



*European Spatial Data Research*

December 2006

The EuroSDR Test  
“Checking and Improving of Digital Terrain Models”

Report by Joachim Höhle and Marketa Potuckova

Reliability of Direct Georeferencing  
Phase 1: An Overview of the Current  
Approaches and Possibilities

Report by Jan Skaloud

Reliability of Direct Georeferencing  
Phase 2: A Case Study on Practical  
Problems and Solutions

Report by Klaus Legat, Jan Skaloud, and Ronald Schmidt

The present publication is the exclusive property of  
European Spatial Data Research

All rights of translation and reproduction are reserved on behalf of EuroSDR.  
Published by EuroSDR

Printed by Gopher, Utrecht, The Netherlands

## EUROPEAN SPATIAL DATA RESEARCH

### PRESIDENT 2006 – 2008:

Stig Jönsson, Sweden

### SECRETARY-GENERAL:

Kevin Mooney, Ireland

### DELEGATES BY MEMBER COUNTRY:

Austria: Michael Franzen

Belgium: Ingrid Vanden Berghe

Cyprus: Christos Zenonos; Michael Savvides

Denmark: Joachim Höhle; Lars Jørgensen

Finland: Risto Kuittinen; Juha Vilhomaa

France: Marc Pierrot-Deseilligny; Franck Jung

Germany: Dietmar Grünreich; Günter Nagel; Dieter Fritsch

Hungary: Arpad Barsi

Ireland: Colin Bray

Italy: Carlo Cannafoglia; Riccardo Galetto

Netherlands: Jantien Stoter; Aart-jan Klijnjan

Norway: Jon Arne Trollvik; Ivar Maalen-Johansen

Portugal: Berta Cipriano

Spain: Antonio Arozarena, Francisco Papí Montanel

Sweden: Stig Jönsson; Anders Östman

Switzerland: Francois Golay; André Streilein-Hurni

United Kingdom: Keith Murray; David Chapman

### COMMISSION CHAIRPERSONS:

Sensors, Primary Data Acquisition and Georeferencing: Michael Cramer, Germany

Image Analysis and Information Extraction: Juha Hyypä, Finland

Production Systems and Processes: Eberhard Gülch, Germany

Core GeoInformation Databases: Keith Murray, United Kingdom

Integration and Delivery of Data and Services: Mike Jackson

### OFFICE OF PUBLICATIONS:

Bundesamt für Kartographie und Geodäsie (BKG)

Publications Officer: Andreas Busch

Richard-Strauss-Allee 11

60598 Frankfurt

Germany

Tel.: + 49 69 6333 312

Fax: + 49 69 6333 441

## CONTACT DETAILS:

Web: [www.eurosdrr.net](http://www.eurosdrr.net)  
President: [president@eurosdrr.net](mailto:president@eurosdrr.net)  
Secretary-General: [secretary@eurosdrr.net](mailto:secretary@eurosdrr.net)  
Secretariat: [admin@eurosdrr.net](mailto:admin@eurosdrr.net)

EuroSDR Secretariat  
Faculty of the Built Environment  
Dublin Institute of Technology  
Bolton Street  
Dublin 1  
Ireland

Tel.: +353 1 4023933

The official publications of EuroSDR are peer-reviewed.

## TABLE OF CONTENTS

*J. Höhle and M. Potuckova:*

<b>The EuroSDR Test "Checking and Improving of Digital Terrain Models"</b>	9
<b>ABSTRACT</b>	11
<b>1 INTRODUCTION TO THE TOPIC</b>	11
<b>2 METHODS FOR THE GENERATION OF DIGITAL TERRAIN MODELS</b>	11
<b>3 CHECKING AND IMPROVING OF DTMS</b>	12
3.1 Accuracy of DTMs	13
3.2 Completeness of DTMs	14
3.3 Economy of the checking methods	14
<b>4 OBJECTIVES OF THE EUROSDR PROJECT</b>	15
<b>5 THE DIFFERENT TASKS OF THE PROJECT</b>	15
<b>6 ACTIVITIES OF THE WORKING GROUP</b>	18
<b>7 PRACTICAL HANDLING OF THE PROJECT</b>	18
<b>8 CONTENTS OF THE REPORT</b>	18
<b>9 DTM BY DIGITAL PHOTOGRAMMETRY (TASK A)</b>	19
9.1 General considerations and principles	19
9.2 Test areas	19
9.3 Test data for the participants	19
9.3.1 Aerial images	19
9.3.2 DTM data	19
9.3.3 Other material	20
9.4 Evaluation procedures by the pilot centre	20
9.4.1 Reference data	20
9.4.2 Evaluation of the accuracy	20
9.4.3 Evaluation of the completeness	20
9.4.4 Evaluation of the economy	21
<b>10 DTM BY SCANNING OF CONTOUR LINES (TASK B)</b>	21
10.1 General considerations and principles	21
10.2 Test areas	21
10.3 Test data for the participants	21
10.3.1 Aerial images	21
10.3.2 DTM data	22
10.3.3 Other material	22
10.4 Evaluation procedures by the pilot centre	22
10.4.1 Reference data	22
10.4.2 Evaluation of the accuracy	22
10.4.3 Evaluation of the completeness	23
10.4.4 Evaluation of the economy	23
<b>11 DTM BY LASERSCANNING (TASK C)</b>	23
11.1 General considerations and principles	23
11.2 Test areas	23
11.3 Test data for the participants	23
11.3.1 Aerial images	23
11.3.2 DTM data	24
11.3.3 Other material	24
11.4 Evaluation procedures by the pilot centre	24
11.4.1 Reference data	24
11.4.2 Evaluation of the accuracy	25
11.4.3 Evaluation of the completeness	25
11.4.4 Evaluation of the economy	25

<b>12</b>	<b>DESCRIPTION OF THE METHODS OF THE PARTICIPATING GROUPS</b>	25
12.1	Skarlatos/Georgopoulos	25
12.2	Potuckova	26
12.3	Paszotta/Szumilo	26
12.4	Fiala/Sima	27
12.5	Jancso/Zavoti	27
12.6	Kim/Shan	28
<b>13</b>	<b>TYPES OF METHODS APPLIED BY THE PARTICIPANTS</b>	28
<b>14</b>	<b>ANALYSIS OF THE DELIVERED DTMS</b>	29
14.1	Absolute vertical accuracy	29
14.2	Relative vertical accuracy	31
14.3	Ratio between the relative and absolute accuracy of the tested DTMs	34
14.4	Ratio between the delivered DTMs and the improved DTMs	36
14.5	Number of blunders	37
14.6	Positional accuracy	39
14.7	Completeness of the checking	40
14.7.1	General remarks	40
14.7.2	Results of the participants	41
14.8	Economy of the checking methods	42
<b>15</b>	<b>DISCUSSIONS</b>	43
15.1	Results of task A	43
15.2	Results of task B	45
15.3	Results of task C	46
15.4	Joint results	47
<b>16</b>	<b>COMPARISONS OF THE METHODS</b>	50
<b>17</b>	<b>PROBLEMS IN THE INVESTIGATION</b>	50
<b>18</b>	<b>COMPARISON WITH RESULTS OUTSIDE OF THIS INVESTIGATION</b>	51
<b>19</b>	<b>NEW DEVELOPMENTS</b>	52
<b>20</b>	<b>PRACTICAL CONCLUSIONS</b>	52
<b>21</b>	<b>PROPOSALS FOR FUTURE WORK</b>	53
21.1	Practical work	53
21.2	Scientific research and investigation	53
21.3	Disseminations of the work	54
<b>ACKNOWLEDGEMENTS</b>		54
<b>REFERENCES</b>		54
<b>APPENDICES</b>		57
<b>Appendix I</b>		57
Publications of the participants		
	D. Skarlatos, A. Georgopoulos. The method of two overlapping orthoimages for checking the produced DTM	59
	M. Potuckova. Checking and improvements of DTMs in the EuroSDR test	69
	Z. Paszotta, M. Szumilo. Application of a statistical test of hypothesis to check DTM accuracy over the Internet	79
	R. Fiala, J. Sima. The Czech method of DTM checking	87
	T. Jancso, J. Zavoti. Quality control of Digital Terrain Models using different autocorrelation techniques	95
	J. S. Kim and J. Shan. A statistical approach to DTM quality evaluation	113
Special contribution		
	W. Karel and K. Kraus. Quality parameters of Digital Terrain Models	125
<b>Appendix II</b>		141
	Programme of the seminar "Automated DTM checking"	141

*J. Skaloud:*

**Reliability of Direct Georeferencing**

<b>Phase 1: An Overview of the Current Approaches and Possibilities</b>	143
---	-----

<b>ABSTRACT</b>	145
-----------------	-----

<b>1 INTRODUCTION</b>	145
1.1 Background	145
1.2 Motivation	145
1.3 Limits	146
1.4 Outline	146
<b>2 RELIABILITY AND INTEGRITY</b>	146
2.1 Definitions	146
2.1.1 Reliability	146
2.1.2 Integrity	146
2.2 Application to DG	147
<b>3 DG IN GENERAL</b>	147
3.1 The method	147
3.2 Technology suppliers	147
3.3 Overview	147
<b>4 GNSS</b>	148
4.1 Current situation	148
4.2 Available technologies	148
4.2.1 RAIM	148
4.2.2 SBAS	148
4.2.3 GPS signal modernization	149
4.2.4 GLONASS and Galileo	149
4.2.5 PPP	149
4.2.6 CP-DGPS	150
4.2.7 Network differential techniques	150
4.2.8 Local and nation-wide networks	150
4.2.9 Differential atmosphere	151
4.3 Summary	151
<b>5 INERTIAL SENSORS AND ESTIMATION METHODS</b>	152
5.1 Current situation	152
5.2 Available technologies	152
5.2.1 The enabling technology	152
5.2.2 Sensor life expectancy	153
5.2.3 Sensor redundancy	153
5.2.4 GPS/INS integration	153
5.2.5 FDE in Kalman filtering	154
5.2.6 FDE in Artificial Neural Networks	154
5.2.7 Limits of GPS/INS and complementary methods	154
5.3 Summary	155
<b>6 INTEGRITY AND COMMUNICATION</b>	155
6.1 Current situation	155
6.2 Available technologies	155
6.2.1 The problem of distributions	155
6.2.2 Avionic approach	156
6.2.3 Pseudolites	156
6.2.4 TCAR	156
6.2.5 Communication technology	156
6.3 Summary	157

<b>7</b>	<b>CALIBRATION AND INTEGRATED SENSOR ORIENTATION</b>	157
7.1	Current situation	157
7.2	Available technologies	158
7.2.1	System calibration in general	158
7.2.2	Lever-arm calibration	158
7.2.3	Boresight calibration for frame and line-based sensors	158
7.2.4	Boresight calibration for LiDAR	158
7.2.5	Synchronization	158
7.2.6	Sensor interior orientation	159
7.2.7	Transformation of EO to national coordinates	159
7.3	Summary	159
<b>8</b>	<b>CONCLUDING REMARKS</b>	159
<b>9</b>	<b>ACKNOWLEDGEMENT</b>	160
	<b>REFERENCES</b>	161
	<b>REFERENCES BY ALPHABETIC ORDER</b>	165

*K. Legat, J. Skaloud and R. Schmidt:*

**Reliability of Direct Georeferencing**

**Phase 2: A Case Study on Practical Problems and Solutions** .....169

**ABSTRACT** .....171

**1 INTRODUCTION** .....171

**2 THEORETICAL BACKGROUND** .....172

2.1 Recording and processing of direct-georeferencing data .....172

2.1.1 Layout of airborne mobile-mapping systems .....172

2.1.2 System calibration .....172

2.1.3 Nominal processing steps of the GPS/INS data .....172

2.2 Potential error sources .....173

**3 CASE STUDY** .....174

3.1 Project characteristics .....174

3.2 Provided data and information .....175

3.3 Identified problems and solutions .....176

3.3.1 Erroneous image positions – Horizontal effects .....176

3.3.2 Erroneous image positions – Vertical effects .....178

3.3.3 Erroneous image-orientation angles .....180

3.4 Summary .....181

**4 CONCLUSIONS AND RECOMMENDATIONS** .....182

**ACKNOWLEDGMENTS** .....183

**REFERENCES** .....183

**INDEX OF FIGURES** .....184

**INDEX OF TABLES** .....184



## **The EuroSDR Test**

### **“Checking and Improving of Digital Terrain Models”**

*Report by Joachim Höhle and Marketa Potuckova*

Aalborg University, Department of Development and Planning  
Research Group “Geoinformatics”



## ABSTRACT

*This report deals with research work how digital terrain models can automatically be checked and improved. Test material consisting of three DTMs of different acquisition methods has been prepared, and six research groups applied their methods with the delivered DTMs. The provided imagery is suitable for the production of orthoimages and serves also as auxiliary material for the checking and improving of DTMs. The results of the participants were analyzed by means of accurate reference material with regard to accuracy. Furthermore, the completeness and degree of automation at the different methods have been evaluated.*

*The report describes in detail the delivered test material, the characteristics of the different methods, the strategy in the evaluation including the applied accuracy measures. The improving of DTMs is also possible to a large extent. A thematic map can give a quick overview where additional measurements are required. The applied methods are compared by means of the accuracy measures derived both from the delivered material and from the accurate reference data of the pilot centre. One method, which derives correction for the delivered DTM by means of parallaxes between two overlapping orthoimages, was applied to all test areas and achieved the best results. The three DTMs could be tested with an accuracy of  $\sigma_h=0.015\%$  of the flying height. Proposals for future practical work and further investigations are given. The results of this investigation will also be disseminated in educational seminars and e-learning courses of the EuroSDR. The contributions of the participating research groups are attached in the appendix of the report.*

## 1 INTRODUCTION TO THE TOPIC

Digital Terrain Models (DTMs) are required for the production of orthoimages. They are often produced for large areas and nowadays at short intervals of time (e.g. two years in Denmark). The geometric accuracy of the DTM influences the quality of the orthoimage very much. The production process requires quality control, and the DTM has therefore to be checked and updated. Changes in the landscape and construction work make an update of the DTM necessary, and the requirements for accuracy become larger. Efficient methods for checking and improving of DTMs are requested by the National Mapping Agencies and private mapping organizations. In 2004 the European Research Organization for Spatial Data Research (EuroSDR) initiated research on checking of digital terrain models (DTMs). Participants in the project should develop methods, apply them to the same test material, and the results should be investigated regarding accuracy, degree of automation and economy. The analysis of the results should give an indication which method would deliver the best results and which problems would remain unsolved.

## 2 METHODS FOR THE GENERATION OF DIGITAL TERRAIN MODELS

The production of orthoimages for large areas and of medium resolution (0.25-0.80 m) uses heights which represent the terrain. Digital Terrain Models (DTMs) are used for this application. The so-called “true orthoimages” require Digital Surface Models (DSMs). They are produced for cities and with a higher geometric resolution, for example 0.05 m - 0.20 m. Both types of height models are sometimes called Digital Elevation Models (DEMs). The use of Digital Terrain Models is not restricted to the production of orthoimages. Other tasks such as planning of construction work or flood studies require higher accuracies than the production of orthoimages. Therefore, a demand to check and to improve the accuracy of existing DTMs exists at National Mapping Agencies and other mapping organizations.

Digital Terrain Models can be produced by different methods and each method has its characteristics. In this investigation the results of three different methods are investigated: Scanning of contour lines,

automated photogrammetry and laser scanning. By means of these three methods, height spots arranged in a grid of equal spacing are produced and can in this form best be used for the production of orthoimages. The heights derived from the contour lines represent the terrain, the heights from automated photogrammetry and laser scanning are on the surface (on top of vegetation, buildings, vehicles, etc.). These raw data can be filtered and thereby be reduced to the terrain (bare earth). The accuracy of the methods for DTM generation are different; contour lines of existing topographic maps, such as 1:25 000, may have standard deviations of  $\sigma_h=1.5 - 3$  m; laserscanning may produce accuracies of  $\sigma_h=0.15 - 0.3$  m. The accuracy of automated photogrammetry is about  $\sigma_h=0.02 - 0.03\%$  of the flying height (h), for example  $\sigma_h=0.8 - 1.2$  m at  $h=4000$  m. The mentioned accuracies refer to the accuracies of the grid posts. The spacing of the height points is 1-2 m at laser scanning, but 10-25 m for the DTMs derived from the contour lines. Automated photogrammetry can also produce dense DTMs. All of the three methods of DTM generation may have blunders. They have to be detected and eliminated because they are easily visible in the orthoimages. Figure 1 shows the required DTM

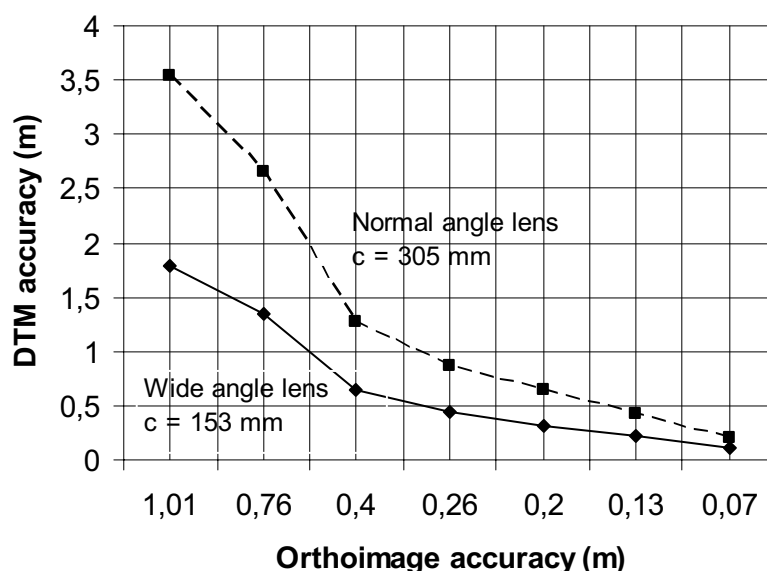


Figure 1: Influence of DTM accuracy on orthoimage accuracy. The data are based on the specifications for orthoimage production in Denmark (GeoForum, 2004).

accuracy in order to maintain the accuracy demands for orthoimages. Such requirements are pretty high, and the existing DTMs have to be improved or new ones have to be measured by the proper methods.

### 3 CHECKING AND IMPROVING OF DTMS

The investigation "Checking of DTMs" should include three parts: Accuracy, completeness and the degree of automation. The checking methods should be universal. The amount of work involved when checking large areas will require automated methods. A visual inspection of the results and other manual work may have to be added. Reliable and economic methods of DTM checking are then becoming semi-automatic methods. Such methods should also include the possibility for improvement of the DTMs.

### 3.1 Accuracy of DTMs

The accuracy of grid-DTMs includes the vertical **and** the horizontal accuracy of the grid posts. If the terrain is hilly or mountainous, a positional error will also result in a height error. If DTMs of such areas are checked, the accuracy can be modelled as a function of the slope and of the grid spacing. Reference values of the check points must have a superior accuracy, which means their accuracy has to be better at least by a factor of 3 to 5. The number of reference values should be as high as possible; the distribution of the check points must be over the whole area. The principle in the checking of the DTMs in this investigation is depicted in figure 2. The DTM accuracy is characterized by the root mean square error (RMSE value), the maximum error, the mean error, the standard deviation, and the number of blunders. The threshold for blunders may be defined as  $3 * \text{RMSE}$ , and all blunders should be removed before the calculation of the mean and the standard deviation. This threshold is special for each type of landscape. A constant threshold should be used when comparing the results of the different methods. It will be set according to the checking method (photogrammetry or ground surveying). Table 1 shows the accuracy measures as they are used in this investigation.

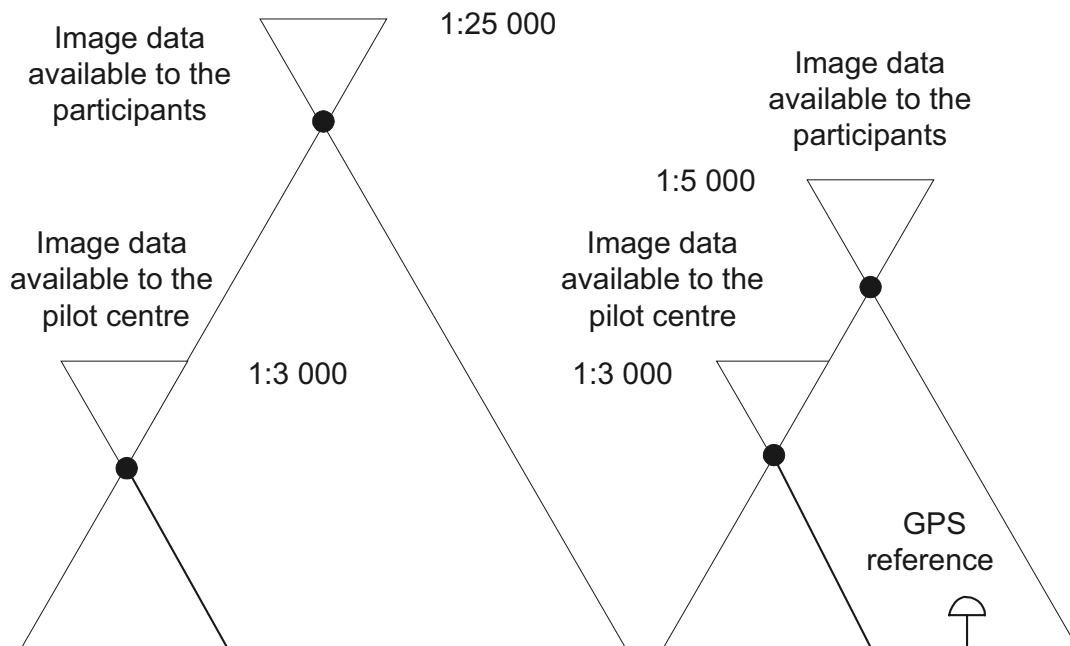


Figure 2: Principle of checking DTMs in this investigation.

The left configuration is used for DTMs derived by digital photogrammetry (task A) and scanning of contour lines (task B), the right one for DTMs derived by laser scanning (task C).

Special attention has to be given to the mean error because a systematic shift of the heights may lead to problems in the calculation of volumes or the directions of water flow.

<b>Vertical Accuracy</b>	
Difference from reference data	$\Delta h$
Number of tested points	$n$
Root Mean Square Error	$RMSE = \sqrt{\frac{\sum \Delta h^2}{n}}$
Maximum difference	$ \Delta h_{\max} $
Definition of a blunder (threshold)	$S > 3 * RMSE$
Number of blunders	$N$
Number of points without blunders	$n' = n - N$
Mean	$\mu^* = \frac{\sum \Delta h}{n'}$
Standard deviation	$\sigma^* = \sqrt{\frac{\sum (\Delta h - \mu^*)^2}{(n'-1)}}$
<b>Horizontal Accuracy</b>	$\sigma_P = \sqrt{(\sigma_x^2 + \sigma_y^2)}$

Table 1: Accuracy measures for DTMs as they are used in this investigation.

### 3.2 Completeness of DTMs

The DTM cannot be determined in all areas. Excluded areas can be areas with objects above the terrain, for example houses and trees. Photogrammetric methods require contrast and structure in the imagery, and if these conditions do not exist, such areas must also be excluded. Laser scanning requires roughness at the terrain surface and blunders may occur due to multi-path in the neighbourhood of buildings. This may also lead to “excluded areas” and grid posts without heights. The amount of the missing areas in relation to the whole area in percent will give a value for the completeness. Furthermore, the applied checking method should give an overview where problematic areas are situated. By means of a thematic map, for example, the zones of intolerable errors can be visualized and the efforts for updating of the DTM can then be estimated.

### 3.3 Economy of the checking methods

The economy of the checking methods is influenced by the degree of automation and the amount of manual work. Other factors are investments for tools (e.g. software packages) and training of the personnel. The easiness in use of the method is also an economic factor. Most important for the economy

is the availability or generation of reference data with the required accuracy and distribution. If DTMs are used for orthoimage production, the same imagery can be used for the checking and improving of the existing DTMs. This will, of course, save a lot of costs. Methods and procedures which avoid reference data and will test for blunders and inconsistencies in the DTMs only, are more economic, but they are not complete checking methods.

#### 4 OBJECTIVES OF THE EUROS DR PROJECT

This EuroSDR project should lead to experience with various automatic and semi-automatic checking methods. EuroSDR research usually uses test material which is sent to different researchers or research groups. The pilot centre of the project, the research group “Geoinformatics” of Aalborg University, compiled three different data sets and sent them to the interested participants. The test material included three DTMs, which were derived by the three methods of data collection: Automated photogrammetry, digitizing of contour lines, and laser scanning. Beside the DTMs, two stereopairs and some control points for the orientation of the imagery were available for the participants. The image scale is the same as in the orthophoto production. Also some profiles were marked in orthoimages. The participants of the test with the laser scanning data had to check the height values in these locations. If possible, the method should also be used for improving the delivered DTM. Details of the test material will be presented in the next chapters.

#### 5 THE DIFFERENT TASKS OF THE PROJECT

The investigation has been separated into three tasks (A, B and C). In each of the tasks the data acquisition technology, the spacing of the grid points and the magnitude of errors are different. Specific checking methods and standards may be necessary for each DTM type. Also the type of landscape (for example open area or built-up area) may have an influence. A universal method for checking and improving of DTMs would, however, be of advantage.

**Task A** deals with a DTM derived by digital photogrammetry. The provided DTM has a relatively low density (grid spacing = 25 m), a relatively low accuracy ( $\sigma_h = 0.7$  m) and only a few blunders ( $N=41$ ). The images for the investigation have a scale of 1: 25000. The reference data for the evaluation are derived by low altitude photography ( $m_b=1:3000$ ) and its accuracy amounts to  $\sigma_h = 0.09$  m, which means that the accuracy of the reference data is better than the DTMs accuracy by a factor of 8. The subareas I-IV have 2033 reference points, that is 59% of all grid posts in these subareas. The landscape type is open area. Figure 3 shows the test areas of task A (and B).

The DTM of **task B** is derived from 5m contours of a topographic map by scanning. The contours themselves are compiled from different sources (plane table surveying and analogue photogrammetry). These older data acquisition methods surveyed only a few points and lines and/or plot the contours continuously. A generalization of the contours took place in the cartographic process afterwards. The scanning of the final contour lines required automated labelling of the contours which is a difficult procedure and which may produce blunders. However, improvements thereafter took place by means of data fusion with more accurate height data from new photogrammetric mapping.

The DTM delivered to the participants has a modest density (grid spacing = 10 m), a relatively low accuracy ( $\sigma_h = 1.4$  m) and a relatively large number of blunders ( $N=165$ ). The reference data for the evaluation by the pilot centre are again derived from low altitude photography and its accuracy is  $\sigma_h = 0.09$  m, which means that it is better by a factor of 15 in regard to the accuracy of the DTM. The sub-areas (I-IV) have 10390 reference points, which is 47% of all the grid posts. The images for the



Figure 3: Test areas of task A and B.

investigation by the participants are the same as in task A ( $m_b = 1: 25000$ ). Figure 3 shows the test areas of the tasks A and B.

**Task C** will check the DTM derived by laser scanning. This DTM has a high density (grid spacing = 1 m), a relatively high accuracy ( $\sigma_h = 0.10$  m) and very few blunders ( $N=9$ ). The reference data for the evaluation are derived by GPS (RTK) and low altitude photography ( $m_b = 1: 3000$ ). The accuracy of the reference data is relatively high ( $\sigma_h = 0.02$  m and  $\sigma_h = 0.06$  m, respectively); that means the accuracy is better by a factor of 5 and 1.7, respectively. The condition of superior accuracy is fulfilled for the GPS derived reference data only. The areas 'L' and 'R' cover 1412 reference points, which is 3% of all grid posts in these areas.

The GPS data are arranged in 9 profiles. The provided images for the investigation by the participants have a scale of 1: 5000. The landscape of Task C is a built-up area (compare figure 4). Table 2 summarizes the details of the different tasks for the participants in the test.



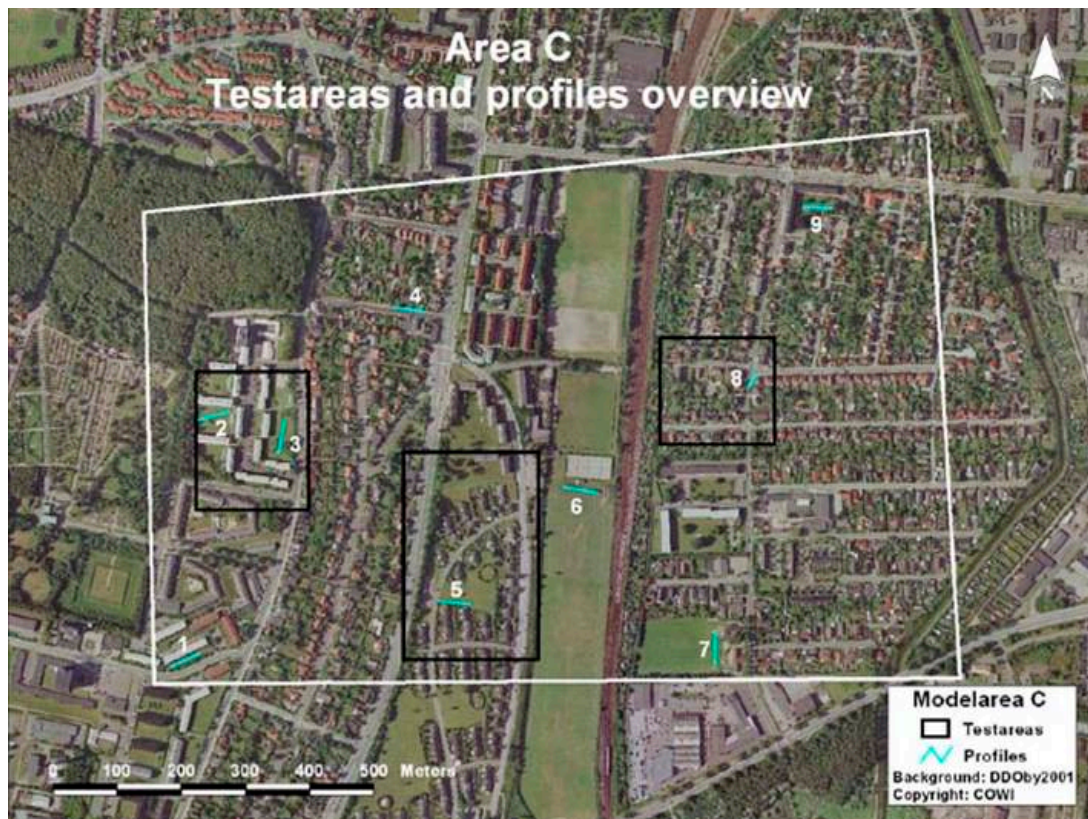


Figure 4: Test areas and profiles of task C (checking the DTM derived by laser scanning).

Task/Test	A	B	C
<b>DTM</b>			
Derived by:	Photogrammetry, automatic procedures	Digitizing of contour lines of topographic maps	Laser scanning
Grid spacing	25 m	10 m	1 m
<b>Aerial images</b>			
Scale	1:25 000	1:25 000	1: 5 000
Pixel size (im- age)	0.021mm	0.021 mm	0.015 mm
Pixel size (ground)	0.525 m	0.525 m	0.075 m
<b>Landscape</b>	Open area	Open area	Built-up area
<b>Control points</b>	Sketches, XYZ co-ordinates	Sketches, XYZ co-ordinates	Sketches, XYZ co-ordinates
<b>Other data</b>	Border lines of test areas	Borderlines of test areas	Borderlines of test areas, Profile positions where heights have to be measured

Table 2: Characteristics of test data and areas of task A, B and C.

## **6 ACTIVITIES OF THE WORKING GROUP**

In order to carry out this project several people had to agree to do voluntary research work.

Information about the project was spread via different channels, among others via a homepage.

The following researchers participated in the project:

D. Skarlatos and A. Georgopoulos (National Technical University of Athens, School of Surveying, Laboratory of Photogrammetry, Athens, Greece)

Z. Paszotta and M. Szumilo (University of Warmia and Mazury, Department of Photogrammetry and Remote Sensing, Olsztyn, Poland)

R. Fiala and J. Sima (University of West Bohemia in Pilsen, Department of Geomatics, Czech Republic)

T. Jancso and J. Zavoti (University of West Hungary, Faculty of Geoinformatics, Szekesfehervar)

J. S. Kim and J. Shan (Purdue University, West Lafayette, Indiana, USA)

The authors of this paper participated with contributions to the project as well. The method of automated parallax measurements between two orthoimages was investigated and improved in the PhD thesis of M. Potuckova. The preparation of the test material and the analysis of the results were carried out by both authors. Project leader was Prof. J. Höhle, Aalborg University.

A seminar "Automated Quality Control of Digital Terrain Models" with most of the working group members and a few experts of related knowledge was held at Aalborg University, 18.-19.8.2005. The seminar programme is attached in Appendix II.

## **7 PRACTICAL HANDLING OF THE PROJECT**

The participants in the project downloaded the test material from the homepage of the project. It was their decision which task (A, B or C) they wanted to solve. The focus in the project was on the methods how the DTM could efficiently be checked and improved. The description of the method and the achieved results were sent to the pilot centre. The results (accuracy measures for the original DTM, a corrected DTM and/or a list of blunders) were analyzed by the pilot centre by means of accurate reference data and a preliminary report was compiled. The participants had then the opportunity to comment the preliminary report. This final report was compiled afterwards.

## **8 CONTENTS OF THE REPORT**

The report deals with the three tasks (A, B, and C) separately.

Each task contains general considerations and principles, a more detailed description of the test area and of the test data, and remarks on the evaluation procedures. After a description of the methods of the participating research groups the analysis of the delivered DTMs follows. The discussion of the results of the participants ends in a conclusion and proposals for future work. The original contributions of the authors (including some editing by the authors of this report) are attached to this report (see Appendix I).

## 9 DTM BY DIGITAL PHOTOGRAMMETRY (TASK A)

### 9.1 General considerations and principles

A DTM derived by digital photogrammetry has to be checked with regard to accuracy and completeness of improving the height values at all grid posts. As assistance a stereopair in the scale which also enables orthoimage production is available together with control points and orientation data. Accuracy measures for the delivered DTM including a list of blunders and a revised DTM had to be sent to the pilot centre for evaluation. The used method for checking and improving of the DTM had to be described by the participants. The pilot centre will check the revised DTM by means of accurate reference data. The evaluation will comprise the accuracy, completeness and economy. It is the goal of this investigation to develop and test automatic or semi-automatic methods for checking and improving of such a DTM.

### 9.2 Test areas

The test areas (samples) of task A can be seen in Figure 3. It consists of four sub-areas (I-IV), which are very similar regarding the type of landscape. The area is mainly hilly and open land with fields, meadows, roads, and paths. A small part is built-up area. Altogether about 2033 reference points are available, which is 59% of all grid posts. They are lying in the terrain and have good texture and contrast. The test areas cover 11% of the stereo model.

### 9.3 Test data for the participants

The data provided to the participants in the project comprise two overlapping aerial images, the interior orientation of the used camera, control points for the derivation of the exterior orientation, and the DTM to be tested. The reference data used by the pilot centre for evaluation consisted of accurate height values determined from low altitude photography.

#### 9.3.1 Aerial images

The images delivered to the participants of the test were taken in 2003 by an analogue camera (RMK TOP 15) from an altitude of 3800 m above ground. The scale of the colour images is about 1:25 000. The images have been digitized by a precision scanner using a pixel size of 21  $\mu\text{m}$ . The interior orientation of the images used the data from the camera calibration report of the camera manufacturer. An affine transformation has been carried out in order to establish the image co-ordinate system and to define the fiducial centre.

#### 9.3.2 DTM data

The provided DTM is derived by digital photogrammetry using the program “Automatic Elevations” of Z/I Imaging (version 04.04.06.00). The used control parameters had the following values: Threshold for correlation coefficient = 0.7, parallax bound = 8 pixels (pel), adaptive matching strategy = yes. The derived height (elevation) model is basically a surface model. It has a grid spacing of 25 m. The planimetric co-ordinates (Easting and Northing) are in the UTM system based on the Euref89 datum. The heights are given in the Danish Vertical Reference (DVR90). The DTM has been derived for the whole model area (about 20  $\text{km}^2$ ). The vertical accuracy of the DTM is  $\sigma_h = 0.7$  m which was calculated from the four sub-areas (I-IV) by means of the accurate reference data (compare chapter 9.4).

### 9.3.3 Other material

Other material provided for the participants of task A were co-ordinates of the borders of the test areas, sketches of the control points, and the description of the delivered files.

## 9.4 Evaluation procedures by the pilot centre

The evaluation of the results of the participants in task A will comprise the vertical accuracy and the completeness of the improvement. Reference values for the heights (elevations) will be derived by means of photogrammetry. The accuracy measures of table 1 will be derived. The horizontal accuracy is checked by means of the residuals in the absolute orientation of the stereo pair.

### 9.4.1 Reference data

Reference data for the evaluation of the delivered results were derived by the pilot centre from black&white photographs, which were taken from an altitude of 460 m in the same year as the photographs used by the participants. The large-scale photographs ( $m_b=1:3000$ ) were digitized in a precision scanner with a pixel size of 21  $\mu\text{m}$ . Semi-automatic measurements were carried out in the stereomodel at the places of the grid posts. When such a grid post was lying on the top of a house or a tree or the condition for good correlation (correlation coefficient  $r>0.5$ , standard deviation of subpixel calculation  $\sigma<0.25$  pel) was not fulfilled, the point was skipped. This means that only points on the ground were used as reference data and that the measured height at such a point is reliable. 59% of all grid posts were used as reference data only. This amount of points is enough for checking the DTM.

The accuracy of reference data has been estimated by double measurements of grid posts and the deviations at check points after the orientation of the model. A total error of  $\sigma_h = 0.09$  m was calculated for the reference points in test area A. The accuracy of the reference data is superior to the accuracy of the delivered DTM ( $\sigma_h=0.7$  m).

### 9.4.2 Evaluation of the accuracy

The vertical accuracy of DTMs is derived by comparison of the DTM height with the reference height. The accuracy measures of table 1 will be calculated from these differences. If the reference data of the pilot centre are used, an absolute accuracy can be determined. If the participants have derived own reference values by means of the delivered images, then a relative accuracy is calculated. The ratio between the relative and the absolute accuracy will also be determined by the pilot centre. This ratio will normally exceed 1.0 because the reference values of the participants are less accurate due to the large difference in the scales of the photography. The obtained ratios can be used for a comparison of the different methods. The number of blunders, which are detected by a checking method, is also used for comparison of the methods. It has to be defined what a blunder is. A threshold has to be set and this can be done in two ways. The threshold can be adapted to the area and the actual errors when using  $S=3*RMSE$ . Secondly, a constant value (for example  $3*0.015\%*\text{flying height}$ ) can be used as a threshold. By means of a constant threshold the different methods of checking can be compared regarding their effectiveness in blunder detection. For task A (and B) the threshold  $S_{\text{constant}} = 3*0.00015*3800 \text{ m} = 1.7 \text{ m}$  was selected.

### 9.4.3 Evaluation of the completeness

A DTM consists of grid posts with elevations. In this investigation not all of the grid posts have reference values (due to elevated objects and due to poor condition for correlation) and not all reference

points have height values in the delivered DTM. The ratio between the number of the measured points and the number of reference points is here used as a measure for completeness. In addition, a thematic map is compiled showing the areas where DTM specifications are met and areas where improvements by other methods are still necessary. By such a map the efforts for updating of the DTM can be estimated.

#### 9.4.4 Evaluation of the economy

The proposed methods are new and not yet prepared for production. A judgment will be made whether a method has the potential for automation. Two classes (high and low) are used in the evaluation of the methods. A table with the advantages and disadvantages of each method will be compiled in addition.

## 10 DTM BY SCANNING OF CONTOUR LINES (TASK B)

### 10.1 General considerations and principles

A DTM derived by scanning of contours has to be checked with regard to accuracy and completeness of improving the DTM. A stereopair in the scale which also enables orthoimage production is given together with control points and orientation data as assistance. Accuracy measures for the delivered DTM including a list of blunders and a revised DTM had to be sent to the pilot centre for evaluation. The method used for checking and improving of the DTM had to be described by the participants. The pilot centre checks the revised DTM by means of accurate reference data. The evaluation will comprise the accuracy, completeness and economy.

### 10.2 Test area

The test areas of task B consists of four sub-areas (I-IV), which are very similar (compare Figure 3). It is mainly hilly and open area with fields, meadows, roads, and paths. A small part is built-up area. Altogether about 10000 reference points are available, which is 47% of all grid posts. They are lying in the terrain and have good texture and contrast. The test area covers 11% of the stereo-model. The test areas (and the delivered aerial images) are the same as in task A.

### 10.3 Test data of the participants

The data provided to the participants of the test comprise two overlapping aerial images, the calibration report of the applied camera, control points for the derivation of the exterior orientation, and the DTM to be tested. The reference data used by the pilot centre for evaluation consisted of accurate height values determined from low altitude photography.

#### 10.3.1 Aerial Images

The images delivered to the participants were taken by an analogue camera (RMK TOP 15) from an altitude of 3800 m above ground. The scale of the colour images is about 1:25 000. The two images have been digitized by means of a precision scanner using a pixel size of 21  $\mu\text{m}$ . The interior orientation of the images used the data from the camera calibration report of the camera manufacturer. An affine transformation has been carried out in order to establish the image co-ordinate system and the fiducial centre. The images are the same as for task A.

### 10.3.2 DTM data

The provided DTM is derived by scanning of contour lines. It has a grid spacing of 10 m. The planimetric co-ordinates (Easting and Northing) are in the UTM system based on the Euref89 datum. The heights are given in the Danish Vertical Reference (DVR90). The DTM was derived for the whole model area (about 20 km<sup>2</sup>). The vertical accuracy of the DTM is  $\sigma_h=1.4$  m which was determined from checking the four sub-areas (I-IV) by means of the accurate reference data (compare chapter 10.4).

### 10.3.3 Other material

Other material provided for the participants of task B were co-ordinates of the borders of the test areas, co-ordinates and sketches of the control points, and a description of the delivered files.

## 10.4 Evaluation procedures by the pilot centre

The evaluation of the results of the participants in task B will comprise the vertical accuracy and the completeness of the improvement. Reference values for the heights (elevations) will be derived by means of photogrammetry. The horizontal accuracy can be checked by means of the residuals in the absolute orientation of the stereopair.

### 10.4.1 Reference data

Reference data for the evaluation of the delivered results were derived from black&white photographs, which were taken from an altitude of 460 m in the same year as the photographs used by the participants. The large-scale photographs 1:3000 were digitized in a precision scanner using a pixel size of 21  $\mu$ m. Semi-automatic measurements were carried out in the stereomodel at the places of the grid posts. If such a grid post was on the top of a house or a tree, or the condition for correlation (correlation coefficient  $r>0.5$ , standard deviation of subpixel calculation  $\sigma<0.25$  pel) was not fulfilled, the point was skipped. This means that only points on the ground were used as reference data and that the measured elevation at such a point is reliable. Only 47 % of all grid posts could be used as reference data. The accuracy of the reference data was estimated by double measurements of grid posts and by means of the deviations at check points after the orientation of the model. A total error of  $\sigma_h = 0.09$  m was calculated for the reference points in test area B. The number of reference points is 10 390.

### 10.4.2 Evaluation of the accuracy

The vertical accuracy of the DTM is derived by comparison of the DTM elevation with the reference elevation. The accuracy measures of table 1 will be calculated from these differences. If the reference data of the pilot centre are used, an absolute accuracy can be determined. If the participants have derived own reference values by means of the delivered images, then a relative accuracy is calculated. The ratio between the relative and the absolute accuracy will also be determined by the pilot centre. This ratio will normally exceed 1.0 because the reference values of the participants are less accurate due to the large difference in the scales of the photography. The obtained ratios can be used for a comparison of the different methods. The number of blunders which are detected by a checking method, is also used for comparison of the methods. It has to be defined what a blunder is. A threshold has to be set and this can be done in two ways. The threshold can be adapted to the area and the actual errors when using  $S=3*RMSE$ . Secondly, a constant value (for example  $3*0.015\%*$ flying height) can be used as a threshold. By means of a constant threshold the different methods of checking

can be compared regarding their effectiveness in blunder detection. For task B (and A) we select the following threshold,  $S_{\text{constant}} = 3 * 0.00015 * 3800 \text{ m} = 1.7 \text{ m}$ .

#### 10.4.3 Evaluation of the completeness

The ratio between the number of the measured heights and the number of reference heights is here used as a measure for completeness. In addition, a thematic map is compiled showing the areas where DTM specifications are met and areas where improvements by other methods are still necessary.

#### 10.4.4 Evaluation of the economy

The proposed methods are not yet prepared for production. Their potential for automation will be judged. Two classes (high and low) are used in the evaluation of the methods.

### 11 DTM BY LASER SCANNING (TASK C)

#### *11.1 General considerations and principles*

A DTM derived by laser scanning has to be checked by the participants with regard to accuracy and to be improved in all posts of the grid which have reference data. A stereopair in the scale 1:5000 which also enables the production of high resolution orthoimages is given together with control points and orientation data as assistance. A revised DTM, accuracy measures and a list of blunders should be delivered to the pilot centre for evaluation. The used method for checking and improving of the DTM had to be described by the participants. The pilot centre checks the revised DTM by means of accurate reference data. The evaluation will comprise the vertical and horizontal accuracy, completeness of the checking and economy of the applied checking method. Goal of this investigation is to develop and to test automatic or semi-automatic methods for checking and improving such a DTM.

#### *11.2 Test area*

The test areas of task C consists of three sub-areas, L(ef), M(iddle), and R(ight), and nine profiles (compare Figure 4). About 2153 reference points are available, which is 3% of all grid posts. They are situated in the terrain and have good texture and contrast. The test areas cover 13% of the stereo-model. In the nine profiles 417 points are measured by GPS in 2005.

The imaged landscape of task C can be classified as built-up area. Houses, roads, meadows and gardens are present. The elevations range from 2-56 m.

#### *11.3 Test data for participants*

The data provided to the participants in the project comprise two overlapping aerial images, the interior orientation of the used camera, control points for the derivation of the exterior orientation, and the DTM to be tested. In addition, planimetric co-ordinates of reference points within profiles were delivered, at which the participants had to determine heights by means of the delivered stereopair.

##### 11.3.1 Aerial images

The images delivered to the participants were taken in 2001 by an analogue camera (RMK TOP 15) from an altitude of 765 m above ground. The scale of the colour images is about 1:5 000. The two

images have been digitized by means of a precision scanner using a pixel size of 15  $\mu\text{m}$ . The interior orientation of the images used the data from the camera calibration report of the camera manufacturer. An affine transformation has been carried out in order to establish the image co-ordinate system and the fiducial centre. The exterior orientation of the images could be derived by control points. The co-ordinates of the control points were determined by GPS/RTK. Its accuracy is  $\sigma_E = \sigma_N = 0.01\text{m}$  and  $\sigma_h = 0.02\text{m}$ .

### 11.3.2 DTM data

The DTM to be tested by the participants is derived by laser scanning in 2001. The DTM has a grid spacing of 1m. The planimetric co-ordinates (Easting and Northing) are in the UTM system based on the ED50 datum. The heights are given in the Danish Normal Null (DNN) system. The vertical accuracy of the DTM was assumed to be  $\sigma_h = 0.15\text{m}$ . The actual accuracy of the delivered DTM has been derived from comparison of the DTM heights with the heights determined by GPS. It turned out that the vertical accuracy was much higher than assumed ( $\sigma_h = 0.03\text{m}$ ).

### 11.3.3 Other material

Other material for the participants in task C were co-ordinates of the borders of the sub-areas and co-ordinates of the profile points, co-ordinates and sketches of the control points, and a description of the delivered files.

## 11.4 Evaluation procedures by the pilot centre

The evaluation of the results of the participants in task C will comprise the vertical accuracy, the number of blunders, the completeness and the economy. Reference values for the heights (elevations) are derived by means of photogrammetry and by means of ground surveying. The accuracy measures of Table 1 will then be derived. The horizontal accuracy of the DTM will be checked by means of some additional photogrammetric measurements, which are carried out by the pilot centre only.

### 11.4.1 Reference data

Reference data for the evaluation of the delivered results were derived from black&white photographs, which were taken from an altitude of 460 m in the spring of 2003. The large-scale photographs 1:3000 were digitized in a precision scanner with a pixel size of 21  $\mu\text{m}$ . Semi-automatic measurements were carried out in the stereomodel at the places of the grid posts. If such a grid post was on the top of a house or a tree, or the condition for correlation (correlation coefficient  $r > 0.5$ , standard deviation of subpixel calculation  $\sigma < 0.25\text{ pel}$ ) was not fulfilled, the point was skipped. This means that only points on the ground were used as reference data and that the measured elevation at such a point is reliable.

1412 grid posts were used as reference data. The accuracy of the reference data was estimated by double measurements of grid posts and by means of the deviations at check points after the orientation of the model. A total error of  $\sigma_h = 0.06\text{ m}$  was calculated for the reference points in test area C.

The reference heights of 417 points in 9 profiles are determined by GPS (RTK); they have an estimated accuracy of  $\sigma_h = 0.02\text{ m}$ .

The condition of superior accuracy is fulfilled for both types of reference data if a height accuracy  $\sigma_h = 0.15\text{ m}$  at laser scanning is assumed.



#### 11.4.2 Evaluation of the accuracy

The vertical accuracy of a DTM is derived by comparison of the DTM elevation with the reference elevation. The accuracy measures of Table 1 will be calculated from these differences. If the reference data of the pilot centre are used, an absolute accuracy can be determined. If the participants have derived own reference values by means of the delivered images, then a relative accuracy is calculated. The ratio between the relative and the absolute accuracy will also be determined by the pilot centre. This ratio will normally exceed 1.0 because the reference values of the participants are less accurate due to the large difference in the scales of the photography. The obtained ratios can be used for a comparison of the different methods. The number of blunders which are detected by a checking method is also used for a comparison of the methods. It has to be defined what a blunder is. A threshold has to be set and this can be done in two ways. The threshold can be adapted to the area and the actual errors when using  $S=3*RMSE$ . Secondly, a constant value (for example  $3*0.015\%*$  flying height) can be used as a threshold. By means of a constant threshold the different methods of checking can be compared regarding their effectiveness in blunder detection. For task C we select the following threshold,  $S_{\text{constant}} = 3*0.00015*765 \text{ m} = 0.34 \text{ m}$ .

#### 11.4.3 Evaluation of the completeness

The ratio between the number of the measured heights and the number of reference heights is again used as a measure for completeness. In addition, a thematic map is compiled showing the areas where DTM specifications are met and areas where improvements by other methods are still necessary.

#### 11.4.4 Evaluation of the economy

The proposed methods are not yet prepared for production. Their potential for automation will be judged. Two classes (high and low) are used in the evaluation of the methods.

## 12 DESCRIPTION OF THE METHODS OF THE PARTICIPATING RESEARCH GROUPS

The participating research groups wrote an article about their method. It can be found in Appendix I. In the following a short summary of the methods is presented.

### 12.1 Skarlatos/Georgopoulos (S/G)

Errors in DTM appear as parallaxes between corresponding points in two overlapping orthoimages. Corrections of DTM can be derived from the measured parallaxes (Norville 1996). By applying a rigorous mathematic solution, not only height corrections but also shifts in position from the DTM posts are calculated. Corresponding points are found by means of area-based matching. A novel sub-pixel matching technique using elliptical templates was developed (Skarlatos, Georgopoulos 2004). Moreover, an adaptive template size and the strategy allowing for skipping homogenous areas were applied. Height corrections are calculated with a higher density than an original DTM grid. Due to positional shifts, a TIN of corrections or corrected heights is delivered as a result. In order to improve reliability and decrease the number of mismatches, only points with a correction within the interval of  $\langle m-0.6745\sigma_0, m+0.6745\sigma_0 \rangle$  (50% confidence level test) were accepted.  $m$  is the mean value of corrections and  $\sigma_0$  the standard deviation.

All calculations are carried out fully automatically. The areas, which are not suitable for correlation, are excluded. A high density of corrections gives the advantage that the terrain can be modeled in detail.

### 12.2 Potuckova (P)

The applied method is based on the same principle as the S/G solution. Corresponding points are found in two overlapping orthoimages and height corrections are calculated from discrepancies in their position.

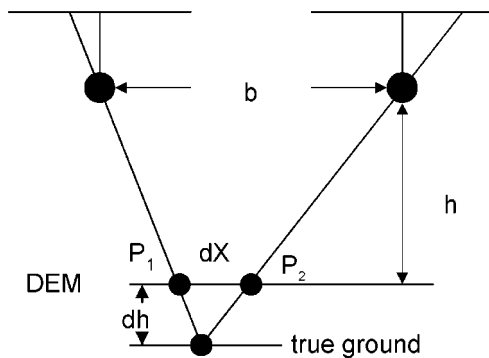


Figure 5: Method of two overlapping ortho images. A parallax ( $dX$ ) between the two overlapping ortho-images will appear when the DTM/DEM has an error. These parallaxes are automatically measured and height errors ( $dh$ ) are derived from them.

Cross-correlation and least squares matching are techniques applied for searching corresponding points. The original RGB images were converted to gray scale images first. In order to eliminate errors in image matching, the following approaches were used:

- setting thresholds for the correlation coefficient and for the standard deviation of shift parameters derived in least squares matching
- searching corresponding points along epipolar lines (which are parallel to the line of flight)
- setting thresholds for differences between matching from the left orthoimage (template) to the right one (search area) and vice versa (L/R method)
- calculating corrections also in the surrounding of the DTM posts and statistical evaluation of these corrections (histogram method)

The histogram method combined with epipolar geometry and thresholds for the correlation coefficient and the accuracy of least squares matching gives the best results. Height corrections are applied directly at DTM posts. Built-up and forest areas can be excluded in advance using map data. In the EuroSDR test, all calculations are restricted to DTM posts covered by reference data. After applying the proposed method, each point of the checked DTM is assigned into one of two groups:

- Points where the method is applied and the DTM is corrected and
- points where the testing method fails and matching criteria are not fulfilled.

Superimposition of these two groups of points in different colors on the orthoimage gives a quick overview where the problems within the DTM and correlation occur. The principle of the method is depicted in Figure 5.

### 12.3 Paszotta/Szumilo (P/S)

The presented approach uses a stereo-pair of aerial images for deriving a DTM of the same point density and size as the DTM to be checked. Discrepancies between the original and the derived DTMs are evaluated.

First, control points are measured and orientation parameters of the stereo-pair are determined. The measurement of control points is carried out semi-automatically. An operator has to point out the

positions of the control points in the images. The measurement itself as well as the automatic derivation of the DTM is based on area-based matching. An analysis of height differences between the derived and original DTMs follows. A hypothesis about a mean error of the sample is tested at a certain level of significance provided a sufficient sample size is available. At the same time a map of height differences is plotted. It gives a quick overview where the discrepancies of the compared DTMs are largest.

The algorithms are implemented at the Internet. The aerial images, the parameters of interior and exterior orientation and an original DTM are saved on a server. A standard Internet browser allowing for running Java applets is required at the client site. A user defines subsections of a stereo-pair where the DTM is checked. Homologous points at original DTM posts are found automatically by means of correlation. A mean value and a standard deviation of the differences between the derived heights and the original DTM are calculated and the mean error hypothesis is tested. More details about the implementation can be found at the given Website (*WebPhotogrammetry*).

#### *12.4 Fiala/Sima (F/S)*

This method carries out a statistical evaluation of height differences between two TINs. The first TIN represents a DTM to be evaluated. The second one is produced as a reference data set and it is assumed that its quality is higher. It can be obtained by digitizing contour lines from large-scale maps or by stereoscopic measurements in the stereomodels. In the test, manual photogrammetric measurements of characteristic spot heights and break lines were carried out. Three statistical measures, namely average error, mean error and root mean square error are derived from volume differences between the TINs by means of the software package ATLAS DMT. Contour lines of the height differences between TINs give a quick overview on errors in the checked DTM.

#### *12.5 Jancso/Zavoti*

The proposed DTM checking method is based on back projection of a grid point into the original images. Area-based matching is used for finding corresponding points.

Two geometrical approaches are applied:

1. Corresponding points are searched on epipolar lines.
2. The height is changed within a given interval (vertical line locus approach).

Different correlation methods are applied. They include e.g. correlation in R(ed), G(reen), B(lue) channels separately, a conversion of colored images into gray scale images followed by correlation, correlation in images with reduced resolution. In order to ensure good conditions for image matching, a texture coefficient is calculated and evaluated. No subpixel methods are applied. Two methods are considered as most successful and are used in the evaluation of results in this report:

- Correlation in the RGB channels. The channel with the maximal value of the correlation coefficient is chosen for further calculations. The size of the template is constant by 15 pixels. The vertical line locus approach is used.
- Correlation is applied in the RGB channels at reduced image resolution. The searching occurs along an epipolar line with a variable size of the search window.

The designed software solution gives a user the possibility of setting several parameters such as the size of correlation matrix, thresholds for correlation and texture coefficients, maximal height error, etc. Based on values of the correlation coefficient, texture coefficient and the height error each point is evaluated and assigned into one of three categories – accepted, rejected, or skipped point. All calculations run fully automatically. An output text file comprises, among others, corrected heights.

Checking of the exterior orientation of an aerial image is done before the checking of a DTM. The principle of the back projection method is depicted in Figure 6.

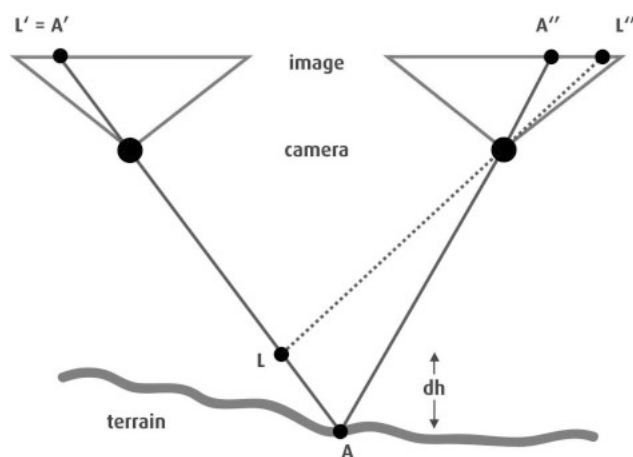


Figure 6: The back projection method. A DTM point (L) is projected onto both aerial images. A corresponding point to L' is searched in the right aerial images along an epipolar line. The height error (dh) will appear as a difference between the points L'' and A''.

#### 12.6 Kim/Shan (K/S)

A height at the DTM post ( $Z$ ) is compared with the surrounding heights. A mean value ( $Z_{\text{mean}}$ ) of the heights of eight neighboring DTM posts as well as a standard deviation ( $\sigma$ ) are calculated. The value  $c = |Z - Z_{\text{mean}}| / \sigma$  is compared with two thresholds  $c1$  and  $c2$ . Only DTM points where  $c \leq c2$  are considered as correct. DTM posts where  $c2 \leq c \leq c1$  are labeled as 'caution area' and values  $c > c1$  indicate blunders. The thresholds  $c1$  and  $c2$  are determined empirically based on diagrams of blunder ratio decrements. They depend on the quality of an original DTM. There is no need for additional data sets (e.g. aerial images) when applying this checking method.

### 13 TYPES OF METHODS APPLIED BY THE PARTICIPANTS

The participants developed different methods and applied it to one or several tasks/DTMs (A, B, C). The participants used their method in three different applications regarding the quality control of DTMs:

- Checking and improving (C&I),
- Checking for relative accuracy (C),
- Checking for blunders (CB).

'Checking for relative accuracy' means that the accuracy has been checked by the participants with their derived reference data and that an improved DTM has not been delivered to the pilot centre.

Table 3 provides an overview for which task the participants delivered results and for which of the three categories of application their method was used.

The three applications (C&I, C and CB) use three different technologies (photogrammetry, ground surveying and statistics). Statistical methods (as used by K/S for example) do not introduce new measurements of heights. The DTM is searched by means of an algorithm for blunders. Ground surveying cannot be used for extensive DTMs. Table 4 shows the applied technologies in the three applications. The table shows the fact that ground surveying can be used for checking only, statistics can be

used for blunder detection only, and that photogrammetry can also solve the checking and improving of DTMs.

Method	Task A	Task B	Task C
S/G	C&I		C&I
P	C&I	C&I	C&I
P/S	C		
F/S	C	C	
J/Z	C&I		
K/S	CB	CB	CB

Table 3: Overview for which task/DTM the participants delivered results and how the application is characterized. It means: C&I...checking and improving, (C)...checking for relative accuracy, (CB)...checking for blunders.

	Statistics	Photogrammetry	Ground surveying
C&I		x	
C		x	x
CB	x	x	

Table 4: Applicable technologies for the checking of DTMs. It means: C&I...checking and improving, (C)...checking for relative accuracy, (CB)...checking for blunders.

## 14 ANALYSIS OF THE DELIVERED DTMS

### 14.1 Absolute vertical accuracy

The accuracy of the delivered DTMs can be determined by comparing the heights at the grid posts with the accurate reference data. The accuracy measures of Table 1 can then be derived and the results of the different methods can be evaluated and compared.

Improved DTMs were delivered by S/G, P and J/Z only. Their data will be compared with the accurate reference values, which are derived by the pilot centre. These results are named as absolute accuracy.

The position of the height values should be the same at the delivered DTM and at the DTM used as the absolute reference. A small difference in the position was tolerated (2 m in the DTM of task A and B and 0.5 meter in task C). If the DTM has been delivered as a TIN model, a grid model has first been derived by linear interpolation.

Tables 5 and 6 show the results for the test areas of task A, Table 7 for the task B areas and Table 8 for the areas and profiles of task C with the two types of reference data.

Participant	S/G					P				
Test Area	AI	AII	AIII	AIV	A	AI	AII	AIII	AIV	A
<b>n</b>	841	112	107	729	1789	726	121	135	747	1729
<b>RMSE [m]</b>	1.2	0.9	1.1	2.0	1.6	0.5	0.4	0.6	0.4	0.5
<b><math> \Delta h_{\max} </math> [m]</b>	5.4	2.4	3.2	9.7	9.7	2.6	1.4	1.8	4.6	4.6
<b>N(&gt;1.7m)</b>	97	7	15	244	363	5	0	1	2	8
<b><math>\mu^*</math> [m]</b>	0.2	0.0	0.0	0.1	0.1	-0.1	-0.1	0.3	0.2	0.1
<b><math>\sigma^*</math> [m]</b>	0.8	0.8	0.8	0.9	0.8	0.5	0.4	0.5	0.4	0.4

Table 5: Results of the participants regarding the absolute vertical error in the test areas of task A.

N ...number of blunders

$\sigma^*$ ...standard deviation, derived after excluding blunders and systematic shift ( $\mu^*$ )

Participant	J/Z*	J/Z**
Test Area	A1	A1
n	414	383
RMSE [m]	0.7	1.3
$ \Delta h_{\max} $ [m]	1.9	4.2
N(>1.7m)	4	60
$\mu^*$ [m]	-0.2	0.3
$\sigma^*$ [m]	0.6	0.9

Table 6: Results of the participant 'J/Z' regarding the absolute vertical error at area A.  
 $\sigma^*$ ...standard deviation, derived after excluding blunders and systematic shift ( $\mu^*$ )  
J/Z\*...M6 (RGB-H,V), dynamic CM  
J/Z\*\*...M7 (RGB-H,V), CM=15 pel

Participant	P
Test Area	B
n	8973
RMSE [m]	0.4
$ \Delta h_{\max} $ [m]	6.0
N(>1.7m)	27
$\mu^*$ [m]	0.1
$\sigma^*$ [m]	0.4

Table 7: Results of method 'P' regarding the absolute vertical error at area B.  
 $\sigma^*$ ...standard deviation, derived after excluding blunders and systematic shift ( $\mu^*$ )

Figure 7 shows the position of blunders ( $\Delta h > 1.7$  m) for area B graphically.

Participant	S/G	P	S/G	P	P	S/G
Test Area	$C_{LR}$	$C_{LR}$	$C_{LR}$	$C_{LR}$	$C_M$	$C_M$
Reference	PHM	PHM	GPS	GPS	GPS	GPS
n	1398	1099	120	94	50	50
RMSE [m]	0.72	0.26	0.44	0.19	0.18	0.46
$ \Delta h_{\max} $ [m]	2.54	2.69	1.27	0.97	0.28	1.39
N(>0.34 m)	840	57	53	2	0	14
$\mu^*$ [m]	0.00	0.15	0.02	0.15	0.17	-0.05
$\sigma^*$ [m]	0.20	0.08	0.19	0.05	0.07	0.19

Table 8: Results of the participants regarding the absolute vertical error at area C.  
 $\sigma^*$ ...standard deviation, derived after excluding blunders and systematic shift ( $\mu^*$ )  
PHM...reference data derived by images 1:3000  
GPS... reference data derived by GPS

The reference data for area 'M' could not be measured by photogrammetry due to lack of coverage with images 1:3000.

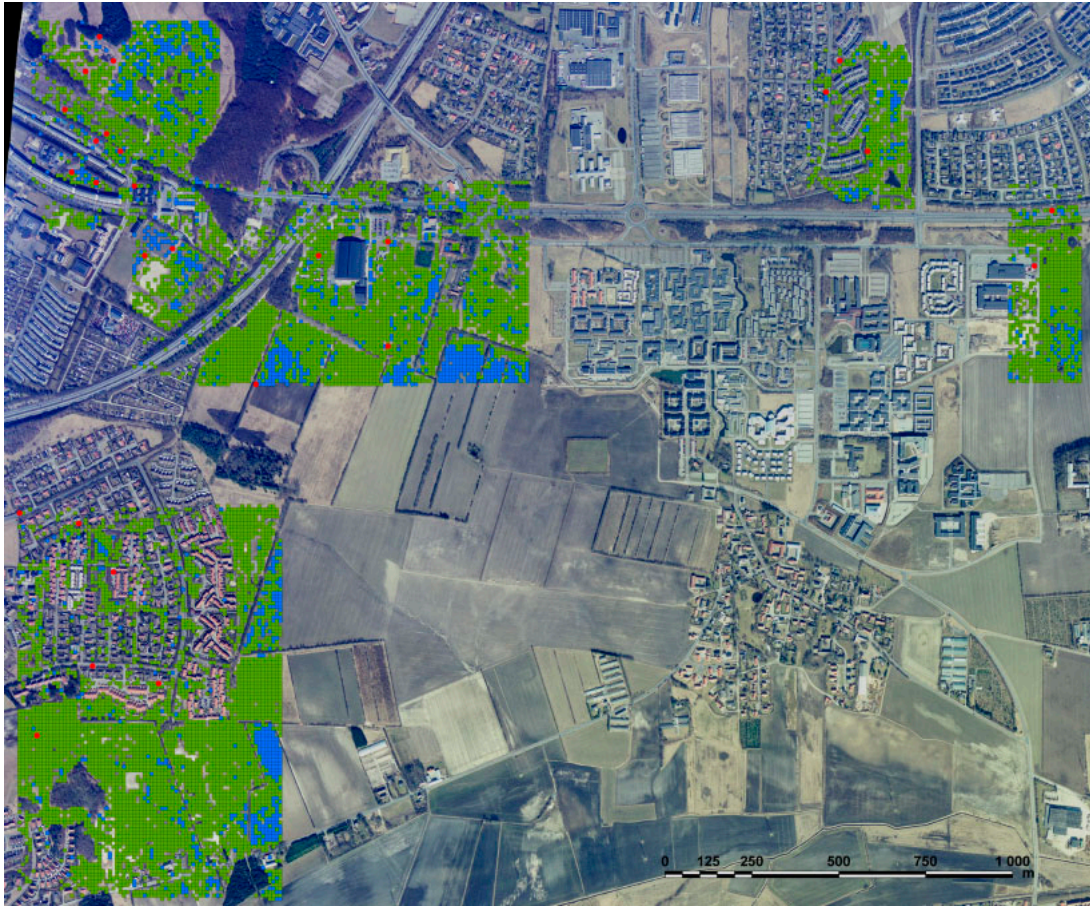


Figure 7: Results of the checking of the improved DTM derived by method P. The colors mean: Green...corrected DTM points fulfilling the specification ( $\Delta h < 1.7$  m), red ... blunders ( $\Delta h > 1.7$  m), blue ... rejected points by the method 'P'.

#### 14.2 Relative vertical accuracy

Some of the participants used reference data, which they derived from the delivered images. The calculated accuracy (RMSE and standard deviation) is less accurate due to the small scale of the delivered images. Therefore, the results are here named “relative accuracy”. Furthermore, some of the participants used different accuracy measures than those of Table 1. The results of the different participants will therefore be presented individually. Results with the same accuracy measure will be compared to each other at the end of this chapter. The results of the different authors/methods are presented in Tables 9 - 13.

S/G

Participant	S/G			
area	AI	AII	AIII	AIV
<b>n</b> 50%	17291	3372	875	11823
$\mu \Delta h$ [m]	0.14	0.57	-1.55	0.07
$\sigma \Delta h$ [m]	4.96	4.86	7.46	4.60

Table 9: Relative accuracy presented by S/G for the four sub-areas of task A.

The presented standard deviations for the differences in height ( $\Delta h$ ) by S/G for the sub-areas are very large and do not agree with the data derived by the pilot centre (see Table 9). The values are based on points whose height differences passed the 50% level of confidence test. The remaining number of checked heights is relatively high.

P

The method of 'P' derives the errors of the delivered DTM and uses them (with a different sign) as corrections to this DTM. The derived corrections/errors are considered as relative accuracy as well.

Participant	P		
area	A	B	C <sub>LR</sub>
<b>n</b>	1729	8973	1021
<b>RMSE</b> $\Delta h$ [m]	0.7	1.5	0.19
$\mu \Delta h$ [m]	-0.1	-0.2	0.18
$\sigma \Delta h$ [m]	0.7	1.4	0.06

Table 10: Relative accuracy achieved with method 'P'.

Method 'P' was applied for all three test areas. Blunders were not removed.

P/S

The authors of this method derived a DTM for the whole model by digital photogrammetry and used it as reference data. In comparison with the delivered DTM the accuracy measures 'systematic shift' ( $\mu$ ) and standard deviation ( $\sigma$ ) were derived. The method P/S is therefore a typical checking method. Heights of an improved DTM were not delivered. Only areas of task A have been tested.

Participant	P/S
<b>area</b>	A
<b>RMSE*</b> [m]	1.5
$\mu$ [m]	0.3
$\sigma$ [m]	1.5

Table 11: Results of method 'P/S' for test area A.  
The value for RMSE\* is calculated from the delivered values ( $\mu$ ,  $\sigma$ ).

F/S

For the delivered DTMs the authors derived an average error ( $az$ ), which then was converted to a root mean square error by the formula:  $RMSE = 1.25 * az$ . Furthermore, a systematic error is given for the investigated DTMs. A standard deviation ( $\sigma^{**}$ ) could be calculated from these two values.



Participant	F/S			
area	AII	AIV	BII	BIV
n	4016	17953	9392	43952
RMSE[m]	1.3	1.2	1.1	1.3
$\mu$ [m]	1.0	0.8	0.7	0.7
$\sigma^{**}$ [m]	0.8	0.9	0.8	1.1

Table 12: Results of method ‘F/S’.  
 $\sigma^{**}$ ...standard deviation (calculated from given RMSE and  $\mu$ )

#### J/Z

Several methods of Jancso and Zavoti have been applied to the sub-area I of task A. Table 13 the results are presented for one method of (J/Z) only. It is assumed that the standard error of J/Z corresponds to the standard deviation ( $\sigma$ ).

Participant	J/Z
area	AI
n	780
$\sigma$ [m]	0.8

Table 13: Results of method ‘J/Z’ with accepted points.  
Details about this method (M6, (RGB-H,V), dynamic window size (CM)) can be found in Appendix I.

#### K/S

This method does not compute a relative accuracy for the delivered DTMs.

A comparison of the relative accuracy achieved by different participants is given in table 14. The values for methods ‘S/G’ and ‘J/Z’ are computed by the pilot centre from the delivered data at DTM posts only. Three methods (P, S/G, and J/Z) are nearly the same for the RMSE value at test area AI.

When comparing all the values, it is obvious that the results for area A differ between 0.7 m and 1.5 m in the RMSE- and  $\sigma$ -values. This is a considerable difference. For the sub area AI the results of three participants (J/Z, S/G, and P) are nearly equal regarding the RMSE value and the standard deviation (0.6 m – 0.8 m). There is a good agreement between the results of P and F/S. A large difference of 0.5 m in the RMSE-value and of 0.6 m in the  $\sigma$ -value exists between the results of S/G and P at the area  $C_{LR}$ .

Participant	area	RMSE [m]	$\sigma$ [m]
S/G	A	1.2	1.2
P	A	0.7	0.7
P/S	A	1.5	1.5
S/G	AI	0.7	0.7
P	AI	0.8	0.8
J/Z	AI	0.6	0.6
P	B	1.5	1.4
P	BII	0.9	0.9
F/S	BII	1.1	0.8
P	BIV	1.1	1.1
F/S	BIV	1.3	1.1
S/G	$C_{LR}$	0.7	0.7
P	$C_{LR}$	0.2	0.1

Table 14: Comparison of the results of participants regarding the relative accuracy.

The relative accuracy has been determined differently by the participants and the results differ therefore quite a lot in the three test areas. Figure 8 illustrates this. But more important is an investigation whether the relative accuracy has a certain ratio with the absolute accuracy and whether the accuracy of the delivered DTM could be improved by the applied methods. These investigations are carried out in the next two chapters.

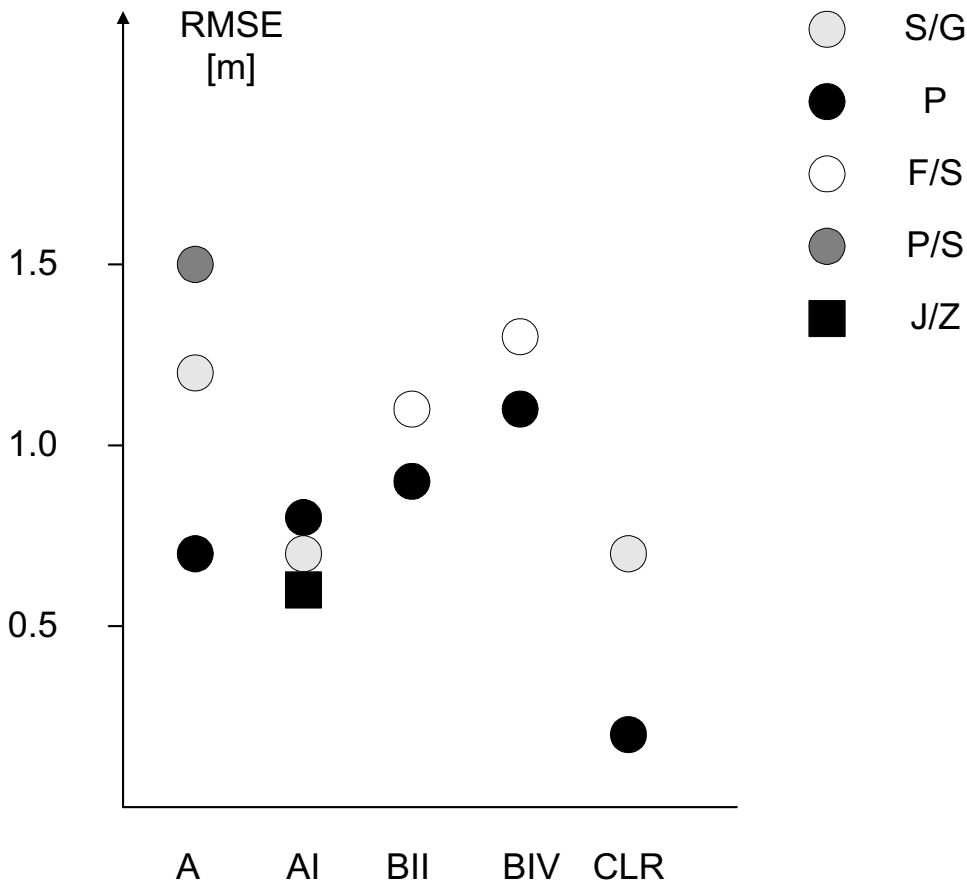


Figure 8: Relative accuracy as determined by the different methods.

#### 14.3 Ratio between the relative and the absolute accuracy of the tested DTMs

The investigation about the relation between relative and absolute accuracy of the tested DTMs requires the absolute accuracy of the delivered DTMs. It is determined by comparison with the accurate reference data of the pilot centre (DTM\_ref and profiles\_ref). Table 15 displays the absolute accuracy of the delivered DTMs.

area	n	RMSE [m]	$\mu$ [m]	$\sigma$ [m]	N	$ \Delta h_{\max} $ [m]
AI	907	0.7	0.2	0.7	30	3.9
AII	139	0.4	-0.1	0.4	1	1.8
AIII	152	0.4	-0.2	0.4	1	2.1
AIV	835	0.7	0.2	0.7	27	4.9
A	2033	0.7	0.2	0.7	59	4.9
B	10390	1.4	0.3	1.4	1636	10.9
C <sub>PHM</sub>	1412	0.13	-0.07	0.10	10	1.18
C <sub>GPS</sub>	170	0.08	-0.08	0.02	0	0.15

Table 15: Absolute accuracy of the delivered DTM (DTM\_orig) derived by comparison with the accurate reference DTM (DTM\_ref and profiles\_ref). The area C<sub>GPS</sub> includes four profiles (2, 3, 5, 8) of the three sub-areas L, M and R. The threshold for blunders has been set to S = 1.7 m (area A and B) or S = 0.34 m (area C). (The results for area C are given in cm due to a higher accuracy).

The results of Table 15 confirm the fact that the DTM derived from laser scanning is the most accurate one (RMSE<sub>PHM</sub>=0.13 m). The checking with reference data from photogrammetry gives nearly the same RMSE value as with GPS data as reference data (RMSE<sub>GPS</sub>=0.08 m). Automated photogrammetry with images 1:25 000 produced an accuracy of RMSE = 0.7 m or 0.018% of the flying height. The DTM derived from 5 m contours has only a modest accuracy in this test area (RMSE=1.4 m).

In order to find out if there is a relation between the relative and the absolute accuracy, Table 16 is compiled. The values for the absolute accuracy will differ somewhat for each participant because they are here derived at the locations where the participants delivered height values. The number of points differs then for each participant and therefore also the values for RMSE and for  $\sigma$ .

It can be seen from Table 16 that the relative accuracy and the absolute accuracy in the DTMs of task A and B are approximately the same. In area C, however, the two values are very different and the ratio is much higher than 1.0. This confirms the fact that the laser scanning data in this test cannot be improved reliably by means of images at 1:5000. On the other hand, the DTMs of task A and B can be checked and improved by imagery at 1:25 000.

		Relative accuracy		Absolute accuracy		Ratio	
		cor		DTM_orig		cor/DTM_orig	
method	area	RMSE [m]	$\sigma$ [m]	RMSE [m]	$\sigma$ [m]	RMSE	$\sigma$
S/G	AI	0.7	0.7	0.7	0.7	1.0	1.0
P	AI	0.8	0.8	0.7	0.7	1.1	1.1
J/Z*	AI	0.6	0.6	0.5	0.5	1.2	1.2
J/Z**	AI	1.0	0.9	0.8	0.8	1.3	1.1
S/G	A	1.2	1.2	0.7	0.7	1.7	1.7
P	A	0.7	0.7	0.7	0.7	1.0	1.0
P	B	1.5	1.4	1.4	1.4	1.1	1.0
S/G	C	0.73	0.68	0.13	0.10	5.6	6.8
P	C	0.30	0.16	0.13	0.10	2.3	1.6
S/G	C_GPS	0.44	0.44	0.08	0.02	5.5	22.0
P	C_GPS	0.26	0.13	0.09	0.02	2.9	6.5

Table 16: Ratio between the relative and the absolute accuracy of the tested DTM by different methods. It means:

cor/DTM\_orig...ratio corrections/original DTM

J/Z\*...M6 (RGB-H,V), dynamic CM

J/Z\*\*...M7 (RGB-H,V), CM=15 pel

C\_GPS...reference data are profiles measured by GPS

(The results for area C are given in cm due to a higher accuracy).

#### 14.4 Ratio between the delivered DTMs and the improved DTMs

In order to find out the relation between the delivered DTM and the improved DTM, Table 17 is compiled. It shows the results for the participants who delivered a corrected DTM. If the ratio is above 1.0, then the DTM has been improved.

In the following the results of the different participants regarding the ratios are discussed individually.

S/G

This method could not improve the RMSE or the standard deviation of the delivered DTMs at the areas AI, A and C.

P

In test area A the method 'P' could improve the DTM by a factor of 1.4 or 40%. At the test area B a factor of improvement was even higher (3.5). In test area C the DTM could not be improved by the images 1:5000. The delivered DTM had already a very high accuracy ( $\sigma=0.02$  m).

J/Z\*/J/Z\*\*

Both methods of J/Z could not improve the accuracy of the delivered DTM at area AI.

method	area	Absolute accuracy		Absolute accuracy		Ratio	
		DTM orig		DTM cor		DTM_orig/DTM_cor	
		RMSE [m]	$\sigma$ [m]	RMSE [m]	$\sigma$ [m]	RMSE	$\sigma$
S/G	AI	0.7	0.7	1.2	1.2	0.6	0.6
P	AI	0.7	0.7	0.5	0.5	1.4	1.4
J/Z*	AI	0.5	0.5	0.7	0.6	0.7	0.8
J/Z**	AI	0.8	0.8	1.3	1.3	0.6	0.6
S/G	A	0.7	0.7	1.6	1.6	0.4	0.4
P	A	0.7	0.7	0.5	0.5	1.4	1.4
P	B	1.4	1.4	0.4	0.4	3.5	3.5
S/G	C	0.13	0.10	0.72	0.70	0.2	0.1
P	C	0.12	0.09	0.26	0.19	0.5	0.5
S/G	C_GPS	0.09	0.02	0.44	0.44	0.2	0.1
P	C_GPS	0.09	0.02	0.19	0.13	0.5	0.2

Table 17: Ratio between delivered DTM (DTM\_orig) and corrected DTM (DTM\_cor).

J/Z\*...M6 (RGB-H,V), dynamic CM

J/Z\*\*...M7 (RGB-H,V), CM=15 pel

C\_GPS...reference data are profiles measured by GPS

(The results for area C are given in cm due to a higher accuracy).

Altogether the proposed methods are sensitive to errors in the absolute orientation of the images and require good conditions for correlation. This cannot be achieved at all positions of the DTM, but for checking of DTMs such areas with good conditions for automated measurements can be found. The sample size will still be large enough. It is also obvious that the accuracy in a DTM is hard to characterize by a single number for RMSE,  $\mu$  and  $\sigma$ . These values vary within the DTM and a graphic display of the quality of the DTM should be added.

The task remains whether the methods can find and remove blunders in the DTMs (compare next chapter).

#### 14.5 Number of blunders

The checking method should be able to detect blunders in the DTM. In order to compare the results of the participants the same threshold should be applied. Furthermore, the number of blunders detected and corrected by the method is of interest. Then a blunder detection ratio and a blunder ratio can be derived which will characterize the methods. The size of the RMSE for the detected blunders may help to interpret the results. Table 18 shows results with areas AI, A and B (threshold  $S=1.7$  m) and the results for area C (threshold  $S=0.34$  m).

With the selected threshold (1.7 m) up to 6% of blunders were present in the DTM derived by digital photogrammetry and up to 16% in the DTM derived from contours of a topographic map.

In the DTM derived from laser scanning data less than 1% of the heights were over the selected threshold (0.34 m). For testing the DTMs the chosen thresholds correspond to  $3 \cdot 0.015$  % of the flying height from which images are taken. The thresholds are then equal for A and B, but different for C. If another threshold was selected, the number of blunders would change. A threshold could also be defined as  $S = 3 \cdot \text{RMSE}$ , which means  $S=2.1$  m for A,  $S=4.2$  m for B and  $S=0.34$  m for C. The values

for RMSE were not known from the beginning; therefore the other definition ( $3 \cdot 0.015\%$  h) has been used.

method	area	N	N [%]	N*	N'	N'/N	N*/N	RMSE* [m]
J/Z*	AI	1	0.2	4	1	1.0	4.0	1.9
J/Z**	AI	23	6.0	60	6	0.3	2.6	2.0
P	AI	27	3.7	5	25	0.9	0.2	2.7
S/G	A	50	2.9	8	47	0.9	0.2	2.6
P	A	50	2.9	8	47	0.9	0.2	2.6
P	B	1389	15.5	27	1385	1.0	0.0	3.0
S/G	C	10	0.7	840	1	0.1	84.0	0.49
P	C	6	0.5	57	2	0.3	9.5	0.45

Table 18: Number of blunders for test areas in task A, B and C.

It means:

J/Z\*...M6 (RGB-H,V), dynamic size of the correlation matrix (CM)

J/Z\*\*...M7 (RGB-H,V), CM=15 pel

N...number of blunders after checking the original DTM with reference values

applying a threshold  $S = 1.7$  m for areas of task A and B. The threshold  $S=0.34$  m has been used for the areas of task C.

N [%]...number of blunders in % of the total number of points in the original DTM

N\*...number of blunders in the corrected DTM

N'...number of blunders detected and corrected by the method

N'/N ... blunder-detection-ratio (where  $1.0 = 100\%$  detection rate)

N\*/N ...blunder-ratio

RMSE\*...root mean square errors for blunders detected and corrected by the method

(The RMSE\* for area C are given in cm due to a higher accuracy).

The methods for checking and improving of DTMs were different with respect to finding blunders. Method 'P' could detect and correct 93% of the blunders in DTMs of task A, 100% in the areas of task B, but only 30% in the areas of task C. In this respect the other methods (S/G, J/Z\*) were also successful in the areas of task A. As it can be seen from the RMSE\* values of the detected and corrected blunders, the values are different in the three tasks (2.6 m in A, 3.0 m in B and 0.47 in C). They are larger than the threshold by the factor 1.5, 1.8 and 1.4. It may be remembered that the RMSE values of the three DTMs were derived with 0.7 m (areas in task A), 1.4 m (areas in task B), and 0.13 m (areas in task C).

The evaluation for blunders derived by the **method 'K/S'** has to be dealt with separately. No reference values were derived from the available imagery, but the heights of the surroundings were used for the detection of blunders. The positions (co-ordinates) of detected blunders were delivered to the pilot centre. True reference values in the same position were derived for the evaluation. The results are presented in Table 19. The sub-areas of task 'A' are presented separately.

There is not much difference in the results between the areas AI-AIV. The areas of task 'B' and 'C' are presented as mean of all subareas. The second last column shows the success rate in %. It is nearly 0%. The detected blunders in method 'K/S' are therefore no blunders which the RMSE\* value confirms.

Area	N	N[%]	N*	N'	success rate [%]	RMSE* [m]
AI	30	3	7	0	0	0.2
AII	1	1	3	0	0	0.2
AIII	1	1	3	0	0	0.5
AIV	27	3	3	0	0	0.2
B	1636	16	5	2	0.1	1.7
C	12	1	99	1	8.0	0.1

Table 19: Number of blunders, success rate for method K/S and RMSE\* of the blunders found by method K/S at the areas AI-AIV, B and C.

N...number of (real) blunders after checking with accurate reference values

(threshold for areas A/B:  $S = 1.7 \text{ m} = 0.015\% \text{ h}$ ; for areas C:  $= 0.34 \text{ m} = 0.015\% \text{ h}$ )

N[%] ... number of blunders in %

N\*...number of blunders derived by method 'K/S'

N'...number of blunders at the positions which were marked in K/S as blunders

success rate [%]... $N' \cdot 100/N$

RMSE\*...root means square errors for N' blunders.

#### 14.6 Positional accuracy

Vertical errors can also be caused by positional errors. Especially in mountainous and hilly areas an error in position has influence on the height. The height errors depend on the slope and on the occurrence of breaks and extreme points in the terrain (top of the hill or bottom of the valley). Digital photogrammetry and laser scanning determine a surface model. The correction to the terrain by filtering may also create height errors. If points on top of houses and trees remain in the data set, the calculated DTM will have considerable height errors. Heights of objects on the ground (persons, cars) and the air (birds) have also to be removed from the laser scanning data. The laser beam can be reflected from the ground **and** from buildings (so-called multi-path effect) which leads to positional and height errors. Furthermore, the checking of DTMs by means of photogrammetry or GPS requires the same reference system and datum for the reference data. Erroneous control points may lead to wrong orientation data and thereby to positional errors.

This project did not include the investigation of the positional errors by the participants. The pilot centre had to make sure that systematic errors of the position do not exist or can be neglected. The following precautions have been made.

The ground control points for task A, B and C were delivered to the participants in the same reference system as the DTMs. The residuals after orientation of the models revealed a sufficient accuracy in planimetry and in the height (compare Table 20).

task	image scale	number of control points	$\sigma_P$ [m]	$\sigma_Z$ [m]
A/B	1:25 000	17	0.14	0.20
C	1: 5 000	12	0.06	0.07

Table 20: Standard deviation of the residuals after absolute orientation of the stereo-models.

It is assumed that the participants oriented the stereo-models with a similar accuracy. Some participants reported about their calculated residuals at the control points (J/Z, F/S). A special test for the detection of blunder is suggested in (Jancso 2005).

The reference data of the pilot centre are based on GPS measurements in the field. The planimetric accuracy of the control points and of the points in the profiles is  $\sigma_P = 0.015 \text{ m}$ . The standard deviation

of the residuals after absolute orientation of the stereo-models is  $\sigma_p = 0.04$  m and the grid posts will have the same positional accuracy.

The co-ordinates of the reference-DTM posts did not coincide precisely with the co-ordinates of the (improved) DTMs of the three participants. A deviation of 2.0 m (at task A and B) and of 0.5 m (at task C) has been accepted in the search routines for finding corresponding grid posts. The data of S/G needed an interpolation.

Special emphasis has been given to the positional errors in laser scanning (task C). The planimetric accuracy of the laser scanning data can be derived by comparing points and lines of hip roofs which are determined by intersection of planes and by manual photogrammetric measurements (compare Figure 9).

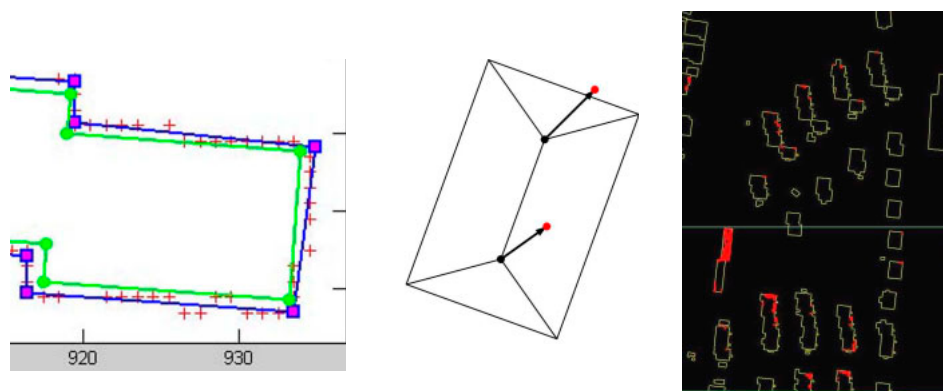


Figure 9: Planimetric errors of laser scanning data when comparing with a vector map. Errors of roof corners (left image), errors of roof points at hip houses (middle image), and blunders within houses (right image).

When checking roof corners, the positional error at a single house amounted to  $\sigma_p = 1.0$  m. The checking of 31 roof points of hip houses revealed a positional error of  $\sigma_p = 0.65$  m.

The superimposition of vector maps and laser scanning data shows laser points within the building areas and having the heights of the roof (compare right image of Figure 9). The filtering should have removed such points. A graphical display in planimetry together with a height profile discovers such blunders.

## 14.7 Completeness of the checking

### 14.7.1 General remarks

The amount of elevations which is tested in comparison with the total number of available reference points is a measure for the completeness of checking. In this investigation the delivered DTMs consisted of all grid posts in the area, but the reference values were not available for all of the grid posts. The pilot centre measured only at such grid posts where the bare ground could be measured and where good conditions for correlation existed. The measure for completeness is therefore a relative number. In this case it will be calculated as a percent value which is related to the amount of available reference points. The automated procedures for checking will lead to a large number of test points. The sample size will be large and the statistical values (RMSE,  $\mu$ ,  $\sigma$ ) will be reliable.



If the DTM should also be improved then it will be important to produce an overview about how many points are accepted (regarding a DTM specification) and how many are not tested and improved. Such a graphical display will help in the decision making.

The density of the data is another item for the completeness of the checking. The delivered DTM is given with a fixed spacing between the grid posts. It varies between 25 m (task A), 10 m (task B) and 1 m (task C). Automated methods can achieve a high density in the checking. If the checking is carried out manually, only a few points of the DTM can be checked. Another approach could be to test the DTM at critical positions, for example along break lines or in the neighbourhood of buildings.

#### 14.7.2 Results of the participants

The checking of completeness has been handled differently by the participating research groups. Their procedures and results will be dealt with separately in the following.

S/G

The method of S/G tested the four sub-areas of task A and characterized them according to the number of points which qualified as test points. This coverage with test points was divided into four classes: excellent, very good, medium, and poor (compare Table 21). According to S/G the class ‘poor’ should be excluded from checking due to an insufficient number of test points.

test area	AI	AII	AIII	AIV
coverage	very good	excellent	poor	medium

Table 21: Evaluation of completeness of the checking at method S/G.

The tested points were displayed on top of an orthophoto so that the coverage was displayed visually.

P

All test areas (A, B and C) have been checked and values for the (relative) completeness are given in Table 22. In addition, graphs are given about how many points of the DTM are accepted (regarding the DTM specification) and how many are not tested and improved compare Figure 3 in (Potuckova, Appendix I).

area	total number of reference points	accepted points	completeness [%]
A	2033	1729	85
B	10390	8973	86
C	1412	1099	78

Table 22: Evaluation of the (relative) completeness of the checking by method ‘P’.

P/S

The method ‘P/S’ derived a new DTM by digital photogrammetry and compared it at all grid posts. The completeness of the checking is thereby 100%. The differences between the two DTMs and their distribution are displayed in a graph.

F/S

The method used manual measurements for deriving a DTM. These measurements were carried out at points and lines which characterize the terrain. The density of the measured points is not as high as in the automated methods. The derived differences in height are displayed as contour lines, which gives a good insight where problem areas are.

J/Z

A value for the absolute completeness of checking in this method is derived for a small area (AI). The results are displayed in Table 23. This area comprised 1569 grid posts. Only 42% points of the points were accepted. Points were rejected and skipped due to a low correlation coefficient and some other criteria.

area	total number of grid posts	accepted points	completeness [%]
AI	1569	658	42

Table 23: (Absolute) completeness of the checking in method J/Z\* in the area AI. J/Z\*...M6 (RGB-H,V), dynamic CM.

K/S

This statistical method checks all the grid posts. The (absolute) completeness is therefore 100%.

In order to give a summarized evaluation of the completeness of the checking a table with three categories (good, medium, poor) is compiled (see Table 24).

method	degree of completeness		
	good	medium	poor
S/G		x	
P		x	
P/S	x		
F/S			x
J/Z		x	
K/S	x		

Table 24: Comparison of the methods with respect to completeness of the checking.

A good degree of completeness is possible in the methods 'P/S' and 'K/S'. The manual measurement has a poor degree of completeness. The other methods (S/G, P, J/Z) are characterized as 'medium'. They test only in positions where good conditions for correlation exist.

#### 14.8 Economy of the checking methods

The economy of the checking method can be evaluated when the amount of time necessary for the checking (and improving) of the DTM is known. It is influenced by the computer, the programming, the size of the DTM, the preparation work, and the checking method itself. None of the participants reported how much time they needed for the checking of the DTMs. The pilot centre only estimates the degree of automation. Two categories (high and low) are used (compare Table 25). This rough estimation is based on the amount of manual work which is necessary.

The estimation has to be related to the quality of the results. The method 'K/S' can be applied to all types of DTM data and it is therefore a universal method. If stereo-photogrammetry is used as a checking method, the image scale has to be of such a magnitude that the required accuracy can be reached.

method	degree of automation	
	high	low
S/G	x	
P	x	
P/S	x	
F/S		x
J/Z	x	
K/S	x	

Table 25: Degree of automation at the applied methods for checking of DTMs.

high...potential for full automation  
low...manually measured

## 15 DISCUSSIONS

The objectives in this project were to obtain experience with different methods of checking and improving of DTMs. Test material consisting of three DTMs and auxiliary material (overlapping images and control points) has been made available to interested research groups. Six groups have sent results to the pilot centre which evaluated the delivered results regarding accuracy, completeness and degree of automation. The provided imagery is in a scale which is adequate both for the production of orthoimages and for the checking and improving of DTMs. The three DTMs have had different acquisition methods, accuracy, and density. They were handled separately and the results will be discussed separately as well.

Besides automated photogrammetry, also manual photogrammetry and a statistical method without using reference values have been used by the participants. The participating research groups applied their methods to some of the delivered test areas. A comparison of the methods will be carried out with the selected test areas.

### 15.1 Results of task A

The DTM of task A has been produced by digital photogrammetry from imagery 1:25 000. The result has been a digital surface model. No correction to the bare earth has taken place. All the reference points, however, have been on the bare earth.

The results achieved by the participants with the provided test material have been named as 'relative accuracy'. It is of interest to know how these results compare with the absolute accuracy of the delivered DTMs, which was obtained by comparison with the accurate reference data of the pilot centre. In Figure 10 the result of the comparison is depicted. It can be seen that the standard deviation ( $\sigma$ ) for the sub-area AI is the same for the relative and the absolute accuracy, but for the whole area A (including AI) it is true only for the method 'P'. The two other methods (S/G and P/S) have a considerable difference between the relative and the absolute accuracy regarding the standard deviation. With method 'P' it was possible to check the DTM by means of the images 1: 25 000 accurately and reliably. The same results have been obtained for the standard deviation calculated from the differences to the accurate reference data. This agreement of the relative and absolute accuracy is the precondition that the DTM can also be improved by such a method.

The (absolute) accuracy of the DTM derived by digital photogrammetry is relatively high ( $\sigma=0.7$  m). It is of great interest whether the accuracy of the DTM can be improved and which of the methods can do this best. Figure 11 gives an answer to this question.

It is obvious from Figure 11 that only method 'P' can achieve an improvement of these DTMs. The accuracy of the photogrammetrically improved DTM is  $\sigma_h = 0.5\text{m}$  or 0.013 % of the altitude from

which the images were taken and then used for the corrections by means of the orthoimage method. Method J/Z\* is second best, but no improvement is achieved.

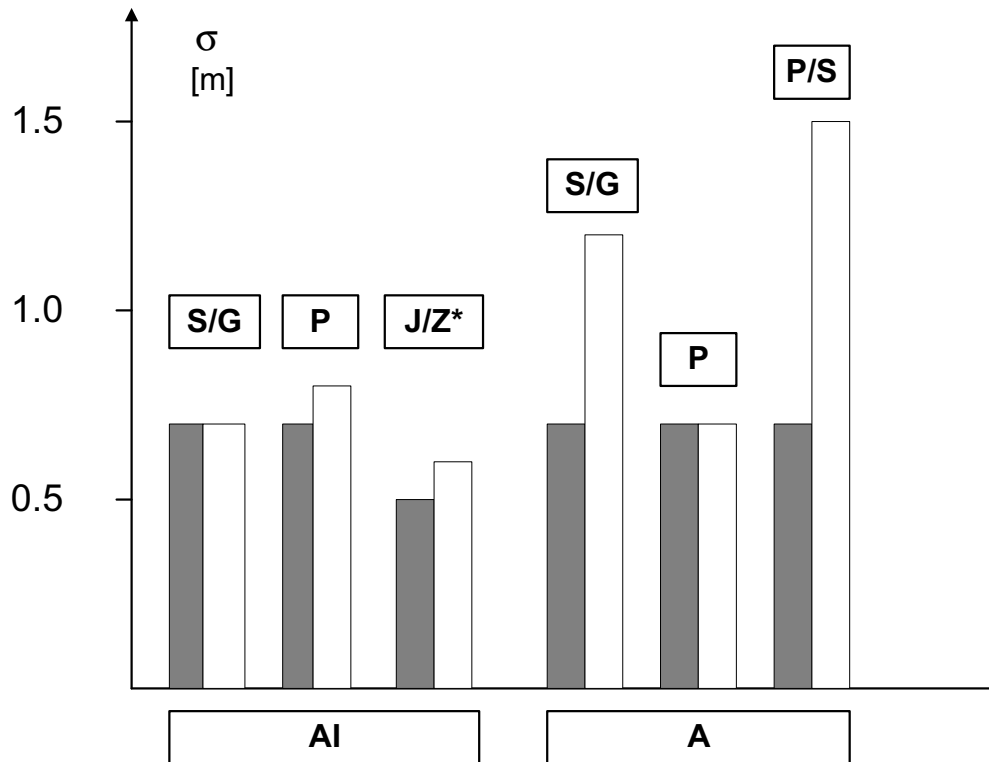


Figure 10: Absolute accuracy (grey columns) and relative accuracy (white columns) for areas of task 'A'.

Regarding the **number of blunders** which could be detected and corrected, the methods of S/G, P and J/Z\* are equal. At least 93% of the blunders could be detected and corrected (compare Table 18). The method of K/S provided a list of blunders. The evaluation with reference data revealed that the method 'K/S' is not able to find real blunders.

The (relative) **completeness** of the checking is with 85% sufficient at method 'P'. Method 'J/Z\*' checks only at 42% of the reference points. The method of S/G has characterized the completeness of checking by four classes. A comparison with the other methods is not possible. The methods (P/Z, F/S) have tested the DTM completely at all grid posts. A graphical display of the tested points, for example as in Figure 7, helps to obtain a quick overview.

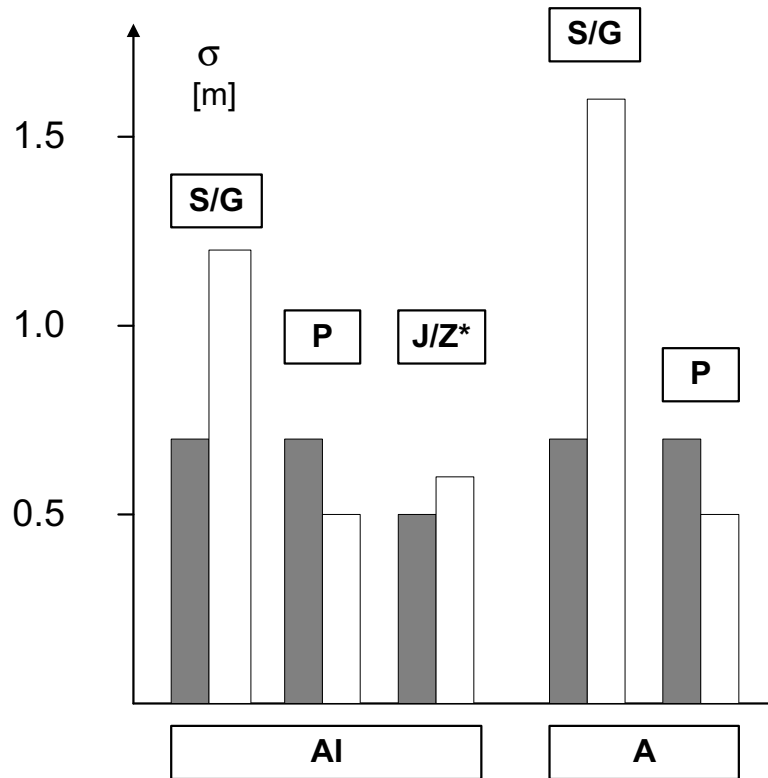


Figure 11: Comparison between the delivered DTM (DTM\_orig, grey columns) and the corrected DTM (DTM\_cor, white columns) for areas of task A.

### 15.2 Results of task B

The DTM of task B has been produced from scanning of 5m contours of a topographic map. The errors in this DTM are relatively large ( $\sigma = 1.4$  m) and there are quite a lot of blunders present ( $N=1389$  or 15.5%). Only three participants (P, F/S and K/S) checked this DTM. Method 'P' checked and also improved this DTM. The DTM could be improved considerably to  $\sigma=0.4$  m, that means by a factor of 3.5. Also the systematic errors of the original DTM could be reduced from  $\mu=0.3$  m to  $\mu=0.1$  m. The achieved improvements are visualized by Figure 12.

In addition, nearly all of the blunders were detected and corrected by this method. The achieved accuracy ( $\sigma=0.4$  m) is about the same accuracy which has been achieved for the DTM of task A ( $\sigma=0.5$  m), where the corrections are derived by means of the **same** images.

The results of method 'P' prove the fact that automated photogrammetry can check and improve different DTMs with respect to accuracy and the number of blunders and achieve the same results. Regarding the relative accuracy, a good agreement between the results of method 'P' and 'F/S' has to be mentioned. Method 'K/S' detected only 2 of the 1636 blunders which corresponds to 0.1%. The success rate of this method is therefore poor.

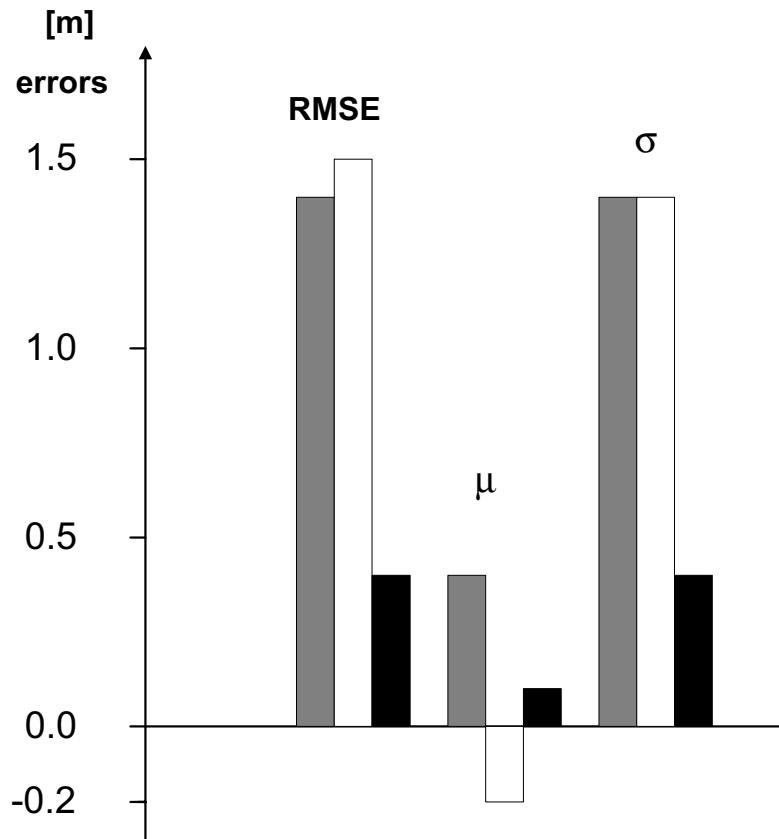


Figure 12: Result of method 'P' regarding the errors (RMSE, $\mu$ , $\sigma$ ) in the delivered DTM (grey columns), the found corrections (white columns), and the corrected DTM (black columns) for the test areas of task B.

### 15.3 Results of task C

The DTM of task C has been produced by laser scanning. Filtering took place in order to reduce the heights from the surface to bare earth. All the reference points have been on the bare earth. They were determined by semi-automated photogrammetry from images 1:3000 and by GPS measurements in the field. The corrections for the delivered DTM were derived by the participants from images of 1:5000. The result of method 'P' ( $\sigma_h = 0.19$  m) is a better result than that of S/G ( $\sigma_h = 0.70$  m). The diagram also shows the influence of the reference data. The reference data are more accurate when determined by means of GPS, but only a few points can then serve as reference points.

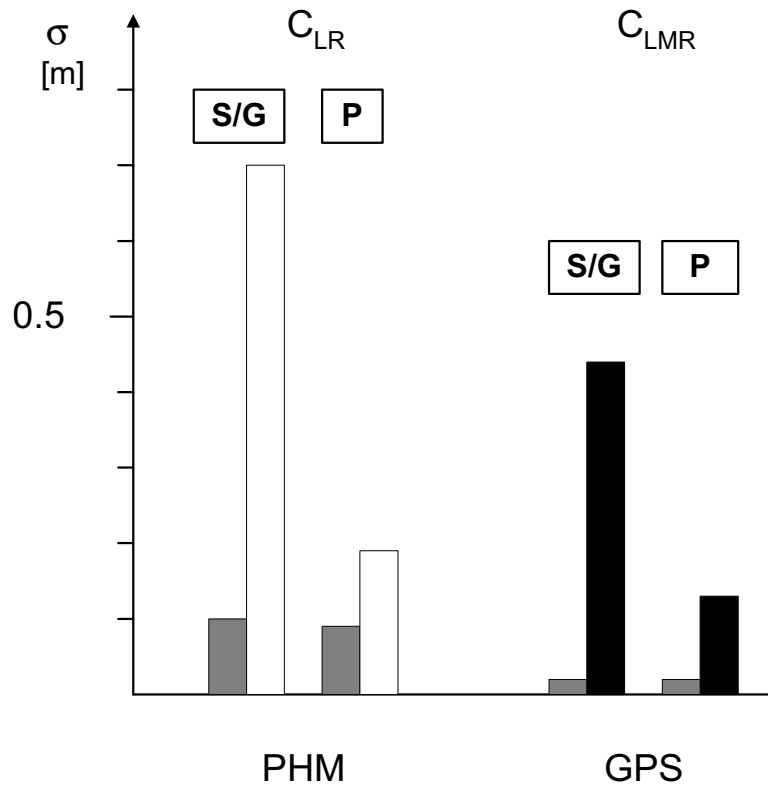


Figure 13: Comparison between the delivered DTMs (grey columns) and the corrected DTM (white and black columns) for areas of task C. The corrections for the DTM were derived from images 1:5000. The reference data for the evaluation of the results have been determined either by images 1:3000 (PHM) or by ground surveying of profiles (GPS).

**Additional investigations** by the pilot centre with imagery 1:3000 demonstrated that better results in the correction of a DTM can be achieved ( $n = 116$ ,  $RMSE = 0.06$  m,  $\mu = 0.04$  m,  $\sigma = 0.04$  m). Reference data were the heights of three profiles measured by GPS. The delivered DTM is already very accurate ( $RMSE = 0.08$  m,  $\mu = -0.08$  m,  $\sigma = 0.02$  m) so that improvements in the standard deviation ( $\sigma$ ) are difficult to achieve and very likely not required in most of the applications. The detection and the removal of the systematic error and of blunders are then the main objectives. The systematic error of the delivered DTM ( $\mu = -0.08$  m) is reduced at the 'DTM\_cor' ( $\mu = 0.04$  m); four new blunders ( $\Delta h > 0.34$  m) were, however, introduced. Other DTMs derived by laser scanning may have larger errors and larger numbers of blunders.

#### 15.4 Joint results

The use of photogrammetry for checking and improving of DTMs has been successful in tasks A and B. At task C where the DTMs derived by laser scanning had to be tested, the corrections can not be derived from the delivered images at 1:5000. The use of larger scale imagery (1:3000) reduced the systematic errors of the DTM. Accurate orientation data for the images are a precondition for applying

the photogrammetric method for checking and improving of DTMs. In the following the obtained results will be generalized.

The theoretical accuracy of the corrected height at the 'orthoimage method' can be derived by formula (1).

$$\sigma_{DTM\_cor} = (\sigma_{cor}^2 + \sigma_{h\_ori}^2)^{1/2} \quad (1)$$

It means:

$\sigma_{DTM\_cor}$  ...final accuracy of the corrected height

$\sigma_{cor}$  ...accuracy of the derived correction

$\sigma_{h\_ori}$  ...influence of the accuracy of the image orientation on the DTM

The accuracy of the derived correction depends on the accuracy of the matching and can be derived by formula (2).

$$\sigma_{cor} = \sigma_{LSM} \cdot h/b \quad (2)$$

It means:

$\sigma_{LSM}$  ...accuracy of least squares matching

$h$ ...flying height over terrain

$b$ ...distance between the two overlapping images (basis)

From the achieved results we may now estimate the accuracy of the matching and derive a formula which can also be used for other imagery than the used one. The base/height ratio ( $b/h$ ) is a constant and about  $1/1.67$  at 60% overlap and wide angle lenses ( $c=15$  cm).

$$\sigma_{LSM} = \sigma_{cor} / (1.67 \cdot m_b \cdot pel)$$

It means:

$\sigma_{LSM}$  ...accuracy of least squares matching

$\sigma_{cor}$  ...accuracy of the derived correction

$m_b$  ...image scale number

$pel$  ...pixel size in the image

The influences of the matching accuracy and of the orientation accuracy can be estimated. For example,  $\sigma_{h\_ori} = 0.01\% \cdot h$  and  $\sigma_{LSM} = 0.3$  pel can be assumed. But it is difficult to separate both influences on the result.

If we disregard orientation errors and use the achieved standard deviations for the improved DTMs (DTM<sub>cor</sub>) as an approximation for the accuracy of the correction,

$$\sigma_{cor} \approx \sigma_{DTM\_cor}$$

the accuracy for the matching accuracy can then be derived as



$$\sigma_{LSM} = \sigma_{DTM\_cor} / (1.67 \cdot m_b \cdot pel)$$

Table 26 shows the results for all tests of method ‘P’, which has been applied to all test areas.

test	$\sigma_{DTM\_cor}$ [μm]	$m_b$	pel [μm]	$\sigma_{LSM}$ [pel]	$\sigma_{LSM}$ [μm]
<b>A</b>	0.5	25 000	21	0.57	12
<b>B</b>	0.4	25 000	21	0.46	10
<b>C</b>	0.19	5 000	15	1.52	23
<b>C GPS</b>	0.13	5 000	15	1.04	16
<b>C GPS</b>	0.04	3000	21	0.38	8
<b>mean</b>				0.79	14

Table 26: Derivation of the matching accuracy from results of method ‘P’ at tasks A, B and C.

The derived standard deviations for this ‘matching accuracy’ differ from 0.38 pixel to 1.52 pixel and from 8 μm to 23 μm, respectively. The result with the accurate reference values (C\_GPS) and the largest image scale is the optimum result (8 μm or 0.38 pel). The mean values are 14 μm or 0.79 pel at the image.

If the orientation data and the reference data have a superior accuracy regarding the matching accuracy then the accuracy of the orthoimage method can check and improve the DTMs with an accuracy of

$$\sigma_{cor} = \sigma_{LSM\_mean} \cdot h / b = 14 \mu m \cdot m_b \cdot 1.67$$

$$\sigma_{cor} \approx 0.023 \text{ mm} \cdot m_b \quad (3)$$

The achievable DTM accuracies with the method of ‘P’ are then for example at images 1: 8 000  $\sigma_{cor} = \sigma_{DTM\_cor} = 0.18$  m or at images 1: 33 000  $\sigma_{cor} = \sigma_{DTM\_cor} = 0.76$  m. Orthoimages can be produced with such DTMs and images with a pixel size of 10 cm or 40 cm on the ground, respectively. Formula (3) can also be transferred into another form

$$\sigma_{cor} \approx 0.023 \text{ mm} \cdot h / c .$$

It means:

c...camera constant

with c = 15 cm

$$\sigma_{cor} \approx 0.015\% \cdot h \quad (4)$$

The checking cannot occur at all positions of the DTM. The (relative) completeness has been at least 78% at method ‘P’, but less at other methods. This is still sufficient for checking of DTMs, but for improving of DTMs a more complete coverage would be desirable. At least a graphical display of the areas with the need for further actions should be produced.

## 16 COMPARISON OF THE METHODS

A comparison of the methods can be done by means of table 27 containing the items of the investigation and the judgement of the performance after the experiences made in this project.

method	detection & correction of blunders	detection & correction of systematic errors	improvement of standard deviation	completeness of checking & improvement	potential for full automation
S/G	+	+	-	-	+
P	+	+	+	-	+
P/S	-	+	-	+	+
F/S	+	+	-	+	-
J/Z	+	+	-	-	+
K/S	-	-	-	+	+

Table 27: Advantages (+) and disadvantages (-) of the participating methods.

The method 'P' has a positive evaluation in most items of the investigation. It uses parallax measurements between two overlapping orthoimages. Original images are used by J/Z. It can be assumed that the original images give better results in the matching and thereby in the accuracy of the corrections, but this could not be confirmed by the results of this investigation. Nearly all methods have the potential for full automation. It needs more programming before the methods can be used in production. Only then a comparison regarding the time consumption can be carried out.

## 17 PROBLEMS IN THE INVESTIGATION

In order to check and improve DTMs by means of photogrammetry and ground surveying, the data acquisition and the checking should be carried out at the same point of time. But this is difficult to realize. Changes in the nature by human activity and by growing of vegetation may have caused some of the errors.

The ground control for area A and B has not been measured by the pilot centre. It was taken from the library of the Danish Mapping Agency (KMS). It turned out that some of the points are not optimal for this purpose. But there has been a large redundancy and the orientation data could be determined with suitable points and sufficient accuracy.

The reference points were measured semi-automatically in stereomodels 1:3000. Only points on the ground with good results in the correlation coefficient and in the accuracy of the matching have been accepted. Therefore, the reference data were not available for all grid posts. However, a huge number of reference points were available.

The participants in the test have been free to select the DTMs of their interest and time available. Some of the participants did not deliver a corrected DTM but only a statistical evaluation of the DTM(s). Thus, only a few results could be compared for the same test area.

The DTM of task C has been very accurate and with a few blunders only. Therefore, it was difficult to improve the DTM with the provided imagery (1:5000). It would have been a possibility to use images in a larger scale for the derivation of corrections and/or to introduce some blunders and systematic error in the DTM to be tested. But the provided material has been taken from practice.

## 18 COMPARISON WITH RESULTS OUTSIDE OF THIS INVESTIGATION

Several investigations dealing with automated checking and improving of DTMs have been published during the last decade. Some examples comparable with the results of this investigation follow here.

Norvelle describes the “Iterative Orthophoto Refinements” (IOR) method that is based on finding horizontal parallaxes, between two overlapping orthoimages derived from a stereopair of images and a DEM to be refined (Norvelle 1996). Using a simple formula represented by the multiplication of the height/base ratio and a discovered horizontal parallax, a height correction at a chosen point can be calculated. The proposed algorithm was tested on two data sets, 1:40 000 photographs scanned with 50  $\mu\text{m}$  pixel size and 1:20 000 photographs scanned with 25  $\mu\text{m}$  pixel size. The initial DEMs were derived automatically from the stereopairs. Only the second data set is to a certain extent comparable with the task A of the EuroSDR investigation. The terrain elevations varied about 110 m, and the terrain was mainly covered by grass and trees. The spacing of the initial DEM was 10 m and it was derived from images of reduced resolution (2 m ground-sample distance). The IOR was applied in several iteration steps. A refined DEM was used for deriving new orthoimages after each iteration step. The process stopped when the horizontal parallaxes did not exist or were neglectable. In order to minimize the influence of large x-parallaxes on trees and shadows, the method was first applied on orthoimages with a reduced resolution. No comparison with reference data is mentioned. It is only stated that the heights of trees in the refined DEM were not accurate ( $\pm 3\text{m}$ ) and that positional shifts between corresponding points can be found in areas of low texture at the final orthoimages.

The orthoimage method described above has been further developed (Skarlatos and Georgopoulos 2003, 2004). The approximate solution has been replaced by a rigorous mathematical model. Except of a height correction, a shift to a new position from the DTM post is calculated. Furthermore, a matching algorithm containing adaptive templates and elliptical areas was applied. The test material comprised a stereopair of coloured images at the scale of 1:17000 and the pixel size of 21  $\mu\text{m}$ . The method was tested on automatically derived DTMs with a spacing of 10 m. A comparison with manually measured reference data showed an improvement of a corrected DTM in the RMSE value from 0.9 m to 0.6 m which corresponds to an improvement from 0.035% to 0.022% of the flying height.

Potuckova (2004) also built up on finding parallaxes in two overlapping orthoimages. An investigation regarding different similarity measures and elimination of blunders in image matching was carried out. The suggested “histogram method” and “L/R method” (compare chapter 12.2) were applied on a DTM automatically derived from a stereopair of black and white aerial images at the scale 1:25 000 that was scanned with the geometric resolution of 30  $\mu\text{m}$ . The comparison of the corrected DTM with reference data measured manually in stereomodels at the scale of 1:5 000 revealed similar results as in task A of this project. Height corrections were only applied at the DTM posts with good conditions for correlation which corresponded to 80% of the tested area. The standard deviation of the corrected DTM was below 0.02% of the flying height and the number of blunders was not higher than 1%.

The back projection method was applied for an accuracy study of data acquired with the Airborne Topographic Mapper laser system (Schenk et al. 2001). Expected accuracy of these data was 8 cm. Stereopairs of aerial images at the scale of 1:2435, scanned with the pixel size of 28  $\mu\text{m}$ , were available. The laser points were projected to the images. The template size was chosen according to the gradients and entropy within the patch. Position of the best fit of the left patch in the right image was found by least squares matching. Only points with good conditions for correlation were taken into the calculation. This caused a considerable reduction of the tested points (from 860 to 106 points). The results showed a good correspondence with the accuracy values estimated a priori and a high accuracy of the laser scanning data. An investigation concerning the planimetric accuracy was also carried out. Linear features were extracted from laser points and from aerial images and then compared. Some of the results were satisfactory (accuracy about 20 cm) but some results showed larger discrepancies. They were mainly caused by modelling roof planes, which contained many chimneys.

All the mentioned examples allow for fully automated procedures for accuracy assessment of DTMs.

## 19 NEW DEVELOPMENTS

These investigations have been started in November 2004. In the meantime, new developments have taken place. One of the major innovations in the last years is the use of digital aerial cameras. These digital cameras have a small pixel size and a high radiometric resolution. The new Vexcel Ultra CAM-X camera, for example, has now a pixel size of 7.2  $\mu\text{m}$  and a radiometric resolution of more than 12 bit in each colour channel. The matching of corresponding image points can then be done with a higher accuracy.

On the evaluation side new software packages were introduced which enable the interactive editing of the terrain model. The DTM can be superimposed on the stereoscopic model, displayed in profiles or together with vector maps or orthoimages. Visual inspections are necessary when problems are discovered in the automated derivation of heights or corrections.

Airborne laser scanning is more and more applied in the production of surface and terrain models, especially for cities and forest areas. Filtering of the raw data, which reduces the heights from the surface to the bare earth, is then important and new programs have been created and are continuously improved.

Airborne Interferometric Synthetic Aperture Radar (InSAR) has been applied for DTM generation of medium accuracy ( $\sigma_h=1\text{-}2\text{ m}$ ) and for large areas.

The accuracy of the DTM is variable across the terrain. Graphical displays of the density of the original data set, or of the distances between points of the DTM grid and the next point of the original data set, the curvature of the terrain, etc. may supplement the quality measures as used in this investigation. The article of Kraus and Karel in Appendix I of this report gives some details regarding such supplements.

DTMs became an important subject and general literature about the theory and methodology of DTM modelling has been published, for example (ASPRS 2001) and (Li et al. 2005).

## 20 PRACTICAL CONCLUSIONS

At National Mapping Agencies and other mapping organizations the quality control of DTMs has become an important task today. One of the major applications is the production of orthoimages in short intervals of time. This investigation concentrated on the automatic and semi-automatic checking of the DTM grid posts and the derivation of adequate quality measures. Several new methods for checking and for improving of DTMs have been developed by six international research groups. The methods have been applied to three different DTMs, and the results of the participants were checked by means of accurate reference data produced by the pilot centre.

The emphasis in this investigation has been on the photogrammetric approach. The provided auxiliary material consisted of a stereomodel and control points from which quality measures should be derived and by which the delivered DTM could be improved. One group used only the delivered DTM and derived a list of blunders from the surrounding heights.

The result of the investigation proved that automatic checking **and** improving of DTMs is possible by aerial images which can also be used for the orthoimage production. For this purpose a dense DTM of sufficient accuracy and without blunders is required.

One method of checking has been applied to all test areas and from these results a relation for the achievable accuracy could be derived. The heights of an existing DTM can automatically be checked by means of wide-angle images with 60% overlap, and an average accuracy of  $\sigma_{\text{DTM}} = 0.023 \text{ mm} \cdot \text{image scale}$  can be obtained. The automatically corrected DTM will then have the same accuracy. 85% of the available reference points could be tested. The grid posts which could not be tested were visualized graphically in this method.

Other methods also checked the DTMs with good accuracy by means of photogrammetry. The back-projection-method works with the original images, but the results were not better than the methods using orthoimages for deriving the corrections. The image scale has to be large enough in order to obtain the required accuracy. The DTMs derived by laser scanning may also need ground measurements in order to detect small systematic errors.

## 21 PROPOSALS FOR FUTURE WORK

This project had its limitations, for example regarding the available resources. Promising results have been achieved. It is the wish of the authors that the results of the report should be used in practice, that new investigations and research about the topic should be started, and that the results of the report should be disseminated. Some proposals for future work will be made in the following.

### 21.1 *Practical work*

This project used DTMs of Danish landscapes, which are rather flat. Landscapes with larger height differences or other texture may produce different results. The successful methods should be applied to other test material in order to get more experience. A digital camera should take the images. The programs used in the methods should be adapted for production and then be implemented in the professional workstations. Map data in vector form should be used to exclude the areas with houses, forests and other vegetation. In the very end of supplementary work the national and international standards for checking and improving of DTMs should be formulated and put into practice.

### 21.2 *Scientific research and investigation*

This investigation revealed that the improving of the DTM by automated photogrammetry could not be carried out accurately at areas with low texture and contrast. The completeness in the checking and especially in the improving of DTMs suffered. The completeness should be improved by more advanced methods in matching, but it will never become 100%. The remaining gaps have to be filled by other methods, for example by manual photogrammetry. A proper interpolation from surrounding areas may be an approach, which should then be supplemented by graphical displays about distances between grid posts and data points.

The largest errors occur along break lines. These break lines can be derived from a dense net of data points and then be supplemented to the DTM as an additional information layer. Digital photogrammetry is able to produce such a dense net of DTM points. DTM points on top of elevated objects like houses or trees have to be reduced by filter programs. The same has to be done with unwanted objects like cars and persons on roads or footpaths. The other approach is to use information from vector maps and exclude such areas already in the data acquisition.

Airborne laser scanning depends very much on the direct georeferencing by means of GPS and IMU. Positional errors may occur and have to be detected and corrected. The accuracy demands are very

high when checking and improving such DTMs by photogrammetry. It can be achieved by large-scale images and accurate ground control.

The modelling of the landscape has to incorporate houses, bridges, and other objects above the ground. Such 3D models are necessary for the production of true orthoimages. The quality of such DTMs/3D models is another important task where new investigations are required.

The use of InSAR as a rather new method of data acquisition needs quality control as well. All these investigations should lead to national and international standards for quality control of DTMs.

### *21.3 Dissemination of the work*

The results of this project will be disseminated by this Official Publication of EuroSDR. Another form of dissemination of EuroSDR research projects is an educational seminar together with e-learning courses. They are organized by EuroSDR as 'EduServ modules'. A course on "Methods for Checking and Improving of DTMs" has been carried out by the two authors within the module 'EduServ4' which was started with a seminar at the ITC in the Netherlands, and it is planned to repeat the seminar in Praha, Czech Republic, in spring 2007 as part of the 'EduServ5' module.

## **ACKNOWLEDGEMENTS**

This investigation was financially supported by EuroSDR and Aalborg University. The Danish mapping agency (KMS), Aalborg municipality and the Danish company COWI A/S provided test material. Two students of Aalborg University, Peter Erbs and Arnt Elgaard Madsen, measured control points and reference data in the field. Nicole Bogadczyk, student at the University of Applied Sciences Stuttgart/Germany, acquired reference data by means of semi-automatic measurements and carried out other practical work. Birthe Nørskov improved the English language of this report. The project was also supported by a research grant of the Ministry of Education, Youth and Sports, of the Czech Republic, No. MSM 0021620831. Many thanks belong to the participating researchers who developed new methods and derived results with the delivered test material.

## **REFERENCES**

- ASPRS, 2001. Digital Elevation Model Technologies and Applications: The DEM Users Manual, 539 p., ISBN 1-57083-064-9, Bethesda, Md. 20814, USA.
- Geoforum, 2004. Vejledning om ortofotos (Guidance for orthoimage production), november 2004, [http://www.geoforum.dk/Files/Filer/Arbejdsgrupper/Ortofoto/Orto2004\\_version\\_8.pdf](http://www.geoforum.dk/Files/Filer/Arbejdsgrupper/Ortofoto/Orto2004_version_8.pdf) (in Danish).
- Georgopoulos, A., Skarlatos D., 2003. A Novel Method for Automating the Checking and Correction of Digital Elevation Models Using Orthophotographs, *Photogrammetric Record*, 18(102), pp. 156-163.
- Höhle, J., Potuckova, M., 2005. Automated Quality Control for Orthoimages and DEMs , *Photogrammetric Engineering & Remote Sensing*, Vol. 71, Number 1, pp. 81-87.
- Höhle, J., 2005. International Seminar "Automated Quality Control of Digital Terrain Models" at Aalborg University, 18-19 August 2005, *Photogrammetrie, Fernerkundung, Geoinformation Heft 7/05*, s. 565-568, ISSN (print): 1432-8364.
- Li, Z., Zhu, Q., Gold, C., 2005. Digital Terrain Modeling, Principles and Methodology, 323 p., CRC Press, ISBN 0-415-32462-9.

Norvelle, F.R., 1996. Using Iterative Orthophoto Refinements to Generate and Correct Digital Elevation Models. Digital Photogrammetry, an Addendum to the Manual of Photogrammetry, ASPRS, ISBN 1-57083-037-1, pp. 151-155.

Potuckova, M., 2005. International Symposium "Modern Technologies, Education and Professional Practice in Geodesy and Related Fields, 03-04 Nov., Sofia, Bulgaria, 2005.

Potuckova, M., 2006. Image Matching and its Applications in Photogrammetry, 132 p., PhD thesis, in: Working papers from the Department of Development and Planning, nr. 314, ISBN 87-91830-00-1, ISSN 1397-3169.

Schenk, T., Seo S., Csatho, B., 2001. Accuracy Study of Airborne Laser Scanning Data with Photogrammetry, International Archives of Photogrammetry and Remote sensing, Volume XXXIV-3/W4, pp.113-118.

Skarlatos, D., Georgopoulos, A., 2004. A new matching algorithm using elliptical areas: Results, accuracy, advantages and disadvantages. IAPRS XXXIV, Istanbul, 2004.

Skarlatos, D., Georgopoulos A. 2004. Automating the Checking and Correcting DEMs without Reference Data, International Archives of Photogrammetry and Remote sensing, Volume XXXV-B2, pp. 553-558.

*WebPhotogrammetry* [online], visited 29.8.2006 <http://www.kfit.uwm.edu.pl/zp/zp.html>





## **APPENDIX I**



# THE METHOD OF TWO OVERLAPPING ORTHOIMAGES FOR CHECKING THE PRODUCED DTM

Dimitris Skarlatos\*, Andreas Georgopoulos

NTUA, School of Rural & Surveying, Laboratory of Photogrammetry, 9 Iroon Polytechniou, Athens 15780, Greece

(dskarlat,drag)@central.ntua.gr

## ABSTRACT

*The need for Digital Elevation Model (DEM) checking becomes apparent as more and more data need updating and validation. Often automatic DEM extraction techniques prove to be inadequate and extensive manual checking is necessary. Since the use of reference data is a luxury and, therefore, cannot be used in all cases, a novel method for DTM checking through orthophotographs created from the two photographs of the stereopair has been developed and introduced by the authors (Georgopoulos, Skarlatos 2003, 2004). The mathematical model is loosely based on Norvelle's method (1994), and translates discrepancies between two orthophotographs created from two overlapping photographs into precise corrections of the DEM. These corrections are the differences from the real surface and, if applied over the existing DEM, can produce a more accurate one. The mathematical model is rigorous and straightforward, it does not approximate, and therefore there is no need for iterations.*

*This paper is mainly concerned with the results of the proposed method, over artificial data, manually collected DEM and an artificially distorted version thereof and the EuroSDR data of the project "Automated DTM checking". Until now tests over artificial data and other areas have proved that the method can be used for improvement of DEMs even when differences are crude. Once again, the method proved to be able to cope with the problematic areas. Therefore the use of the method for DTM correction is valid. The use of the method as checking and validation procedure is also feasible, provided that the specifications impose strict criteria for acceptance or rejection.*

*The comparison shows that statistically the corrections have the same values as the differences between automatic DEMs and the reference; hence the proposed method might be used as a check of DEMs. This means that one can estimate the quality of a DEM without having any reference data, just by analyzing the results from the proposed algorithm. This solves a common problem to a number of governmental organizations who cannot reliably check their contractor's deliveries.*

*The quality of the corrected DEMs after the application of the corrections will also be analyzed. Results indeed show a clear improvement and are encouraging. It should be mentioned though that in any case the best method for checking DEMs is an existing reference DEM. This method comes as a solution in cases where reference DEM is or cannot be present.*

## 1 INTRODUCTION

Digital Elevation Model (DEM) production is currently the bottleneck of the photogrammetric workflow. Automated aerial triangulation (using GPS and INS) and orthophoto map creation (automatic mosaicking) has stressed the problem. Orthophoto maps are becoming a standard and therefore DEMs become necessary in most photogrammetric projects.

Although nowadays all consulting companies own automatic DEM creation software, the production rate does not rise, simply because the editing needed is almost as time consuming as the manual collection. Experience has shown e.g. that in a certain project with 60 colour photographs of 1:6000

scale, with the DEMs being collected automatically overnight, each user could correct 3 models during a shift. On the other hand if random points and breaklines had been collected manually, 2.5 models per shift of an experienced user could be expected.

A new matching algorithm has been developed in the Laboratory of Photogrammetry of the School of Rural and Surveying Engineering of the National Technical University of Athens (NTUA). During its last stages, where customization and final adjustments were necessary, the urge of checking the results over different types of landscape became obvious. Manual collection of a reference DEM is the most reliable and obvious solution, but if a number of models is under investigation then it becomes impractical, tedious and time consuming.

Another possible solution for checking could be the use of internal statistics, which provide a measure of precision but not a measure of accuracy, hence it was also rejected. Simple overlay of the two orthophotos and subtraction of the gray level values provide a coarse measure for spatial distribution of errors, but do not describe their exact magnitude. Therefore this was also rejected.

Norvelle (1994) has introduced Iterative Orthophoto Refinement (IOR), a method where the discrepancies between two orthophotos were translated into height displacement and used to correct the initial DEM. Although theoretically the orthophotograph should be independent of the initial photograph, in practice orthophotographs created from overlapping photographs differ. The mathematical model of the corrections was simple and approximate. Height correction was calculated using the approximate formula:

$$dh = dx \frac{H}{B},$$

where

dh, the height correction

dx, the x difference (in ground units) between orthophotographs created from the left and the right photographs of a pair

B, base

H, flying height.

Although the formula was approximate, multiple iterations were utilized to produce promising results. Since 1996, there wasn't any other report on this subject that the authors are aware of. The idea of using the discrepancies between two orthophotographs to correct the underlying DEM has a strong geometric background and seemed attractive to the authors, who decided to investigate further and work out a precise mathematical model for the height error in any given position using orthophotographs created from the left and the right photographs of a pair (from now on referred freely as left and right orthophotographs). The advantages of such a method are obvious; automation of checking or correcting DEMs becomes feasible.

Previous tests of artificial data, which supported further examination, will be presented, as well as initial results of EuroSDR data.

## 2 METHODOLOGY

The principle of the method is quite simple. Using the DEM under investigation, one can produce two orthophotographs from two overlapping photographs. Matching the two orthophotographs locates the position of discrepancies and by applying the suggested mathematical model, height discrepancies from original DEM can also be calculated. Running statistics over the TIN of the height discrepancies could be a way to check DEMs. On the other hand addition of the discrepancies' TIN over the initial DEM could produce a more accurate one.

Calculation of the height discrepancy is a two-step problem. It begins with two matched points in left and right orthophotographs as input data and returns a height correction and the application position over the DEM. The calculation of the height correction is one thing, and the calculation of the exact position is another. It is not to forget that if the matched points in the two orthophotographs do not coincide (that is they do not have exactly the same geodetic co-ordinates), neither of them is correct, hence the exact position must be calculated. The key point is that the planimetric displacement due to height error is always radial to the nadir of the corresponding photograph (Kraus, 1992).

It is critical to calculate the exact height error in each planimetric position. The basic quantities can be seen in Figure 1, and the basic formula for the height discrepancy calculation is

$$\frac{R2''}{M''R''} = \frac{Dh''}{1''Acorr} \Rightarrow Dh'' = \frac{R2''}{M''R''} 1''Acorr$$

Hence  $Dh''$  and similarly  $Dh'$  can be calculated exactly. The final  $Dh$  on the point can be the average of the two values. The complete theoretical model is described in detail by Georgopoulos and Skarlatos (2003). The flow chart of the suggested method is described in Figure 1.

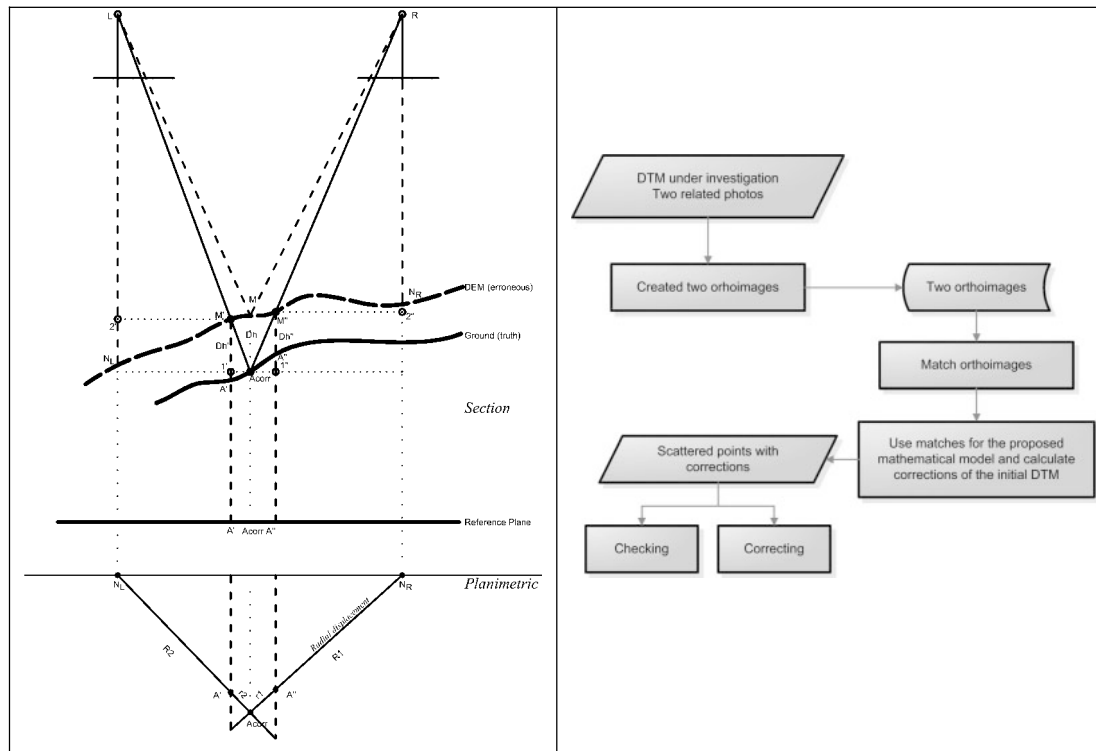


Figure 1. Left: Diagram of the basic concept of the proposed method. Right: Flow chart of the proposed method.

### 3 VERIFICATION OF THE PROPOSED METHOD

The verification of the method has been checked twice. Once using purely artificial data and another one using manually collected DEM. The use of purely artificial data has been proved necessary due to the size of the expected differences. Given any pair of photographs, the accuracy of a single manual height measurement is not accurate enough to check matching techniques. It has been reported that the

accuracy of image matching is in the range of 1/10 (Schenk, 1999) to 1/100 of the pixel size (Zhizhuo, 1990, McGlone, 2004). A human operator cannot rival these figures. On the other hand he is able to collect a better overall DEM, because he is able to deal reliably with breaklines and large discrepancies in x-parallax. Therefore the check should cover both the accuracy aspect as well as the reliability which is more critical.

Artificial data include a mathematical function like DEM (Fig. 2) and two artificially created aerial photographs. These images have been created using a real aerial photograph scanned in 1800 dpi as pattern. The final photographs were of a 1200 dpi resolution (Fig. 2) and the approximate photo scale 1:12000. The advantage of the artificial data is the accuracy and reliability of the height information and the exact knowledge of exterior and interior orientation. Therefore the suggested method will be held responsible for any deviation between expected and detected DEMs.

The artificial DTM was altered by adding an inclined plane (Fig. 3a) with deviations in the range of  $\pm 34$  m. The new “corrupted” DTM has been checked using the proposed methodology. The raw differences detected follow generally the pattern of the applied deviations (Fig. 3b), with a few blunders, mainly in the area between the two projection centers. These blunders can be eliminated using a threshold on checked points, depending on the triangle formed with the projection centers (Fig. 3c). By applying a simple smoothing filter on the remaining detected differences the final surface of errors is created (Fig. 3d), which is identical to the artificial deviations with opposite sign. Therefore the method successfully detected the deviations and can be considered for further investigation.

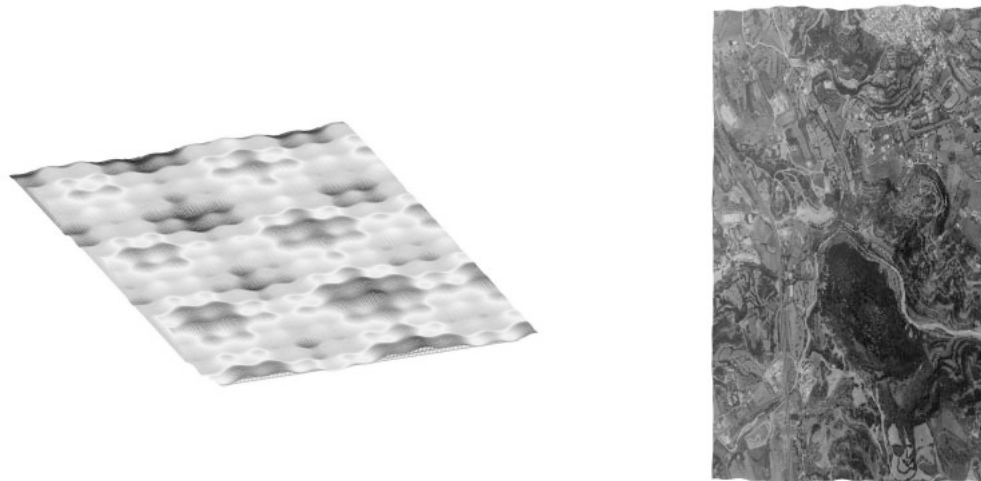


Figure 2. Artificial data. Left: Mathematical function used as DEM. Right: Left aerial photograph created using the DEM and a true photo as pattern.

#### 4 APPLICATION ON REAL DATA

The next step was the verification of the method using real data. In this test, the ability of the method to correct an existing DTM has also been tested. The selected area covers 1500x1200 metres with a height range of 58 metres, with minimum and maximum 54 and 169 metres respectively. The flying height was 2650 metres above mean sea level. The original photographs were scanned at 21 microns, or 0.364 metres in ground units. The area selected includes many features such as a quarry or several agricultural and semi urban areas, thus being ideal as test area. The DTM has been collected manually over a 10 m grid, allowing the user to deviate up to 7.5 m from the original position of the grid. In this

way the collected DTM was very good because it resembles a TIN with characteristic points on surface discontinuities and slope changes.

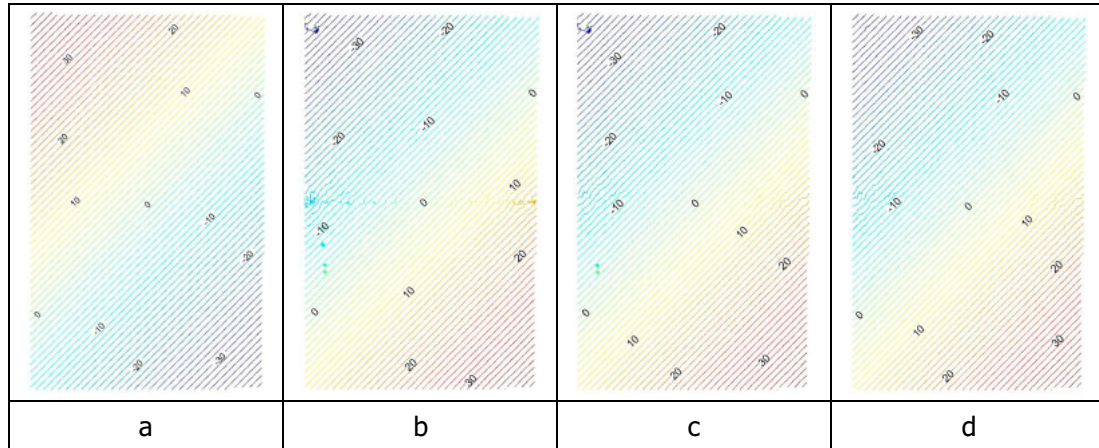


Figure 3. a: Deviations applied to original DTM. b: Raw detected differences. c: Filtered differences for points with bad geometry as to projection centres. d: Final filtering of remaining spikes and final result of the checking.

The same method was also used in this case. An inclined plane has been added as deviation and the new DTM has been checked with the proposed method. In addition to the artificially distorted DTM two more DTMs, created from commercial software, were used for checking (marked as DTM and TIN in Table 1). All three DTMs were corrected using the proposed method. The initial DTM and the corrected one were compared using the manually collected DTM as reference data. The results of the comparison are displayed in Table 1. In the case of the artificially distorted DTM the improvement is clear. RMS and all statistical measures were improved a lot. In the case of the commercial software, the RMS has been improved by 36-37% along with MAD and standard deviation. The mean in all three cases has improved, but not significantly. Therefore there was no systematic error in the surfaces. On the other hand the fact that the RMS has been improved much more than the mean suggests that the variations in the new DTMs follow the reference surface much better.

In any case this test can also be considered successful because all surfaces under investigation have been improved, hence deviations, artificial or not, have been detected correctly.

## 5 APPLICATION ON EUROS DR DATA

EUROS DR and the related test was an ideal opportunity to test again the proposed method. The data provided cover two areas and the presented results concern test area A (Fig. 3). The available data for this area were a pair of aerial photos, direct orientation data, the calibration report of the camera, sketches of the control points, as well as their ground coordinates. Four areas of the model have been designated as the test areas.

For the creation of the two necessary orthophotographs, the complete DTM and the 6 parameters of exterior orientation have been used. The pixel size was equivalent to the ground pixel size of the original images (50 cm), and the bi-cubic resampling method has been used in order to keep as much information as possible. The image matching has been restricted only to the four areas of interest (Fig. 4). It is obvious that the proposed method is very sensitive to the image matching method. The method used in this particular application is a combination of a dynamically adaptive template size and a modified Gotcha strategy. The latter has the ability to skip areas with uniform tones and therefore

avoid blunders (Fig. 4, areas 1 and 4). On the other hand this might cause problems in some isolated areas in terms of propagation (Fig. 4, area 3), especially since the matching has been restricted in the areas of interest and not in the whole orthophoto model.

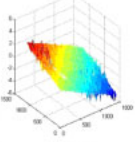
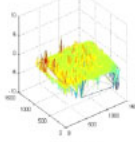
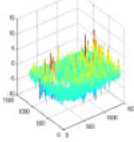
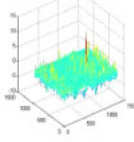
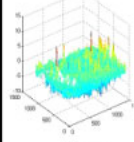
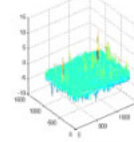
	Artificially Distorted		DTM		TIN	
	Initial	Corrected	Initial	Corrected	Initial	Corrected
Difference from reference						
Mean	-0.54	-0.11	-0.10	-0.09	-0.09	-0.09
Std. Dev.	1.75	0.59	0.93	0.58	0.87	0.56
RMS	1.82	0.60	0.94	0.59	0.88	0.56
MAD	1.42	0.36	0.65	0.36	0.62	0.35
Range	10.25	12.43	20.82	20.74	20.33	20.70
Kurtosis	2.45	16.92	12.41	28.78	12.87	30.11

Table 1. Comparison of the artificially distorted DTM with the corrected version of it against the reference (manually collected). The same comparison for the two DTMs created using commercial s/w.



Figure 4. EuroSDR test area A, with raw matched points over the left orthophoto.



The raw image matching data have been analyzed using the proposed method, and for each matched point a difference from the “correct” but unknown position has been calculated. A statistical analysis of these differences over each area separately may provide necessary information for DTM rejection or acceptance. Since the calculated differences are to be used for DTM checking, the values used should be very reliable. A 50% level of confidence test (if  $m$  is the mean and  $\sigma_o$  the standard deviation of the calculated differences then only values within the limits  $[m-0.6745*\sigma_o, m+0.6745*\sigma_o]$  are accepted) was used in all four cases. The points excluded are not as many as expected (approx. 25% instead of 50%), hence suggesting that the differences do not follow the normal (Gaussian) distribution (Table 2). The remaining points are considered correct and therefore contribute to the final results and evaluation of each area of interest (Table 2). In addition to the internal statistical values, comprehensive plots of errors can be plotted as contours over the area of interest (example in Fig. 5).

Areas with poor coverage such as area 3 should be excluded from the checking. Perhaps a more appropriate matching algorithm could provide more matched points as check points over poor contrast areas. It is the authors’ intentions to rerun the test with a customized version of the matching algorithm to improve matching results hence better checking accuracy.

Areas 1, 2 and 4 from the table have similar standard deviation results. The value of approximately 5 m is rather high implying that the DTM is not very good. The means in areas 1 and 4 are well within the expected accuracy, while area 2 has a rather big value, implying that there might be a systematic error on the surface. The final conclusions can only be reported after the comparison made by EuroSDR with reference data.

	DTM checking area (TEST A)			
	1	2	3	4
Raw matched points	22630	4625	1189	15470
After 50% level of confidence test on dZ	17291	3372	875	11823
Coverage	Very Good	Excellent	Poor	Medium
Mean of dZ [m]	0.14	0.57	-1.55	0.07
Std dev of dZ [m]	4.96	4.86	7.46	4.60

*Table 2. Results and final evaluation of the interest areas.*

## 6 DISCUSSION AND CONCLUSIONS ABOUT THE METHOD

The advantages of the proposed method can be summarized as follows:

1. It is a rigorous method
2. It does not need reference data
3. It produces an excessive amount of check data
4. It can be fully automated
5. It can be used for checking, correction or even updating of DTMs

There are also two disadvantages which may be argued.

The first and obvious one is the fact that the method is heavily dependent on the image matching algorithm utilized for the collection of check points. In any case blunders cannot be avoided and therefore filtering is necessary. In this application two stages of filtering have been used. The first one is based on the well known and widely used hypothesis that the detected differences follow the normal distribution. Therefore a strict 50% confidence level filter will only let correct points to pass. A further

smoothing filtering is used to form the final surface of differences. The acceptance or not of the checked area based on the calculated differences is the next important step.



*Figure 5. Test Area A1 with overlaid contours of the calculated differences. Green points the given DTM and red points the calculated check points with the proposed method, after 50% confidence level filtering.*

The second argument against the proposed method is the usage of image matching to check DTM produced with image matching. In addition, image matching is applied on resampled images, which degrades the quality of the original photographs, hence results could be dubious. These statements are indeed true, but resampling using bi-cubic interpolation takes some care of the problem, while there still are four good reasons why this method can be applied as DTM checking:

1. Initial approximations, which is the main problem of least squares image matching and often the basic reason of blunders, has been almost eliminated in the orthophotographs used.
2. The affine transformation, which in real photographs might be inadequate due to strong slopes, has almost been eliminated in orthophotos and therefore matching is faster and more reliable.
3. Any two overlapping photographs can be used, not only the two photographs which formed the original stereopair.
4. Using image matching in orthophotos for DTM checking, provides a very strong and redundant system. Since the main scope of this application is checking and there is no need for complete coverage of the area of interest, a loss of a large number of matched points (i.e 50%) can be tolerated, in order to increase reliability of the rest. The remaining thousands of points are still plenty for DTM checking.

Therefore the proposed method has a strong theoretical and practical background that supports its usage for DTM checking.

## 7 DISCUSSION ABOUT DTM CHECKING

A couple of interesting points should be stressed here. When a large number of check points is available, the differences do not seem to follow the normal distribution. This has been reported not only in tests referred to here, but in a number of DTM checking cases against reference data (Papasaika, 2002). If this holds, then a number of assumptions and formulae used widely are not valid. The adoption of a new distribution function for DTM checking, presuming there is one, and the enactment of criteria for DTM rejection is very difficult.

The standardization of rejection criteria is a big issue by itself. There are two main measures that need to be defined. One measure should describe the surface quality and another one the area this measure applies to. In other words, a problematic area representing 10% of the project's area might not be represented in the measure of 'goodness' of the whole project's area. Therefore the area under check should be broken down in smaller parts where checking will take place and measure of goodness will be calculated. These smaller parts should be defined by the specifications.

The measure of goodness itself might be RMS, standard deviation, MAD or something similar. The mean is inappropriate for such purpose since it is always well within the limits and can only describe whether there is a systematic error on the surface or not.

## REFERENCES

- Al-Tahir, R., Schenk, T., 1992. On the interpolation problem of automated surface reconstruction. *International Archives of Photogrammetry and Remote Sensing*, 29(3):227-232.
- Förstner, W., 1986. On feature based correspondence algorithm for image matching and least squares matching, *International Archives of Photogrammetry and Remote Sensing*, Vol. 26, P3, Rovaniemi, pp. 150-166.
- Georgopoulos, A., Skarlatos, D., 2003. A novel method for automating the checking and correction of digital elevation models using orthophotographs. *Photogrammetric Record*, 18(102):156-163.
- Kraus, K., 1993. *Photogrammetry. Volume I. Fundamentals and standard processes*. Dümmler, Bonn. 397 pages.
- McGlone, J., C., Mikhail, E., M., Bethel, J., 2004. *Manual of photogrammetry*, fifth edition. ASPRS, Maryland, p. 1151.
- Norville, F., R., 1996. Using iterative orthophoto refinements to generate and correct digital elevation models (DEM's). *Digital Photogrammetry: An addendum to the Manual of Photogrammetry*. American Society for Photogrammetry and Remote Sensing. Bethesda, Maryland, USA. 247 pages:151-155.
- Norville, F.R., 1994. Using iterative orthophoto refinements to generate and correct digital elevation models (DEMs). *Proceedings: Mapping and remote sensing tools for the 21st century*. American Society for Photogrammetry and Remote Sensing, Washington:134-142.
- Papasaika H., 2002. *Digital Terrain Modeling from color aerial photographs*. Diploma thesis, N.T.U.A., 89 pages.
- Schenk, T., 1999. *Digital Photogrammetry*. TerraScience, Laurelville, 428 pages.
- Skarlatos D., 2000. Image matching towards maturity. *IAPRS XXXIII, Amsterdam 2000*, TP III-03-03.
- Skarlatos, D., Georgopoulos, A., 2004. A new matching algorithm using elliptical areas: Results, accuracy, advantages and disadvantages. *IAPRS XXXIV, Istanbul, 2004*.

Zhilin L., 1993b, Theoretical models of the accuracy of digital terrain models: an evaluation and some observations. *Photogrammetric Record*, 14(82):651-660.

Zhilin, L., 1988. On the measure of digital terrain accuracy. *Photogrammetric Record*, 12(72):873-877.

Zhizhuo W., 1990. Principles of photogrammetry (with remote sensing). Press of Wuhan University of Surveying and mapping. Publishing house of surveying and mapping Beijing. Pages 575.

# Checking and Improvements of DTMs in the EuroSDR Test<sup>1</sup>

Marketa Potuckova

Charles University in Prague, Department of Applied Geoinformatics and Cartography  
Czech Republic

## ABSTRACT

*The methodology of checking digital terrain models (DTMs) based on finding horizontal parallaxes in two overlapping orthoimages is described. Attention is paid to the detection and elimination of errors in image matching that is crucial for a successful application of the method. Results based on the EuroSDR test data comprising DTMs derived by means of photogrammetry, digitized contour lines and laser scanning are presented.*

## 1 INTRODUCTION

DTMs used for orthoimage production or engineering applications have to fulfil high requirements for geometrical accuracy and have to be up to date. Considering most used approaches to a DTM collection such as digitizing contour lines, photogrammetry, or laser scanning, all provide DTMs suitable for the mentioned applications. Nevertheless, none of these techniques provides an error-free DTM. Errors caused by inaccurate georeferencing or image matching appear. Manual editing is time consuming and costly. Therefore methods with a high degree of automation are demanded.

The methodology presented in this paper is based on the 'Iterative Orthophoto Refinements (IOR)' method proposed by Norvelle (1996). The main idea is based on finding corresponding points in two overlapping orthoimages and comparing their position. If a discrepancy in the position exists, it is recalculated into a height correction. The original method has been improved with respect to an elimination of blunders that appear in image matching. Tests of the proposed methodology are carried out on EuroSDR project data. The available reference data are used for an evaluation of the results.

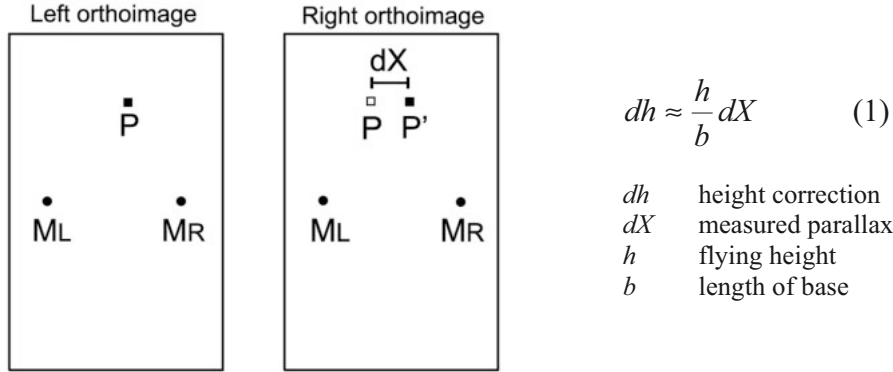
In this experiment, only the height accuracy at the grid posts is tested. The fit between a 'model' and a 'real terrain' is not evaluated (density of points, omission of break lines and other morphological features, suitable interpolation methods, etc.). The goal is to find blunders and systematic errors in the tested data sets.

## 2 METHODOLOGY

Assuming error-free image orientation and error-free DTM, bare earth points should have the same plane coordinates in the overlapping orthoimages. If DTM errors exist, false horizontal parallaxes  $dX$  appear (Fig. 1). The height errors  $dh$  are proportional to these parallaxes according to the formula 1 (Norvelle 1996, Höhle, Potuckova 2005). In the solution to be described, a found height correction is assigned directly to a grid point. A correct position can also be derived as proposed in (Skarlatos, Georgopoulos 2004).

---

<sup>1</sup> Written version of the lecture at the seminar "Automated Quality Control of Digital Terrain Models", 18-19<sup>th</sup> of August 2005 at Aalborg University



$P$  ... DTM point in the left and the right orthoimage (given  $X, Y$  coordinates)

$P'$  ... point corresponding to  $P$  from the left orthoimage found by image matching

$M_L, M_R$  ... centres of the left and right aerial images

Fig.1 Effect of DTM errors in orthoimages

Corresponding points in images can be found by means of image matching. In this test, area based matching (ABM), namely cross-correlation and least squares matching, are applied. Accuracy of a derived corrected height can be estimated as follows:

- Accuracy of a derived correction  $\sigma_{dh}$

$$\sigma_{dh} = \sigma_{LSM} \frac{h}{b}$$

$$\sigma_{LSM} = 0.3 \text{ of pixel size (or better)}$$

$\sigma_{LSM}$  ... accuracy of least squares matching (shift parameters)

- Accuracy of orientation  $\sigma_{h\_ori}$

$$\sigma_{h\_ori} = 0.01\%h$$

- Final accuracy of a corrected height  $\sigma_{h\_corr}$

$$\sigma_{h\_corr} = (\sigma_{dh}^2 + \sigma_{h\_ori}^2)^{1/2}$$

In order to avoid blunders in matching that would result in introducing false height corrections, three restrictions are applied in the first place:

- Based on existing topographic maps, all areas covered with objects rising above terrain (houses, forests) are excluded from further calculations, as image matching finds corresponding points on the surface of objects.
- Matching is carried out along an epipolar line only (+/- 1 row due to remaining orientation errors)
- Thresholds for similarity measures, namely a minimal value of correlation coefficient and a maximal value of a standard deviation of a shift parameter derived by least squares matching, are set. The choice of threshold values is based on previous experiments (Potuckova 2006).

A comparison with reference data showed that applying above-mentioned criteria is not sufficient for an elimination of mismatches. Therefore two new approaches are presented. Both of them have been developed with respect to a quite flat area covered by the test material.

The first approach is based on an assumption that a derived height correction should be nearly the same regardless of a ‘direction’ of image matching, i.e. regardless whether a template is chosen from the left orthoimage and a search area from the right one or vice versa. Based on this assumption, a new threshold for a difference between corrections obtained from the double matching procedure  $\Delta h_{LR}$  can be set:

$$|\Delta h_{LR}| < 3\sigma_{LR}$$

$$\sigma_{LR} = \sqrt{2}\sigma_{dh}$$

This method is referred as the ‘L-R method’ in the following text.

The second approach is inspired by software packages for DTM generation where matching in lots of points is carried out and the grid points are interpolated afterwards (the redundancy principle). Several points in the neighbourhood of a grid point are matched. It is assumed that the neighbourhood is planar, not necessarily horizontal. A histogram of corrected heights is created. An interval of the range  $\pm t\sigma$  with highest occurrence of corrected heights is sought. The parameter  $t$  is usually chosen between 2 and 3.  $\sigma$  is an expected accuracy of the corrected model (e.g. 0.01%h). At the same time a threshold for a number of points within this interval must be fulfilled. Due to the size of the sample (e.g. 25 points) the conditions of the normal distribution are not fulfilled. The amount of points within the interval with the highest occurrence of points is smaller than a value corresponding to the variable  $t$  of the normal distribution (for  $t=3$  number of points should be 99.7% but the threshold is set to e.g. 75%). The final value of the corrected height is calculated as an average of the heights within the interval. This method is called the ‘histogram method’ in the following text. A similar result can be achieved if the surrounding points are used for defining a plane and a corrected height of a grid point is derived from this plane. This approach was also tested but is not discussed further.

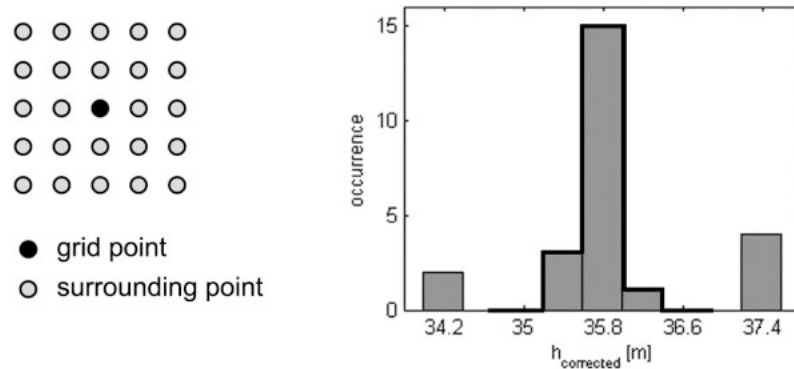


Fig. 2 Principle of the histogram method. Matching is carried out in 25 points (a grid point and 24 surrounding points). After applying criteria for similarity measures, height corrections are calculated and assigned to heights of surrounding points interpolated from DTM. A histogram of corrected heights is created. An interval of the range  $\pm 3\sigma$  with the highest occurrence of points is found (points under the red line). The number of points in this interval has to be higher than a given limit; otherwise it is excluded from ‘accepted points’. In a given example  $\sigma=0.4m$ , the limit for number of points is 19 (75%).

### 3 TEST DATA

The EuroSDR test comprises three DTMs with parameters summarised in Tab. 1. All DTMs were delivered as ASCII files containing X, Y, Z coordinates of grid points. Furthermore, stereopairs of coloured aerial images including their inner and exterior orientation parameters were provided for the purpose of DTM checking. Their properties are shown in Tab. 2.

Tab. 1 DTMs in the EuroSDR test

DTM	Test A	Test B	Test C
Origin of data	Digital photogrammetry (stereopair of aerial images at the scale of 1:25 000, pixel size 21 $\mu$ m)	Digitized contour lines from a topographic map 1:50 000, basic contour line interval 5 m	Laser scanning
Grid interval	25 m	10 m	1 m
Expected accuracy ( $\sigma$ )	0.4 m	1-2 m	0.10 m
Date	Images from spring 2003	Maps updated in 1984/85 *	Spring 2001

\* <http://www.geodata-info.dk>

Tab. 2 Parameters of aerial images used for DTM checking

	Scale	Pixel size	Accuracy of image orientation*	Date
Test A & B	1:25 000	21 $\mu$ m	$\sigma_X=\sigma_Y=0.1$ m, $\sigma_Z=0.2$ m	Spring 2003
Test C	1: 5000	15 $\mu$ m	$\sigma_X=0.03$ m, $\sigma_Y=0.05$ m, $\sigma_Z=0.07$ m	Spring 2001

\* Standard deviation on control points after absolute orientation

Orthoimages were derived from available images, orientation parameters and DTMs using the software package Base Rectifier from Intergraph. In each test, two orthoimages ('left' and 'right') covering the area of forward overlap between aerial images were produced. In order to minimize possible artefacts, orthoimages were derived with the smallest possible sampling distance of 1 pixel using the bilinear interpolation. A pixel size of 0.5 m and 0.1 m is chosen in Tests A&B and Test C, respectively. Expected accuracy of corrected heights derived by means of matching orthoimages is calculated in Tab. 3.

Tab. 3 Expected accuracy of the orthoimage method

Test	$\sigma_{dh}$ [m]	$\sigma_{h\_ori}$ [m]	$\sigma_{h\_corr}$ [m]
A&B	0.25	0.40	0.47
C	0.05	0.07	0.09

Based on Tab. 2 and 3, the orthoimage method should be sufficient for finding blunders in all three tests. Systematic errors can be discovered in Tests B and C. Orientation parameters in Test A were the



same as the parameters used for automatic DTM generation, and therefore the existence of any systematic errors due to inaccurate orientation of images could be found. Because of lower accuracy of the DTM in Test B, this DTM can be also improved in general by the suggested method.

A validation of the obtained results is carried out by a comparison of the corrected heights with the reference data. The reference data of Tests A&B were obtained by semiautomatic measurement of grid points at the distances of 25 m and 10 m, respectively in stereopairs of aerial images at the scale of 1:3 000 and a pixel size of 21 $\mu$ m. Each measurement was done twice and the final accuracy of the heights of reference points (including orientation errors) corresponds to 0.09 m. Profiles measured by GPS (RTK method) with the step of 1 m are used as reference data in Test C. The accuracy of the reference points was estimated to 0.02 m. The root mean square error (RMSE), standard deviation ( $\sigma$ ), mean, and maximal difference between original/corrected height and the reference height are calculated as statistical measures for evaluation of the results of the proposed method and are presented below.

#### 4 TEST RESULTS

The described methodology was first applied to Test B data as the largest changes had been expected on this data set (compare to Tab. 3). The calculations were carried out only on points with available reference data. In this way, all points on man-made and natural object surfaces were avoided. The size of image patches for ABM was chosen as 19 x 19 pixel<sup>2</sup> (or 9.5 x 9.5 m<sup>2</sup>) for templates and 27 x 47 pixel<sup>2</sup> (or 13.5 x 23.5 m<sup>2</sup>) for search areas. The size of the templates was chosen empirically. Several calculations were carried out with a different template size and the success (number of mismatches) of the results was evaluated. Image patches were matched along an epipolar line  $\pm 1$  row. The angle between the base line and the X axis of the reference coordinate system was about 5 gon. Therefore the size of the search area across the epipolar direction was chosen to be  $19 + 2 \times 4 = 27$  pixels. The biggest height error was estimated to 11 m, which corresponds to a planimetric shift of 7 m or 14 pixels (considering 60% overlap). The size of the search area along the epipolar direction was set to  $19 + 2 \times 14 = 47$  pixels. As the matching algorithm was designed only for one channel, original RGB image patches were converted to gray tone images.

Altogether 10 390 DTM points were evaluated in Test B. After applying thresholds for similarity measures and other constraints mentioned in the paragraphs about the L-R and the histogram method, corrections were applied on more than 80% of the points and improvements were achieved as Tab. 4 and Tab. 5 demonstrate. The expression ‘before correction’ is connected to a comparison of the original DTM points and reference points while ‘after correction’ reflects the situation after applying derived height corrections.

Both approaches proved to be quite successful with the given data set. As the results of the histogram method showed to be slightly better than those of the L-R method, the histogram method was applied to other data sets. The results of Test A are summarised in Tab. 6. Again, only points at reference data posts were evaluated, i.e. the test was carried out on 2 033 points. Because the orientation and resolution of the original images were the same as in Test B, the same threshold for similarity measures and the range of interval were chosen.

A direct comparison of heights acquired by laser scanning with heights measured by GPS (417 points in 9 profiles) in Test C revealed quite favourable results: RMSE = 0.08 m, mean = -0.06 m,  $\sigma$  = 0.04 m, maximal error of 0.31 m. The evaluated points comprised only one blunder. Orthoimages with a pixel size of 0.1 m were derived from aerial images at the scale of 1:5 000. The estimated accuracy of the orthoimage method was at the level of accuracy of laser scanning (compare Tab. 3). The orthoimage method has not been applied to low flying height images before. Therefore in this first try the calculation was carried out on 120 points (3 profiles) only and was used as an evaluation of the

method and finding its limitations. The only thresholds set were for the correlation coefficient ( $r > 0.5$ ) and accuracy of least square matching ( $\sigma_{LSM} < 0.2$  pixel). After excluding four blunders, a comparison with GPS points showed an unacceptable systematic shift of 0.15 m. The relative and absolute orientation of the stereopair was carried out again. The RMSE on check points equalled 0.01 m, 0.05 m, and 0.03 m in X, Y, Z coordinates, respectively. New orthoimages were derived and height corrections were calculated using the orthoimage method. Four blunders appeared again due to soft criteria for elimination of mismatches. The comparison with GPS measurements revealed RMSE = 0.06 m, mean = 0.05 m,  $\sigma = 0.04$  m. Such a result is acceptable and shows a potential of the orthoimage method for finding blunders and systematic errors in DTMs derived from laser scanning.

Tab. 4 Test B, results of L-R method

<b>Test B L-R method</b> $T_{hLR}, T_r, T_{LSM}$	Before correction	After correction
Number of points	8481 (82% of all tested points)	
RMSE	1.4 m	0.5 m
Mean	0.3 m	0.1 m
$\sigma$	1.4 m	0.5 m
$\max  \Delta h $	10.8 m	10.3 m
Number of outliers $ \Delta h  < 1.2$ m	2321 (27% of 8481 p.)	229 (3% of 8481 p.)

Thresholds for similarity measures were set as follows: correlation coefficient  $r > T_r$ ,  $T_r = 0.5$ ; accuracy of least squares matching  $\sigma_{LSM} < T_{LSM}$ ,  $T_{LSM} = 0.3$  pixel; difference of two corrected heights obtained by double matching for one grid point  $\Delta h_{LR} < T_{hLR}$ ,  $T_{hLR} = 1.1$  m

## 5 DISCUSSION

L-R and histogram methods allow for dividing the whole investigated DTM into two categories:

1. Points where all the set criteria are fulfilled. The number of blunders is minimized. If the accuracy of the orthoimage method is higher than an accuracy of the original DTM, applying corrections brings an improvement of an overall accuracy of the tested DTM (Test B, possibly Test A).
2. The criteria are not fulfilled; the points in this category must be checked by means of another method, e.g. manual measurement in stereomodels.

The division is carried out fully automatically. The result is presented graphically in Fig. 3.

The suggested approaches check as many points as possible. If only a random check is required, radiometric measures as contrast, entropy, or parameters  $w$  and  $q$  of the Förstner operator that assure good matching conditions should be calculated for templates on grid points. Only templates fitting the high criteria required for the mentioned measures would be matched. Based on literature and own experience (Schenk et al. 2001, Potuckova 2006) the number of checked points can decrease down to 10%.

Tab. 5 Test B, results of histogram method

<b>Test B</b> <b>Histogram method</b> $T_r, T_{LSM}, T_{\#p}$	Before correction	After correction
Number of points	8973 (86% of all tested points)	
RMSE	1.4 m	0.4 m
Mean	0.3 m	0.1 m
$\sigma$	1.4 m	0.4 m
$\max  \Delta h $	10.9 m	6.0 m
Number of outliers $ \Delta h  < 1.2 \text{ m}$	2400 (27% of 8973 p.)	95 (1% of 8973 p.)

Thresholds for correlation coefficient  $r > T_r$ ,  $T_r = 0.3$ , accuracy of least squares matching  $\sigma_{LSM} < T_{LSM}$ ,  $T_{LSM} = 0.3 \text{ pixel}$ , and a number of points within an interval  $\pm 3\sigma$ ,  $\sigma = 0.4 \text{ m}$  with highest occurrence of points  $T_{\#p} = 75\%$  were applied

Tab.6 Test A, results of histogram method

<b>Test A</b> <b>Histogram method</b> $T_r, T_{LSM}, T_{\#p}$ (see Tab. 5)	Before correction	After correction
Number of points	1729 (86% of all tested points)	
RMSE	0.7 m	0.5 m
Mean	0.2 m	0.1 m
$\sigma$	0.7 m	0.5 m
$\max  \Delta h $	4.9 m	4.6 m
Number of outliers $ \Delta h  < 1.2 \text{ m}$	35 (2% of 1729 p.)	19 (1% of 1729 p.)

All the calculations concerning image matching, height corrections, and their evaluation were carried out by own developed MATLAB scripts. This caused quite a long calculation time especially when the image matching was carried out several times per grid point. More effective programming might speed up the whole process.



*Fig. 3 Division of the tested DTMs into two categories, example of Test B, subarea A\_I. White (green) points fulfilled all set criteria and comprise a minimum of blunders, dark (red) points must be checked by other methods. The distance between points is 10 m.*

## 6 CONCLUSION

Application of the orthoimage method proved to be successful in approximately of 85% of the tested DTM posts in Tests A&B. In comparison to reference data, a systematic error was minimised and a standard deviation improved. This achievement was possible when matching was not carried out in grid posts only but also in their surroundings. Thresholds for the correlation coefficient and the accuracy of least square matching were applied at the same time. Test C showed the importance of accurate orientation of images taken from a lower flying height. If images 1:5 000 are used for checking DTMs derived from laser scanning, only points where calculated corrections exceed a certain limit (e.g. 10 - 15 cm) should be revised. Applying corrections in other points does not bring any improvement and is not recommended due to remaining mismatches that might occur.

The tested method showed to be promising especially for 'smaller scale' images and DTMs. The degree of automation is very high. By its origin, it is a 'surface' method and a combination with other data sets is necessary for its restriction to bare earth points only. Blunders in matching must be eliminated e.g. by setting thresholds for similarity measures and applying the redundancy principle. Measuring of several check points is recommended in order to eliminate systematic errors due to orientation. In order to check an entire DTM, the method must be supplied by other measurements such as manual measurements in stereomodels or GPS measurements on the ground to cover areas where the automated procedure fails.

## ACKNOWLEDGEMENT

All the presented work was carried out at Aalborg University, Laboratory for Geoinformatics in cooperation with Prof. Joachim Höhle.

The work has also been supported by the research grant of the Ministry of Education, Youth and Sports, the Czech Republic, No. MSM 0021620831.

## REFERENCES

- Höhle, J., Potuckova, M., 2005, Automated Quality Control for Orthoimages and DEMs, *Photogrammetric Engineering and Remote Sensing*, Vol. 71, No. 1, pp. 81 - 87
- Norvelle, F. R., 1996, Using Iterative Orthophoto Refinements to Generate and Correct Digital Elevation Models (DEM's), In: *Digital Photogrammetry: An Addendum to the Manual of Photogrammetry*, American Society for Photogrammetry and Remote Sensing, pp. 151 - 155
- Potuckova, M., 2006, Image Matching and its Applications in Photogrammetry, Ph.D. dissertation, Czech Technical University in Prague, 132 p., in: *Working papers from the Department of Development and Planning*, Aalborg University
- Schenk, T., Suyoung, S., Csathó, B., 2001, Accuracy Study of Airborne Laser Scanning Data with Photogrammetry, *International Archives of Photogrammetry and Remote Sensing*, Vol. XXXIV-3/W4, pp. 113-118
- Skarlatos D., Georgopoulos, A., 2004, Automating the Checking and Correcting of DEMs without Reference Data, *International Archives of Photogrammetry and Remote Sensing*, Vol. XXXV/B2, pp. 553-558



# Application of a statistical test of hypothesis to check DTM accuracy over the Internet

**Zygmunt Paszotta, Malgorzata Szumilo**  
University of Warmia and Mazury in Olsztyn, Poland

## ABSTRACT

*This paper analyses automated checking of DTM quality. The method of automatic assessment of DTM accuracy is elaborated using an existing DTM and taking measurement on a stereo-pair of photos. Both data (DTM and Photos) are available as Test A materials. Statistical approaches for determining quality DTM are presented using a statistical test of hypothesis for this purpose. The article also describes an internet application based on a test of hypothesis, which determines whether existing, available DTM meet accuracy specifications sufficient for a user's requirements.*

## 1 INTRODUCTION

Currently, the Digital Terrain Model DTM has become a standard geospatial product. It can be used in the fields of civil engineering, surveying and mapping, land management and many others. Orthophoto (orthoimage), the most often-used photogrammetric product, is generated by means of a single photo (image) and a DTM. Thus, the DTM which users require should have appropriate quality (accuracy) for these applications.

The existing DTM may be good enough for some purposes, but as the demand for higher resolution and more accurate data rises, they cannot meet the requirement due to some errors introduced from the source data and production methods. On the other hand, some changes may occur in the terrain relief because of the natural erosion, earthquake and human activity. These changes should be reflected in the DTM and users should have tools for determining whether their DTM meets the specifications of the intended applications.

DTMs are generated in different ways: derived from contours lines of topographic maps, generated by automatic methods using aerial photos or satellite images or done by laser scanning. National Mapping Organizations often describe the quality of DTMs offered for sale by describing the sources of data origin, grid interval, the point density of the data set and the root mean square error (RMSE). The knowledge of these parameters is insufficient to determine if the existing DTM meets a client's needs.

In this paper, the authors not only propose an algorithm for statistical testing of the DTM accuracy, but also present an internet solution of the algorithm. The results of comparisons DTMs available in test A materials with a DTM derived by automatic photogrammetric measurements is also described.

## 2 THE MOST COMMON PARAMETER OF DTM QUALITY

The surface described by DTM,  $z' = \hat{f}(x, y)$ , is only an approximation of the genuine terrain defined  $z = f(x, y)$ . The error of the DTM is the difference between these above-mentioned surfaces, which can be calculated as following:

$$\Delta z = z - z'$$

$$d(x, y) = f(x, y) - f'(x, y)$$

The variance of the DTM error is defined as

$$\sigma^2 = \frac{1}{LX * LY} \int_0^{LX} \int_0^{LY} d(x, y) dx dy$$

In practice, the true terrain surface is unknown, thus the variance between the estimated and genuine terrain cannot be calculated. The common method of approximation  $\sigma^2$  is calculated with the difference between the elevation value of check points and the corresponding elevation value in the DTM as following

$$RMSE = \sqrt{\frac{\sum (z_i - z'_i)^2}{n}}$$

This estimator of the variance is known as Root Mean Square Error (RMSE) and is the dominant parameter in the DTM accuracy report. According to literature (Kraus 2004), the RMSE is not appropriate to report the error of the DTM. There are a lot of problems with the RMSE measure. The first one is the assumption that the error is the same everywhere in the area of the DTM; the RMSE is stationary over any single study area. Secondly, there is the assumption of no bias in the error.

DTM quality control can be done on different methods, such as point examination, visual checking, random sampling, join map checking (Zhu, Wei et al 2003), but in order to do this it is necessary to have a more accurate DTM covering the same area than the checked one.

### 3 DESCRIPTION OF THE PROPOSED METHOD

Quality measures can also be acquired through the analysis of the difference between two DTMs. Assume that we have two DTMs and they have the same dimensions, k rows by m columns, the difference between them can be calculated with the equation:

$$\Delta Z = Z_{DTM1} - Z_{DTM2}$$

The variance of  $\Delta Z$  is defined as

$$\sigma_{\Delta Z}^2 = \frac{1}{k * m} \sum_{i=1}^k \sum_{j=1}^m (\Delta Z_{i,j} - xs)^2$$

where  $xs$  is the mean difference between both compared DTMs.

$$xs = \frac{1}{k * m} \sum_{i=1}^k \sum_{j=1}^m \Delta Z$$

The value of  $xs$  corresponds to the mean error if one of the two DTMs takes the role of the check-points. In further considerations,  $xs$  will be used as the quality parameter of DTM.



Suppose that we want to know whether on the test area the mean error  $m$  of DTM is equal the assumed value of it -  $m_0$ . We have also a large sample of differences between the elevation value of check-points and the corresponding elevation value in the tested DTM. In order to check this assumption we have to create and carry out two tests of hypothesis.

First of all we have to check the sample size. According to central limit theorem, a random sample of  $n$  observation is selected from any population then when  $n$  is sufficiently large, the sampling distribution of  $xs$  (mean value) will be approximately a normal distribution. The larger the sample size,  $n$ , the closer the sampling distribution of  $xs$  is to a normal distribution. In our case, we will use the normal approximation for the sampling distribution of  $xs$  when the sample size is at least 30.

The next step is defined the elements of the test of hypothesis. It could be done as below

- $H_0$  – null hypothesis is  $m = m_0$ ,
- $H_A$  – alternative hypothesis is  $m > m_0$  (or  $H_A: m < m_0$ )
- Test statistic (a sample statistic used to decide whether to reject a null hypothesis):

$$u = \frac{xs - m_0}{\sigma_{xs}}$$

$$\text{where } \sigma_{xs} = \frac{\sigma_x}{\sqrt{n}} \approx \frac{s}{\sqrt{n}}$$

- Rejection region is  $u > u_\alpha$  (or  $u < -u_\alpha$  when  $H_A: m < m_0$ )

$u_\alpha$  is chosen by an analyst so that  $P(u > u_\alpha) = \alpha$

$\alpha$  is referred to as the level of significance

Now some points should be noted concerning the conclusions in the test of hypothesis. If the numerical value of the test statistic falls in the rejection region, we may reject null hypothesis  $H_0$  and conclude that the alternative hypothesis is true. The hypothesis-testing process will lead to this conclusion incorrectly only 100  $\alpha$  % of the time when  $H_0$  is true. On the other hand, if the test does not fall in the rejection region, it can be concluded that the sampling experiment does not provide sufficient evidence to reject  $H_0$  at the  $\alpha$  level of significance.

#### 4 PREVIOUS WORK

The test material contains two aerial photos (stereo-pair) on a 1:25000 scale. We received them in digital form with a pixel size of 21 $\mu$ m. The camera constants were 152,734 mm. The DTM derived by digital photogrammetry was available in text file form. From this data we interpolated and visualized one of the DTM used in our research (Figure 1).

The X,Y,Z co-ordinates of control points and their sketches were also included in the test material. It allowed all elements of stereo-pair orientation to be determined using ImageView software. Table 1 presents the elements of relative and absolute orientation. These data are essential to build a three-dimensional stereo-model, measure and transform all points' co-ordinates from pixel co-ordinate to the Danish co-ordinate system. After these preparations, the second DTM was generated using available photos and obtained data. (Figure 2).

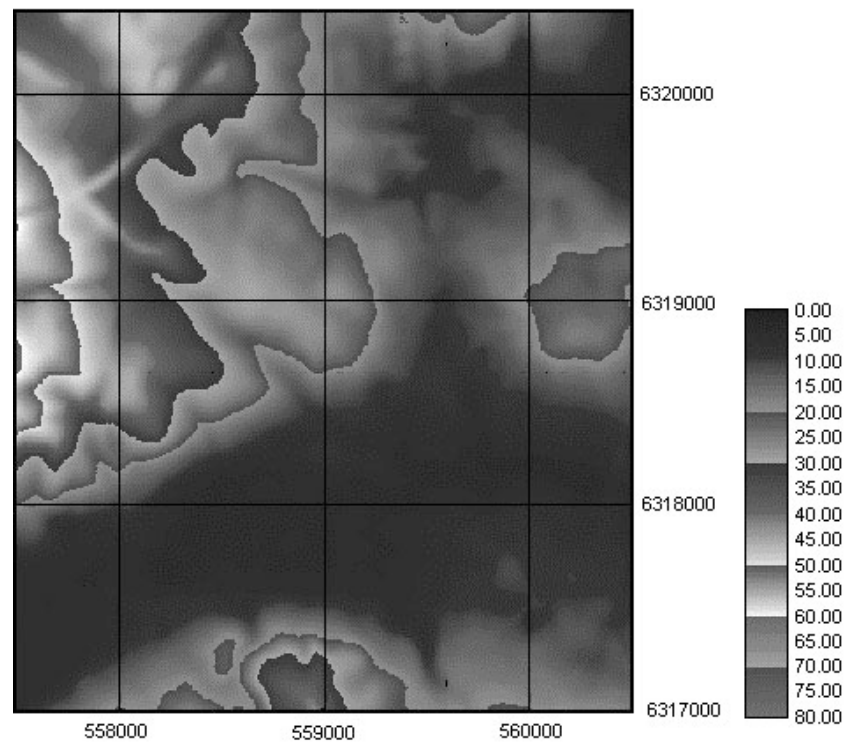


Figure 1 - DTM generated from photogrammetric data available in Test A material of the EuroSDR project.

Table 1 - Elements of relative and absolute orientation for stereo-pair 1526-1525

Elements of relative orientation		Elements of absolute orientation	
By	0.087121m	X <sub>0</sub>	558888,875m
		Y <sub>0</sub>	6317990,262m
Bz	0.001017m	Z <sub>0</sub>	29,82m
		$\lambda$	2173,47
$\omega$	0,00957893 (rad)	$\varphi$	-0,1082098 (rad)
$\varphi$	0,0129089 (rad)	$\omega$	0,0350755 (rad)
$\kappa$	-0,022194 (rad)	$\kappa$	0,0873882 (rad)

Then, with two DTMs covering the same area, the differences between them were calculated. The results of computations are shown in figure 3. The mean value of difference amounted to 0.28 m, the standard deviation of the difference was 1,48 m. The maximum and minimum equalled 18.77m and -14,12 m correspondingly. The distribution of the differences was also checked. This test confirmed the authors' presumption that the difference between the compared DTMs is a random variable and its distribution is a normal distribution. It means that all statistical methods could be applied to this data set.

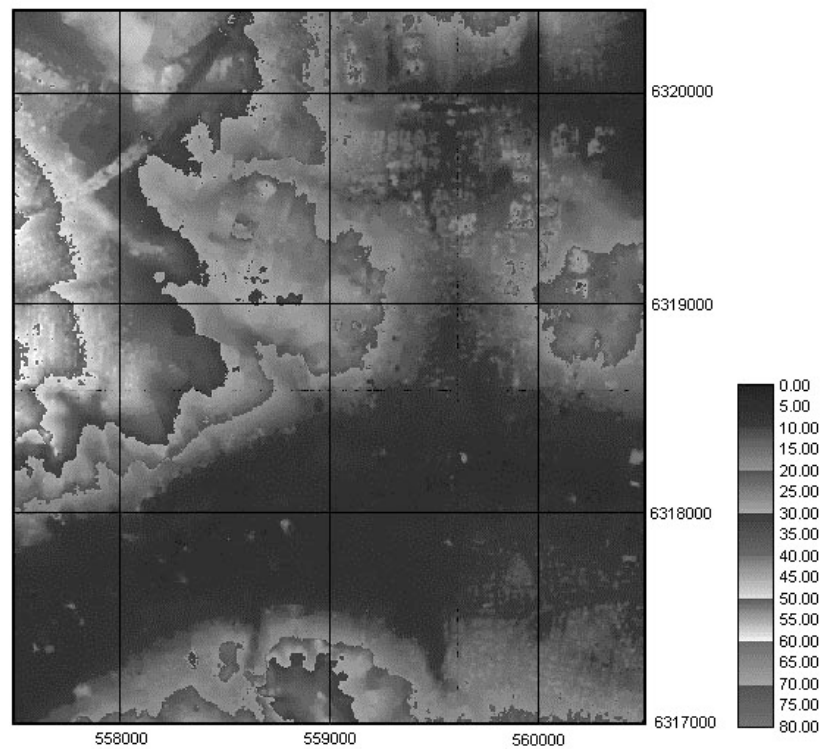


Figure 2 – DTM generated from photogrammetric data, which was measured automatically.

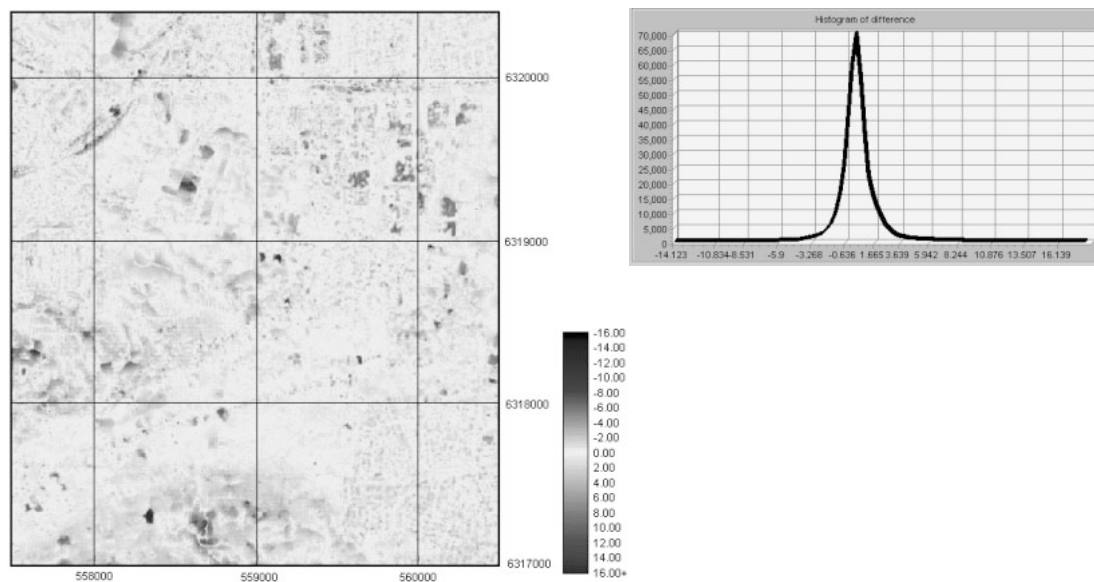


Figure 3 – The differences between two compared DTMs and their distribution.

## 5 THE INTERNET SOLUTION OF THE ALGORITHM

This part of the article presents the internet tool for the DTM and its quality control. Practical application of the proposed above algorithm is based on the system of a central unit - a server of applications and Internet pages and client computers equipped with standard Internet browsers (e.g. Internet Explorer, Netscape, Opera). Clients communicate with the server through a web page and the server provides its photogrammetric resources to clients.

Images and their orientation parameters, which were previously determined, are stored on the server. In order to obtain the necessary photograph fragment, the user determines its centre, the size of the fragment and the pyramid level. These parameters, together with the user login, are sent by the applet to the server. Next, on the server images in the BMP format from the advisable pyramids level can be found in a catalogue, unavailable through the Internet, and they are transformed in JPEG format. All data – images and orientation parameters of these photos – are sent back to the client. The user is now able to automatically measure the point for the DTM built. As a method of homologous point determination applied in this solution, the authors use the method of area matching. The measure of similarity between pixel sets is the coefficient of correlation, calculated in the JAVA applet on the client side.[Paszotta 2000] In addition, the user has the possibility of defining the magnitude of the correlation.

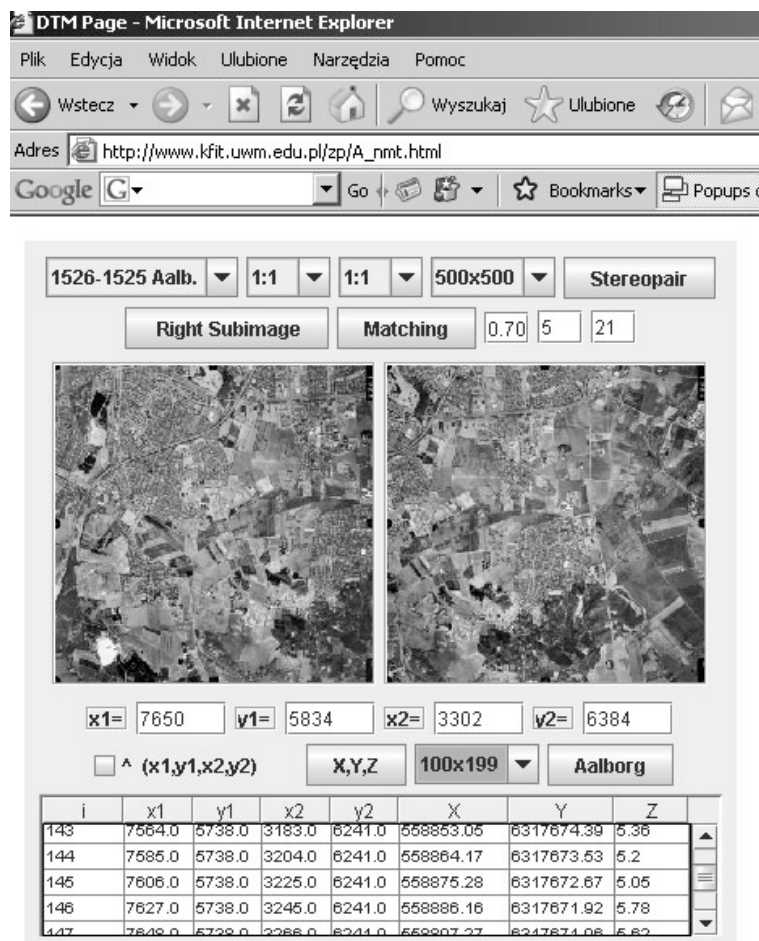


Figure 4 - Aerial photograph in the JAVA applet on the Web.

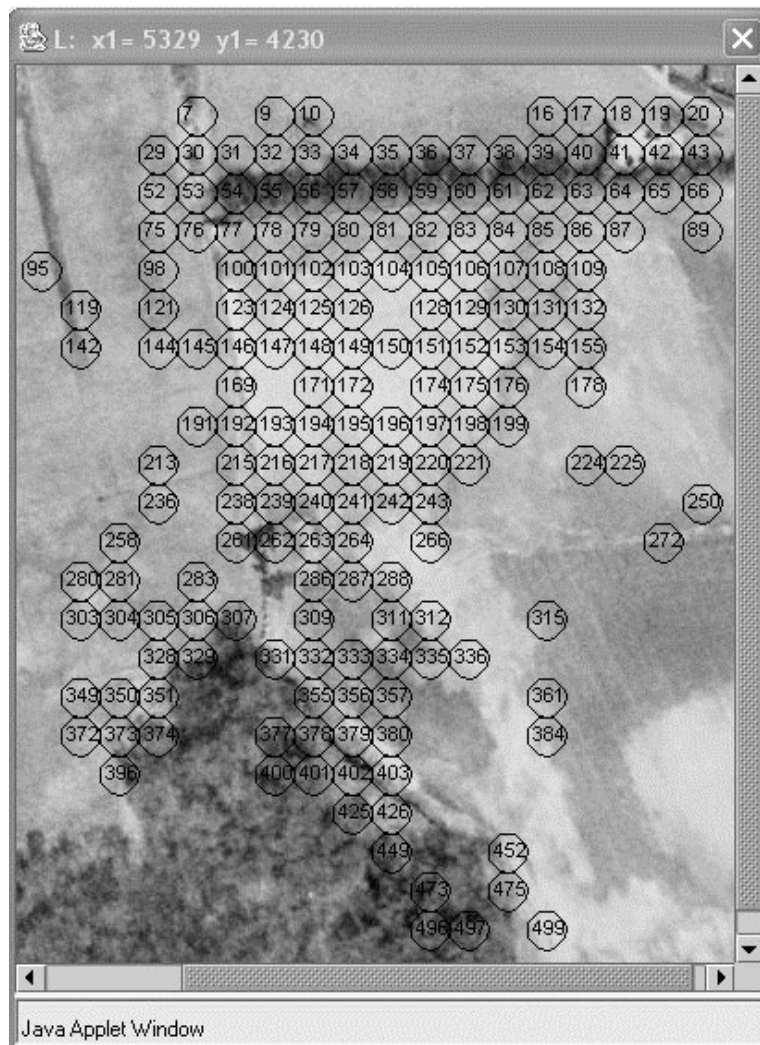


Figure 5 – Results of automatic measurement of homologous points.

The software applied in browsers not only presents photographs and determines co-ordinates, but can also compare results of measurement with the referencing DTM, which is provided at the same time as the images and their orientation parameters. The Z co-ordinates of points that were measured by user is compared with a Z co-ordinate of the same points determined based on the referencing DTM, which is designed for checking the quality of the newly generated DTM. The system then automatically calculates the differences between Z co-ordinations and all statistics (mean value and standard deviation). The client is now able to carry out two test of hypothesis and check if the new DTM, generated by himself/herself, meets the quality specification. On the other hand, this application can check whether the available (referencing) DTM is appropriate enough for user's needs, based on the new measurement of the homologous points.

At present, the system is employed at the Department of Photogrammetry and Remote Sensing, University of Warmia and Mazury in Olsztyn. All users using a browser can perform the following tasks:

- choose any fragment of a photograph from any level of a photograph pyramid,
- determine the pixel coordinates of homologous points and match them automatically,

- determine the coordinates of a point in a Danish coordinate system,
- compare Z co-ordinates from new automatic measurements and from referencing DTM,
- check whether the DTM meets the quality specification through a test of hypothesis

The above functions are performed by means of HTML elements, using JAVA applets and servlets.

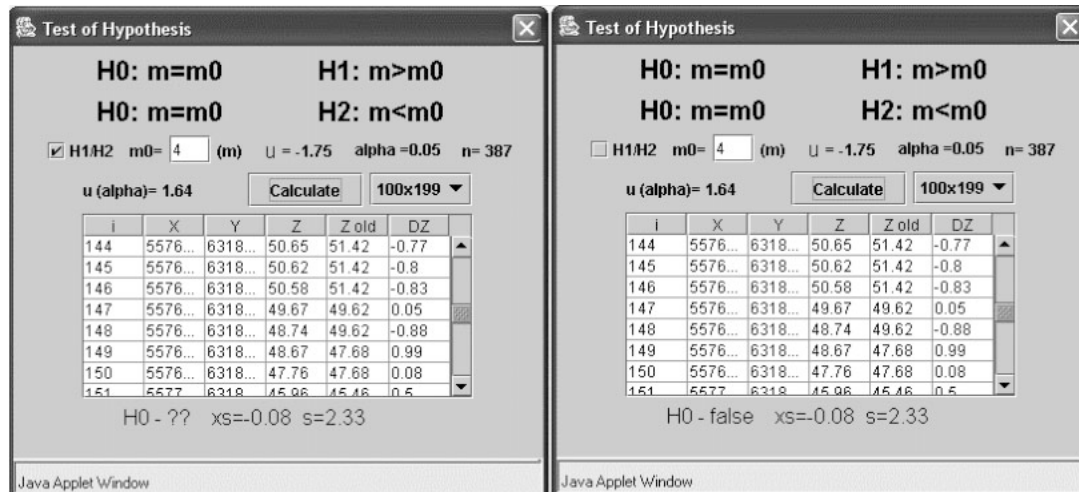


Figure 6 – Example of test of hypothesis.

## REFERENCES

- ACKERMANN, F., 1996, *Technique and strategies for DEM generation*. Digital photogrammetry: an addendum to the manual of photogrammetry. American Society for Photogrammetry and Remote Sensing, 135-141
- FISHER, P., 2003, *Data quality and uncertainty: ships passing in the night*. The second international symposium on spatial data quality 2003, Hong Kong
- [KRAUS K., 2004 *Quality measures for Digital Terrain Models*, XX<sup>th</sup> Congress International Society for Photogrammetry and Remote Sensing, Istanbul 12-23 July 2004
- MAURE, D, 1996, *Introduction to Digital Elevation Models*. Digital photogrammetry: an addendum to the manual of photogrammetry. American Society for Photogrammetry and Remote Sensing, 131-134
- SCHENK, A. 1996 *Automatic generation of DEM's*. Digital photogrammetry: an addendum to the manual of photogrammetry. American Society for Photogrammetry and Remote Sensing, 145-151
- SITEK Z. 1990, *Fotogrametria ogólna i inżynieryjna*, Warszawa
- PASZOTTA, Z., 1999, *Matching Orthoimages and Direct Method Determining Exterior Orientation Elements*, OEEPE.s Official Publication nr. 36, ISSN 0257-0505, pp. 145-150.
- PASZOTTA, Z., 2000, *Method of Exterior Orientation of Aerial Images by Matching Orthoimages*. Dissertations and Monographs 28, University of Warmia and Mazury in Olsztyn, ISBN 83-88343-79-3.
- ZHU Z., Y. WEI, 2003, *Research on methods of DEM quality control*. The second International Symposium on Spatial Data Quality, Hong Kong.

# The Czech Method of DTM Checking

Radek FIALA<sup>1</sup>

Jiří ŠÍMA<sup>2</sup>

## ABSTRACT

*This paper describes a robust DTM quality evaluation method originally used for checking of official DTM created by Czech National Mapping Agency. The method has been applied both to 25 m DTM grid acquired by digital photogrammetric measurement and 10 m DTM grid derived from the Danish topographic map with 5 m contour interval. For comparison a DTM created by automatic image correlation has been also evaluated. As a result, 12 % of the checked area in case of the 25 m DTM and up to 19 % in case of the 10 m DTM has been found to contain gross errors. However, both DTMs are fit for orthophoto production at scale 1:10 000.*

## 1 INTRODUCTION

The goal of this paper is a brief description of the Czech method of DTM quality checking which has been applied to robust accuracy evaluation of the official DTM ZABAGED in the Czech Republic. This model has been created by the National Mapping Agency at the whole state territory within the period 1994–2000. It has the form of a 3D contour model originated from digitized 2 m contours of the State topographic map on scale 1 : 10 000. As a standard the contour large scale maps (1 : 2000, 1 : 1000) served for comparison. They were at disposal in many localities scattered at 10 % of the state territory. Their contour interval is 1 m and the accuracy of altimetry is approx. 3 times higher than that of the ZABAGED. The principle of the Czech method of DTM checking consists in superimposing of both TINs (ZABAGED and large scale map) at the same check area, computing of height differences and statistical evaluation of their propagation.

## 2 PROCESSED DATA AND ESTIMATION OF HEIGHT MEASUREMENT ACCURACY

The Czech method of DTM checking has been applied at the Photogrammetric Laboratory of the University of West Bohemia in Pilsen to data provided by the Aalborg University within the bounds of the EuroSDR project „Automated checking of DTMs“ (namely to „A“ and „B“ data sets). As a standard the CZMAN DTM, created by „manual“ digital photogrammetric measurement of typical spot heights and terrain break lines, has been used. Another CZCOR has been created by automatic image correlation as a regular 5 m grid using the ERDAS software. The corresponding DKA25 DTM (25 m grid acquired by digital photogrammetric measurement) and DKB10 DTM (10 m grid derived from the Danish topographic map with 5 m contour interval) have been used from data provided by the Danish organizer. Known parameters of obtained digital aerial photographs made it possible to estimate the relative (internal) accuracy of spot height measurement using our own and other experience from abroad.

---

<sup>1</sup> Assistant, Faculty of Applied Sciences, Department of Geomatics, University of West Bohemia in Pilsen. e-mail: fialar@kma.zcu.cz

<sup>2</sup> Senior Lecturer, Faculty of Applied Sciences, Department of Geomatics, University of West Bohemia in Pilsen. e-mail: simaj@kma.zcu.cz

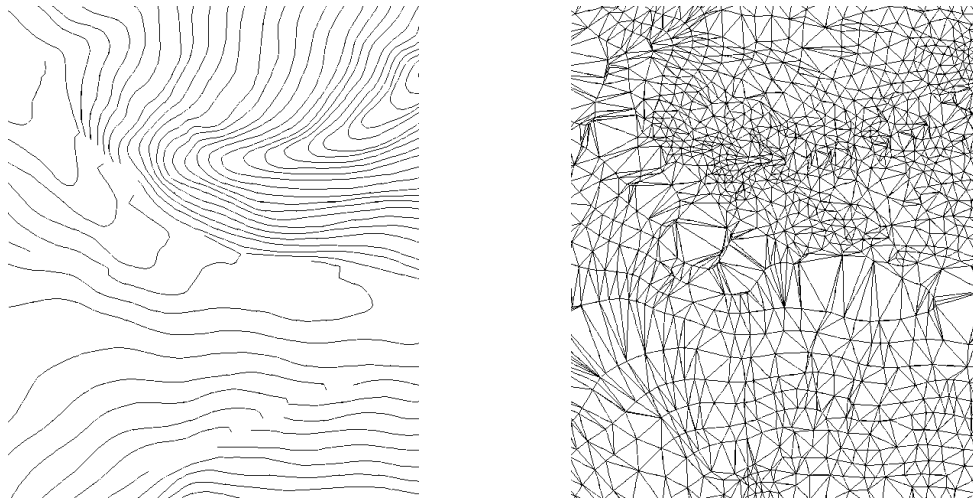


Fig. 1 3D contour DTM ZABAGED and its TIN

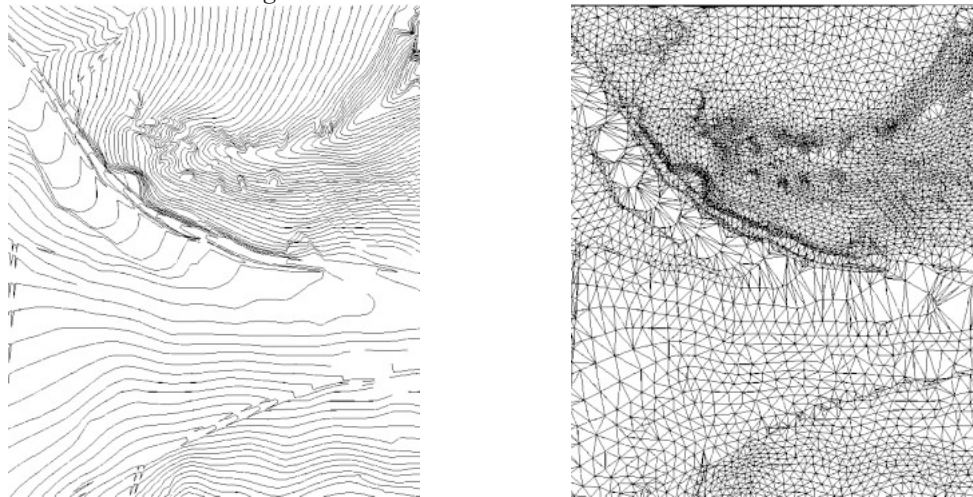


Fig. 2 3D contour DTM of a large scale map and its TIN

stereo pair	No 1526 – 1525
image scale	appr. 1 : 25 000
focal length	$f = 152.734 \text{ mm}$
flight height	$h = \text{appr. } 3820 \text{ m}$
relative (internal) accuracy of spot height measurement	$\sigma_z = 0.010 \% h = 0.38 \text{ m}$

Table 1 Parameters of digital photogrammetric measurement

20 ground control points within the stereo pair were supplied by the Danish organizer. 12 of them showed the best results of absolute orientation (they were considered as control points), 5 other points were considered as check points. 3 points were excluded because of significant deviations of coordinates exceeding 3 multiples of the standard deviation derived from parameters of digital photogrammetric measurement (Table 1). The results of absolute orientation, computed by means of ERDAS software (Table 2), showed minimal systematic errors of coordinates of 12 selected control points and also very favourable mean square errors. Analogous results concerning the check points were less



satisfactory but still within the limits of the digital photogrammetric measurement of aerial photographs on scale 1 : 25 000.

number of control points used	12
root mean square errors of residuals	
mZ = 0.338 m    mX = 0.130 m    mY = 0.147 m	
mean values of residuals (systematic errors)	
sZ = 0.000 m    sX = -0.009 m    sY = 0.002 m	
control points excluded	
15 (y,z), 612523 (z), 612524 (x)	
number of check points used	5
root mean square errors of residuals	
mZ = 0.451 m    mX = 0.239 m    mY = 0.194 m	
mean values of residuals (systematic errors)	
sZ = 0.275 m    sX = -0.081 m    sY = 0.122 m	

*Table 2 Results of absolute orientation*

The total (external) accuracy of spot height measurement has been derived provided that the height accuracy of control and check points attained by their preceding geodetic measurement or aerotriangulation with the aerial photographs on scale 1 : 25 000 has reached 0.10 m. Using the law of error propagation we got the value of the total (external) accuracy of the photogrammetric height measurement represented by the root mean square error (RMSE):

$$\begin{aligned} \text{RMSE} &= (\sigma_Z^2 + m_{AO}^2 + \sigma_G^2)^{0.5} \\ &= (0.38^2 + 0.34^2 + 0.10^2)^{0.5} = 0.52 \text{ m} \end{aligned}$$

The gross (evident) error has been considered as larger than 3 RMSE, that is  $\pm 1.56$  m.

### 3 EVALUATION OF HEIGHT DIFFERENCES

The Czech software ATLAS DTM makes it possible to determine height differences  $\Delta Z$  between standard and checked DTMs so that for each node of the first TIN (e.g. CZMAN) a height of corresponding points on the same perpendicular is interpolated in the second TIN (e.g. DKA25) and vice versa (see *Fig. 3*).

SW „ATLAS DTM“ computes the volume of a model shaped by positive height differences (Vol<sub>+</sub>) and of another model shaped by negative height differences (Vol<sub>-</sub>). The common area of both standard and checked DTMs is also computed.

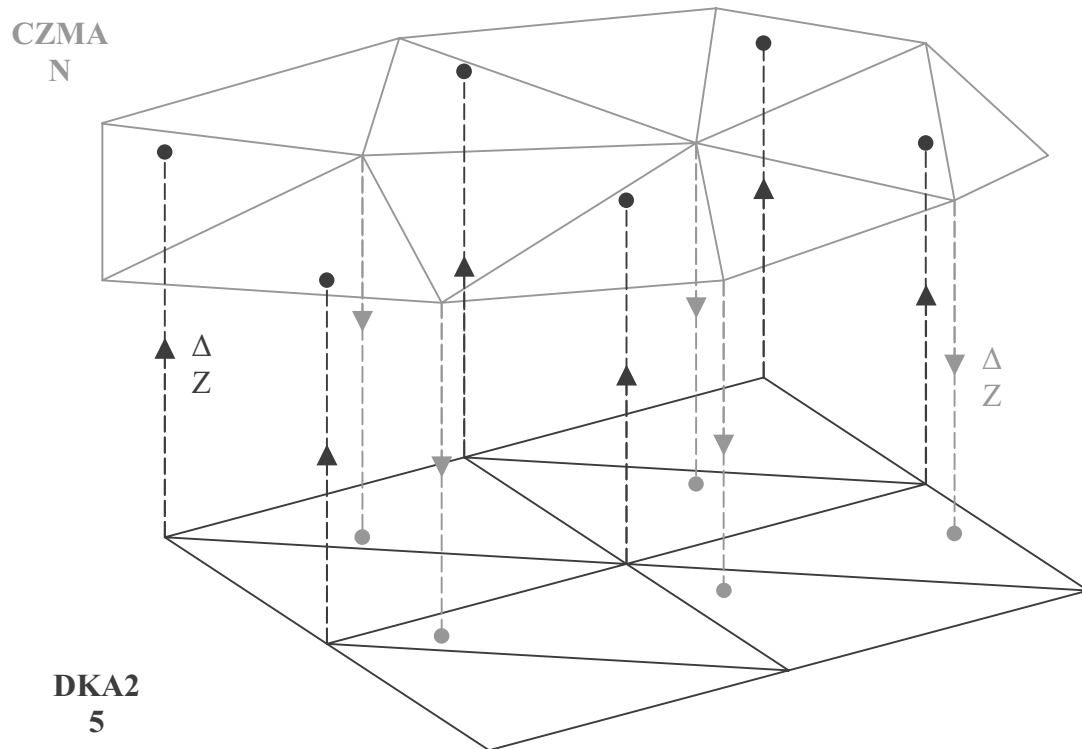


Fig. 3 SW „ATLAS DTM“ – Computation of height differences

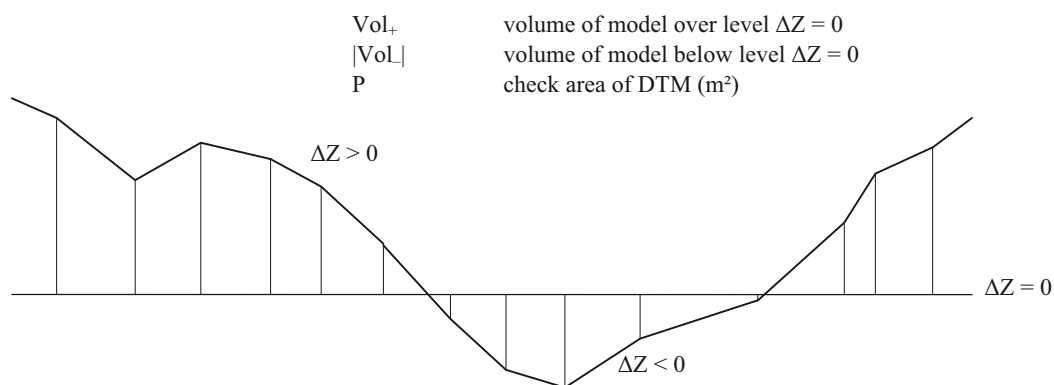


Fig. 4 Volume and check area computation

The accuracy evaluation of the checked DTM (for instance DKA25) has been realized by computing the **average error**  $a_Z$  (average of absolute values of height differences taken into consideration) and the **systematic error**  $s_Z$  (mean value of all positive and negative height differences). According to the theorem of adjustment calculus the **root mean square error**  $m_Z$  can approximately be estimated as 1.25 multiple of the average error.

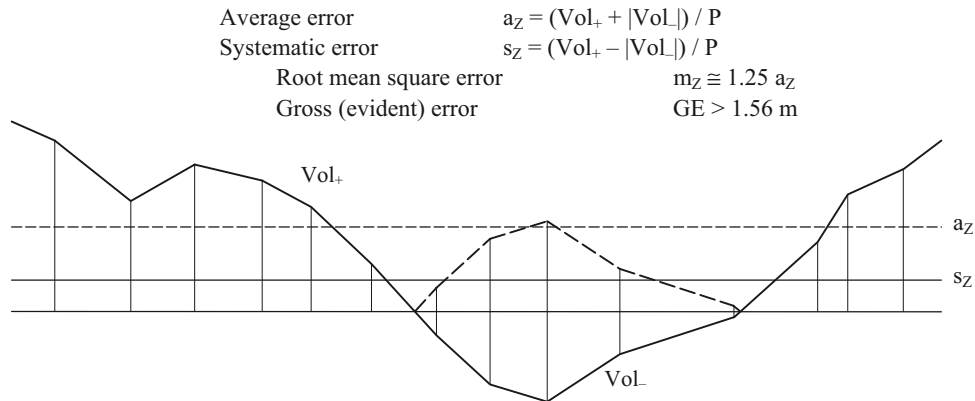


Fig. 5 Accuracy evaluation of DTM

#### 4 RESULTS

For each DTM checked by the Czech method a new model of height differences has been created over the check area. If the part of **checked DTM** is situated **higher** the height difference is **positive** and will be represented by a **red colour density** corresponding to the real value of the height difference. **Negative** differences will be represented in **blue color** by the same method. 1 m „contours“ of height differences have been constructed for better understanding of the graph. For the distribution of  $\Delta Z$  for the case of DKA25 DTM evaluation (check area IV) see in *Annex 1*. Gross (evident) errors larger than  $\pm 1.56$  m (positive in red, negative in blue on the orthophoto background) see in *Annex 2*.

The results of the DTM accuracy evaluation in *Table 3* are relevant to Check areas II and IV as defined by the Danish organizer. This table presents the values of systematic, average and root mean square errors resulting mainly from computations by the ATLAS DTM software. Both DKA25 and DKB10 DTMs are fit for orthophoto production on scale 1:10 000. DTMs created by automatic image correlation must be modified in the sites with buildings and dense vegetation cover.

DTM	Check area	$s_z$ (m)	$a_z$ (m)	$m_z$ (m)	n	$\Delta Z_{\max}$ (m)	$P_G/P$ (%)
DKA25	II	0.996	1.016	1.270	4 016	4.81	12.5
	IV	0.801	0.947	1.183	17 953	8.90	11.8
DKB10	II	0.686	0.846	1.057	9 392	3.79	12.7
	IV	0.710	1.054	1.318	43 952	9.71	19.1
CZCOR	II	0.930	1.039	1.299	16 232	5.13	19.4
	IV	0.907	1.035	1.294	68 349	11.23	19.3

Explanations:

$s_z$  systematic error (mean value of all positive and negative height differences within the Check areas II and IV)

$a_z$  average error (average of absolute values of height differences within the Check areas II and IV)

$m_z$  complete root mean square error (containing also systematic component)

n number of height differences

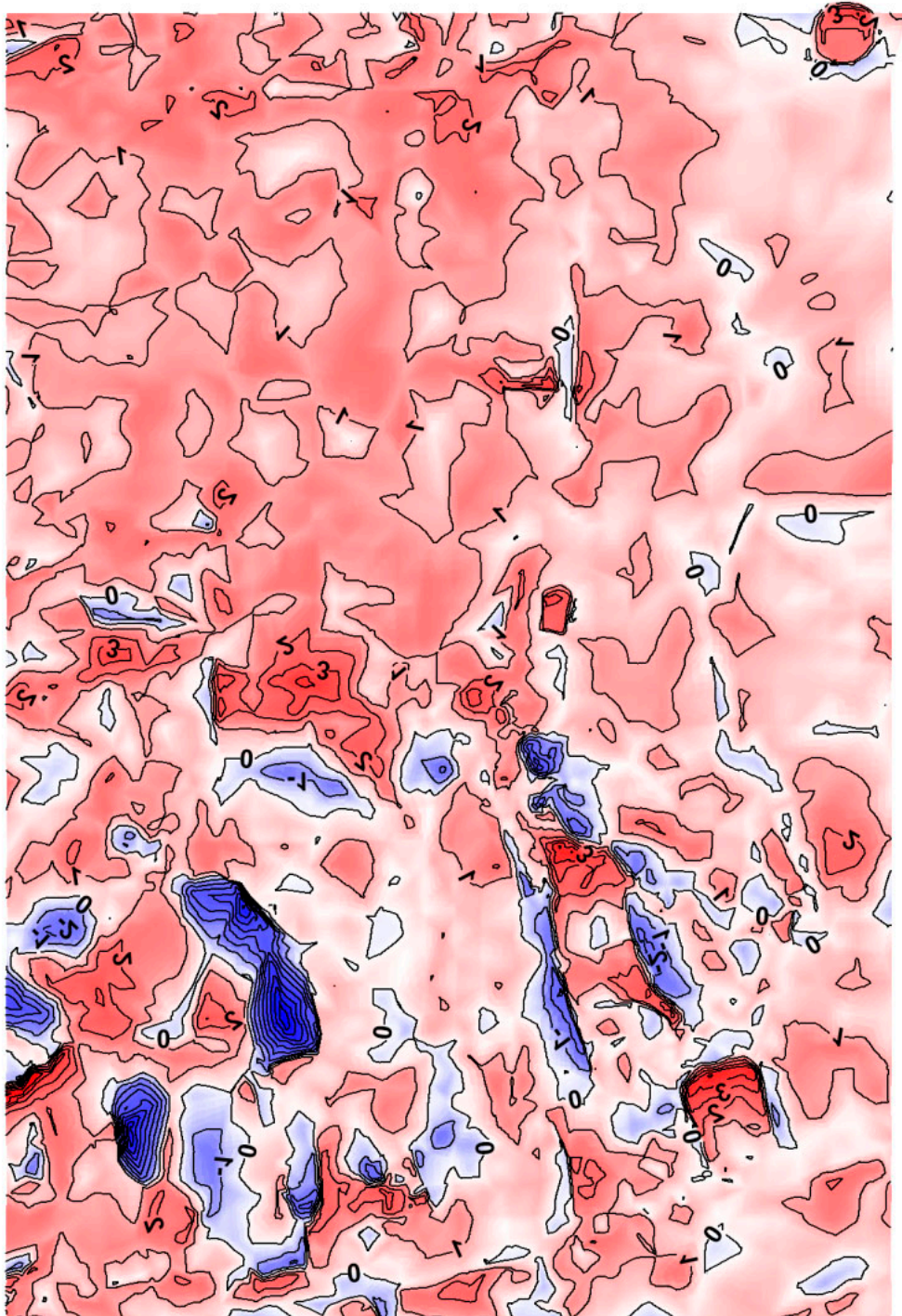
$P_{GE}$  part of the Check area containing height differences larger than  $\pm 1.56$  m

*Table 3 Results of DTM accuracy evaluation*

## 5 CONCLUSION

The reasons of gross errors occurrence may be found in following typical situations:

- DKA25 and DKB10 DTMs contain spot heights outside the forest periphery only. CZMAN DTM registers as many random spots heights in clearings inside the forest as possible.
- DTMs with regular grids (25 m, 10 m) cannot represent reliably the terrain break lines. CZMAN DTM registers all significant natural and artificial terrain break lines in a special layer.
- Some recent changes in terrain (progressive excavations in sandpits and quarries, new roads, new settlements), which happened between creating the evaluated DTMs and taking the aerial photographs, are obvious.



**Annex 1. Height differences DKA25 DTM minus CZMAN DTM**





**Annex 2. Gross errors (larger than  $\pm 1.56\text{m}$ ) of DKA25 DTM**

# QUALITY CONTROL OF DIGITAL TERRAIN MODELS USING DIFFERENT AUTOCORRELATION TECHNIQS

**T. Jancso**

Department of Photogrammetry and Remote Sensing, College of Geoinformatics, University of West Hungary

H-8000, Szekesfehervar, Pirosalma u. 1-8. , Hungary

e-mail: t.jancso@geo.info.hu

and

**J. Zavoti**

Geodetic and Geophysical Research Institute, Hungarian Academy of Sciences

H-9400, Sopron, Csatkai u. 6-8., Hungary

e-mail: zavoti@ggki.hu

**KEY WORDS:** stereo-pairs, space resection, gross error detection, cross-correlation, median difference filter

## ABSTRACT

*The paper demonstrates modified cross-correlation methods to detect height errors of DTM points based on stereo-pairs of aerial images. The usual cross-correlation method is extended using dynamic dimensioning and different structures of the correlation matrix. Also a texture coefficient is introduced which makes the auto-correlation procedure more robust. Before starting the cross-correlation procedure the accuracy of the exterior orientation elements is checked by application of a direct analytical space resection in conjunction with effective gross-error detection. Also as a separate method the paper points at the importance of examination of the possibilities of the median difference filter for detection of "sensitive" areas on the digital terrain models as a method to visualize and separate the areas where more thoroughly checking procedures would be necessary. Also some experimental results are demonstrated which were produced by a software application especially developed for the checking of DTM points.*

## 1 INTRODUCTION

### 1.1 Aims

There is given a stereo-pair made by a RMK TOP aerial frame camera. We have control points covering the whole image area. The DTM of Test area A was produced on a digital photogrammetric workstation ImageStation Z/I imaging with a grid spacing of 25 m. Our goal is to check automatically the DTM points, especially the height errors. The expected ideal height accuracy can be derived mainly from the assumption that the derived heights of a single point correspond to 0.01% of the flying height, which for the Test areas A and B means an expected height accuracy of approx.  $\sigma = 40$  cm. In this case - following the usual gross-error theory - our aim is to detect and allocate the points where the height error is larger than  $3-5 \sigma$ . To detect the height errors there a series of extended area-based image-matching techniques have been applied based on the well-known cross-correlation formula.

## 1.2 Procedure

The whole procedure is summarized in Figure 1. In this figure we separate the input data and the procedures derived from them. On the procedure list the checking of horizontal parallaxes is divided into two parts, although here we could mention the feature-based matching, but this method is not part of the present paper.

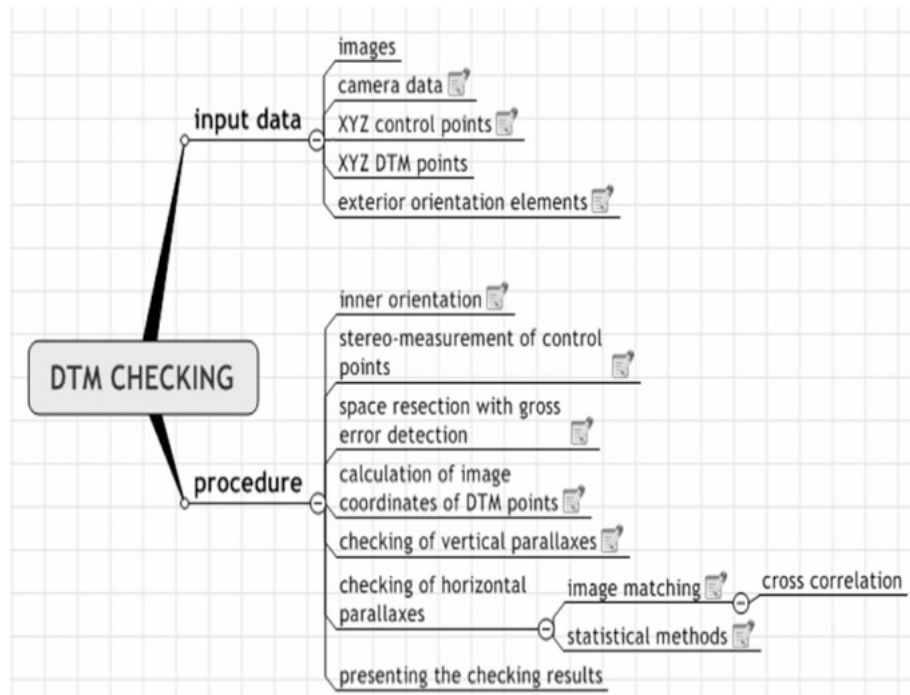


Figure 1. DTM checking procedure

We have the following input data:

- Images used at Test A and Test B
- Camera data
  - calibrated focal length
  - image coordinates of fiducial marks
- List of XYZ coordinates of control points
- List of XYZ coordinates of DTM points
- Exterior orientation elements of left and right images

*We can add the following comments on the procedure steps:*

### - Inner orientation

It includes the following:

1. Measurement of fiducial marks (registration of pixel coordinates)
2. Affine transformation
3. Storage of the affine transformation parameters



This orientation can be done on any digital photogrammetric workstation. For example on a Leica LPS system.

**- Stereo-measurement of control points**

The goal is to measure and register the image coordinates of control points. These image coordinates together with the XYZ coordinates are necessary to carry out the space resection, for which we also need to use the calibrated focal length.

**- Space resection with gross error detection**

See more details in [Jancso 2004].

**- Calculation of image coordinates of DTM points**

The calculation is made by the collinear equations. It also means, that later the image coordinates of the same DTM point can be calculated twice on one image, since the image coordinates can be calculated by the given exterior orientation elements and also by the exterior orientation elements derived from the space resection.

**- Checking of vertical parallaxes**

Checking the residual  $dp_y$  parallax we can determine the points which were measured with wrong stereoscopic matching. To calculate  $dp_y$  we should calculate first the theoretical image coordinate  $y''^0$  of the normal image:

$$y''^0 = \frac{\begin{vmatrix} b_x & b_y & b_z \\ \bar{x}''^0 & \bar{y}''^0 & \bar{z}''^0 \\ \bar{x}' & \bar{y}' & \bar{z}' \end{vmatrix}}{\begin{vmatrix} b_x & b_y & b_z \\ \bar{x}' & \bar{y}' & \bar{z}' \\ r''_{12} & r''_{22} & r''_{32} \end{vmatrix}} \quad (1)$$

Notations:

$b_x, b_y, b_z$  : basis components of  $O_1O_2$  basis

$\bar{x}', \bar{y}', \bar{z}', \bar{x}'', \bar{y}'', \bar{z}''$  : model coordinates of  $P', P''$  image points

$r''_{12}, r''_{22}, r''_{32}$  : rotation matrix elements at the right image

$\bar{x}''^0, \bar{y}''^0, \bar{z}''^0$  : theoretical model coordinates of  $P''$  (condition is  $y'' = 0$ )

**- Checking of horizontal parallaxes by image matching**

We can distinguish two approaches for image matching:

1. Image matching means matching of left image points  $x', y'$  to the right image. The search area on the right image is determined by the location of the right image point  $x'', y''$  calculated from the back projection by the collinear equations. After the image matching we gain

a new image point on the right image ( $x''_{new}, y''_{new}$ ). Comparing  $x'', y''$  with  $x''_{new}, y''_{new}$  we can calculate  $dx$  and  $dy$ . The point P is wrong if the differences are over the gross-error limit (usually  $3-5 \sigma$ ) (Figure 2).

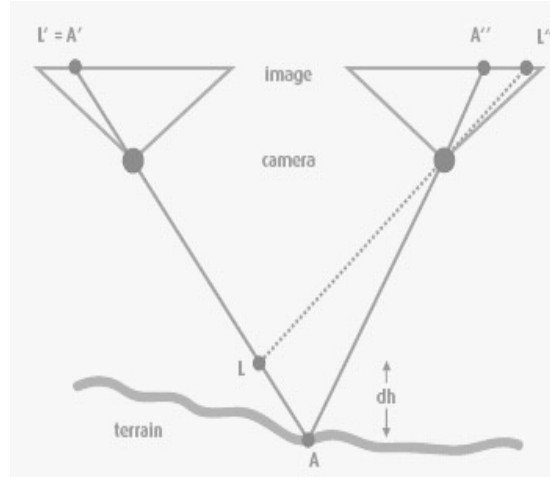


Figure 2. Back projection method, where the left image point is fixed

2. At the checking of DTM points we can follow the way where the X,Y coordinates of the examined DTM point are fixed, and the appropriate back-projected points are calculated at different Z coordinates. This procedure assumes to have the area based image matching several times and we will choose that Z coordinate where the cross-correlation coefficient reaches the maximal value. After this we can calculate the difference of Z coordinates comparing the original Z coordinate of the DTM point with the gained Z coordinate corresponding to the maximal cross-correlation coefficient (Figure 3) [Schenk 2001].

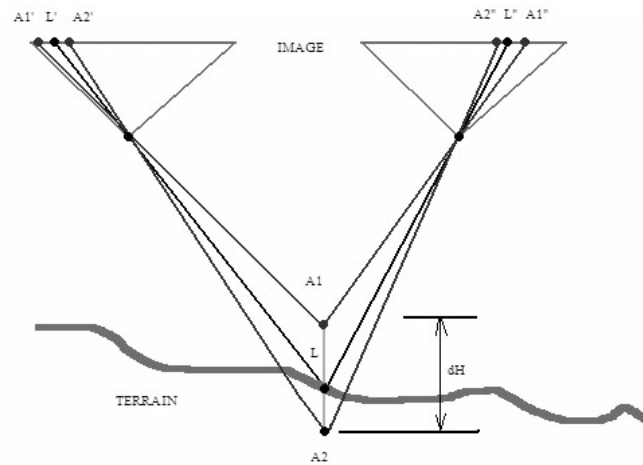


Figure 3. Back projection method, where the DTM X,Y is fixed

### - Statistical methods

The "statistical methods" means the examining the neighbouring DTM points ( $P_i$ ,  $i=4,8,16$  or  $24$ ) at a certain DTM point  $P$ . Based on the surrounding points we extrapolate the point  $P'$ . Comparing it with  $P$  we can calculate the  $dZ$  differences at each point. Based on the differences we do a statistical procedure to find the probable outliers. As a good example the median difference filter can be used effectively.

## 2 CHECKING OF THE EXTERIOR ORIENTATION ELEMENTS

### 2.1 Space resection

Before starting to check the DTM points we should check the control points. If a gross error exists among the control points and the exterior orientation elements were calculated by the control points, then we should check and revise the exterior orientation elements as well, since these errors cause absolute positional errors in the DTM points. A new adjustment and gross-error detection method was applied on control points based on the Jacobian Mean Theorem. The main core of this theorem is that the adjusted values of exterior orientation elements can be calculated from the weighted mean values of solutions from a minimally necessary number of control points and it is done in every combination. For the space resection we need at least three control points (Points  $A, B, C$ ) as it is shown in Figure 4.

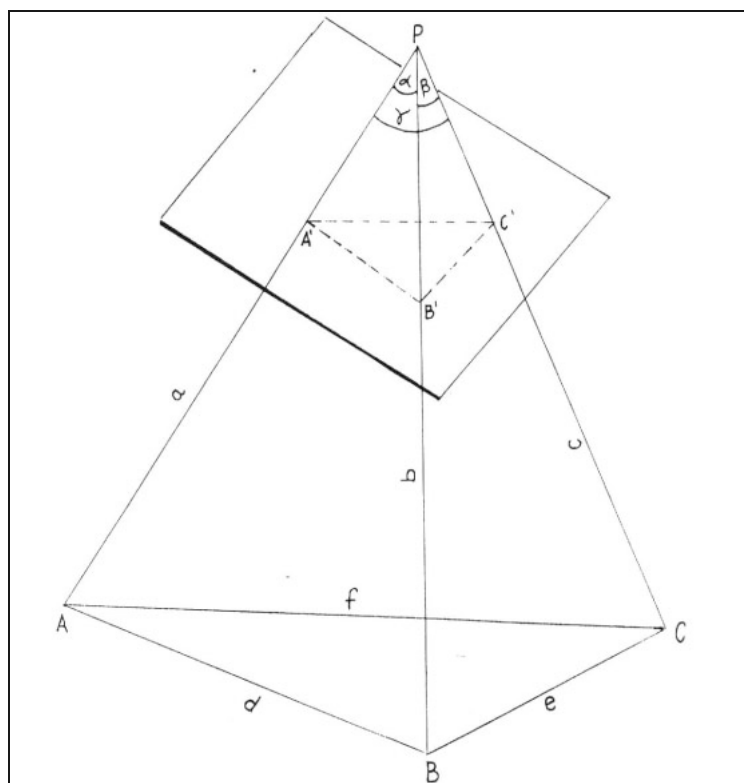


Figure 4. Space resection using three control points

We calculate the adjusted values of unknowns by the Jacobian Mean Theorem as follows:

$$X = \left( \sum P_i \right)^{-1} \times \sum (P_i L_i) \quad \text{or} \quad X = Q_{xx} \times \sum (P_i L_i) \quad \text{where} \quad L_i = \begin{bmatrix} X_i \\ Y_i \\ Z_i \end{bmatrix} \quad (2)$$

and it contains the solutions from each group (combination) consisting of three control points. The whole procedure can be followed in [Jancso 2004].

## 2.2 Comparison of the exterior orientation elements

As an alternative checking method the exterior orientation was carried out on a Leica LPS DPWS system. Three different tests were made.

1. The given exterior elements were set in LPS and the control points were measured by manual stereo-measurement. Based on this image coordinates applying the collinear equations the geodetic coordinates of control points were calculated and compared with the given X,Y,Z coordinates. The RMS values and residuals on the control points were calculated as follows:

mX	mY	mZ	[m]
0.5410	0.4827	0.3363	
Max. residuals of Control Points [m]			
No.	rX	rY	rZ
2	0.4899	0.1852	-0.8845
9	-0.6086	1.1544	-0.3524
524	-1.9588	-1.3449	-0.1164
525	0.4564	-0.4892	-0.4120

Table 1. RMS and max. residuals based on the given exterior orientation elements

2. Here we used the given exterior orientation elements (EOE) as initial values for the space resection carried out on the Leica LPS. In Table 2 we can notice that the RMS values become slightly better, but these errors are still far from the expected RMS values.
3. Here we used the given exterior orientation elements (EOE) as initial values for the space resection carried out on the Leica LPS, but in this case we omitted the points 9, 524, 525. In Table 3 we can see that the RMS values are very close to the expected RMS values of RMS\_X=0.10 m, RMS\_Y=0.11 m, RMS\_Z=0.16 m.

Also the space resection was made by the direct method described in [Jancso 2004]. In Table 4 we can compare the results with the RMS values indicated in Table 3.

The exterior orientation parameters						
image ID	Xs	Ys	Zs	OMEGA	PHI	KAPPA
1526	557846.0391	6318015.9213	3886.0353	-2.2280	1.4049	195.9758
1525	560141.8591	6318070.5686	3856.6372	-1.6780	0.5390	194.5252
The accuracy of the exterior orientation parameters						
image ID	mXs	mYs	mZs	mOMEGA	mPHI	mKAPPA
1526	0.7743	0.6332	0.3242	0.0080	0.0120	0.0038
1525	0.7447	0.7029	0.3493	0.0087	0.0115	0.0042
mX	mY	mZ				
0.4833	0.4329	0.3260				
Max. residuals of Control Points						
No.	rX	rY	rZ			
2	0.2833	0.4540	-0.6817			
9	-0.1052	1.1112	0.0641			
524	-1.7571	-1.1342	0.0087			
525	0.7446	-0.1691	-0.0984			

The exterior orientation parameters						
image ID	Xs	Ys	Zs	OMEGA	PHI	KAPPA
1526	557846.2262	6318015.1645	3886.0708	-2.2179	1.4093	195.9766
1525	560142.4973	6318069.9771	3856.3137	-1.6703	0.5506	194.5235
The accuracy of the exterior orientation parameters						
image ID	mXs	mYs	mZs	mOMEGA	mPHI	mKAPPA
1526	0.3454	0.2951	0.1325	0.0039	0.0053	0.0017
1525	0.3625	0.3086	0.1810	0.0038	0.0056	0.0019
mX	mY	mZ				
0.1790	0.2001	0.2882				

Table 3. RMS and max. residuals based on the given EOE not including the points 9,524,525

image ID	Xs	Ys	Zs
1526	557846.212	6318015.068	3886.066
1525	560142.622	6318070.216	3856.245
<b>DIFFERENCES TO THE RMS VALUES OF TABLE 3.</b>			
image ID	dXs	dYs	dZs
1526	0.22	-0.45	-0.10
1525	0.05	-1.37	-0.04

Table 4. EOE gained from the direct space resection method

In Table 4 the differences of dYs. indicate too large differences while the differences of DXs and dZs are well correlated.

### 3 IMPLEMENTATION OF THE CROSS-CORRELATION METHOD

#### 3.1 Cross-correlation procedures

The area-based image matching is based on the well-known cross-correlation formula [Höhle 2003]:

$$\rho = \frac{\sum_{r=1}^R \sum_{c=1}^C (g_1(r,c) - \mu_1)(g_2(r,c) - \mu_2)}{\sqrt{\sum_{r=1}^R \sum_{c=1}^C (g_1(r,c) - \mu_1)^2 (g_2(r,c) - \mu_2)^2}} \quad (3)$$

Where:

$g_1$  - gray value of a pixel in the template area

$g_2$  - gray value of a pixel in the search area

$r, c$  - row, column

$\mu_1, \mu_2$  - arithmetic mean of the gray values in the template area

$R, C$  - arithmetic mean of the gray values in the search area

This basic idea was extended and investigated on seven different methods like:

1. Cross Correlation (RGB)
2. Cross Correlation (RGB- weighted)
3. Cross Correlation (Gray)
4. Cross Correlation (RGB – 0,1)
5. Cross Correlation (Gray – 0,1)
6. Cross Correlation (RGB – H,V)
7. Cross Correlation (RGB – DTM)

Let's comment each method:

- **Cross Correlation (RGB):** It is a usual cross-correlation made by each colour channel. Then the max. correlation is chosen.
- **Cross Correlation (RGB)-P :** This method is using the same procedure as above, but here the cross correlation coeff. is altered by the weight and the texture coeff. Also the threshold for correlation is set to 0.7:

$$P = \frac{(c_m + 2)^2 - (c_m)^2}{(c_m + 4)^2 - (c_m + 2)^2}, \quad corr_P = corr \cdot P \quad (\text{for R,G,B}) \quad (4)$$

Then the correlation coeff. is calculated as the weighted mean:

$$corr = \frac{corr_R \cdot tu_R + corr_G \cdot tu_G + corr_B \cdot tu_B}{tu_R + tu_G + tu_B} \quad (5)$$

$$corr_{\min} = \frac{0.4666669}{P} \quad (6)$$

Table 5 shows the weights and the acceptable correlation coefficients for different correlation matrices of  $c_m$  :

cm	weight	corr_min
3	0.666667	0.7
5	0.75	0.622223
7	0.8	0.583334
9	0.833333	0.56
11	0.857143	0.544445
13	0.875	0.533334
15	0.888889	0.525
17	0.9	0.518519
19	0.909091	0.513334
21	0.916667	0.509091
23	0.923077	0.505556
25	0.928571	0.502564
27	0.933333	0.5

Table 5. The weights and the acceptable correlation coefficients for different cm correlation matrices

The calculation of the texture coefficient  $t_u$  is made by the following formula:

$$t_u = q \cdot \frac{n_c}{c_m^2} \quad (7)$$

where

$n_c$  : number of different colours (gray values) in the correlation matrix

$c_m^2$  : number of pixels in the correlation matrix

$$q = 1 \text{ if } c_m \leq 15 \text{ else } q = \frac{c_m^2}{256}$$

- **Cross Correlation (GRAY):** Here the RGB values are changed to gray values as an average, and after this a usual cross correlation is made on pixel level.
- **Cross Correlation (RGB)-(0,1):** Here each RGB value is changed to 0 or 1 depending on the mean value. So, we will have 3 correlation matrices (for each colour channel). Then a usual cross correlation is made by the first method.
- **Cross Correlation (GRAY)-(0,1):** Here each gray value is changed to 0 or 1 depending on the mean value. If the gray value is larger than the mean value, it is converted to 1. If the gray

value is smaller than the mean value, it is converted to 0 (see Figure 5). Then a usual cross correlation is made.

126	234	101	45	230
98	99	102	65	210
4	230	56	45	212
34	255	87	34	189
176	20	145	21	173

0	1	0	0	1
0	0	0	0	1
0	1	0	0	1
0	1	0	0	1
1	0	1	0	1

Figure 5. Conversion of the correlation matrix into a binary matrix

- **Cross Correlation (RGB)-(H,V):** Here two correlation matrices are derived from the original one. The first one consists only of every second horizontal row, the second one only consists of every second vertical column. This means some „polarization” of the data (see Figure 6). Then a usual cross correlation is made by the first method.

126	234	101	45	230
98	99	102	65	210
4	230	56	45	212
34	255	87	34	189
176	20	145	21	173

126	234	101	45	230
4	230	56	45	212
176	20	145	21	173

126		101		230
98		102		210
4		56		212
34		87		189
176		145		173

Figure 6. Polarization of the correlation matrix



In this case the mean values are calculated differently:

$$\mu_H = \frac{\sum_{r=1}^{c_m, step2} \sum_{c=1}^{c_m} g_{r,c}}{c_m^2 - ((c_m - 1) / 2) \cdot c_m}$$

$$\mu_V = \frac{\sum_{r=1}^{c_m} \sum_{c=1}^{c_m, step2} g_{r,c}}{c_m^2 - ((c_m - 1) / 2) \cdot c_m} \quad (8)$$

- **Cross Correlation (DTM):** Here the vertical locus method is used, which means that the DTM X,Y coordinates are fixed and the cross correlation is calculated for different Z values. The Z value is incremented each time by 0.1 m until the max. H error value is reached in both directions.

Mainly, the procedure steps are the same for the methods 1-6 (see Figure 7) , only the algorithm of the last method (RGB-DTM) is different (see Figure 8).

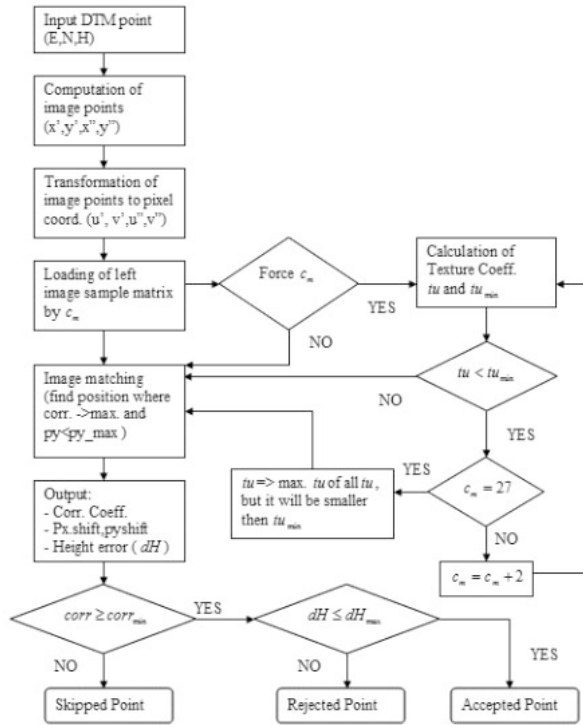


Figure 7. Algorithm for methods 1-6

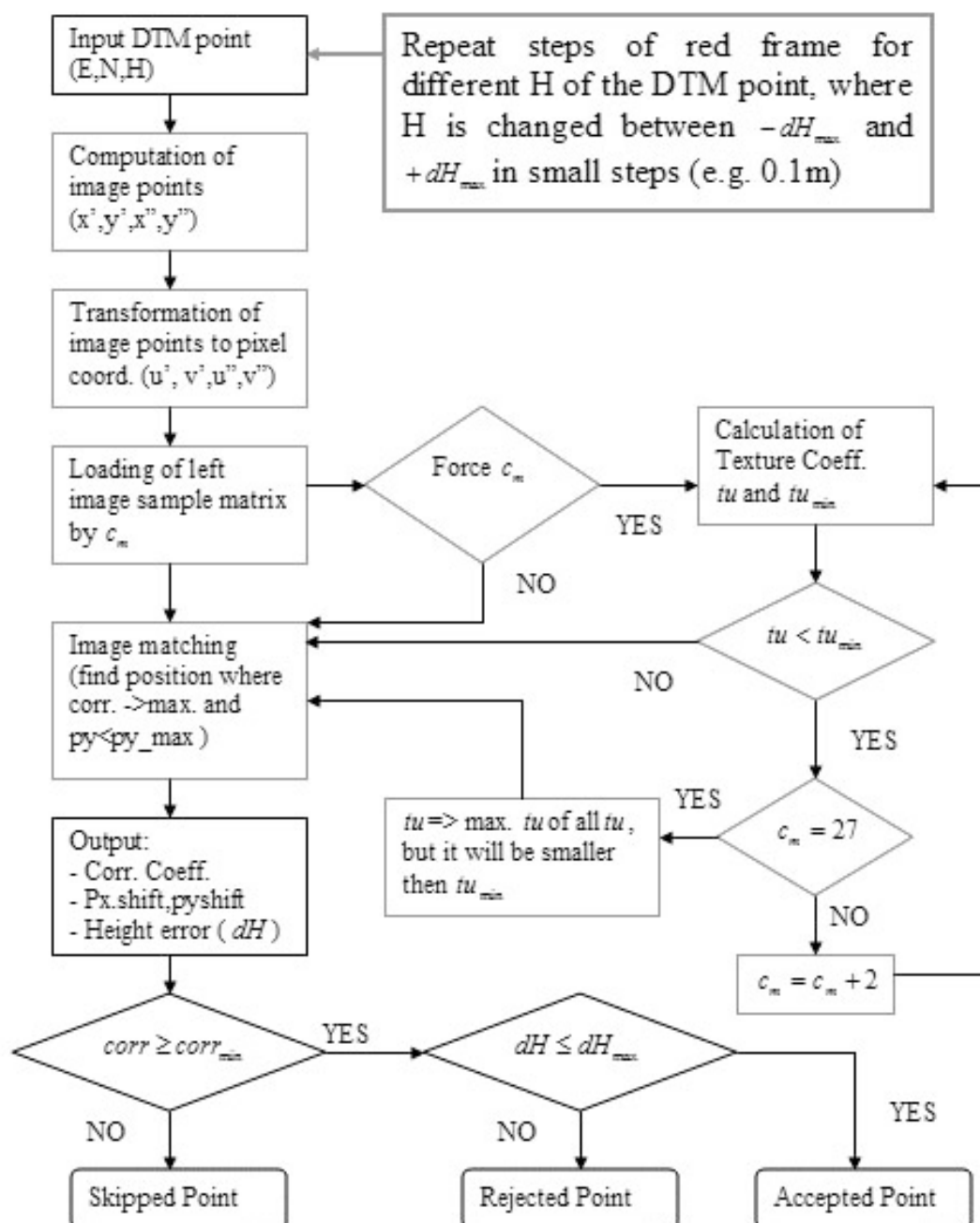


Figure 8. Algorithm for method RGB-DTM

### 3.2 Experimental results

To investigate the different cross-correlation methods a software application was developed (Figure 9).

**Area Based Matching**

DTM point Number:  Max. H error:

E:  N:  H:

Correlation Matrix:  ☒ Force Dimension

Correlation Coeff.  Threshold:

Texture Coeff.  Threshold:

Max. Shift x:  Max. Shift y:

Max. Py error:  Py error:

----- Height Error -----

Pixel x	Pixel y	Image [mm]	Ground [m]
<input type="text" value="1"/>	<input type="text" value="0"/>	<input type="text" value="0.021"/>	<input type="text" value="0.85048"/>
E: <input type="text" value="558267.132"/>	N: <input type="text" value="6320553.254"/>	H: <input type="text" value="43.42"/>	

☒ Point accepted ☐ Point rejected ☐ Skipped point

Figure 9. Area based matching application – setup window

First the input data should be loaded in the „input data” frame as:

- Load the right image file (the image data should be in raw format).
- Load the left image file (the image data should be in raw format).
- Load the DTM file (simple XYZ text file).
- Load the exterior orientation elements (EOE). The file extension is .eoe
- Load the affine transformation parameters (IOP). These parameters are necessary to transform image coordinates to pixel coordinates.
- Load the affine transformation parameters (IOI). These parameters are necessary to transform pixel coordinates to image coordinates.

After this we should determine and edit the following parameters:

- **Max. H error:** Maximally allowed height error. It is usually considered from the expected height error, and the max. H error is about 3 times more than the expected height error. For example: the expected height error is 0.5 m, then the max. H error is about 1.5 m
- **Threshold for the correlation coefficient:** Its usual value is 0.7 but you can change it between 0 and 1, although there are two methods when the threshold is automatically calculated. These methods are the „Cross Correlation (RGB)-P” and the „Cross Correlation (RGB)-DTM” (see later).
- **Max Shift x and Max Shift y:** These values are considered in pixel coordinates and they are used to determine the right image sample search area in both directions. For example Max Shift x=10 and Max Shift y=4 means that the right image sample will be shifted +/-5 pixels in direction x and +/-2 pixels in direction y. So it means that Max Shift x and y should always be given as an even number.
- **Max Py error:** Maximally allowed Py error given in mm. It is considered from the relative orientation result or just simply from the accuracy of an image coordinate measurement. The Max Py error is usually 3 times more than the gained Py accuracy. For example, if the gained Py accuracy is 5 microns, it means that the Max Py error is about 0.015 mm.
- **Correlation matrix:** You should indicate here the dimension of the correlation matrix (the dimension of the left image sample). The acceptable values are 3, 5, 7, 9, 11, 13, 15, 17, 19, 21, 23, 25, 27. It means that this number is always an odd number.
- **Force dimension:** This option is used to force the dimension of the correlation matrix. If the dimension is not forced, the program will try all the dimensions until it reaches the maximum correlation coefficient.

All the other parameters are controlled and calculated automatically.

After choosing the correlation method in the “Correlation” frame panel we can choose the command buttons in the „Correlation” frame to investigate different methods. Visually you will see how successful the correlation was. The small red circle indicates the back-projected point on the right image sample. The green circles indicate the final stage of the cross correlation procedure (see Figure 10).

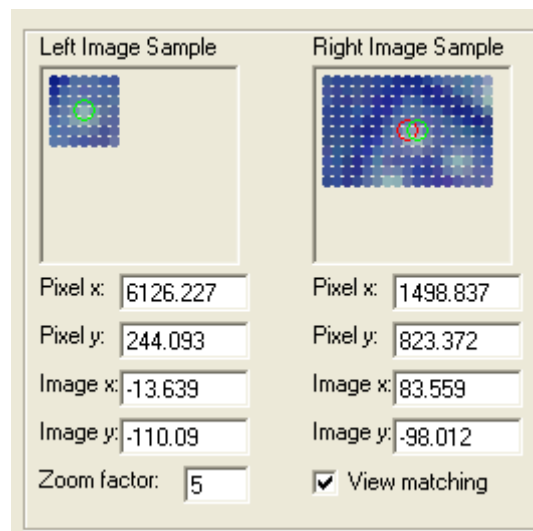


Figure 10. The result of the image matching

When you choose the command button „Matching All Points”, the program calculates the cross-correlation for each DTM point. You should wait until it finishes the calculation; then you can examine the „Error Report”.

The correlation calculates the following parameters:

- Correlation Coeff.
- Height errors in pixels (Pixel x, Pixel y)
- Height error on the image in mm.
- Height error on the ground in m.
- Recalculated coordinates of the DTM point. (If you chose the „Cross Correlation (DTM)” method, the E and H coordinates are not changed, only the H.
- The program indicates whether the DTM point can be accepted, rejected or it is just skipped. The DTM point is accepted if the corr. coeff. is larger than the threshold; otherwise it is rejected. The point is skipped if the achieved corr. coeff. is smaller than the threshold.

Comparison of methods was applied for the Test Area I. and the results are summarized in Tables 6, 7 and 8. The blue values indicate the best results if we omit the results which were gained at the correlation matrix dimension of 5x5.

Number of accepted points							
CM	M1 (RGB)	M2 (RGB-P)	M3 (GRAY)	M4 (RGB-0,1)	M5 (GRAY-0,1)	M6 (RGB-H,V)	M7 (RGB-DTM)
5	433	139	421	193	228	540	704
7	477	287	475	188	258	570	675
9	520	396	517	213	281	566	689
11	591	479	570	237	305	626	751
13	633	557	628	272	322	669	762
15	670	624	673	287	335	704	805
Number of rejected points							
CM	M1 (RGB)	M2 (RGB-P)	M3 (GRAY)	M4 (RGB-0,1)	M5 (GRAY-0,1)	M6 (RGB-H,V)	M7 (RGB-DTM)
5	404	75	304	211	261	605	108
7	285	128	243	178	190	335	112
9	257	167	228	166	172	302	110
11	237	181	212	161	144	259	97
13	229	196	204	149	146	244	112
15	219	204	197	142	142	234	96
Number of skipped points							
CM	M1 (RGB)	M2 (RGB-P)	M3 (GRAY)	M4 (RGB-0,1)	M5 (GRAY-0,1)	M6 (RGB-H,V)	M7 (RGB-DTM)
5	732	1355	844	1165	1080	424	714
7	807	1154	851	1203	1121	664	782
9	792	1006	824	1190	1116	701	770
11	741	909	787	1171	1120	684	721
13	707	816	737	1148	1101	656	695
15	680	741	699	1140	1092	631	668

Table 6. Number of accepted, rejected and skipped points at each method

Dynamic CM methods							
St. Error	M1 (RGB)	M2 (RGB-P)	M3 (GRAY)	M4 (RGB-0,1)	M5 (GRAY-0,1)	M6 (RGB-H,V)	M7 (RGB-DTM)
All	1.96	1.939	1.912	2.316	2.131	1.934	0.928
Accepted	0.654	0.628	0.648	0.617	0.645	0.648	0.794
Rejected	2.919	2.927	2.968	3.006	3.213	2.958	1.506
Dynamic CM methods							
Point	M1 (RGB)	M2 (RGB-P)	M3 (GRAY)	M4 (RGB-0,1)	M5 (GRAY-0,1)	M6 (RGB-H,V)	M7 (RGB-DTM)
Accepted	572	416	585	208	273	658	780
Rejected	304	156	259	187	193	337	121
Skipped	693	997	725	1174	1103	574	668

Table 7. The standard errors and the number of accepted, rejected and skipped points at each method but with dynamic handling of the correlation matrix dimension

Standard height error for all points							
CM	M1 (RGB)	M2 (RGB-P)	M3 (GRAY)	M4 (RGB-0,1)	M5 (GRAY-0,1)	M6 (RGB-H,V)	M7 (RGB-DTM)
5	2.454	2.41	2.35	2.615	2.552	2.458	0.953
7	2.187	2.176	2.118	2.535	2.334	2.179	0.956
9	2.015	2.006	1.969	2.368	2.187	2.014	0.952
11	1.878	1.87	1.835	2.24	1.998	1.862	0.92
13	1.767	1.753	1.721	2.123	1.906	1.768	0.927
15	1.701	1.688	1.649	2.071	1.862	1.669	0.918
Standard height error for accepted points							
CM	M1 (RGB)	M2 (RGB-P)	M3 (GRAY)	M4 (RGB-0,1)	M5 (GRAY-0,1)	M6 (RGB-H,V)	M7 (RGB-DTM)
5	0.653	0.61	0.643	0.662	0.656	0.652	0.827
7	0.659	0.651	0.647	0.612	0.636	0.64	0.808
9	0.66	0.64	0.634	0.643	0.652	0.659	0.803
11	0.643	0.627	0.626	0.64	0.64	0.646	0.803
13	0.642	0.622	0.631	0.63	0.646	0.65	0.796
15	0.652	0.608	0.629	0.644	0.644	0.644	0.799
Standard height error of rejected points							
CM	M1 (RGB)	M2 (RGB-P)	M3 (GRAY)	M4 (RGB-0,1)	M5 (GRAY-0,1)	M6 (RGB-H,V)	M7 (RGB-DTM)
5	3.145	3.094	3.127	3.115	3.217	3.192	1.507
7	2.967	3.016	3.009	3.036	3.183	3.008	1.507
9	2.857	2.841	2.878	3.009	2.935	2.856	1.507
11	2.842	2.94	2.883	2.865	3.018	2.841	1.508
13	2.903	2.916	2.858	2.913	2.89	2.874	1.507
15	2.95	2.921	2.897	2.865	2.876	2.913	1.507

Table 8. Standard errors at each method

From Table 8 we can see that the standard height error for the accepted points is around 0.6 m. The standard errors of the rejected points are around 3 m, and finally if we do not filter the DTM points it means that the height error is varying between 0.918 m and 2.615 m depending on the correlation method and the correlation matrix dimension.

#### 4 MEDIAN DIFFERENCE FILTER

As a separate method for detecting the outliers in the DTM grid we can produce a median difference image and table. The median difference filter means that for each grid node ( $r, c$ ) we identify the set of non-blank, neighbouring input grid values; then we compute the median of these neighbouring values. If  $B$  represents this median value then the output grid node value is set to  $Z_{out}(r, c) = Z(r, c) - B$ . The effect of this filter is to emphasize the outliers in the grid. For the Test Area I before applying the median difference filter a Kriging interpolation method was applied with 1/10 grid size of the original DTM grid size. The median difference filter was applied on this interpolated grid and the result can be seen in Figure 11.

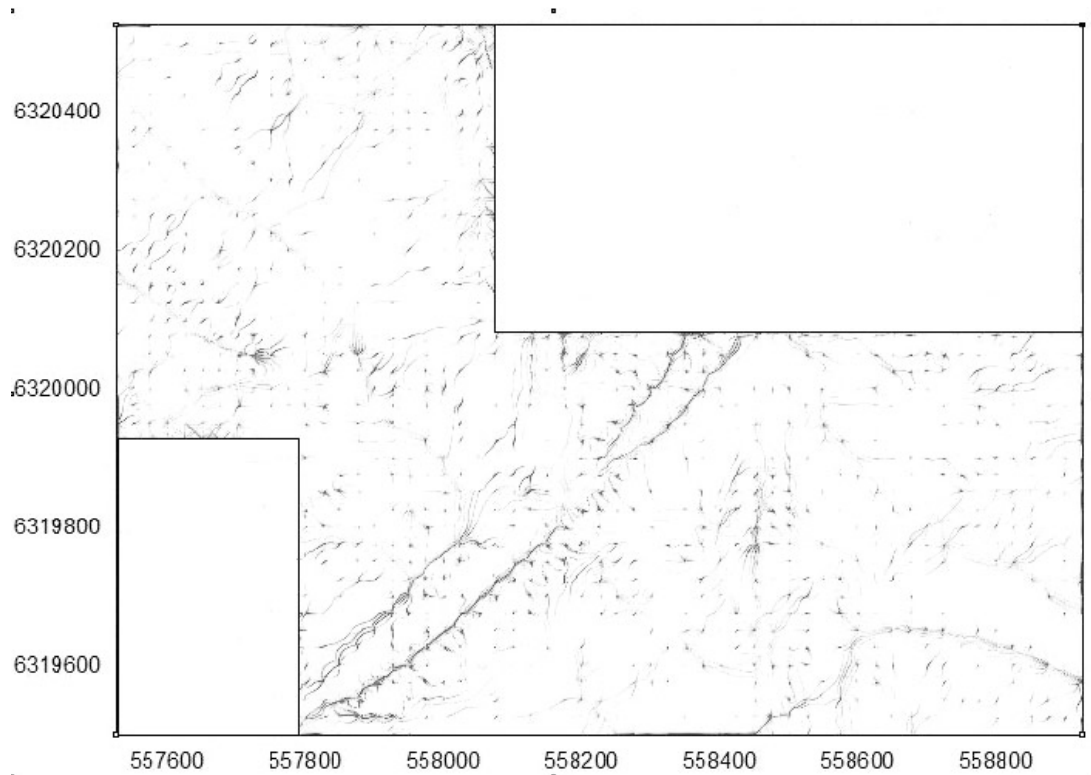


Figure 11. Resulting image of the median difference filter

From the image we can distinguish the main geo-morphological elements, and the small red dots and lines mean smaller or larger outliers in the grid. By this method we can allocate the sensitive areas and as a tool we can target the areas where we need more detailed investigation and quality checking of DTM points.

## 5 CONCLUSIONS

Let us summarize the conclusions referring to the applied methods:

- Before testing the quality of DTM points first we should check the exterior orientation elements by an independent calculation or by re-measurement of the control points on a different DPWS.
- The median difference filter is a very fast and effective method to detect the sensitive areas of DTM points.
- It is necessary to test and investigate the proposed extended and modified cross-correlation methods. By the first experiments an order of effectiveness can be listed as follows:
  - M7 (RGB-DTM)
  - M6 (RGB – H,V)
  - M1 (RGB)
  - M3 (GRAY)
  - M4 (RGB -0,1)
  - M5 (Gray -0,1)
  - M2 (RGB-P)

## REFERENCES

- Höhle, J., Potuckova M. 2003. Automated quality control for orthoimages and DEMS, Aalborg University, Aalborg, 41 p.
- Jancsó T. 2004. Gross Error Detection of Control Points with Direct Analytical Method, ISPRS Volume XXXV Part B3/W3, Istanbul, pp. 678 ff.
- Schenk T., Seo S., Csathó B. 2001. Accuracy study of airborne laserscanning data with photogrammetry, ISPRS Volume XXXIV-3/W4 Annapolis, MD, pp. 113-118.



# A Statistical Approach to DTM Quality Evaluation

Jae Sung Kim & Jie Shan

Geomatics Engineering  
School of Civil Engineering  
Purdue University  
550 Stadium Mall Drive  
West Lafayette, IN 47907

## 1 INTRODUCTION

Since the quality of digital terrain model (DTM) determines the accuracy of orthoimage, it is important to find out where the DTM has problems. According to EuroSDR (2004), the goal of this project is “to receive an overview of which areas of the DTM have to be revised and which areas can be solved by automated procedures, before the orthophoto production can start”. Therefore, we focus on finding problematic cells or areas, which are potential blunders. The basic assumption is that the terrain relief changes rather continuously. Hence, cells with a significant height difference compared to their neighbour cells will be regarded as blunders. In this study, the problematic cells are determined based on the heights of the eight neighbouring cells and their standard deviation. We compare the difference between the height of the centre cell and the mean height of its eight neighbour cells with the standard deviation of the eight surrounding cells. The test material is provided by EuroSDR project (2004).

## 2 DATA SETS

The DTM data are provided by EuroSDR (2004). They represent the bare ground elevation in raster format. The properties of such data sets are summarized in Table 1. Test material A is collected from digital photogrammetry, while test material B is from map digitization. As shown in Figure 1, test material A consists of four sub areas. Test material C is generated by removing the buildings and other non-ground features over a built-up area measured by airborne lidar. The cell size of DTM for test material A, B, C is respectively 25m, 10m, and 1m, respectively.

Table 1. Properties of the test data

	Test material <b>A</b>	Test material <b>B</b>	Test material <b>C</b>
DTM source	Digital Photogrammetry	Digitizing contours of topographic maps	Laser scanning
Cell size	25m	10m	1m
Landscape	Open	Open	Built-up
Test area	Check area 1,2,3,4	Entire area	Check area Left, Middle, Right
Image / Map Scale	1:25000	1:25000	-
Number of cells	3431	220400 (400 × 551)	72339
Remarks	21 $\mu$ m pixel size	2.5m contour interval	-

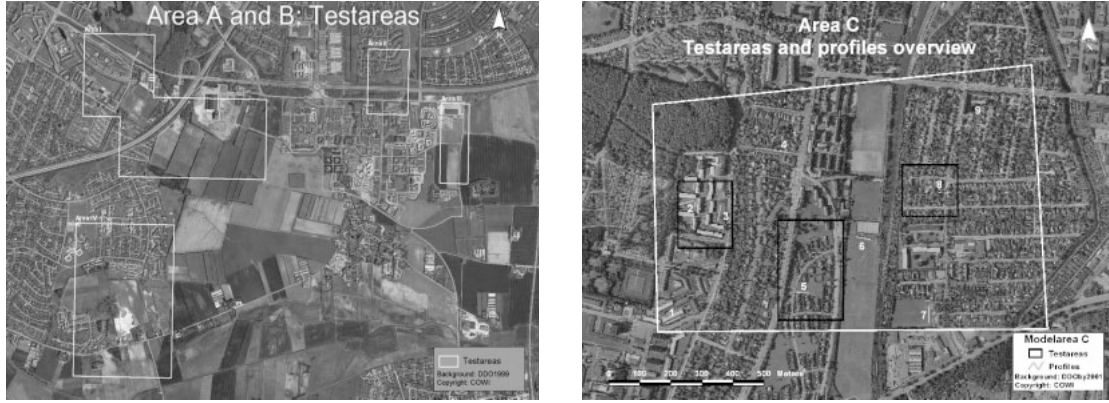


Figure 1. Test materials. A: the four polygons, B the entire image; C: the three small polygons

### 3 METHODOLOGY

The proposed approach is based on the relationship of a target (central) cell and its eight surrounding cells. As shown in Figure 2, the mean height of the eight surrounding cells, the difference of the target cell relative to the mean, and their standard deviation are respectively

$$Z_{mean} = \frac{1}{8} \sum_{i=1}^8 Z_i \quad (1)$$

$$\Delta Z_c = Z_c - Z_{mean} \quad (2)$$

$$\sigma = \sqrt{\sum_{i=1}^8 (Z_i - Z_{mean})^2 / (n-1)} \quad (3)$$

$Z_1$	$Z_2$	$Z_3$
$Z_4$	$Z_c$	$Z_5$
$Z_6$	$Z_7$	$Z_8$

Figure 2. Target cell and surrounding cells

We compare the height difference magnitude between the target cell and mean with respect to the standard deviation of eight neighbour cells.

$$c = |Z_c - Z_{mean}| / \sigma \quad (4)$$

Using the value of  $c$  in Eq (4), we can classify the DTM cells into three categories, eg. normal, caution, and blunders based on the following relationship

$$c = \begin{cases} > c_1, \text{blunder} \\ c_2 < c \leq c_1, \text{caution} \\ \leq c_2, \text{normal} \end{cases} \quad (5)$$

The determination of  $c_1$  is critical for the performance of the proposed approach. It is seen that if  $c_1$  is too small, the blunders found based on Eq (5) will include the normal cells. Likewise, if  $c_1$  is too big, the blunders will be underestimated. Hence, we propose to determine  $c_1$  so that the numbers of detected blunders are stabilized. Figure 3 shows the relationship between  $c_1$  and the blunder percentage for test material A, B and C. As is shown, the blunder percentage decreases as  $c_1$  increases and stabilizes after certain points. This critical point varies depending on the test materials. Therefore, we use the blunder decrement ratio to determine  $c_1$ . Figure 4 plots the decrement of percentage of blunders on the vertical-axis with varying value of  $c_1$  on the horizontal axis. In the case of test material A, the decrement of the blunder ratio stabilizes after  $c_1=1.5$ , and this value is regarded as the critical point which divides the region of overestimating and underestimating blunders. Likewise, values of 2.8 and 2.1 are chosen as critical values of  $c_1$  for test material B and C, respectively.

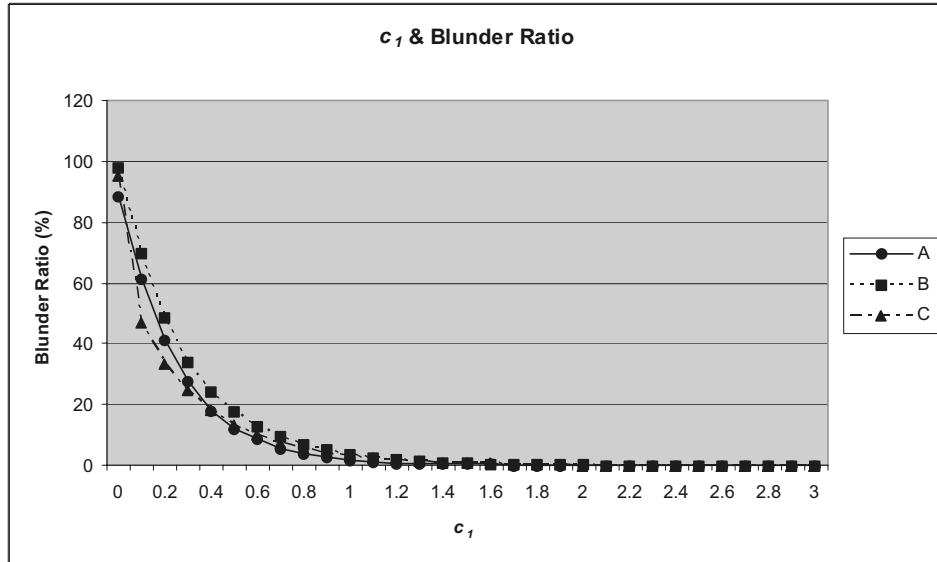


Figure 3. Relationship between  $c_1$  and blunder percentage

We regard 0.5 as a safety factor and can compute the value of  $c_2$  by subtracting the safety factor from  $c_1$ . If  $c$  at a target cell is between  $c_1$  and  $c_2$ , it will be regarded as a caution cell.

If  $c$  at target cell is less than  $c_2$ , the cell is regarded as a normal cell. Table 2 shows the critical values for each test material A, B, and C. It is noticed that the order of threshold values is B, C and A.

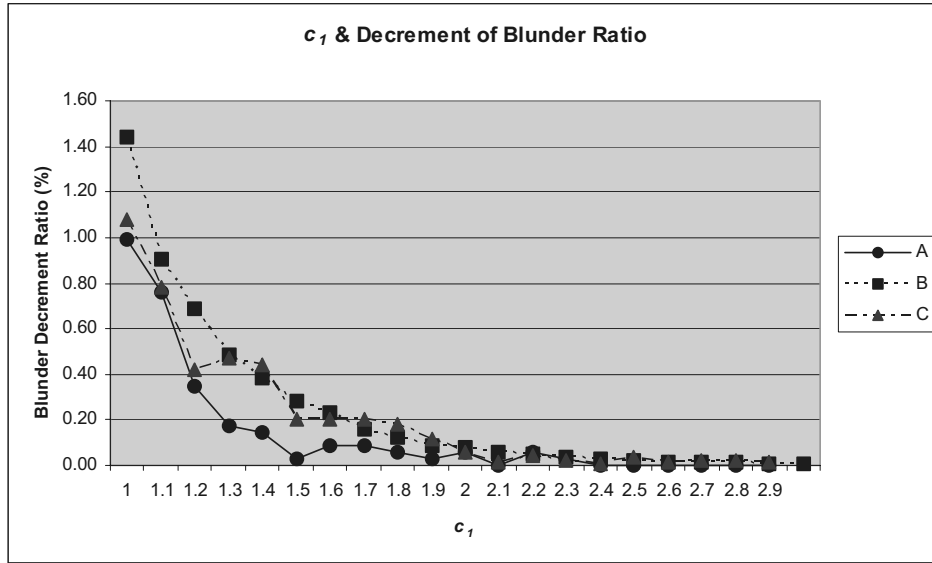


Figure 4. Relationship between  $c_1$  and blunder decrement ratio

Table 2. The critical values of  $c_1$  and  $c_2$

Test Material	c1	c2
A	1.5	1.0
B	2.8	2.3
C	2.1	1.6

In addition to the above intrinsic properties of the data, the methods (extrinsic properties) used to produce the DTM must also be taken into account for blunder detection. For test material A, the mean difference (mean of differences between the height of the target cell and those of the eight neighbour cells) over the entire area is compared with the standard deviation of the height difference  $\Delta h$  determined with parallax measurements. According to Mikhail et al. (2001), the standard deviation of  $\Delta h$  is

$$\sigma_{\Delta h} = \frac{(H - h)}{b} \sigma_{\Delta p} \quad (6)$$

For test material A,  $\sigma_{\Delta p}$  is assumed to be 0.5 pixel,  $H-h= 3838.19m$ ,  $b=0.09188m$ ,  $\sigma_{\Delta h}$  is then determined as 0.44 meter. As for the test material B, we assume that  $\sigma_{\Delta h}$  is one half of the contour interval. The standard deviation is then determined as 1.25 meters based on the contour interval 2.5 meters on the topographic map at 1:25,000 scale. Since test material C is derived from laser scanning, its  $\sigma_{\Delta h}$  is regarded as 10 cm. For all the data sets we use the following ratio to check the blunders

$$\alpha = \frac{\sum_{i=1}^n |Z_c - Z_{mean}|}{n\sigma_{\Delta h}} \quad (7)$$

Where,  $\alpha$  is the degree of deviation relative to the estimated standard deviation of the data collection method,  $Z_{mean}$  is calculated by Eq (1) and  $n$  is the total number of cells in a study area.

#### 4 RESULTS AND EVALUATION

Test materials A, B, and C are evaluated with the suggested method and each cell is categorized as normal, caution, or blunder. In the following figures, caution and blunder cells are represented as hollow circle and solid circle, respectively. For test material B, the result is superimposed on DTM to show the problematic areas in the topographic map. For test material C, some regions with dense blunder cells are represented by superimposing them on the image to show where problems occur in laser scanning. Table 3 shows the critical values for the purpose of comparing the results across the test materials, where maximum difference, minimum difference and mean difference were computed by equation 2 for each blunder cell.

Table 3. The magnitude of differences for test materials

Test Material	$\sigma_{\Delta h}$ (m)	Mean difference(m)	Max difference(m)	Min difference(m)	$\alpha$
A	0.44	0.72	1.94	0.26	1.63
B	1.25	0.29	1.35	0.0088	0.23
C	0.10	0.030	0.49	0.0087	0.30

It is seen that test material B from map digitization is the most reliable because it has the smallest  $\alpha$ . However, test material C is the most accurate in the view of the absolute value of the differences and it seems reasonable because laser scanning is known to have a high accuracy. Test material A (DTM by digital photogrammetry) is the least reliable because it has the highest value of mean, maximum and minimum difference.

Fig. 5 shows the histogram of differences at blunder cells for each test material, and we can see that the shape of histograms positively skewed and the distribution of difference is abnormal. Each test material A, B and C has most blunders at the class of 0.4, 0.2 and 0.02 which corresponds to the quality in the order of C, B and A.

Table 4 shows the number and rate of caution and blunder cells. If we consider the rate of blunders, test material B is most reliable and it has fewer blunders than test material C. Because test material C is derived from laser scanning, it considers small deviations as blunders. That is the reason why test material C has a higher blunder rate than test material B though the absolute difference of test material C is the lowest. Test material A is still the least reliable in the view of blunder rate.

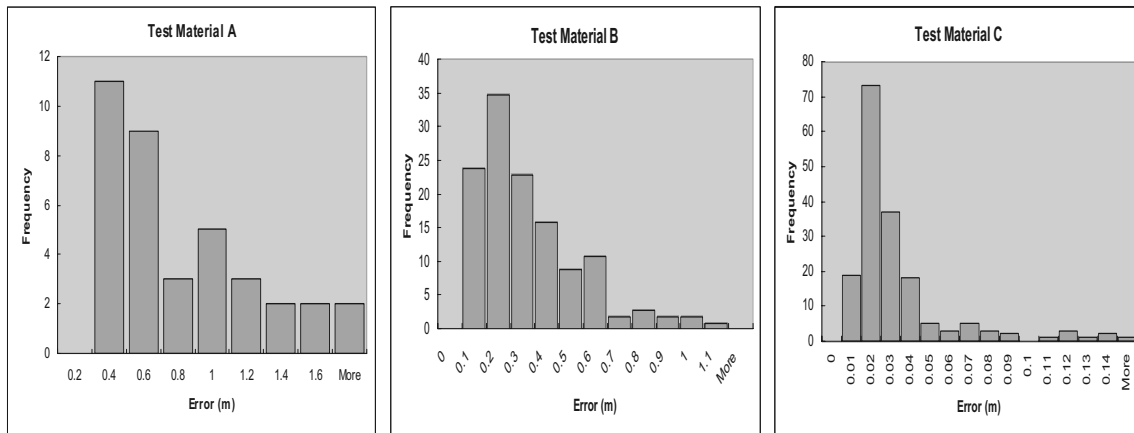


Figure 5. Histogram of errors for each test material

Table 4. The number and percentage of caution and blunder cells

Test material	Total number	Caution	Percentage (%)	Blunder	Percentage (%)	Total	Percentage (%)
A-1	1569	37	2.36	18	1.15	55	3.51
A-2	247	12	4.86	5	2.02	17	6.88
A-3	216	14	6.48	7	3.24	21	9.72
A-4	1399	36	2.57	7	0.5	43	3.07
A	3431	99	2.89	37	1.07	136	3.96
B	220400	235	0.11	128	0.06	363	0.16
C-L	22507	190	0.84	84	0.37	274	1.22
C-M	38373	119	0.31	32	0.08	151	0.39
C-R	11459	131	1.14	57	0.50	188	1.64
C	72339	440	0.61	173	0.24	613	0.85

Figure 6 presents the result of test material A. In test material A-1 there are 18 blunders which are represented as filled solid circles. Likewise, there are 5, 7 and 7 blunders in test material A-2, A-3 and A-4. Those numbers must not be neglected if we consider the small data size.  $\alpha = 1.6$  in Table 3 suggests that the blunders have a mean deviation of 0.8 pixel in parallax measurement. Attention has to be paid to the caution cell because those cells might have problems. However, it might be the result of the inherent characteristics of terrain such as severe slope changes, and a site of summit. Hence, caution cells need to be examined before a decision is made.

Figure 7 shows the superimposed result on the DTM of test material B. It shows that test material B has 235 caution cells and 128 blunder cells. Apparently, it seems to be a great number but if we consider that there are 220400 cells, the percentage is about 0.16 percent. Many caution and blunder cells are located on Mid-South, North-East, South-West, and South-East areas of the lowest height. Hence, the lowest regions in the contour map are probably not well interpolated. Especially, the Mid-South and South-West region has conspicuously focused on caution cells, and those regions are likely problematic. Table 3 shows that the mean error is 0.286m which is about 0.23 times half of the contour interval.

Figure 8 shows the result of test material C-L, C-M and C-R. In test material C, there are relatively more caution and blunder cells compared to test material A and B if we consider the area that the data represent. The first reason for increasing the number of those cells is that test material C's cell size is

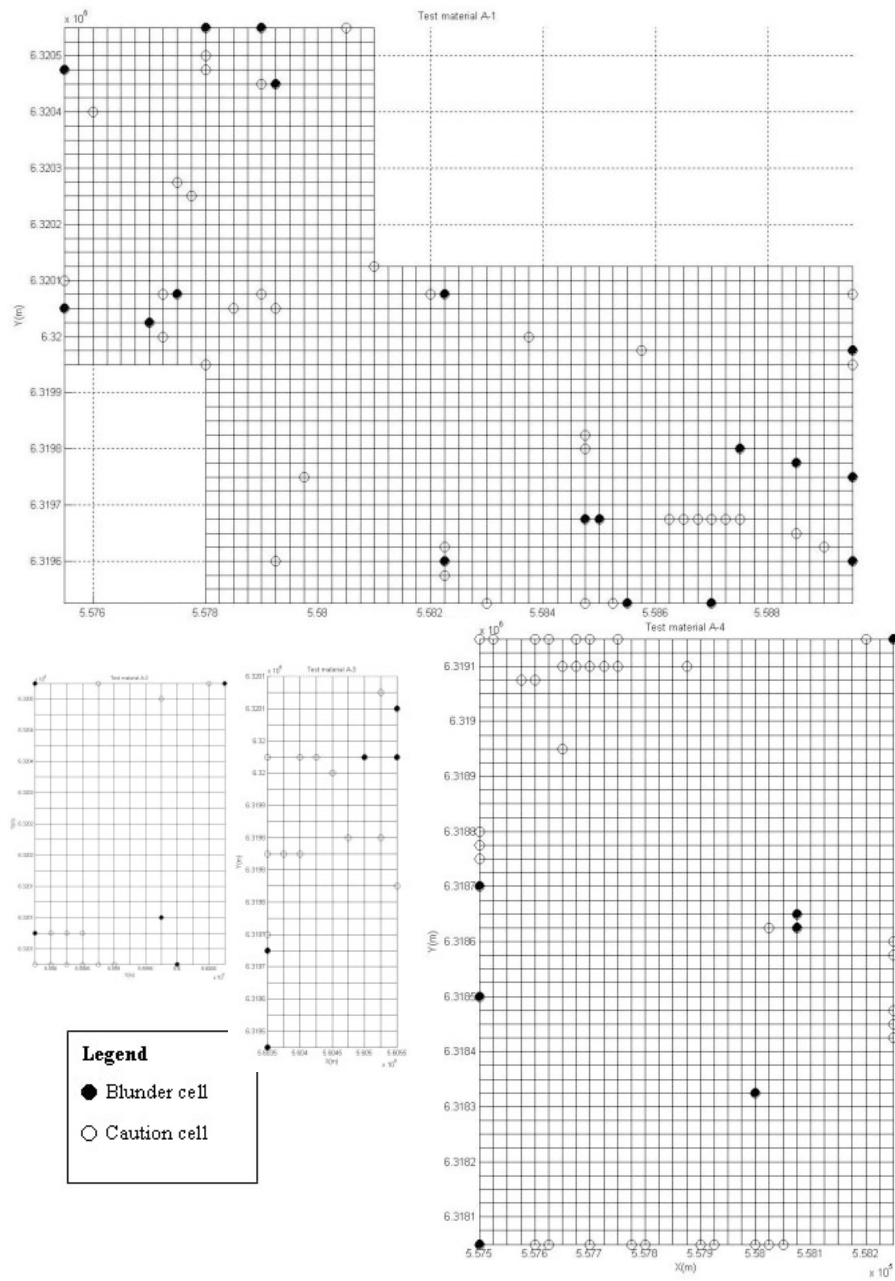


Figure 6. Result of test material A-1, A-2, A-3, A-4

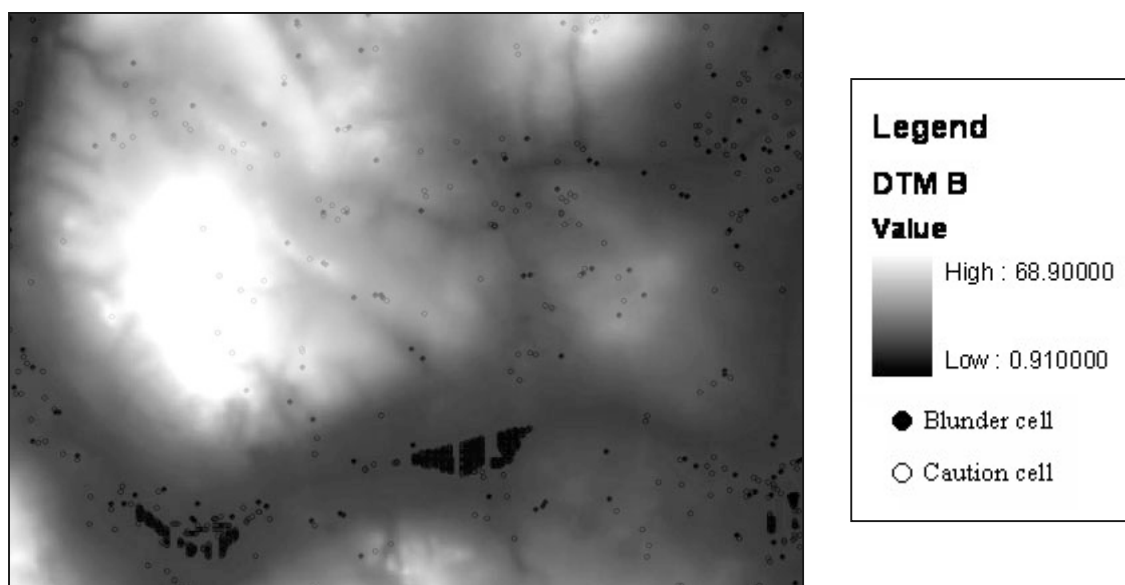


Figure 7. Result of test material B

1m and that is 1/25 and 1/10 compared to test material A and B. The second reason is that the test material C represents built-up areas, where DTM is less accurate than in open areas such as test material A. Figure 9 shows a superimposed image where caution and blunder cells are focused in test material C. We can see that a lot of caution and blunder cells are located in the middle of roads in the C-L image. That seems to be reasonable, because there are lots of trees, cars, and other objects in or along the roads. Some of the blunders are located in the grass areas. Since there should not be much height variation in those regions, such objects remaining in DTM should be considered as blunders. In C-M and C-R, there are certainly more caution and blunder cells along the roads. Some of caution and blunder cells are located on the edge of buildings, and it seems that those cells are not removed during the filtering process.

To summarize, test material A has the highest percentage of blunders as we expected, while test material C has the second highest blunder rate because the DTM represent built-up areas which have lot of variability such as buildings, trees, and cars, although laser scanning is a highly accurate method. It is noted that test material C-R (right) has the highest percentage of blunders among test material C. As we can see from Figure 9, it is more built up than other regions in C. Test material B has the lowest percentage of blunders because the data represent open areas and it was derived from manual digitization of contour maps.

## 5 CONCLUSION

Blunders need to be quantitatively defined for DTM quality control and evaluation. A reasonable reference is the estimated standard deviation of the input data and local height variation as used in this study. To comprehensively evaluate the DTM quality, its cells are classified into normal, caution and blunder categories by using critical values, which can be determined based on stabilization of blunder decrement.



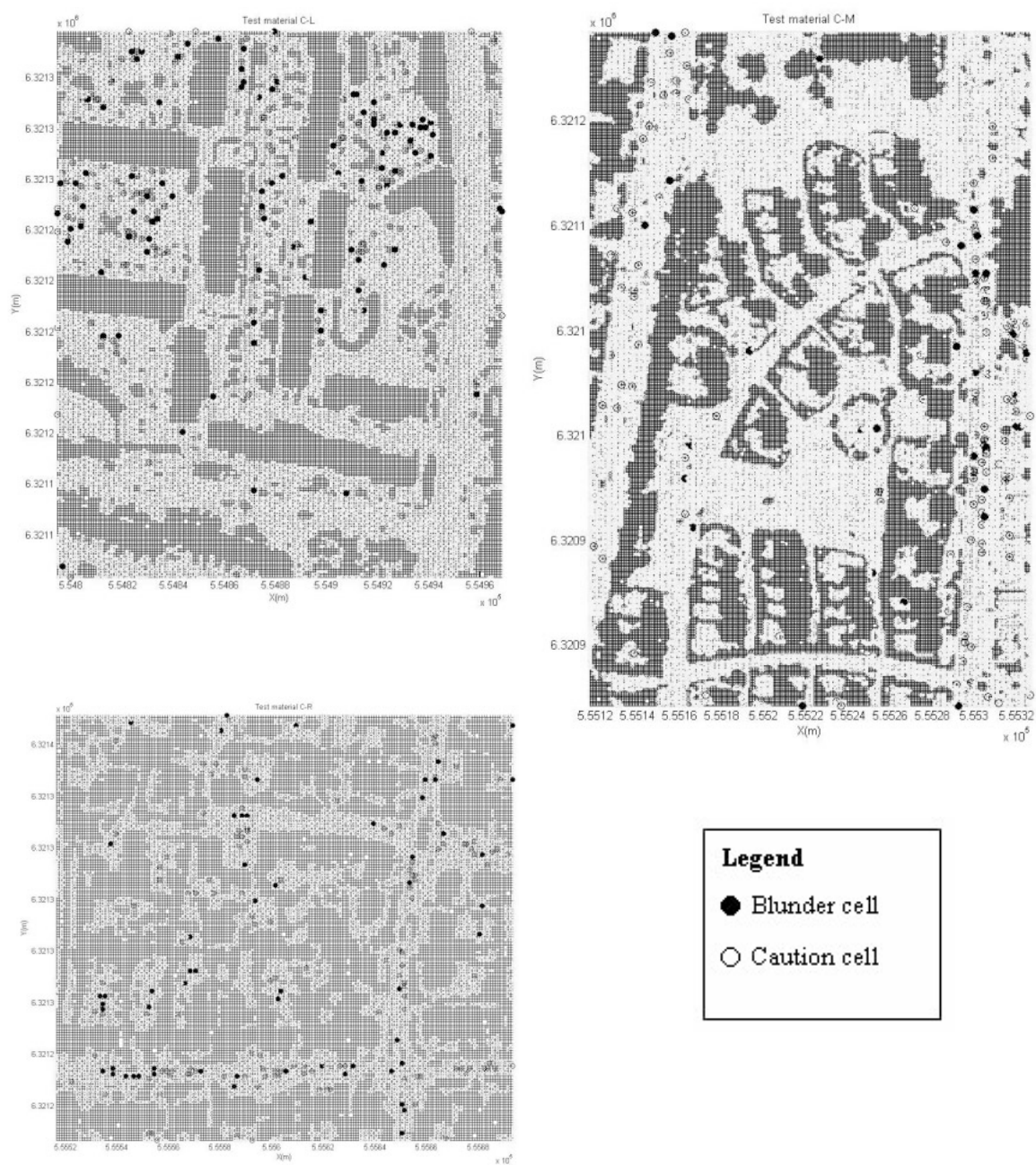


Figure 8. Result of test material C-L, C-M, C-R

C-L

C-M



C-R


**Legend**

● Blunder cell

○ Caution cell

Figure 9. Superimposed image for test material C-L, C-M, C-R

The blunder percentage varies among the test materials. Test material B shows the lowest blunder rate, while test material A has the highest blunders percentage. Blunder cells of test material B are highly focused on the regions with the lowest height as the result of sparse contour lines or poor interpolation. Blunders in test material C are likely caused by the filtering algorithms since they are located mostly along the roads and beside buildings. Test material A has the highest blunder rate and there seems to be no pattern in the spatial distribution of the detected blunders, except that some blunders tend to be located at the boarder of the areas, which are less reliable anyway.

In terms of the magnitude of the detected blunders, the quality of the test materials is in the same order of blunder percentage. However, laser scanning gave the most accurate result in the view of absolute difference. We found that digital photogrammetry sometimes yields larger blunders than digitization of topographic maps. The distribution of errors is positively skewed and it does not suggest any normality.

The advantage of the suggested approach is that it can be used to any case regardless of the method of DTM generation. Therefore, this method is proper for not only DTM generated by photogrammetry, but also map digitization or laser scanning which have no parameters such as inner and exterior orientation.

It should be noted that the above findings are related to our definition and understanding of blunders. A highly accurate data set, such as the test material C may have a high blunder rate. Whereas, the test material B which seems least accurate among the three test materials has the smallest blunder rate. Moreover, the findings may also be subject to the limited size of the test material, such as A.

## REFERENCES

- [1] American Society for Photogrammetry and Remote Sensing (ASPRS) (2004) "ASPRS Guidelines Vertical Accuracy Reporting for Lidar Data", Retrieved May 1st, 2005, from <[http://www.asprs.org/society/committees/lidar/Downloads/Vertical\\_Accuracy\\_Reporting\\_for\\_Lidar\\_Data.pdf](http://www.asprs.org/society/committees/lidar/Downloads/Vertical_Accuracy_Reporting_for_Lidar_Data.pdf)>
- [2] Devore, J. L. (2004). Probability and Statistics for engineering and the sciences (6th ed.), Thomson Brooks/Cole, CA.
- [3] EuroSDR (2004) "Automated checking of DTMs", Retrieved April 1<sup>st</sup>, 2005, from <[http://www.land.aau.dk/~jh/dtm\\_checking/](http://www.land.aau.dk/~jh/dtm_checking/)>
- [4] Mikhail, E. M., Bethel, J. S., McGlone, J. C. (2001). Introduction to Modern Photogrammetry, John Wiley & Sons, Inc., New York.



# QUALITY PARAMETERS OF DIGITAL TERRAIN MODELS

**Wilfried Karel<sup>1</sup>**

Christian Doppler Laboratory for “Spatial Data from Laser Scanning and Remote Sensing”  
at the I.P.F., Vienna University of Technology, Austria

**Karl Kraus<sup>2</sup>**

Institute of Photogrammetry and Remote Sensing (I.P.F.)  
Vienna University of Technology, Austria

## 1 INTRODUCTION

Quality parameters of Digital Terrain Models (DTM) are a hot topic today. This article presents both global and local quality parameters.

Using check points, global quality parameters are determined for a specific measurement technique, for instance airborne laser scanning (ALS), or digital stereo photogrammetry. They describe the whole area of interest with a few parameters only.

Contrary to global quality parameters, local ones describe the quality of a DTM at a high level of detail. The local parameters given in this paper describe the quality of each grid point of a DTM.

In section 6, an ALS project is confronted with a photogrammetric one in the same area through local quality parameters.

## 2 GLOBAL QUALITY PARAMETERS

A formula that describes the height accuracy of topographic measurements is more than a hundred years old. It stems from Carl Koppe:

$$\sigma_H = \sigma_Z + \sigma_G \tan \alpha \quad (1)$$

$\sigma_H$  ... standard deviation in height of topographic maps,  
nowadays of DTM (Kraus 2004)

$\sigma_Z$  ... standard deviation in height

$\sigma_G$  ... standard deviation in planimetry

$\alpha$  ... terrain slope

It has to be mentioned that from the point of view of error propagation, variances should be used instead of standard deviations. However, standard deviations are used in rules of thumb, and (1) is not more than that.

### 2.1 Stereo Photogrammetry

If applied for stereo photogrammetry, (1) has to be used in the following form (Kraus 2004):

---

<sup>1</sup> wk@ipf.tuwien.ac.at

<sup>2</sup> passed away on April 5, 2006.

$$\sigma_H = \pm \left( 0.00015 * h + \frac{0.15}{c} h \tan \alpha \right) \quad (2)$$

$h$  ... flying height

$c$  ... principal distance of the camera [mm]

Formula (2) may only be applied for open terrain. In case of wooded areas, uncertainty increases by approximately 2m.

Example:  $h = 1500\text{m}$ ,  $c = 15\text{cm}$ , 10% terrain slope

$$\sigma_H = 0.22 + 1.5 \cdot 0.1 = \pm 0.37\text{m} \quad \text{open terrain} \\ \pm 2.4\text{m} \quad \text{wooded areas} \quad (3)$$

## 2.2 Airborne Laser Scanning

For ALS, the following formula must be used:

$$\sigma_H [\text{cm}] = \pm \left( \frac{6}{\sqrt{n}} + 50 \tan \alpha \right) \quad (4)$$

$n$  ... points per square metre

Unlike in photogrammetry, the flying height does not affect DTM height accuracy in today's airborne laser scanning. For ALS, point density is the critical influencing factor. However, future scanners will allow for a larger variability in flying height. Thus, planimetric point errors stemming from angular measurement errors of the inertial measurement unit will become distinguishable. This factor will be considered in the second term that describes the impact of planimetric errors on DTM height accuracy.

Example: 2m point spacing, 10% terrain slope

$$\sigma_H = \pm \left( \frac{6}{\sqrt{0.25}} + 50 \cdot 0.1 \right) = \pm 17\text{cm} \quad \text{open terrain, 100\% penetration rate} \\ = \pm \left( \frac{6}{\sqrt{0.0625}} + 50 \cdot 0.1 \right) = \pm 29\text{cm} \quad \text{wooded terrain, 25\% penetration rate} \quad (5)$$

The two constants 6 and 50 were determined using more than 22,000 check points in mountainous and slightly sloped terrain. The height differences between the check points and the DTM were analyzed. These residuals were classified according to the terrain slope and the ALS data density at the respective check point, see Fig. 1.

Subsequently, the standard deviation was computed for each class of residuals. Using these standard deviations as observations, the two constants of equation (4) were determined in an adjustment.

The derived constants already hold high stability. Nevertheless, they are enhanced every time new data are available to the author.

Other alternatives to equation (4) were investigated, like adding a constant term, using terms of higher degrees, or the summation of variances instead of standard deviations. None of the corresponding adjustments yielded convincing results.

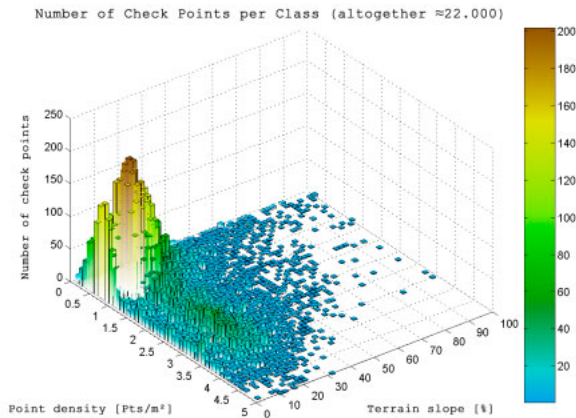


Fig. 1. In order to determine the two constants of formula (4), the residuals in height between 22,000 check points and corresponding ALS DTM were classified according to local terrain slope and data density. Using the standard deviation of each class, the constants of the quality formula were computed in an adjustment.

### 3 TRANSITIONAL REMARKS

Spectral analysis with test profiles resides in an intermediate position between global and local quality parameters, confer (Tempfli 1980), or (Frederiksen 1980). However, according to (Li 1993), the spectral analysis has not found its way to practice.

Another method, which was a focus of the EuroSDR seminar in Aalborg, is interesting mainly from the point of view of automatic DTM enhancement. Overlapping digital orthophotos are generated using the (flawed) DTM. The resulting parallaxes in the orthophotos are a measure for the height accuracy of the DTM. In place of the generation of orthophotos, also a back projection can be done (Schenk 2005).

Alternatively, quality measures may be derived by error propagation. However, users experience this technique as a black box, as no information is given on the impacts of individual factors on quality. Furthermore, this method is not applicable to existing DTM, which is a very important task these days.

As an alternative to error propagation, an empirical, stochastic **step-by-step** approach has been developed that generates very detailed quality measures.

This step-by-step approach can be characterized as follows: it is

- **applicable** in a post-processing phase to **any DTM** existing beforehand, it is
- **independent of the DTM interpolation method**, it
- uses the **original data** (ALS: without eliminated points on trees and buildings), it produces quality measures
- in the **resolution** of the individual **grid points**, and it
- provides **attractive visualizations**.

### 4 LOCAL QUALITY MEASURES

The first parameter of the aforementioned step-by-step approach is the density of the original points  $\bar{n}$ . It is computed as the density in the cells of a regular grid covering the area of interest.

The next local quality measure is the distance  $c_{m_i}$  between each grid point and the data point next to it. This parameter may be computed efficiently using the Chamfer function (Borgefors 1986).

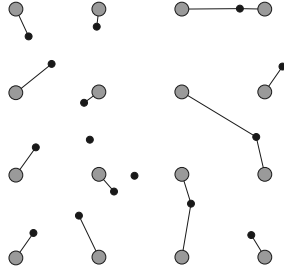


Fig. 2. The distances between each grid point (orange) and the data point next to it (black) are of great importance for DTM quality.

DTM curvature also holds large effects on the quality measure. First, curvatures at each grid point are computed along the grid lines, considering break lines (Fig. 3). Now, maximum and minimum main curvatures are deduced, and with these, the curvature  $1/r_{\alpha_i}$  in an arbitrary direction  $\alpha_i$  can be given.

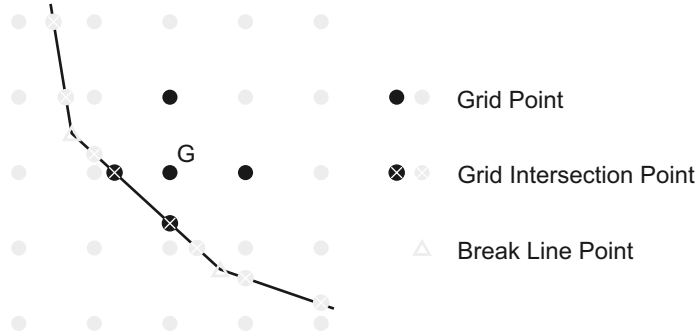


Fig. 3. Computation of the curvature at grid point  $G$ : points used are coloured black.

With both the original data used for DTM generation and the DTM itself, accuracies can be computed that are representative for the surrounding data points of a grid point  $G$ . A weighted  $RMSE$  (6) is used that is calculated using the discrepancies in height  $d_i$  between the original data and the DTM surface (Fig. 4). If the  $RMSE$  results smaller than the a priori known standard deviation of measurement, it is replaced by that value.

$$RMSE = \sqrt{\frac{\sum_i d_i d_i p_i}{\sum_i p_i}} \quad (6)$$

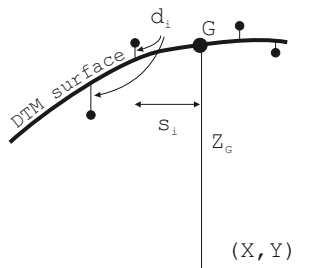


Fig. 4. Discrepancies in height  $d_i$  between the DTM surface and the original data points.



The weights  $p_i$  are defined as follows:

$$p_i = \frac{1}{1 + s_i^2 / r_{a_i}^2} \quad (7)$$

$s_i$  ... distance grid point – original point  
 $r_{a_i}$  ... radius of curvature of the DTM at  
the original point towards the grid point

These weights have the effect that the nearer the data point is to the grid point  $G$ , the more influence on the  $RMSE$  it gets. An analogical effect has curvature. By assigning an adequate threshold, the neighbourhood of a grid point  $G$  may be delimited. Using the information stated above, DTM height accuracies can be computed. Left to answer is the question which interpolation method to take. As for accuracy estimates rather simple interpolation methods can be chosen, the authors decided to apply moving least squares (MLS) with an order one polynomial (plane), weighted with (7). In order to ease computation, each plane is calculated in an own coordinate system whose z-axis goes through the grid point (see Fig. 5).

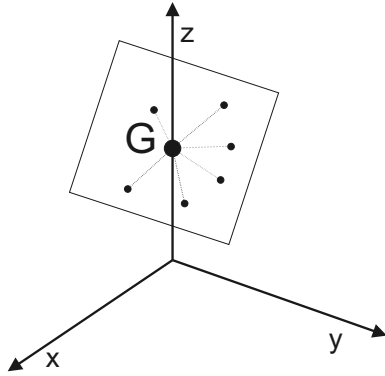


Fig. 5. Adjustment of a plane using the surrounding data points of grid point  $G$ , having defined the z-axis going through  $G$ .

The standard deviation  $\hat{\sigma}_{z_G}$ , which we name  $\hat{\sigma}_{DTM}$ , is computed as (Kraus *et al.* 2005):

$$\hat{\sigma}_{DTM} = RMSE \cdot \sqrt{q} \quad (8)$$

where  $q$  is the cofactor in height of the least squares adjustment of the tilted plane. If  $q$  is 1, then the DTM grid point holds the same accuracy as the surrounding data points. If the cofactor is larger than 1, then the grid point owns an accuracy that is worse than the ones of the neighbouring data points. Reasons for that may be large distances or high curvatures to the next data points. If  $q$  is smaller than one, which should be aimed at, then the DTM holds higher accuracy than the surrounding data points. In the paper (Kraus *et al.* 2005), there are given further details on this theory. Moreover, it presents a drastic example with large data voids, as they may occur in the practice of ALS.

In the next section the quality measures of a high alpine ALS DTM are presented. In the subsequent section a DTM generated with photogrammetric data is confronted with an ALS DTM of the same area of interest.

## 5 LOCAL QUALITY PARAMETERS OF AN ALS PROJECT

The mountainous area of the ALS project described in this section resides in Montafon, Vorarlberg, Western Austria. It covers 1500 by 1100 meters. Height ranges between 1700 and 2600m above sea level. See a shaded view of the digital surface model in Fig. 6.



Fig. 6. Shaded digital surface model, derived from all ALS points. Rocky terrain with relatively little vegetation is visible. Project of the “Landesvermessung Vorarlberg”.

Data capture is done with a mean point density of  $\approx 2$  points per square meter. Using robust filtering, 3.6 million points are classified as terrain points, see Fig. 7.

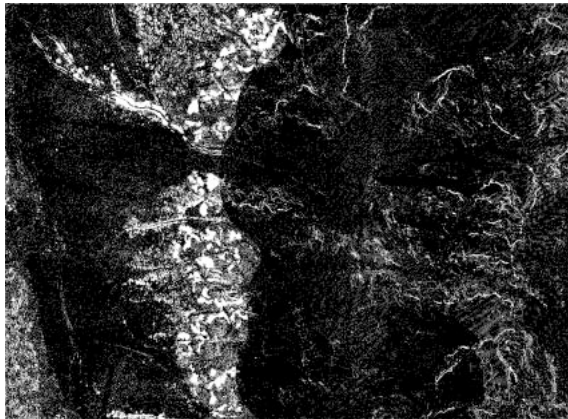


Fig. 7. Classified terrain points (black) of the Montafon project.

Using the classified terrain points, the DTM is interpolated with a grid width of 1m through the linear prediction calculus implemented in the software SCOP++. See a shaded view of the DTM together with derived contour lines on Fig. 8.

As a first quality check, point density is computed. Data characteristics become obvious in the respective colour-coded image (Fig. 9). The broad band of high density in North-South direction stems from the overlap of two laser scanner strips. The three narrow bands of high density in East-West direction are oriented perpendicularly to the flight path and do not correspond to terrain characteristics. They may stem from turbulences during the flight.

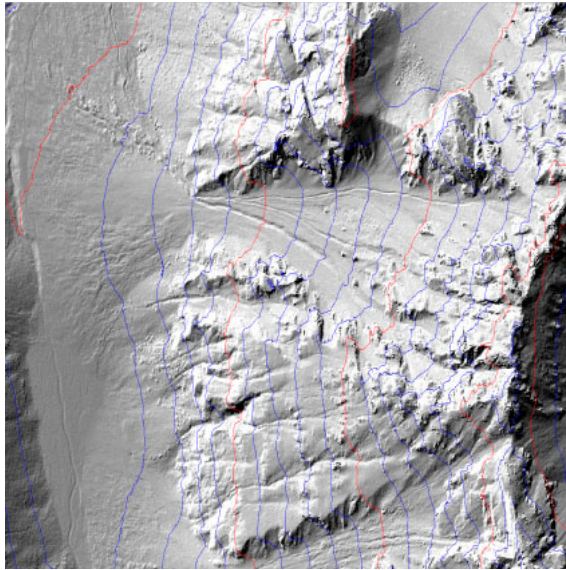


Fig. 8. Shaded DTM together with derived contour lines every 25 meters. The DTM bases on the ALS points classified as terrain points through robust filtering (Fig. 7).

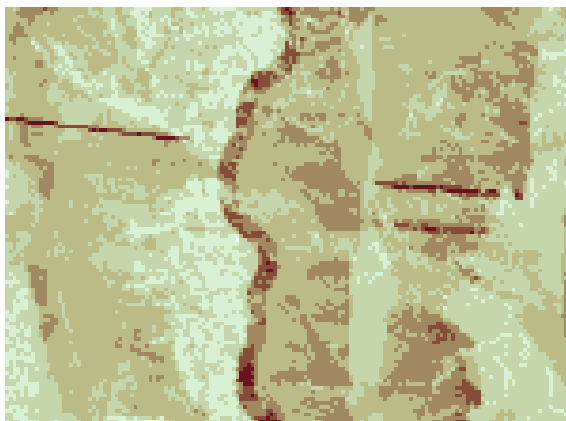


Fig. 9. Density of classified ALS terrain points, computed with a cell size of 100m<sup>2</sup>.

By applying the Chamfer function, the distance from each grid point to its nearest data point is computed. Now, the data voids get visible, of which users should be warned. Thus, grid points that are further away from point data than seven times the DTM grid width, are coloured red (Fig. 10).

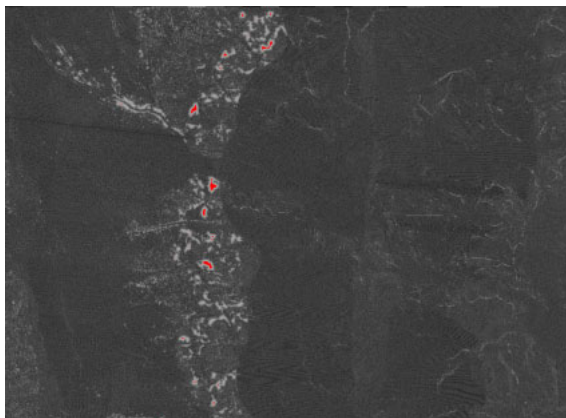


Fig. 10. Distance from each grid point to its nearest data point (see Fig. 2). Grid points with larger distances than seven times the DTM grid width (A7m) are coloured red.

The maximum main curvatures at the grid points (Fig. 11) show up fine terrain characteristics. Crests and rifts become visible. Obviously, this measure is a good representation of the terrain's geomorphology.

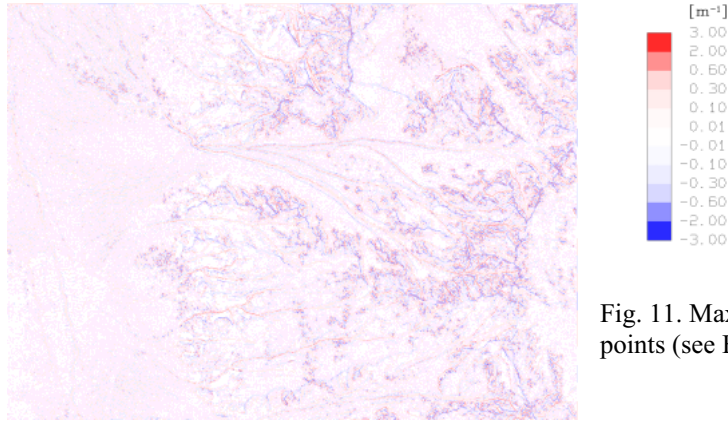


Fig. 11. Maximum main curvatures at the grid points (see Fig. 3).

The colour-coded image of the weighted root mean square error  $RMSE$  in Fig. 12 presents the local accuracy of the data points. Lowest values occur in the non-vegetated, plane zones, while the  $RMSE$  reaches values of up to 5m along the crests. Grid points determined as unusable (Fig. 10) are marked red.

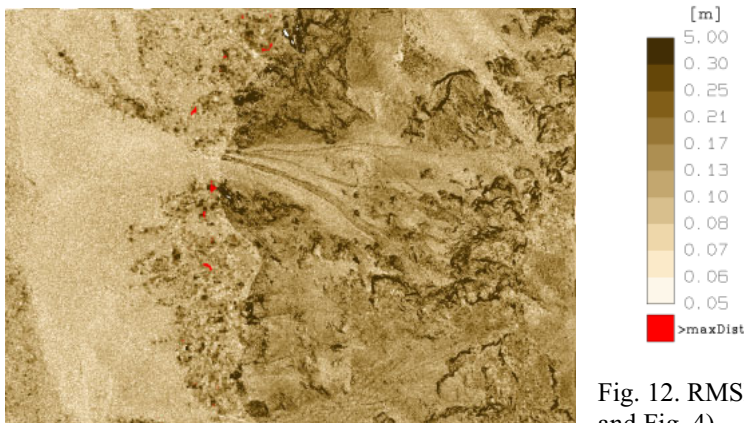


Fig. 12. RMSE at each grid point (see (6), (7), and Fig. 4).

The cofactor in height (Fig. 13) mainly varies around 0.3. Along the crests and in the data voids, values of up to 1 show up. Moreover, the overlap of the two laser scanner strips is distinguishable (compare Fig. 9). Once again, unusable areas are coloured red (see Fig. 10).

Finally,  $\hat{\sigma}_{DTM}$  is computed (Fig. 14). DTM height accuracies around 4cm result in the non-vegetated, plane areas. In the vegetated zones, variation increases with values up to 30cm. The worst accuracies are achieved along the crests. Unusable areas (see Fig. 10) are once again marked red.

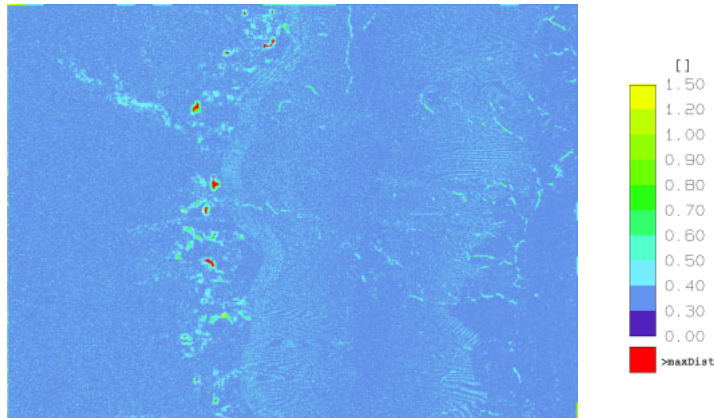


Fig. 13. Cofactor at each grid point (see (7), and Fig. 5).

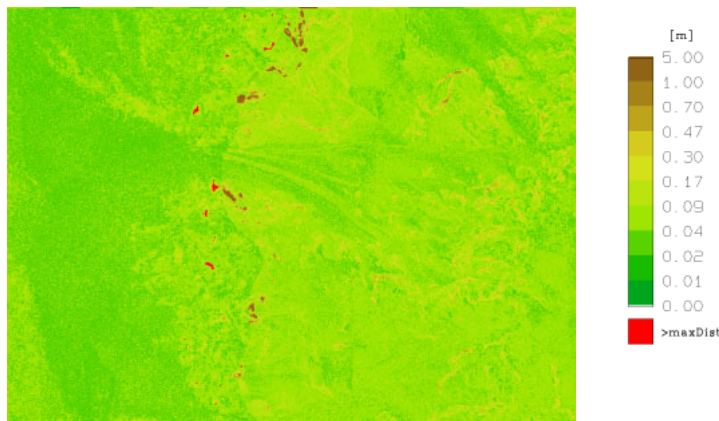


Fig. 14. DTM height accuracy at each grid point (see (8)).

## 6 COMPARISON OF ALS AND PHOTOGRAMMETRY

The slightly sloped area treated in this section is located in the Haselgraben, Upper Austria. It is described by both a photogrammetric and an ALS DTM, whereupon the ALS data were captured with about 1m mean point spacing. The photogrammetric data stem from an aged, countrywide data set that was captured on a scale of 1:30,000 (bulk points), or 1:15,000 (structure information), respectively (*Franzen & Mandlbürger* 2003).

Fig. 15 gives an impression of the test site, as it presents a shaded view of the ALS surface model.

The data sets used as input for DTM interpolation are presented in Fig. 16. The ALS points were classified by robust filtering. Large data voids mainly stemming from buildings show up. The photogrammetric data consist of homogeneously distributed bulk points and additional break and form lines with a high level of detail.



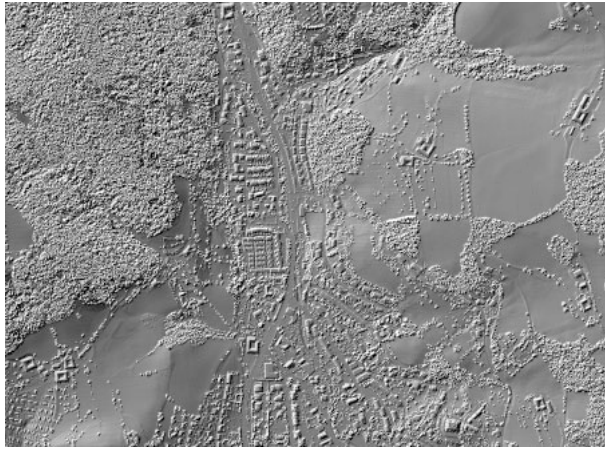


Fig. 15. Shaded digital surface model of the ALS DTM of the Haselgraben test site. Project of the “Oberösterreichische Landesvermessung”.

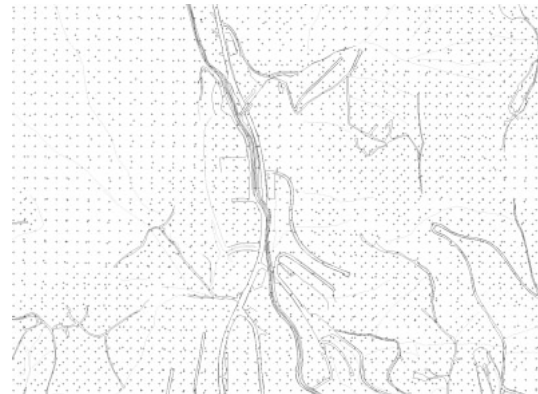


Fig. 16. Input data for the interpolation of the ALS (left) and the photogrammetric (right) DTM. Break lines in the photogrammetric data set are coloured blue, form lines are green.

In Fig. 17, the resulting DTM are presented in shaded views. The ALS DTM has a grid width of 1m and shows up high detail throughout the whole area. The photogrammetric DTM holds a grid width of 10m and is based on bulk points with much larger point spacing. However, through the selective, manual measurement of structure information, the topographically interesting elements are also described by the photogrammetric DTM, at a comparable level of detail. Obviously, the photogrammetric DTM contains some blunders along the inclination in the Northwest. It has to be mentioned that these errors could widely be corrected during a review, leading to an enhanced countrywide DTM (Franzen & Mandlbürger 2003).

The data densities of the two DTM (see Fig. 18) show up that the ALS DTM is covered by four overlapping laser scanner strips, leading to an area of high density in the form of a T standing upside down. The data density of the photogrammetric DTM varies mainly due to additional structure information.

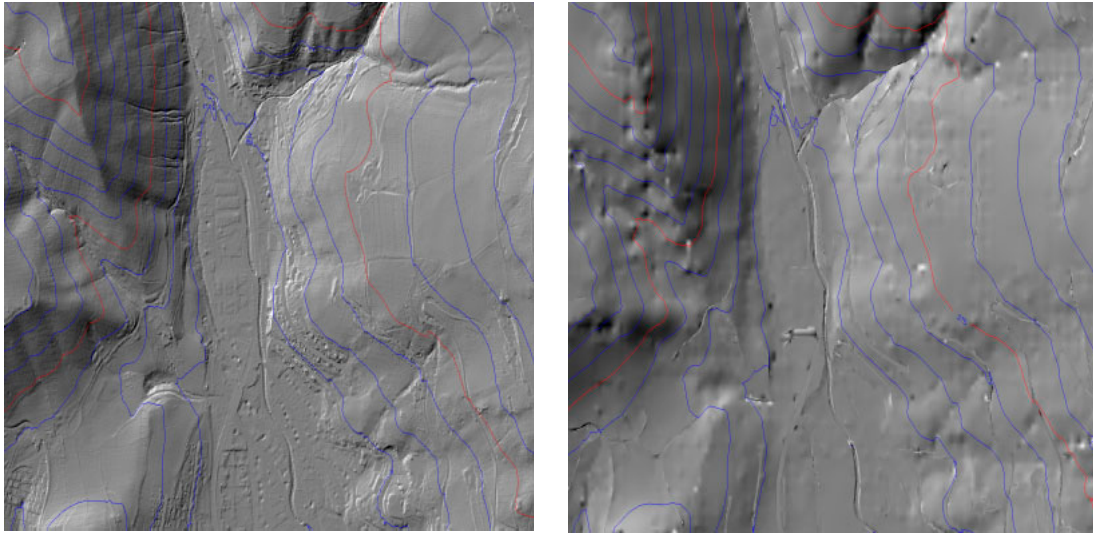


Fig. 17. Shaded ALS (left) and photogrammetric (right) DTM together with contour lines every 25 meters.

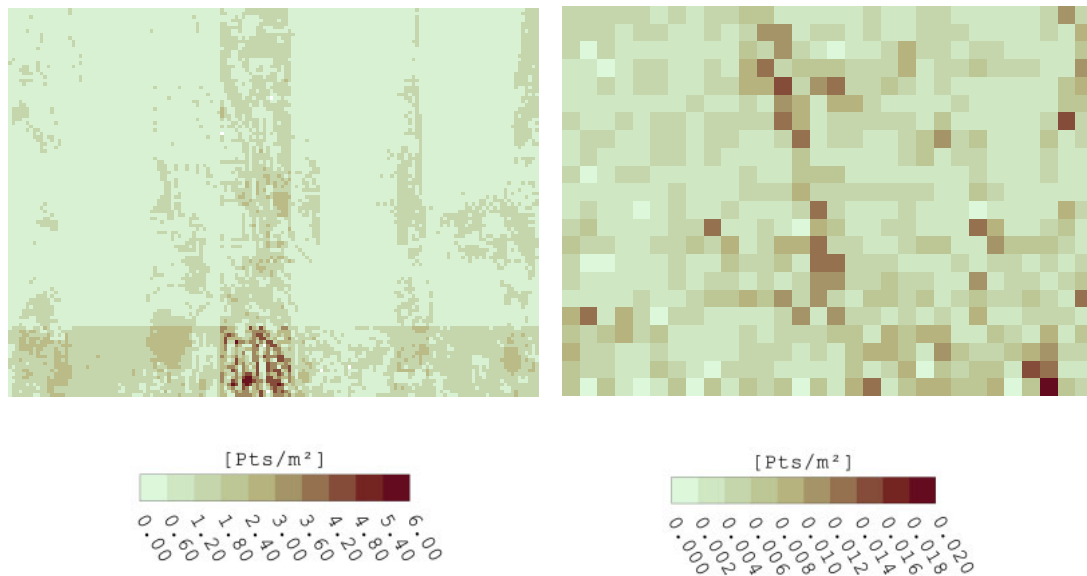


Fig. 18. Point densities, calculated with a cell size of 100m<sup>2</sup> (ALS, left), and 250m<sup>2</sup> (photogrammetry, right). Please note that two different colour tables are used.

Data voids of the ALS data, generated by robust filtering, show up in the colour-coded view of the distance from each grid point to its nearest data point (Fig. 19, left). Distances larger than seven times the grid width are marked red, in order to warn users. The corresponding image of the photogrammetric data (Fig. 19, right) owns an outstanding pattern of extreme distances. It stems from the difference between the bulk point spacing of about 25m and the DTM grid width of 10m, which was chosen according to the higher level of detail of structure information.

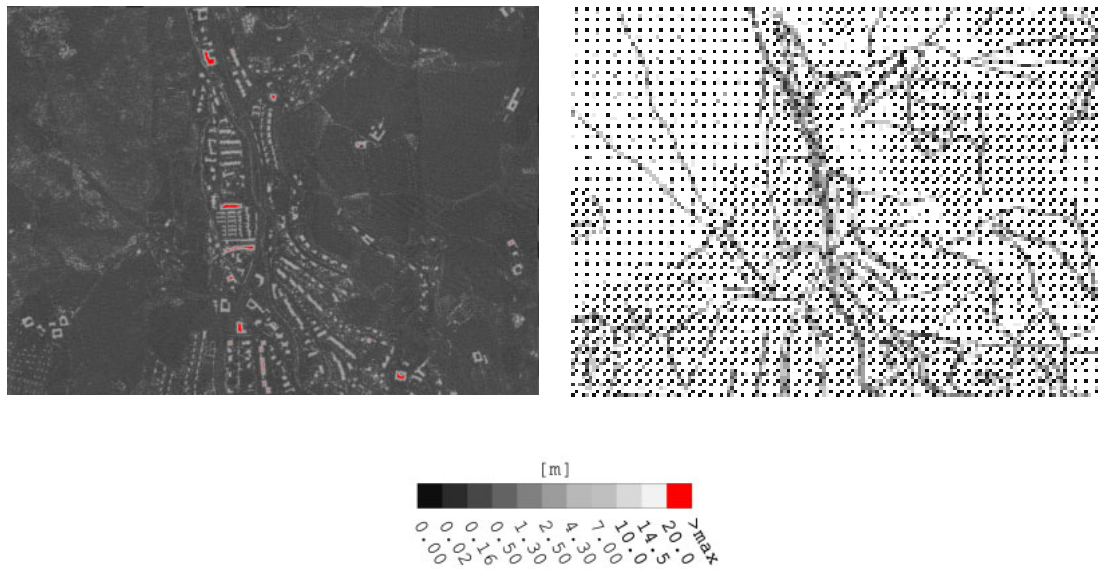


Fig. 19. Distance to nearest data point. In the ALS DTM (left), distances larger than 7m are coloured red. For the photogrammetric DTM (right), an outstanding pattern is noticeable that stems from the difference between the bulk point spacing and the DTM grid width.

Fig. 20 presents the maximum main curvatures at the grid points. The images of the curvatures of both DTM show comparable results. As break lines are considered in the computation of curvature, extreme values mainly occur around form lines of the photogrammetric data set.

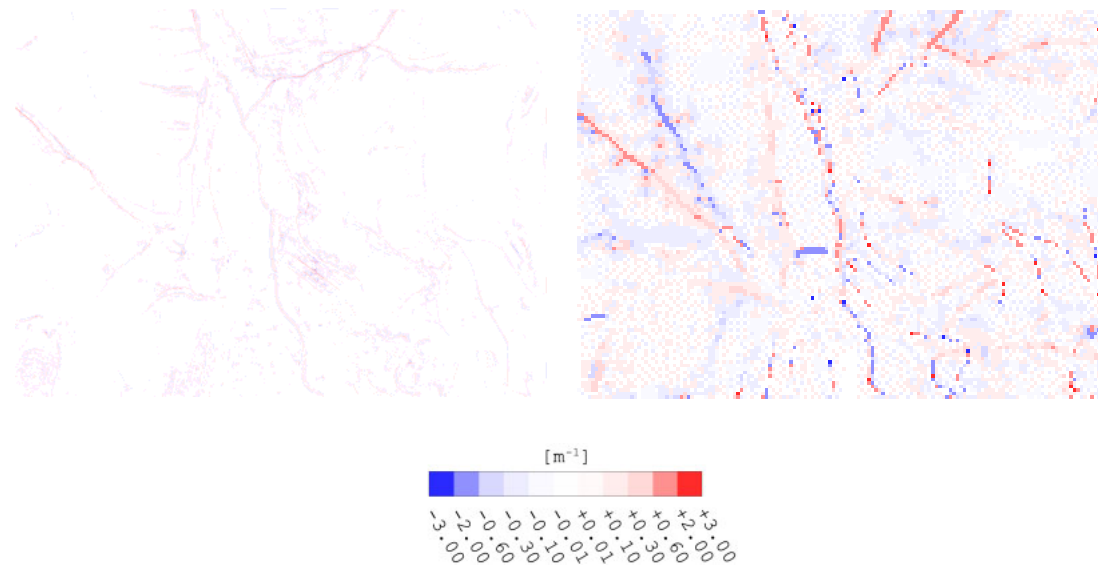


Fig. 20. Maximum main curvature at each grid point of the ALS (left) and the photogrammetric (right) DTM.



The local, weighted *RMSE* of the input data are presented in Fig. 21. For the ALS DTM, values result as near to the standard deviation of measurement (given as  $\pm 5\text{cm}$ ), except for terrain breaks and vegetated zones. For the photogrammetric DTM, the *RMSE* show up the data blunders.

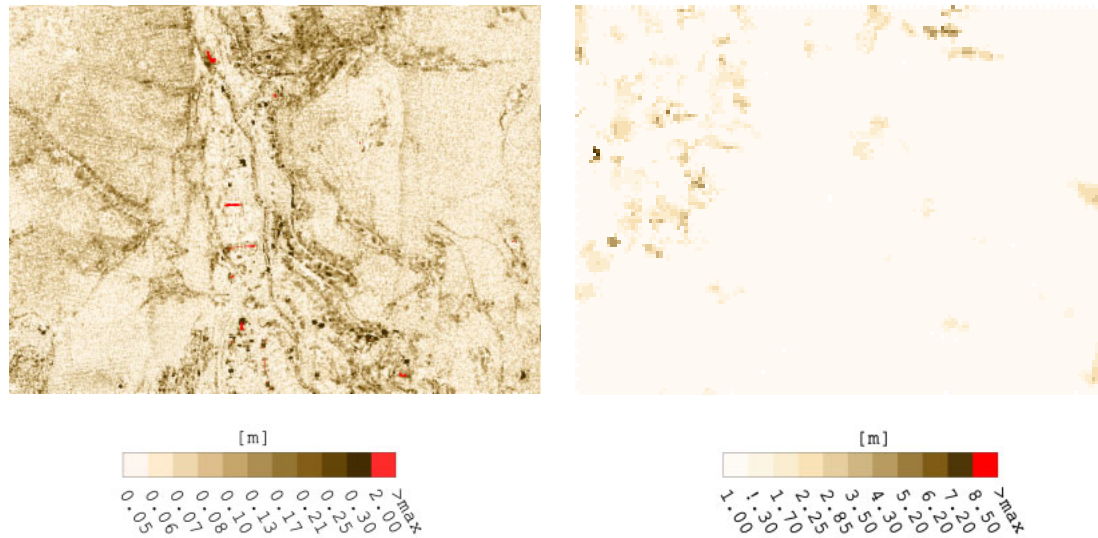


Fig. 21. Weighted RMSE of the ALS (left) and the photogrammetric (right) DTM. The RMSE in the photogrammetric DTM are widely replaced by the a priori known standard deviation of measurement ( $\pm 1\text{m}$ ). Grid points determined as unusable (see Fig. 19) are marked red. Please note that two different colour tables are used.

The cofactors in height (see Fig. 22) show up different characteristics of the data. For the ALS DTM, mainly the overlaps of the laser scanner strips are distinguishable. For the photogrammetric DTM, the cofactors own a much higher variation stemming mainly from inconsistencies between the bulk data and the additional structure information.

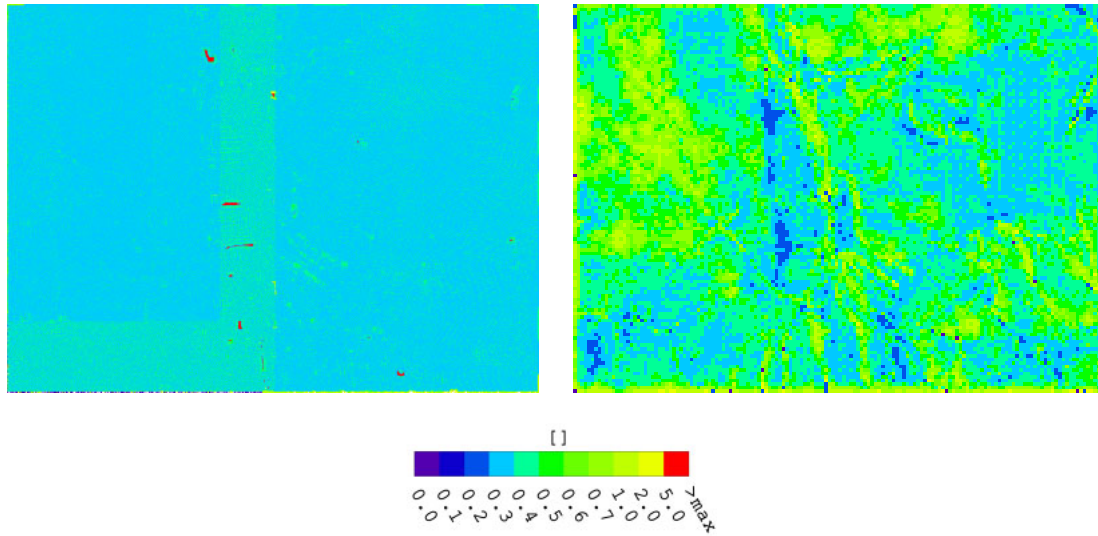


Fig. 22. Cofactors in height of both DTM (ALS: left, photogrammetry: right). Unusable areas (see Fig. 19) are marked red.

The resulting DTM height accuracies are presented in Fig. 23. The quality of the ALS DTM is much better than the one stemming from photogrammetric data. While the accuracy of the ALS DTM is better than 4cm over wide areas, the photogrammetric DTM mainly holds an accuracy of worse than 0.5m, and even reaches values of worse than 5m.

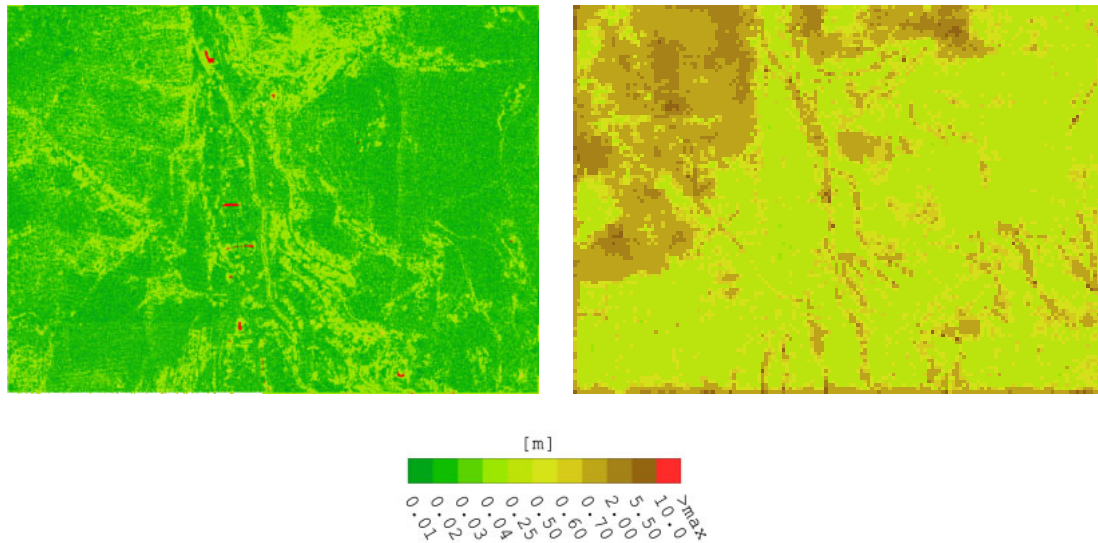


Fig. 23. DTM height accuracy at each grid point (ALS: left, photogrammetry: right). Unusable areas (see Fig. 19) are marked red.

## 7 CONCLUSIONS AND OUTLOOK

Global quality parameters for DTM derived from ALS or photogrammetric data are known by empirical analyses. These global parameters are important for the management of DTM projects.

An approach to derive local DTM quality measures has been developed that holds major advantages in comparison to other methods and generates promising results. Local DTM quality may be expressed by:

- point density
- distance between each grid point and its nearest data point
- curvature
- weighted root mean square error of the surrounding original data (*RMSE*)
- standard deviation of each grid point  $\hat{\sigma}_{DTM}$

The next step is the improvement of software performance. Afterwards, the approach has to be tested with more data sets, which will generate a feedback for improving the theory and the implementation.

In the future, DTM should be handed over to users together with the presented local quality parameters, at best in terms of quality layers.

## REFERENCES

- Borgefors, G., 1986. Distance Transformations in Digital Images. *Computer Vision, Graphics and Image Processing*, CVGIP 34 (3), pp. 344-371.
- Franzen, M. & Mandlbürger, G., 2003. Die neue Generation des digitalen Geländemodells von Österreich. VGI 03/2003.
- Frederiksen, P., 1980. Terrain Analysis and Accuracy Prediction by Means of the Fourier Transformation. *International Archives of Photogrammetry and Remote Sensing*, 23(4); 284-293.
- Kraus, K., 2004. *Photogrammetrie. Band 1: Geometrische Informationen aus Photographien und Laserscanneraufnahmen*, 7. Auflage, Walter de Gruyter, Berlin., Germany, 397 pages.
- Kraus, K., Karel, W., Briese, C., Mandlbürger, G., 2006. Local Accuracy Measures for Digital Terrain Models. *Photogrammetric Record*, 21 (116): 342-354.
- Li, Z., 1993. Theoretical Models of the Accuracy of Digital Terrain Models: an Evaluation and Some Observations. *Photogrammetric Record*, 14(82): 651-660.
- Schenk, T., 2005. The back projection method. Presentation at the EuroSDR seminar in Aalborg on automated checking of DTM, August 2005.
- Tempfli, K., 1980. Spectral Analysis of Terrain Relief for the Accuracy Estimation of Digital Terrain Models. *ITC Journal* 1980-3: 478-510.



## **Appendix II**

### **Programme of the seminar**

## **”Automated Quality Control of Digital Terrain Models” at Aalborg University**

### **Wednesday, 17.8.05**

Icebreaker party 19-21 hours

Aalborg University, Fibigerstraede 11, rooms 1 and 2

### **Thursday, 18.8.05**

8.00 Registration

9.00 Welcome

J. Höhle, Aalborg University, Denmark

9.05 Research of EuroSDR

J. Hyypä, EuroSDR/Finnish Geodetic Institute, Finland

9.10-9.30 The EuroSDR project ”Automated DTM checking” – goals and expectations

J. Höhle, Aalborg University, Denmark

9.30-10.15 The DTM for orthophoto production

P. Reiss, Bavarian State Mapping Agency (BLVA), München, Germany

10.15-10.45 Coffee break

10.45-11.30 Generation and revision of the Danish Elevation Database from multiple data sources

P. Frederiksen, Danish National Mapping Agency (KMS)

11.30-12.15 Quality parameters of DTMs

K. Kraus, Technical University Wien, Austria

12.15-13.30 Lunch

13.30-14.15 Principles of automated DTM generation

D. Wild, Inpho GmbH, Stuttgart, Germany

14.15-15.00 Checking and improvements of DTMs in the EuroSDR test

M. Potucková, Aalborg University, Denmark

15.00-15.30 Coffee

15.30-17.00 Methods and results of participants in the tests

1. The backprojection method  
T. Schenk, B. Csatho, The Ohio State University, USA
2. The method of two overlapping orthoimages  
D. Skarlatos, National Technical University of Athens, Greece
3. The Polish method, M. Szumilo, Z. Paszotta  
University of Olzstyn, Poland
4. The Czech method of DTM quality evaluation  
R. Fiala, West Bohemian University in Pilzen, Czech Republic
5. DTM checking with gross error detection method based on space resection  
with direct analytical approach  
T. Jancso, University of West Hungary, College of Geoinformatics, Szekesfehervar, Hungary

19.30-22.00

Dinner

Hotel 'Hvide Hus' ('White House')

Address: Aalborg, Vesterbro 2

**Friday, 19.8.05**

9.00-9.45 Utilization and checking of DTMs in an orthoimage production flow

T. Nielsen, Scankort A/S, Denmark

9.45-10.15

Developments in DTM generation at BAE Systems

S. Walker, BAE Systems, USA

10.15-10.45 Coffee break

Discussion panel

10.45-12.15

The different approaches to an automated quality control of DTMs will be discussed by

K. Kraus, P. Reiss, O. Jacobi, T. Schenk

12.15-13.30 Lunch

13.30-14.00

Continual developments in Inpho-products: MATCH-T and DTMaster

E. Lysdal, Geoisten/Inpho, Denmark

14.00-14.30 Summary of the results of the seminar

J. Höhle, Aalborg University

15.00-16.30 Visit to the Virtual Reality Media Laboratory of Aalborg University

**EuroSDR-Project**

**Commission 1**

**“Sensors, Primary Data Acquisition and Georeferencing”**

**“Reliability of Direct Georeferencing:  
An Overview of the Current Approaches and Possibilities”  
Final Report on Phase 1**

*Report by Jan Skaloud*  
École Polytechnique Fédérale de Lausanne (EPFL)





## Abstract

After some initial hesitations, the direct georeferencing (DG) of airborne sensors by GPS/INS is now a widely accepted approach in the airborne mapping industry. Implementing DG not only speeds up the mapping process and thus increases the productivity, but also opens the door to new monitoring applications. Although the system manufacturers tend to claim that DG is a well established technique and no longer a research topic, the technology users often encounter pitfalls due to undetected sensor behavior, varying data quality and consistency. One could almost claim that the reliability of DG is the Achilles' heel of this otherwise revolutionary approach in civil airborne mapping. EuroSDR has recognized this problem and would like to address it in several phases. First phase of this effort are some preliminary investigations, charting the current situation and making suggestions for further research. The investigations are divided into the following technology fields: GNSS, inertial sensors and estimation methods, integrity and communication, calibration and integrated sensor orientation. Each field describes the current situation with respect to DG and discusses additional existing possibilities. These do not claim to be complete or exhaustive; however, they claim to address the essential features, methods and processes, the combination of which could increase the reliability of DG substantially without setting large side penalties.

## 1 Introduction

### 1.1 Background

Within the last decade, the application of Direct-Georeferencing (DG) has brought a small revolution into the mapping industry by driving down the cost of mapping products and speeding up the production cycle. At the same time, it has enabled the practical introduction of sensors such as lasers, line scanning cameras, and radar systems into civil airborne mapping. Although DG can now be considered as a well established industrial method, there remain a number of open questions related to its reliability and/or data quality control (QC). These concern both the clients and manufacturers, as they are often related to instrument- or method redundancy which influences the cost of a system and the speed of the production.

### 1.2 Motivation

In 2005, EuroSDR initiated a preliminary investigation into the reliability of direct georeferencing that shall help the future institutional activities in this area. The initial project phase aims at understanding the current situation and sketching an overview of the used or available approaches and technologies related to this topic; it will serve as a base for further decisions. The institutional ambitions can be summarized by two points:

- No commission has ever made a mapping system.
- No mapping or quality standards have ever been made without a commission.

### 1.3 Limits

The study is limited in time and resources and, therefore, its primary aim is to be rather informative than exhaustive. Also, part of the ‘situation map’ was drawn using responses from technical suppliers to a questionnaire. Unfortunately, in some critical cases, no or very limited responses were given. (The author sincerely thanks to those who took the time and effort for replying!) This may eventually distort the given picture in some way, hopefully not decisively.

### 1.4 Outline

After giving some initial definitions, an overview of the current situation is presented. The individual parts of the long chain of DG information flow are treated separately. Each part starts with a problem identification that is followed by a summary of available technologies and an ‘estimate’ of currently used approaches.

## 2 Reliability and Integrity

### 2.1 Definitions

#### 2.1.1 Reliability

Reliability has various interpretations. In the DG context it mainly refers to

- the controllability of observations, that is, the ability to detect blunders and to estimate the effects that undetected blunders may have on a solution;
- the probability of a system to function under stated conditions for a specified period of time.

The former is often decomposed into internal and external reliability. Internal reliability relates to the amount of gross error in an observation, not detectable at a certain probability level while the external reliability relates to the effect of non-detectable blunders on the estimated quantities (for example coordinates).

The latter context can be expressed mathematically as  $R(t) = \int_t^{\infty} f(x)dx$  where  $f(x)$  represents the Failure Probability Density Function (FPDF) and usually refers to physical signal failures.

#### 2.1.2 Integrity

By definition, integrity is a measure of trust which can be placed in the correctness of the information supplied by the total system. Integrity includes the ability of the system to provide timely warnings to the user when the system should not be used for the intended operation [1].

The integrity risk is the probability of an undetected (latent) failure. The systems of highest ambitions are of high reliability (i.e. never break down) and high integrity (i.e. a brake down is immediately detected) but in principle there can be systems of high integrity but low reliability or vice versa.

## 2.2 *Application to DG*

The controllability of observations is closely related to redundancy that significantly increases system reliability; it is often the only viable means of controlling. However, redundancy comes at higher price either due to additional components, signals, or processing methods. Augmenting reliability by redundant observations will be the main interest of this study that follows the individual sensors and data fusion.

The total failure of equipment or one of its parts is usually easily detectable while the occurrence of an unexpected error or performance degradation may be more difficult to notice. Such degradation may bias the DG solution outside its estimated accuracy. This aspect of reliability as investigated here is therefore understood more in a sense of the trustworthiness of the estimated performance.

## 3 **DG in General**

### 3.1 *The method*

Georeferencing can be defined as a process of obtaining knowledge about the origin of some event in space-time. Depending on the sensor type, this origin needs to be defined by a number of parameters such as time, position, attitude (orientation), and possibly also the velocity of the object of interest. When this information is attained directly by means of measurements from sensors aboard the vehicle, the term direct georeferencing is used. In other words, DG comprises a long process of information flow that involves acquisition, synchronization, processing, integration, and transformation of measurement data from navigation (GPS/INS) and remote sensing instruments such as frame or line scan cameras, lasers or radars. The term of DG is sometimes understood as a one-directional data flow from GPS/INS to the mapping sensor(s). When there is a common treatment or a feedback between remotely sensed data and navigation parameters, the term of Integrated Sensor Orientation (ISO) is used.

### 3.2 *Technology suppliers*

The limited field of options that existed only some years ago is diversifying rapidly. This may bring some advantages to the users in terms of pricing; however, it also increases the risk in terms of quality. As will become quickly evident, the purpose of this study is NOT to list or evaluate the technology suppliers! The investigations are limited to the conceptual level of available and future technologies (used/not used) and therefore no concrete references to providers are given.

### 3.3 *Overview*

Most of the technology suppliers have identified that the successful integration of DG into the mapping process requires knowledgeable users as much as good software functionality. Hence, at least the serious players periodically organize and encourage training courses. Those also provide well established workflows; however, these are often optimized for a particular system. The notion of the system- or process reliability is currently traded for a less clear definition of data quality control (QC). The QC comes at different stages of data processing, however, often with substantial delays that do not allow calling a mapping mission successful with good confidence at landing or at the end of the

day. The general lack of redundancy (and thus reliability) in navigation instrumentation (both at the physical and signal level) needs to be compensated by ISO. Hence the requirements on QC as well as on additional important issues such as system calibration are very different depending on whether ISO is used or not.

## 4 GNSS

### 4.1 *Current situation*

In most scenarios, the position of the airborne carrier is determined by one dual frequency GPS receiver (and one antenna) on board of a vehicle. The trajectory accuracy is usually improved off-line by carrier-phase differential data using forward/backward processing and ambiguity determination/validation for one or more base stations. In situations like platform stabilization, real-time GPS/INS integration is performed, however, not in the differential mode. This means that the final answer on data accuracy and reliability cannot be obtained with high confidence during the data acquisition phase. Moreover, possible occurrences of local signal distortions affecting both the GNSS code and phase measurements remain difficult to control and become apparent only later in ISO (bundle adjustment, LiDAR strip adjustment). In general, the reliability measures are replaced by “data QC” that is introduced on different levels. It comprises checks on grammatical (physical) and semantic (validity) aspects of the signal, the geometric situation in real time, and processing residuals in post-processing. Overall, the GNSS-derived position is the decisive factor for trajectory accuracy at lower frequencies ( $<0.1\text{Hz}$ ). With all the progress in carrier-phase differential techniques its application usually marks the mission outcome (i.e. success or failure).

### 4.2 *Available technologies*

#### 4.2.1 RAIM

In terms of physical reliability and integrity, there is a great difference between aviation-certified GPS receivers and the consumer GPS receivers [2]. Apart from the resistance to harsh environment, electromagnetic interference, clearly defined low-dB tracking scenarios and time to first-fix, the avionic receivers use standardized methods for Fault Detection and Exclusion (FDE). The whole process is also known as Receiver Autonomous Integrity Monitoring (RAIM). It requires a minimum of 5 satellites and uses the probability density function and minimum bias or worst bias with fixed or variable threshold [3]. It is based on the Bayesian approach of mixing probability density functions (nominal & failure case) and weighted by their probabilities of occurrence [4]. RAIM can provide alarm during the flight but it is useful only if the operator has access in real time to this information and the possibility to act in order to correct the problem; for example by collecting new data or by changing the trajectory. RAIM is not a standard option in consumer GNSS receiver technology [5] and it is not clear to which extent this is used in the acquisition phase of the DG process.

#### 4.2.2 SBAS

The Satellite-Based Augmentation Systems (SBASs) currently comprise WAAS (Wide Area Augmentation System) covering good part of North America, EGNOS (European Geostationary Navigation Overlay Service) covering Europe and parts of its surroundings, and MSAS (Multi-

Transport Satellite Based Augmentation System) covering part of Asia and Pacific including the Japanese territory. The signal of these systems is interoperable and they offer satellite signal integrity monitoring in flight [1] as well as estimates on ‘normal’ deviations in GNSS signals (such as atmospheric delays, satellite clock-, and ephemeris errors). In other words, such a system ‘flags’ obviously erroneous measurements and computes quality metrics for the others that are broadcast along with the corrections. It is important to note that the decision what to do with this information is left upon the user receiver. Again, the receiver behaviour using SBAS-input is regulated only in case of avionic equipment [6]. The positioning accuracy using the suchlike augmented GPS signal is reported to be 1 to 2 meters vertically and around 1 meter horizontally for EGNOS [7], [8], [9] and slightly worse for WAAS [10] under optimal conditions. Although this accuracy is better than standalone GPS it is still insufficient for most DG applications. Nevertheless, the concept of monitoring the integrity and quality of the code-measurements can well contribute to the DG acquisition phase. Most likely, this has not yet been fully exploited for various reasons.

#### 4.2.3 GPS signal modernization

The modernization of the GPS signal comes in different phases. First, L2C (C/A code on L2) is being introduced on the IIR-M block of satellite. Although one SV has been in orbit since September 2005, the nominal 24 satellites providing this signal are not scheduled before 2012. The main advantages of this enhancement are an improved interference resistance and tracking capability (~3dB higher). Some L2C-ready receivers are already available on the market. The impact on trajectory accuracy and thus DG performance is not expected to be significant before the introduction of the 3<sup>rd</sup> civil carrier frequency (L5) on the Block IIF and Block IIIA satellites. This will take even longer to materialize.

#### 4.2.4 GLONASS and Galileo

The GLONASS constellation is currently enjoying a new boom (13 active SVs in 2005) that is scheduled to continue until reaching a complete constellation of 26 SV in 2012. Its impact on DG applications has been limited up to now but may gain importance once more SVs become available. The proposed signals for Galileo should bring benefits for code multipath mitigation thanks to ‘faster’ codes (steeper slopes of the correlation peaks) and data-free sidelobes. Since end of December 2005, the first experimental Galileo satellite has been transmitting its signal in space [11] that is currently under the process of validation. Its full constellation is scheduled for 2010; however, the ‘five years goal’ has been shifted already several times in the past. Hence, the improved reliability through redundancy of systems, satellites and signals is not expected to happen any earlier before 5-7 years from now.

#### 4.2.5 PPP

The Precise Point Positioning (PPP) is a concept of GPS positioning using data from a single GPS receiver and precise satellite orbit and clock information generated by the International GPS Service (IGS). This technique is reported to achieve decimetre or sub-decimetre accuracy without the need for processing any GPS reference station data. PPP can make use of single- [12] or dual- [13], [14] frequency carrier-phase measurements. The drawback is usually a considerable delay in algorithm initialization and sometimes the method stability as well as the need for an on-line access to IGS-derived products that come also with a certain delay. Nevertheless, there is a significant potential for this already commercially available technique for DG applications with relaxed accuracy requirements or those executed over large remote areas. The saving comes in terms of simplified logistics. Some DG-related research projects focus on this methodology.

#### 4.2.6 CP-DGPS

The double differencing (DD) of GPS carrier-phase (CP) and code data is the most common technique in trajectory estimation that allows achieving cm- to dm- level positioning accuracy under ‘normal’ conditions. For this end, the best estimate of the DD carrier-phase ambiguity needs to be computed (usually by the LAMBDA technique [15] or other least-squares methods) and validated [16]. Although the theory and practice of this process has progressed considerably, open questions still exist especially in the validation area [17]. The expected performance of ambiguity resolution is measured by its success rate given by the probability distribution of the integers. The results are different if the integers are computed based on geometry-free or geometry-based models. Consider an example in the case of DD and the geometry-based model supposing optimal tracking conditions and a short baseline: the instantaneous success rate is ~99.90% with 6 satellites used. However, local disturbances such as multipath, radio interference or ionospheric disturbances can quickly jeopardize this theoretical value. Another limit affecting the ambiguity fixing/reliability is the baseline length between the base station and the rover. Up to distances of 5 km, it is possible to work (at least theoretically) with L1 receivers. For <15 km baseline lengths, a L1/L2 data processing is necessary. For <30 km baseline lengths, additional data/products have to be added to the L1/L2 DD carrier-phase ambiguity fixing resolution [18]. This is usually achieved via a network of reference stations.

#### 4.2.7 Network differential techniques

The network differential GPS techniques fall into one of three categories: (1) measurement domain, (2) position domain, and (3) state-space domain. Category (1) algorithms provide the user with corrections from a reference station or a weighted average of corrections from a network of reference stations. In approach (2), the user derives independent positions using corrections from separate reference stations. A weighted average of these solutions is then computed. The disadvantage of algorithms of group (1) and (2) is a degradation of accuracy with distance from the network centre. Moreover, (2) is not very well suited for ambiguity resolution although it is probably the most common approach used in DG applications (in post-processing). Its alternative is the true multi-baseline processing that is more common in studies of geodynamic phenomena. In this approach, all baselines are computed together, taking into account the inter-baseline correlations which arise from observing a GPS network simultaneously [19]. The approach (3) tries to estimate the real physical parameters as satellite clocks and orbits, reference station tropospheric- and clocks errors. However, its success depends not only on correct modelling but also on parameter observability and correlation. The ionospheric delays can also be modelled from dual-frequency reference station data for single-frequency end users. The recently adopted RTCM 3.0 standard foresees transmitting the reference measurements rather than the corrections or parameters to the user, who is finally left with the option to decide how to exploit them [20]. Hence, some previously investigated concepts of the trajectory reliability within the GPS network may become more practical to apply [21].

#### 4.2.8 Local and nation-wide networks

Only a few GPS receivers offer RTK solutions that work with several bases simultaneously, i.e., the user can set up a mini-network without implementing servers and other network-specialized tools. In one particular case, the firmware of the receiver allows three modes. The first mode selects the best (nearest) base and works with it. The second default mode works with all (up to three) bases independently and provides a weighted solution. The third mode works with all three simultaneously inside the triangle provided the rover belongs to it (firmware-based instant Virtual Reference Station - VRS).

The nation-wide networks have most applications in terrestrial or maritime domains. Many European states are already covered by such systems in total of their territories. The provided correction rates of up to 1Hz are sufficient for the expected flight dynamics when using GPS/INS integration. Their main product are the real time and post-mission corrections, mostly provided as ‘nearest’ or ‘VRS’ modes [22]. Unfortunately, neither of these modes is well suited for trajectories that stretch over larger areas as the base needs to be frequently re-selected to prevent too long baseline lengths. Although some networks propose area-correction parameters (FKP), their derivation uses proprietary (and thus non-transparent) methods where reliability measures cannot be added without difficulties. Hence, the ground reference station measurements are usually applied off-line using the previously mentioned approach (2). The situation for DG applications can, however, improve when all reference data become available to the rover as proposed in the master-auxiliary messages concept [20]. The major challenge will then remain in establishing a robust and fast communication link between the network and the carrier.

#### 4.2.9 Differential atmosphere

The differential atmosphere is obviously not a technology but rather a serious problem that is worth mentioning separately. Its situation is somewhat special as it can be solved through modelling with few parameters that are, however, rarely observed in practice.

The avionic applications of DG involve important height differences between the airborne and reference GPS antennas that bias the trajectory in height when the delay due to the tropospheric refraction is not modelled correctly. If the actual temperature and pressure profiles differ from those assumed by the model (as is often the case), the magnitude of such biases is at least 5-10 cm per 500 m of height difference. Some models are better than the others, but most of the popular ones yield satisfactory results when fed with appropriate meteorological data. Although digital sensors of this type are cheap and available they are rarely exploited and almost never placed on the carrier!

The research activities around atmospheric effects on GPS signals mainly focus on ionosphere modelling with parameters derived from monitoring networks. The tropospheric refraction is usually modelled as a combination of the tropospheric zenith delay and a mapping function. Recently, NOAA (National Oceanic and Atmospheric Administration, USA) started an experimental product that provides tropospheric delay estimates based on a nation-wide GPS network [23].

A first step in mitigating the tropospheric effects is the use of meteorological data at the reference station. Better estimation of model parameters implies the use of environmental data collected at all travelled altitudes. It is therefore advisable to implement a residual tropospheric delay estimation using meteorological data recorded in the aircraft during the flight (not only ‘en route’ but also through the climbing/landing phase) to minimize the systematic errors due to local tropospheric effects that cannot be predicted by global model variables [24].

### 4.3 Summary

Table 1 summarizes the available GNSS methods with respect to the reliability measures and their ‘estimated’ usage in DG. The robustness of GNSS positioning as a method will improve with the increasing number of satellites and signals made available, however, the technologies available today could be better explored.

Segment/Error	Mitigation in RT	Mitigation mission	post	Situation in DG
SV functionality	SBAS	DGPS analyses		Rarely done in RT
Rover functionality	RAIM	Too late		RT—usually only geometry
Base functionality	RT-Network	Network		Sometimes, no RT
Atmospheric Delays	SBAS	PPP, DGPS, CP-DGPS		via CP-DGPS, rarely in RT
Diff. Troposphere	Sensors at carrier + base(s)			Parameters not observed
Multipath/Interference	Receiver and antenna hw/sw design			Follows the evolution
Long Base	Multi-base processing, Master-Auxiliary			Not optimal, no RT
Ambiguity	RTK	CP-DGPS		Separated per base, no RT

**Table 1: Reliability techniques in GNSS.**

## 5 Inertial Sensors and Estimation Methods

### 5.1 Current situation

Although the use of inertial technology in life-critical navigation and guidance applications requires the employment of several (redundant) inertial measurement units (IMU), DG exploits (almost exclusively) only one sensor. Should the unit start malfunctioning, the technology providers rely on detecting obvious failures within the hardware (in real-time) and the detection of eventual performance degradation via the integration with GPS data and its post-mission analysis. The conventional GPS/INS integration tools usually cannot identify sensor degradation from incorrect stochastic/model assumptions without the interpretation of an experienced user. In other words, the models and estimation methods used in DG are generally well optimized for expected sensor behaviour but not for the marginal cases.

### 5.2 Available technologies

#### 5.2.1 The enabling technology

In the context of DG, the primary role of the IMU is in the determination of orientation. The use of GPS/INS integration can be seen as a self-calibration technique for the gyros (the calibrated accelerometers are also needed for that) and a high-frequency interpolator of the GPS position. The inertial technology has been evolving for over fifty years. The most promising technologies enabling the direct measurement of the camera's orientation came with the concepts of ring laser gyros (RLG) and fiber optic gyros (FOG), as well as the later evolution of strapdown dry tuned gyros (DTG) and quartz rate sensors. In general, the sensors of each technology span several orders of magnitude in terms of precision. As a rule of thumb, their precision is proportional to sensor cost and size [25]. The general trend is to rather use smaller and cheaper sensors that rely on calibration by GPS data. The potential of orientation accuracies for today's most popular sensors is summarized in Table 2. The majority of the numbers indicated in the table have been confirmed experimentally during numerous testing.



Time	Navigation grade (usually RLG)		Tactical grade (usually FOG, DTG)	
	roll, pitch (deg)	yaw (deg)	roll, pitch (deg)	yaw (deg)
1 sec	0.0008 - 0.0014	0.0008 - 0.002	0.001 - 0.02	0.001 - 0.05
1-3 min	0.0014 - 0.003	0.004 - 0.005	0.005 - 0.04	0.008 - 0.1
longer time	same as over 1-3 min but manoeuvre-dependent			

**Table 2: Inertial attitude determination performance with GPS aiding.**

### 5.2.2 Sensor life expectancy

The life expectancy of an IMU is usually characterized by its MTBF (Mean Time Between Failures). The users and also the system providers are sometimes less careful about the life-expectancy of the inertial components. At least one provider (and the unfortunate clients) was surprised when the incorporated IMU with the officially stated low MTBF values of 500 hours (originally conceived for missile guidance) manifested its nominal life cycle already within the first year of service in DG applications. Typically, the MTBF figures for IMUs applied in DG exceed 10000 hours. The total failure of some component (not a slow degradation) is usually detected by the IMU hardware and communicated via a predefined message, the interpretation of which, however, is left to the user.

### 5.2.3 Sensor redundancy

A redundant IMU (internally, in terms of sensors) is composed of more than three accelerometers and three gyroscopes. One approach is to combine the inertial observations in the observation space to generate a ‘synthetic’ non-redundant IMU; a second approach is to modify the inertial mechanization equations to account for observational redundancy. The latter may have some economical benefits as it does not require ‘doubling’ of all sensors. On the other hand, doubling or tripling all critical components is most likely the simplest, but not necessary the most economic way for fault detection and isolation. Although the concept of sensor redundancy is a common way for increasing the system reliability in avionics [26, 27], this method is relatively novel in DG [28] and also not available in commercial systems.

### 5.2.4 GPS/INS integration

The inertial system is integrated with GNSS because it cannot navigate accurately in stand-alone mode for extended periods of time due to the rapid accumulation of systematic sensor errors. Besides, an INS can successfully bridge the absence of GNSS signals (due to whatever reason) or smooth its short-term fluctuation. Nonetheless, the traditional GPS/INS integration cannot be considered as a good replacement of sensor redundancy and fault detection for the following reasons: First of all, GPS and inertial sensors do not sense the motion dynamics in the same spectral bands. Second, the integration is usually performed within a Kalman Filter (KF) that is often engineered to trust the inertial sensor more than the GPS in case of unpredicted disagreement. In other words, the KF is configured to reject GPS measurements outside the predicted interval of confidence that is built upon the models. As these models are tuned for the expected stochastic behaviour of the sensors, they are not prepared to react correctly under unexpected conditions.

#### 5.2.5 FDE in Kalman filtering

The chosen architecture of a KF influences not only the optimality of estimation but also the ability of Fault Detection and Exclusion (FDE). In principle, the KF can be of centralized, decentralized or federated architecture and with/without adaptive design.

The centralized KF integrates the data from all available sensors on the measurement level in an optimal manner. However, the fault detection within this architecture is difficult to achieve, even with the use of another (i.e., third) redundant sensor [29, 30]. On the other hand, the decentralised and federated KF have better competences in FDE. These concepts can be described as sets of more than one KF organized into successive integration. A sensor or a subsystem is associated with a sub-KF, the output of which is re-integrated in the overall KF. In the federated design, each sub-KF is accompanied with an index that expresses the trust given to its results (by an internal controlling mechanism). In principle, fault detection can be achieved by comparing the outputs of the different sub-KF [31, 32].

Adaptive filters work on possible modifications of the stochastic assumptions or model parameters [33, 34]. A bank of KFs can be dedicated to run on different stochastic assumptions and models [26]. Although it can be very computational-intensive, the filter banks can provide the FDE via the analyses of innovation or estimate history even for tightly-coupled GPS/INS integration [35]. The available DG systems, though, are usually limited to conventional GPS/INS integration (tightly or loosely coupled) and do not offer specialized fault-detection algorithms.

#### 5.2.6 FDE in Artificial Neural Networks

More recently, the theory of Artificial Neural Networks (ANN) has been applied to the navigation-system modelling and fault detection. The ANN concept is based on a training process by which a set of coefficients are determined, usually without a physical meaning. The disadvantage of this concept in GPS/INS integration is that different motion scenarios require different training procedures and any abrupt change in motion may trigger an alarm that can erroneously be considered as a fault [36]. Again, this technique is not known to be used in DG applications.

#### 5.2.7 Limits of GPS/INS and complementary methods

There is no such thing as a perfect instrument and, despite its undoubted power, the integration cannot completely eliminate all possible errors. In other words, the data integration handled by a Kalman filter/smoothing cancels only the non-overlapping part of the sensor's error budget, i.e. the observable errors. Thus the 'band width' of the error cancellation may overlap only partially with the motion of interest as a function of instrument type and precision and the dynamics of an aircraft. For that reason, de-noising inertial data prior to mechanization has proven in some cases to be indispensable for attitude determination and effective procedures have been developed for that purpose [37]. Another significant portion of the residual orientation errors is most likely to be affected by the quality of the in-flight alignment. Usually, the filter/smoothing keeps on refining the attitude of the inertial platform all along the flight. The strength of this process is its ability to decorrelate the misalignment errors from other error sources and is enhanced when sufficient dynamics are encountered (strong correlation among the desired parameters lowers the trust or the reliability in the estimated performance measures). Its weakness remains in the susceptibility to be influenced by the changes of the accelerometer errors and unmodelled part of the gravity field. Both influences appear as wrongly sensed accelerations that are 'eliminated' by (numerically) re-adjusting the previously aligned platform. Dropping the coupling with the accelerometers is possible once the platform is aligned and high accuracy gyros are available (i.e. 0.002-0.01 deg/h). As the high frequency part of the anomalous gravity field is likely to remain unmodelled, this concept may be appealing for certain types of

applications when operating over a ‘rough, unknown’ gravity field or when flying along survey lines at constant velocity.

### 5.3 *Summary*

In general, the failures and malfunctioning in a GPS/INS solution can be detected and corrected for, or eliminated, by adopting one or more of three possible concepts: (1) sensor redundancy, (2) functional- and error-model modifications, (3) and application of advanced estimation methods. Although centralised KF have proven to provide better estimates, their fault detection capabilities are inferior to the decentralised and federated architectures. However, the centralized KF can be use for fault detection in a setup where a bank of filters of different stochastic assumptions is run in parallel and redundant sensors are provided. In principle, sensor redundancy is a necessity, i.e., without it only ‘massive errors’ or ‘stop-of-operation’ can be quickly detected. Although life-critical applications require triple redundancy as the minimum for the detection of failures and malfunctions, this may seem bit of luxury in DG domain. On the other hand, the evolution of inexpensive MEMS sensors may quickly remove such economical constrains. It also depends on whether it is sufficient to identify a faulty operation within a particular application, or whether exclusion and measurement replacement needs to be provided. In both cases, the currently available DG systems have little to offer as the (additional) sensor redundancy is practically non-existing and FDE not adopted.

## 6 Integrity and Communication

### 6.1 *Current situation*

As formerly defined, integrity asks for the alarm in real-time or with a predefined latency. The bulk of DG applications require the fusion of data collected on the carrier and on the ground (e.g. by CP-DGPS). The prerequisite of integrity-factor calculation on all levels is therefore the establishment of reliable (intra-system) communication links between all important components. This approach is generally applied in avionics by expensive and redundant infrastructure while it is almost non-existing in DG. As the demand on trajectory accuracy in DG applications is usually higher, the approaches pursued in avionics can only be regarded as complementary. On the other hand, the time latency is less critical in DG and therefore the publicly available methods of mobile communication represent an interesting solution.

### 6.2 *Available technologies*

#### 6.2.1 The problem of distributions

From the theoretical and practical point of view, the verification theories applied in integrity monitoring require the use of Gaussian distributions. However, most of the error sources in GNSS (and inertial sensors) do not follow a Gaussian distribution. Worse, some error sources are not always zero mean, especially when observed over a short period of time. The navigation community addresses such problems by ‘overbounding’ [1]. Extension of this concept to the whole complexity of DG is far from being trivial.

### 6.2.2 Avionic approach

Today, only the integrity of code measurements can be estimated efficiently. SBAS, GBAS (Ground-Based Augmentation System) and ABAS (Aircraft-Based Augmentation System) are used in the computation of the integrity level. These techniques include or can be complemented with RAIM and GPS/INS integration. Unfortunately, the applications of DG require a higher level of accuracy than provided by code measurements. Nevertheless, some conceptual approaches or existing integrity algorithms can most likely be applied to carrier-phase data and to GPS/INS integration.

### 6.2.3 Pseudolites

The integrity concept exploiting CP-DGPS technology has been proposed for the CAT-III landing with the help of ground beacons – pseudolites (pseudo-satellites) [38]. The application-based limits when broadcasting integrity messages were identified as multipath and radio interference [39, 40]. The concept of pseudolites is also better suited for locally-limited applications and thus not for DG in general.

### 6.2.4 TCAR

The integrity verification of phase measurements in real time requires redundancy in the computation of the positioning solution. Ideally, a second (redundant and independent) solution is computed. An approach could be based on the new civil signals of GPS and Galileo and the TCAR- (Triple- (or Three-) Carrier-Phase Ambiguity Resolution) [41, 42] or FAMCAR techniques (Factorized Multi-Carrier Ambiguity Resolution) [43]. Thus, over-determination could be provided by a multi-carrier solution and a “traditional” CP-DGPS solution with the possible help of GPS/INS integration.

### 6.2.5 Communication technology

Communication links are required for the real-time transmission of GPS corrections or measurements and integrity information. The transmission of this information ranges from (geostationary) satellites (SBAS) to terrestrial wireless data transmission techniques. For CP-DGPS, radio, cellular terrestrial, satellite, and wireless transmission are compared in Table 3 based on the availability of the communication network, the provided bandwidth, the range, and the cost of the communication link. The integrity requirement in avionics asks for a priority communication link, which is perhaps not necessary in DG. Furthermore, the communication link must not interfere with the GNSS signals (this issue is critical for satellite communication [44]).

	Radio	GSM	GPRS/UMTS	SatCom	802.x
Proprietary	+	+/-	-	+/-	-
Data rate	+	-	+	-	+
Availability	+	-	-	+	+/-
Range	+/-	+	+	+	-
Multi-channel	-	-	+	-	+
Cost	+	-	-	-	+/-

**Table 3: Comparison of communication links.**

Radio transmission is used for the traditional RTK applications. Its inconvenience for DG applications is the low range due to the low transmission power. As (physical) weight (essentially for power

supply) is not critical here, the range can be increased using higher transmission power as long as the legal requirements are fulfilled.

GSM proved to be limited by its data rate of only 9.6 kbps that corresponds approximately to 5 Hz of dual-frequency measurements from one reference station [45]. The network setup or the arrival of new civil GNSS signals further increases the demand on data throughput. The availability of GSM (as well as GPRS and especially UMTS) decreases in rural regions of European countries and these technologies are not ‘generally’ available in many countries. The problems related to cell registration and hand-over are known to occur for fast moving carriers, such as aircrafts.

GPRS has higher data bandwidth as compared to GSM. Unfortunately, the unexpectedly reduced and varying data throughput have proved to be an important inconvenience for kinematic CP-DGPS applications [46]. The newly implemented UMTS technology can handle even higher data transfer rates; however, the transmission is usually handled by ‘bursts’ of packets and therefore has varying latency.

The principle advantage of satellite communication based on Low Earth Orbiting- (LEO) satellites (the availability of GEOs is highly reduced in mountainous regions) is their availability. Some systems are limited to 9.6 kbps (for Globalstar), while the broadband service providers (e.g. skybridge, teledesic) offer somewhat higher data rates.

The 802.x wireless communications techniques (e.g. 802.11x, Bluetooth, ZigBee) are of very short range with the exception of a directive array.

### 6.3 *Summary*

A complete integrity concept for DG would need to face a challenging communication problem when operating over large areas or remote regions. Although the use of dedicated infrastructure would be technically feasible, it is more realistic to foresee sub-optimal or hybrid systems that make a better use of the available technologies such as SBAS, nation-wide GPS networks, and existing communication systems. In smaller projects, the use of radio transmission seems (still) to be the most appropriate communication means for passing GNSS data or corrections and – perhaps in the future – integrity messages.

## 7 **Calibration and Integrated Sensor Orientation**

### 7.1 *Current situation*

In the context of reliability, the Integrated Sensor Orientation (ISO) currently represents the security net for the DG. The net casting can be wider or narrower according to the sensor-type, accuracy requirements, and performance of navigation data. Moreover, the use of ISO is inevitable for the system calibration. The calibration process is not standardized and each technology provider offers some tools for this purpose. The comprehension of the technology’s principles and limits, the ‘savoir faire’, and the judicious data handling seem to be more important than the functionality of a particular tool. Therefore, the users are sincerely invited to follow a specialized formation either in academia or with system providers.

Although the use of ISO requires additional work compared to DG, the process of image orientation is no longer ‘doubled’ in practice (e.g. derivation of exterior orientation with and without GPS/INS). Instead, the complementarities of methods are put upfront as in the self-calibrating GPS/INS-AT where a fast and almost automated transfer of homologous points can be achieved. Although the methods of integrated adjustments have room for improvements, this space is much larger for LiDAR or SAR than for the frame- or line-based sensors.

## 7.2 Available technologies

### 7.2.1 System calibration in general

What is understood by system calibration is the process of finding the relations in position (lever-arm), orientation (boresight), and time (synchronization) between the sensors. The calibration of systematic effects in the imaging/ranging sensors (e.g. parameters of camera interior orientation, LiDAR range-finder offset) can be made either separately or within the same process. The concepts of state-space estimation (KF in GPS/INS) and bundle adjustments (AT) have the ability to accommodate and estimate additional calibration parameters. However, doing so may cause severe correlation among the variables and hamper the reliability of the whole process. Hence, independent methods and parameter separation is recommended whenever feasible.

### 7.2.2 Lever-arm calibration

The lever-arm calibration is a typical example of the previous note on parameter calibration where ISO is not indispensable but (often) used. The lever-arm effects can be correctly modeled and thus calibrated within the KF and/or within the bundle adjustment. However, even good observation conditions cannot match the accuracy of determination by independent geodetic (tachometric) means. Even worse, the lever-arm parameters are often strongly correlated with other systematic errors, e.g., of the inertial or the GPS observations [47]. Nevertheless, the software-driven approach of adding additional parameters represents often the most economic and convenient way for the user that is unaware of the related dangers.

### 7.2.3 Boresight calibration for frame and line-based sensors

Contrary to the lever-arm, the calibration of the boresight requires performing an ISO for attaining sufficient accuracy. The related problems have been addressed by many investigations [48-52]. The situation for frame-cameras is relatively well understood, although some conceptual approaches are better than the others and possibilities for improvements exists [47]. Conceptually, the situation is not very different for line-based scanners when ‘pushbroom’ image blocks are formed and adjusted [53].

### 7.2.4 Boresight calibration for LiDAR

Contrary to well-developed approaches to boresight estimation, the correct recovery of the LiDAR-IMU misalignment is considerably more complicated. The adopted approaches are usually based either on physical boundaries or cross-sections [54, 55], DTM/DSM gradients [56] or signalized target points [57]. These procedures, while functional, are recognized as being sub-optimal since they are labor-intensive (i.e., they require manual procedures), non-rigorous, or they provide no statistical quality assurance measures. The more rigorous class of calibration procedures or strip adjustments uses the modeling of systematic errors directly in the measurement domain [58, 59], yielding practical and adequate results with good de-correlation between all parameters [60].

### 7.2.5 Synchronization

The synchronization between the sensors in airborne applications should be performed with a maximum time tolerance of 0.1ms. Previously, varying time delays used to be a problem especially

when existing image sensors were retrofitted with DG equipment; however, these problems are hopefully eliminated by proper electronic design in the era of new digital instruments. Control of timing can, e.g., be performed by imagery overlaps flown from opposite directions.

#### 7.2.6 Sensor interior orientation

The calibration procedures for digital sensors were recently very well documented by the corresponding EuroSDR-initiated activity [61]. The situation remains less clear for LiDAR [62] and almost proprietary in case of airborne SAR.

#### 7.2.7 Transformation of EO to national coordinates

The choice of a mapping frame and projection is often an underestimated factor causing tensions or distortions. The non-Cartesian character of national (often conformal) projections is causing distortions when DG is performed without special modifications of the bundle adjustment software [63]. Until recently, the problem alleviation by modified transformation of GPS/INS-derived EO was not correctly addressed openly.

Apart from the curvature of the earth, the main problem is that the basic equations of photogrammetry rely on a Cartesian reference frame. National mapping frames, however, are not Cartesian due to the length distortion encountered when projecting an ellipsoid into the plane [63, 64]. Further, national maps are often based on local geodetic datums that differ from the reference frame in which the GPS/INS solutions are obtained.

There are, in principal, three different ways to solve these difficulties: (1) the photogrammetric restitution in a suitable tangential frame and the subsequent transformation of the complete scene to national coordinates, (2) the computation of artificial ground-control points and restitution based on their transformation (imitation of indirect georeferencing), and (3) the restitution directly in national coordinates. The latter approach requires special attention when coping with the earth curvature and the length distortion of the national map projection. A detailed investigation on all these aspects is found in [65].

### 7.3 *Summary*

The concept of ISO is very powerful in the reliability control and needed for system calibration. The main problems of this approach are: (1) the additional work that cannot be fully automated and therefore delays the delivery; and (2) the fact that it comes as a last step and therefore almost too late (from an economical point of view) if the decision to re-fly needs to be taken. The procedures for system calibration can be still improved and the best available methods are not always followed. The latter applies also to the use of DG in map projections and local coordinate systems. Open problems still exist especially in the context of calibration of LiDAR and SAR sensors.

## 8 **Concluding Remarks**

As the GPS/INS technology starts to represent the sole means of sensor orientation (DG) in many projects, the factors concerning its reliability are gaining importance. The reliability is closely related to sensor redundancy and system complexity and thus the overall system cost. However, the higher

‘upfront’ expenses for more reliable systems could be saved later when dropping current (and sometimes less reliable) methods of quality control, consistency checks, or the laborious process of integrated sensor orientation. This is even more evident if integrity concepts (related to reliability checks in real-time) can get introduced.

The chain of data flow in DG is long and the method is only as strong as its weakest link. In the context of reliability, this continues to be the carrier-phase differential GPS, especially over longer baselines. ‘Waiting for Godot’ (represented by Galileo in the context of the famous tragicomedy of two acts) is not most likely the approach to be taken as there is a number of possible technologies existing today, the combination of which may well alleviate the problem. Similarly, there are many possibilities for improvements within the GPS/INS integration itself, both on the hardware- and software level. Finally, although the sensor-to-sensor correlation/calibration problem is no longer a nightmare, the rigorous or standardized approaches are still far from common practice.

## **9 Acknowledgement**

The author would like sincerely thank the doctoral students at EPLF-TOPO, namely Fadi-Atef Bayoud, Valérie Renaudin and Adrian Waegli for their important contributions in literature review and problem synthesis. The time and remarks of Dr. Klaus Legat are greatly appreciated when reviewing this report. Véronique Chazal is thanked for her assistance with final formatting and linking.



## References

- [1] P. B. Ober, "SBAS integrity concept," Eurocontrol, 2001.  
<http://topo.epfl.ch/documents/EuroSDR/ober01.pdf>
- [2] J. Studeny and B. Clark, "The aviation GNSS receiver," *ION Newsletter*, vol. 14, pp. 4-5, 2004. <http://topo.epfl.ch/documents/EuroSDR/studeny04.pdf>
- [3] H. Kuusniemi, G. Lachapelle, and J. H. Takala, "Position and velocity reliability testing in degraded GPS signal environments," *GPS Solutions*, vol. Volume 8, 2004.  
<http://topo.epfl.ch/documents/EuroSDR/kuusniemi04.pdf>
- [4] P. B. Ober, "Integrity according to Bayes," presented at IEEE, 2000.  
<http://topo.epfl.ch/documents/EuroSDR/ober00.pdf>
- [5] W. Y. Ochieng, K. F. Sheridan, K. Sauer, X. Han, P. A. Cross, S. Lannelongue, N. Ammour, and K. Petit, "An assessment of the RAIM performance of a combined galileo/GPS navigation system using the marginally detectable errors (MDE) algorithm," *GPS Solutions*, vol. 5, 2002. <http://topo.epfl.ch/documents/EuroSDR/ochieng02.pdf>
- [6] D. o. T. F. A. Administration, "Airborne navigation sensors using the Global Positioning System (GPS) augmented by the Wide Area Augmentation System (WAAS)," A. C. S. FAA, Ed. Washington, DC, 2002, pp. 8. <http://topo.epfl.ch/documents/EuroSDR/faa02.pdf>
- [7] F. Toran-Marti and J. Ventura-Traveset, "The ESA EGNOS project: The first step of the European contribution to the Global Navigation Satellite System (GNSS)," *GNSS-1 Project Office.*, 2004. <http://topo.epfl.ch/documents/EuroSDR/toranmarti04.pdf>
- [8] A. Waegli and P. Y. Gilliéron, "Le Concept d'intégrité d'EGNOS," *Géomatique Suisse*, vol. 11, 2003. <http://topo.epfl.ch/documents/EuroSDR/waegli03.pdf>
- [9] J. Ventura-Traveset, "EGNOS," *ION NTM*, 2003.  
<http://topo.epfl.ch/documents/EuroSDR/venturatraveset03.pdf>
- [10] R. Yousuf and S. Skone, "WAAS Performance evaluation under Increased ionospheric activity," presented at GNSS 05, Long-Beach, CA, 2005.  
<http://topo.epfl.ch/documents/EuroSDR/yousuf05.pdf>
- [11] G. W. Hein, "From GPS and GLONASS via EGNOS to Galileo positioning and navigation in the third millennium," *GPS Solution*, vol. 3, 2000.  
<http://topo.epfl.ch/documents/EuroSDR/hein00.pdf>
- [12] T. Beran, "High-accuracy point positioning with low-cost GPS receivers: How good can It get?" presented at GNSS 2005, Long-Beach, CA, 2005.  
<http://topo.epfl.ch/documents/EuroSDR/beran05.pdf>
- [13] Y. Gao and A. Wojciechowski, "High precision kinematic positioning using single dual frequency GPS receiver," *Remote Sensing and Spatial Information Sciences*, vol. 34, 2004.  
<http://topo.epfl.ch/documents/EuroSDR/gao04a.pdf>
- [14] R. J. Muellerschoen, B. Iijima, R. Meyer, and Y. Bar-Sever, "Real-time point-positioning performance evaluation of single-frequency receivers using NASA's global differential GPS system," presented at ION GNSS, Long Beach, California, 2004.  
<http://topo.epfl.ch/documents/EuroSDR/muellerschoen04.pdf>
- [15] P. J. G. Teunissen, P. Joosten, and D. Odijk, "The reliability of GPS ambiguity resolution," *GPS Solutions*, vol. 2, pp. 63-69, 1999.  
<http://topo.epfl.ch/documents/EuroSDR/teunissen99.pdf>
- [16] P. J. G. Teunissen and S. Verhagen, "On the foundation of the popular ratio test for GNSS ambiguity resolution," presented at ION GNSS, Long Beach, California, 2004.  
<http://topo.epfl.ch/documents/EuroSDR/teunissen04.pdf>

- [17] S. Verhagen, "Integer ambiguity validation: an open problem?" *GPS Solutions*, vol. 8, pp. 36–43, 2004. <http://topo.epfl.ch/documents/EuroSDR/verhagen04.pdf>
- [18] A. Leick, *GPS Satellite Surveying*, 3 ed: Wiley, 2004
- [19] M. R. Craymer and N. Beck, "Session versus baseline GPS processing," presented at ION GPS, New Mexico, 1992. <http://topo.epfl.ch/documents/EuroSDR/craymer92.pdf>
- [20] N. Brown, R. Keenan, B. Richter, and L. Toryer, "Advances in ambiguity resolution for RTK applications using the new RTCM V3.0 master-auxiliary messages," presented at GNSS 2005, Long-Beach, CA, 2005. <http://topo.epfl.ch/documents/EuroSDR/brown05.pdf>
- [21] J. Talaya, "Robust GPS kinematic positioning for direct georeferencing," *International Archives of Photogrammetry, Remote Sensing and Spatial Information Sciences*, vol. 33, Part B2, pp. 546-551, 2000. <http://topo.epfl.ch/documents/EuroSDR/talaya00.pdf>
- [22] U. Vollath, H. Landau, X. Chen, K. Doucet, and C. Pagels, "Network RTK Versus Single Base RTK - Understanding the Error Characteristics," presented at ION GPS, Portland, OR, 2002. <http://topo.epfl.ch/documents/EuroSDR/vollath02.pdf>
- [23] D. Kim, S. Bisnath, R. B. Langley, and P. Dare, "Performance of long-baseline real-time kinematic applications by improving tropospheric delay modeling," presented at ION GNSS, Long Beach, California, 2004. <http://topo.epfl.ch/documents/EuroSDR/kim04.pdf>
- [24] J. P. Collins and R. B. Langley, "Estimating the residual tropospheric delay for airborne differential GPS positioning," presented at ION GPS, Kansas City, 1997. <http://topo.epfl.ch/documents/EuroSDR/collins97.pdf>
- [25] K. P. Schwarz and N. El-Sheimy, "Mobile mapping systems - state of the art and future trends," *International Archives of Photogrammetry, Remote Sensing and Spatial Information Sciences*, vol. 35, Part B, pp. 10, 2004. <http://topo.epfl.ch/documents/EuroSDR/schwarz04.pdf>
- [26] R. Da and C. F. Lin, "Sensor failure detection with a bank of Kalman filters," *Proceedings of the American Control Conference*, vol. WP4-3:50, 1995. <http://topo.epfl.ch/documents/EuroSDR/da95.pdf>
- [27] Y. Yang and J. A. Farrell, "Magnetometer and differential carrier phase GPS-aided INS for advanced vehicle control," *IEEE Transactions on Robotics and Automation*, vol. 19, 2003. <http://topo.epfl.ch/documents/EuroSDR/yang03.pdf>
- [28] I. Colomina, M. Gimenez, J. J. Rosales, M. Wis, A. Gomez, and P. Miguelsanz, "Redundant IMUs for Precise trajectory determination," *International Archives of Photogrammetry, Remote Sensing and Spatial Information Sciences*, vol. 34, Part B, pp. 7, 2004. <http://topo.epfl.ch/documents/EuroSDR/colomina04.pdf>
- [29] F. Caliskan and C. M. Hajiyev, "Innovation sequence application to aircraft sensor fault detection: comparison of checking covariance matrix algorithms," *Proceedings of the 38th Conference on Decision 81 Control*, 1999. <http://topo.epfl.ch/documents/EuroSDR/caliskan99.pdf>
- [30] Y. Gao, E. Krakiwsky, and M. Abousalem, "Comparison and analysis of centralised, decentralised, and federated filters," *Navigation: Journal of The Institute of Navigation*, vol. 40, pp. 69-86, 1993. <http://topo.epfl.ch/documents/EuroSDR/gao93.pdf>
- [31] S. A. Broatch and A. J. Henley, "An integrated navigation system manager using federated Kalman filtering," *IEEE*, 1991. <http://topo.epfl.ch/documents/EuroSDR/broatch91.pdf>
- [32] M. Wei and K. P. Schwarz, "Testing a decentralized filter for GPS/INS integration," *Proceedings of the IEEE PLANS - Position, Location and Navigation Symposium*, pp. March 1990, 1990. <http://topo.epfl.ch/documents/EuroSDR/wei90.pdf>
- [33] R. Mehra, D. Bayard, S. Seereeram, and F. Hadaegh, "Adaptive Kalman filtering, failure detection and identification for spacecraft attitude estimation," *IEEE*, 1995. <http://topo.epfl.ch/documents/EuroSDR/mehra95.pdf>
- [34] A. H. Mohamed and K. P. Schwarz, "Adaptive kalman filtering for INS/GPS," *Journal of Geodesy*, vol. 73, pp. 193-203, 1999. <http://topo.epfl.ch/documents/EuroSDR/mohamed99.pdf>

- [35] I. Nikiforov, "Integrity monitoring for multi-sensor integrated navigation systems," presented at ION GPS 2002, Portland, OR, 2002.  
<http://topo.epfl.ch/documents/EuroSDR/nikiforov02.pdf>
- [36] M. R. Napolitano, D. A. Windon, J. L. Casanova, M. Innocenti, and G. Silvestri, "Kalman filters and Neural-Network schemes for sensor validation in flight control systems," *IEEE Transactions on Control Systems Technology*, 1998.  
<http://topo.epfl.ch/documents/EuroSDR/napolitano98.pdf>
- [37] J. Skaloud, A. M. Bruton, and K. P. Schwarz, "Detection and filtering of short-term (1/f) noise in inertial sensors," *NAVIGATION, Journal of The Institute of Navigation*, vol. 46, pp. 97-107, 1999. <http://topo.epfl.ch/documents/EuroSDR/skaloud99.pdf>
- [38] B. S. Pervan, C. E. Cohen, D. G. Lawrence, H. Stewa, J. D. Powell, and B. W. Parkinson, "High integrity GPS-based precision landing using beacon pseudolites," presented at ISPA, Braunschweig, Germany, 1995. <http://topo.epfl.ch/documents/EuroSDR/pervan95.pdf>
- [39] M. S. Braasch, "Multipath effects," in *The Global Positioning System - Theory and Application*, A. I. o. A. a. Astronautics, Ed., 1996
- [40] Y. Yang, R. R. Hatch, and R. T. Sharpe, "GPS multipath mitigation in measurement domain and its applications for high accuracy navigation," presented at ION GNSS 2004, Long Beach, California, 2004. <http://topo.epfl.ch/documents/EuroSDR/yang04.pdf>
- [41] B. Forssell, M. Martin-Neira, and R. A. Harris, "Carrier phase ambiguity resolution in GNSS-2," presented at 10th Int. Tech. Meeting of the Satellite Division of the U.S. Inst. of Navigation GPS ION'97, Kansas City, 1997.  
<http://topo.epfl.ch/documents/EuroSDR/forsell97.pdf>
- [42] R. R. Hatch, J. Jung, P. Enge, and B. S. Pervan, "Civilian GPS: the benefits of three frequencies," *GPS Solution*, vol. 3, pp. 1-9, 2000.  
<http://topo.epfl.ch/documents/EuroSDR/hatch00.pdf>
- [43] U. Vollath, "The Factorized Multi-Carrier Ambiguity Resolution (FAMCAR) Approach for Efficient Carrier-Phase Ambiguity Estimation," presented at ION GPS 2004, 2004.  
<http://topo.epfl.ch/documents/EuroSDR/vollath04.pdf>
- [44] J. Burrell, "Disruptive effects of electromagnetic interference on communication and electronic systems," vol. Master, 2003. <http://topo.epfl.ch/documents/EuroSDR/burrell03.pdf>
- [45] J. Skaloud, H. Gontran, and B. Merminod, "GSM-distributed RTK for precise analysis of speed skiing," presented at 8th European Navigation Conference GNSS 2004, Rotterdam, 2004. <http://topo.epfl.ch/documents/EuroSDR/skaloud04.pdf>
- [46] M. Lehmann, "Réalisation d'un serveur de corrections GPS accessible par GPRS," in *TOPO*, vol. master. Lausanne: EPFL, 2005. <http://topo.epfl.ch/documents/EuroSDR/lehmann05.pdf>
- [47] J. Skaloud and P. Schaer, "Towards a more rigorous boresight calibration," presented at ISPRS International Workshop on Theory Technology and Realities of Inertial/GPS/Sensor Orientation, Castelldefels, Spain, 2003.  
<http://topo.epfl.ch/documents/EuroSDR/skaloud03.pdf>
- [48] M. Bäumker and F. J. Heimes, "New calibration and computing method for direct georeferencing of image and scanner data using the position and angular data of an hybrid inertial navigation system," presented at Integrated Sensor Orientation, Proc. of the OEEPE Workshop, Hanover, 2001. <http://topo.epfl.ch/documents/EuroSDR/baeumker01.pdf>
- [49] M. Cramer and D. Stallmann, "System calibration for direct georeferencing," presented at Photogrammetric Computer Vision, ISPRS Commission III Symposium, Graz, Austria, 2002.  
<http://topo.epfl.ch/documents/EuroSDR/cramer02.pdf>
- [50] C. Heipke, K. Jacobsen, and H. Wegmann, "Integrated Sensor Orientation," *OEEPE Official Publication*, vol. 43, 2002. <http://topo.epfl.ch/documents/EuroSDR/heipke02.pdf>
- [51] E. Kruck, "Combined IMU and sensor calibration with BINGO-F," presented at Integrated Sensor Orientation, Proc. of the OEEPE Workshop, Hannover, 2001.  
<http://topo.epfl.ch/documents/EuroSDR/kruck01.pdf>

- [52] M. Mostafa, "Camera/IMU boresight calibration: New advances and performance analysis," presented at ASPRS Annual Meeting, Washington, DC, USA, 2002.  
<http://topo.epfl.ch/documents/EuroSDR/mostafa02.pdf>
- [53] U. Tempelmann and L. Hinsken, "Triangulation of ADS40 pushbroom image blocks - Not much different from classical frame blocks?" in *SGPBF Annual Meeting*. Lausanne, Switzerland, 2005. <http://topo.epfl.ch/documents/EuroSDR/tempelmann05.pdf>
- [54] Optech, "ALTM 30/70/100 user manual," Toronto, Canada 2004.  
<http://topo.epfl.ch/documents/EuroSDR/optech04.pdf>
- [55] T. Schenk, "Modeling and analyzing systematic errors in airborne laser scanners," vol. Technical Notes in Photogrammetry No 19, C. a. E. E. a. G. Science, Ed.: The Ohio State University, 2001. <http://topo.epfl.ch/documents/EuroSDR/Schenk01.pdf>
- [56] H. Burman, "Calibration and orientation of airborne image and laser scanner data using GPS and INS," in *Geodesy and Photogrammetry*. Stockholm: Royal Institute of Technology, 2000, pp. 107
- [57] K. Morin and N. El-Sheimy, "Post-mission adjustment of airborne laser scanning data," presented at FIG XXII International Congress, Washington DC, USA, 2002.  
<http://topo.epfl.ch/documents/EuroSDR/morin02.pdf>  
<http://topo.epfl.ch/documents/EuroSDR/morin02t.pdf>
- [58] S. Filin, "Recovery of systematic biases in laser altimetry data using natural surfaces," *Photogrammetric Engineering and Remote Sensing*, vol. 69, pp. 1235-1242, 2003.  
<http://topo.epfl.ch/documents/EuroSDR/filin03.pdf>
- [59] S. Filin and G. Vosselman, "Adjustment of airborne laser altimetry strips," presented at ISPRS Congress, Istanbul, Turkey, 2004. <http://topo.epfl.ch/documents/EuroSDR/filin04.pdf>
- [60] J. Skaloud and D. Lichti, "Rigorous approach to bore-sight self calibration in airborne laser scanning," EPFL-TOPO, Lausanne, Internal report submitted for publication 2005.  
<http://topo.epfl.ch/documents/EuroSDR/skaloud05.pdf>
- [61] M. Cramer, "The EuroSDR network on digital camera calibration, Phase 1," Stuttgart Oct. 16 2004. <http://topo.epfl.ch/documents/EuroSDR/cramer04.pdf>
- [62] R. Katzenbeisser, "About the calibration of lidar sensors," presented at ISPRS Workshop 3-D Reconstruction from Airborne Laser-Scanner and InSAR data, Dresden, 2003.  
<http://topo.epfl.ch/documents/EuroSDR/katzenbeisser03.pdf>
- [63] C. Ressler, "The impact of conformal map projections on direct georeferencing," presented at Photogrammetric Computer Vision, Vienna, 2002.  
<http://topo.epfl.ch/documents/EuroSDR/ressl02.pdf>
- [64] K. Jacobsen, "Transformation and computation of orientation data in different coordinate systems," *OEEPE Official Publication*, vol. 43, 2002
- [65] K. Legat, "Approximate direct georeferencing in national coordinates," *ISPRS Journal of Photogrammetric Engineering and Remote Sensing*, vol. submitted for publication, 2005.  
<http://topo.epfl.ch/documents/EuroSDR/legat05.pdf>

## References by alphabetic order

- Administration, D.o.T.F.A., 2002. Airborne navigation sensors using the Global Positioning System (GPS) augmented by the Wide Area Augmentation System (WAAS). In: A.C.S. FAA (Editor), Washington, DC, pp. 8. <http://topo.epfl.ch/documents/EuroSDR/faa02.pdf>
- Bäumker, M. and Heimes, F.J., 2001. New calibration and computing method for direct georeferencing of image and scanner data using the position and angular data of an hybrid inertial navigation system, Integrated Sensor Orientation, Proc. of the OEEPE Workshop. CD-ROM, Hanover. <http://topo.epfl.ch/documents/EuroSDR/baeumker01.pdf>
- Beran, T., 2005. High-accuracy point positioning with low-cost GPS receivers: How good can It get? In: T.I.o. Navigation (Editor), GNSS 2005, Long-Beach, CA, pp. 1524-1534. <http://topo.epfl.ch/documents/EuroSDR/beran05.pdf>
- Braasch, M.S., 1996. Multipath effects. In: A.I.o.A.a. Astronautics (Editor), The Global Positioning System - Theory and Application
- Broatch, S.A. and Henley, A.J., 1991. An integrated navigation system manager using federated Kalman filtering. IEEE. <http://topo.epfl.ch/documents/EuroSDR/broatch91.pdf>
- Brown, N., Keenan, R., Richter, B. and Torker, L., 2005. Advances in ambiguity resolution for RTK applications using the new RTCM V3.0 master-auxiliary messages, GNSS 2005. The Institute of Navigation, Long-Beach, CA, pp. 73-80. <http://topo.epfl.ch/documents/EuroSDR/brown05.pdf>
- Burman, H., 2000. Calibration and orientation of airborne image and laser scanner data using GPS and INS, Royal Institute of Technology, Stockholm, 107 pp
- Burrell, J., 2003. Disruptive effects of electromagnetic interference on communication and electronic systems. <http://topo.epfl.ch/documents/EuroSDR/burrell03.pdf>
- Caliskan, F. and Hajiyev, C.M., 1999. Innovation sequence application to aircraft sensor fault detection: comparison of checking covariance matrix algorithms. Proceedings of the 38th Conference on Decision and Control. <http://topo.epfl.ch/documents/EuroSDR/caliskan99.pdf>
- Collins, J.P. and Langley, R.B., 1997. Estimating the residual tropospheric delay for airborne differential GPS positioning. In: U.o.N. Brunswick (Editor), ION GPS, Kansas City. <http://topo.epfl.ch/documents/EuroSDR/collins97.pdf>
- Colomina, I. et al., 2004. Redundant IMUs for Precise trajectory determination. International Archives of Photogrammetry, Remote Sensing and Spatial Information Sciences, 34, Part B(Commission 1): 7. <http://topo.epfl.ch/documents/EuroSDR/colomina04.pdf>
- Cramer, M., 2004. The EuroSDR network on digital camera calibration, Phase 1, Stuttgart. <http://topo.epfl.ch/documents/EuroSDR/cramer04.pdf>
- Cramer, M. and Stallmann, D., 2002. System calibration for direct georeferencing, Photogrammetric Computer Vision, ISPRS Commission III Symposium, Graz, Austria. <http://topo.epfl.ch/documents/EuroSDR/cramer02.pdf>
- Craymer, M.R. and Beck, N., 1992. Session versus baseline GPS processing, ION GPS, New Mexico. <http://topo.epfl.ch/documents/EuroSDR/craymer92.pdf>
- Da, R. and Lin, C.F., 1995. Sensor failure detection with a bank of Kalman filters. Proceedings of the American Control Conference, WP4-3:50. <http://topo.epfl.ch/documents/EuroSDR/da95.pdf>
- Filin, S., 2003. Recovery of systematic biases in laser altimetry data using natural surfaces. Photogrammetric Engineering and Remote Sensing, 69(11): 1235-1242. <http://topo.epfl.ch/documents/EuroSDR/filin03.pdf>
- Filin, S. and Vosselman, G., 2004. Adjustment of airborne laser altimetry strips, ISPRS Congress. International Archives of Photogrammetry and Remote Sensing, Istanbul, Turkey, pp. 285-289. <http://topo.epfl.ch/documents/EuroSDR/filin04.pdf>

- Forssell, B., Martin-Neira, M. and Harris, R.A., 1997. Carrier phase ambiguity resolution in GNSS-2, 10th Int. Tech. Meeting of the Satellite Division of the U.S. Inst. of Navigation GPS ION'97, Kansas City. <http://topo.epfl.ch/documents/EuroSDR/forsell97.pdf>
- Gao, Y., Krakiwsky, E. and Abousalem, M., 1993. Comparison and analysis of centralised, decentralised, and federated filters. *Navigation: Journal of The Institute of Navigation*, 40(1): 69-86. <http://topo.epfl.ch/documents/EuroSDR/gao93.pdf>
- Gao, Y. and Wojciechowski, A., 2004. High precision kinematic positioning using single dual frequency GPS receiver. *Remote Sensing and Spatial Information Sciences*, 34. <http://topo.epfl.ch/documents/EuroSDR/gao04a.pdf>
- Hatch, R.R., Jung, J., Enge, P. and Pervan, B.S., 2000. Civilian GPS: the benefits of three frequencies. *GPS Solution*, 3: 1-9. <http://topo.epfl.ch/documents/EuroSDR/hatch00.pdf>
- Hein, G.W., 2000. From GPS and GLONASS via EGNOS to Galileo positioning and navigation in the third millennium. *GPS Solution*, 3(4). <http://topo.epfl.ch/documents/EuroSDR/hein00.pdf>
- Heipke, C., Jacobsen, K. and Wegmann, H., 2002. Integrated Sensor Orientation. OEEPE Official Publication, 43. <http://topo.epfl.ch/documents/EuroSDR/heipke02.pdf>
- Jacobsen, K., 2002. Transformation and computation of orientation data in different coordinate systems. OEEPE Official Publication, 43
- Katzenbeisser, R., 2003. About the calibration of lidar sensors, ISPRS Workshop 3-D Reconstruction from Airborne Laser-Scanner and InSAR data, Dresden. <http://topo.epfl.ch/documents/EuroSDR/katzenbeisser03.pdf>
- Kim, D., Bisnath, S., Langley, R.B. and Dare, P., 2004. Performance of long-baseline real-time kinematic applications by improving tropospheric delay modeling, ION GNSS, Long Beach, California, pp. 1414-1422. <http://topo.epfl.ch/documents/EuroSDR/kim04.pdf>
- Kruck, E., 2001. Combined IMU and sensor calibration with BINGO-F, Integrated Sensor Orientation, Proc. of the OEEPE Workshop ". CD-ROM, Hannover, pp. 84-108. <http://topo.epfl.ch/documents/EuroSDR/kruck01.pdf>
- Kuusniemi, H., Lachapelle, G. and Takala, J.H., 2004. Position and velocity reliability testing in degraded GPS signal environments. *GPS Solutions*, Volume 8(4). <http://topo.epfl.ch/documents/EuroSDR/kuusniemi04.pdf>
- Legat, K., 2005. Approximate direct georeferencing in national coordinates. *ISPRS Journal of Photogrammetric Engineering and Remote Sensing*, submitted for publication. <http://topo.epfl.ch/documents/EuroSDR/legat05.pdf>
- Lehmann, M., 2005. Réalisation d'un serveur de corrections GPS accessible par GPRS, EPFL, Lausanne. <http://topo.epfl.ch/documents/EuroSDR/lehmann05.pdf>
- Leick, A., 2004. *GPS Satellite Surveying*. Science/Geography. Wiley, 464 pp
- Mehra, R., Bayard, D., Seereeram, S. and Hadaegh, F., 1995. Adaptive Kalman filtering, failure detection and identification for spacecraft attitude estimation. *IEEE*. <http://topo.epfl.ch/documents/EuroSDR/mehra95.pdf>
- Mohamed, A.H. and Schwarz, K.P., 1999. Adaptive kalman filtering for INS/GPS. *Journal of Geodesy*, 73: 193-203. <http://topo.epfl.ch/documents/EuroSDR/mohamed99.pdf>
- Morin, K. and El-Sheimy, N., 2002. Post-mission adjustment of airborne laser scanning data, FIG XXII International Congress, Washington DC, USA, pp. 12. <http://topo.epfl.ch/documents/EuroSDR/morin02.pdf>  
<http://topo.epfl.ch/documents/EuroSDR/morin02t.pdf>
- Mostafa, M., 2002. Camera/IMU boresight calibration: New advances and performance analysis, ASPRS Annual Meeting, Washington, DC, USA. <http://topo.epfl.ch/documents/EuroSDR/mostafa02.pdf>
- Muellerschoen, R.J., Iijima, B., Meyer, R. and Bar-Sever, Y., 2004. Real-time point-positioning performance evaluation of single-frequency receivers using NASA's global differential GPS system, ION GNSS, Long Beach, California, pp. 1872-1880. <http://topo.epfl.ch/documents/EuroSDR/muellerschoen04.pdf>

- Napolitano, M.R., Windon, D.A., Casanova, J.L., Innocenti, M. and Silvestri, G., 1998. Kalman filters and Neural-Network schemes for sensor validation in flight control systems. IEEE Transactions on Control Systems Technology(5).  
<http://topo.epfl.ch/documents/EuroSDR/napolitano98.pdf>
- Nikiforov, I., 2002. Integrity monitoring for multi-sensor integrated navigation systems, ION GPS 2002. The Institute of Navigation, Portland, OR, pp. 579-590.  
<http://topo.epfl.ch/documents/EuroSDR/nikiforov02.pdf>
- Ober, P.B., 2000. Integrity according to Bayes. In: D.U.o. Technology (Editor), IEEE.  
<http://topo.epfl.ch/documents/EuroSDR/ober00.pdf>
- Ober, P.B., 2001. SBAS integrity concept. Eurocontrol.  
<http://topo.epfl.ch/documents/EuroSDR/ober01.pdf>
- Ochieng, W.Y. et al., 2002. An assessment of the RAIM performance of a combined galileo/GPS navigation system using the marginally detectable errors (MDE) algorithm. GPS Solutions, 5(3). <http://topo.epfl.ch/documents/EuroSDR/ochieng02.pdf>
- Optech, 2004. ALTM 30/70/100 user manual, Toronto, Canada.  
<http://topo.epfl.ch/documents/EuroSDR/optech04.pdf>
- Pervan, B.S. et al., 1995. High integrity GPS-based precision landing using beacon pseudolites, ISPA, Braunschweig, Germany, pp. 7. <http://topo.epfl.ch/documents/EuroSDR/pervan95.pdf>
- Ressl, C., 2002. The impact of conformal map projections on direct georeferencing, Photogrammetric Computer Vision. Symposium, Vienna. <http://topo.epfl.ch/documents/EuroSDR/ressl02.pdf>
- Schenk, T., 2001. Modeling and analyzing systematic errors in airborne laser scanners. In: C.a.E.E.a.G. Science (Editor). The Ohio State University.  
<http://topo.epfl.ch/documents/EuroSDR/Schenk01.pdf>
- Schwarz, K.P. and El-Sheimy, N., 2004. Mobile mapping systems - state of the art and future trends. International Archives of Photogrammetry, Remote Sensing and Spatial Information Sciences, 35, Part B: 10. <http://topo.epfl.ch/documents/EuroSDR/schwarz04.pdf>
- Skaloud, J., Bruton, A.M. and Schwarz, K.P., 1999. Detection and filtering of short-term (1/f) noise in inertial sensors. NAVIGATION, Journal of The Institute of Navigation, 46(2): 97-107.  
<http://topo.epfl.ch/documents/EuroSDR/skaloud99.pdf>
- Skaloud, J., Gontran, H. and Merminod, B., 2004. GSM-distributed RTK for precise analysis of speed skiing, 8th European Navigation Conference GNSS 2004, Rotterdam.  
<http://topo.epfl.ch/documents/EuroSDR/skaloud04.pdf>
- Skaloud, J. and Lichti, D., 2005. Rigorous approach to bore-sight self calibration in airborne laser scanning, EPFL-TOPO, Lausanne. <http://topo.epfl.ch/documents/EuroSDR/skaloud05.pdf>
- Skaloud, J. and Schaer, P., 2003. Towards a more rigorous boresight calibration, ISPRS International Workshop on Theory Technology and Realities of Inertial/GPS/Sensor Orientation, Castelldefels, Spain. <http://topo.epfl.ch/documents/EuroSDR/skaloud03.pdf>
- Studeny, J. and Clark, B., 2004. The aviation GNSS receiver. ION Newsletter, 14(3): 4-5.  
<http://topo.epfl.ch/documents/EuroSDR/studeny04.pdf>
- Talaya, J., 2000. Robust GPS kinematic positioning for direct georeferencing. International Archives of Photogrammetry, Remote Sensing and Spatial Information Sciences, 33, Part B2: 546-551.  
<http://topo.epfl.ch/documents/EuroSDR/talaya00.pdf>
- Tempelmann, U. and Hinsken, L., 2005. Triangulation of ADS40 pushbroom image blocks - Not much different from classical frame blocks? SGPBF Annual Meeting, Lausanne, Switzerland. <http://topo.epfl.ch/documents/EuroSDR/tempelmann05.pdf>
- Teunissen, P.J.G., Joosten, P. and Odijk, D., 1999. The reliability of GPS ambiguity resolution. GPS Solutions, 2(3): 63-69. <http://topo.epfl.ch/documents/EuroSDR/teunissen99.pdf>
- Teunissen, P.J.G. and Verhagen, S., 2004. On the foundation of the popular ratio test for GNSS ambiguity resolution, ION GNSS, Long Beach, California, pp. 12.  
<http://topo.epfl.ch/documents/EuroSDR/teunissen04.pdf>

- Toran-Marti, F. and Ventura-Traveset, J., 2004. The ESA EGNOS project: The first step of the European contribution to the Global Navigation Satellite System (GNSS). GNSS-1 Project Office. <http://topo.epfl.ch/documents/EuroSDR/toranmarti04.pdf>
- Ventura-Traveset, J., 2003. EGNOS, ION NTM. <http://topo.epfl.ch/documents/EuroSDR/venturatraveset03.pdf>
- Verhagen, S., 2004. Integer ambiguity validation: an open problem? GPS Solutions, 8: 36–43. <http://topo.epfl.ch/documents/EuroSDR/verhagen04.pdf>
- Vollath, U., 2004. The Factorized Multi-Carrier Ambiguity Resolution (FAMCAR) Approach for Efficient Carrier-Phase Ambiguity Estimation. In: T.T. GmbH (Editor), ION GPS 2004. <http://topo.epfl.ch/documents/EuroSDR/vollath04.pdf>
- Vollath, U., Landau, H., Chen, X., Doucet, K. and Pagels, C., 2002. Network RTK Versus Single Base RTK - Understanding the Error Characteristics, ION GPS, Portland, OR. <http://topo.epfl.ch/documents/EuroSDR/vollath02.pdf>
- Waegli, A. and Gilliéron, P.Y., 2003. Le Concept d'intégrité d'EGNOS. Géomatique Suisse, 11. <http://topo.epfl.ch/documents/EuroSDR/waegli03.pdf>
- Wei, M. and Schwarz, K.P., 1990. Testing a decentralized filter for GPS/INS integration. Proceedings of the IEEE PLANS - Position, Location and Navigation Symposium: March 1990. <http://topo.epfl.ch/documents/EuroSDR/wei90.pdf>
- Yang, Y. and Farrell, J.A., 2003. Magnetometer and differential carrier phase GPS-aided INS for advanced vehicle control. IEEE Transactions on Robotics and Automation, 19(2). <http://topo.epfl.ch/documents/EuroSDR/yang03.pdf>
- Yang, Y., Hatch, R.R. and Sharpe, R.T., 2004. GPS multipath mitigation in measurement domain and its applications for high accuracy navigation, ION GNSS 2004, Long Beach, California. <http://topo.epfl.ch/documents/EuroSDR/yang04.pdf>
- Yousuf, R. and Skone, S., 2005. WAAS Performance evaluation under Increased ionospheric activity. In: T.I.o. Navigation (Editor), GNSS 05. The Institute of Navigation, Long-Beach, CA, pp. 2316-2327. <http://topo.epfl.ch/documents/EuroSDR/yousuf05.pdf>



**EuroSDR-Project**  
**Commission 1**  
**“Sensors, Primary Data Acquisition and Georeferencing”**

**“Reliability of Direct Georeferencing:  
A Case Study on Practical Problems and Solutions”  
Final Report on Phase 2**

*Report by Klaus Legat, Jan Skaloud and Ronald Schmidt*  
Ingenieurgesellschaft Vermessung AVT - ZT GmbH, Austria  
École Polytechnique Fédérale de Lausanne (EPFL)  
Department of Geography, University of Zurich



## **Abstract**

This report studies a practical problem related to the use of GPS/INS technology for sensor direct georeferencing. It is a case study of a specific, yet typical, situation where the performance of a GPS/INS was pronounced unsatisfactory for orientation of an airborne sensor. However, it was in fact not the poor quality of the navigation data but rather numerous disregards occurring in the flight execution and data treatment that have led to this wrong conclusion. The presented analysis reveals the errors committed at different stages of data treatment and quantifies their impact on the sensor exterior orientation. It also explains the remedies employed to mitigate their impact. The recommended procedures are drafted in a summary.

## **1 Introduction**

The method of direct georeferencing (DG) of airborne sensors by GPS/INS is considered by many as a well-established process that increases the productivity of airborne mapping. Nevertheless, the users of this technology often encounter pitfalls related to its reliability (e.g., instrument and/or data quality) or its incorrect use (e.g., an unstable sensor mount, uncompensated effects due to platform stabilization, or inadequate datum/projection transformation procedures). While the recently published EuroSDR report investigated the former (Skaloud, 2006), this study concentrates on the practical aspects. These problems often prevent from benefiting fully from the collected GPS/INS data, or, in extreme (but not rare) cases, lead to a wrong judgment on their adequacy for a stated goal (Kremer 2006).

The core of this report is organized around a case study of a real project (Sect. 3) where such an incorrect conclusion was drawn by a company responsible for the refinement of the image orientation by an automated aero-triangulation (AAT). The first author was given the “detective task” of tracing the origins of the encountered problems. During this investigation, numerous inadequacies were identified which span the whole process from the survey setup to the transformation of the exterior orientation (EO) of the images. These findings are analyzed and their impact on the EO accuracy is quantified in comparison with correct treatment. Finally, the synthesis of the experience serves as a pretext for drafting the recommended procedures in Section 4. These recommendations should not replace but rather complete the existing manuals and suggested measures recommended by technology providers.

Apart a brief theoretical introduction provided in Sect. 2, the reader is further advised to consult the frame definitions given in Kresse et al. (2006) and the introductory material on DG by GPS/INS in Madani (2004) or Legat (2006).

## 2 Theoretical background

### 2.1 *Recording and processing of direct-georeferencing data*

#### 2.1.1 Layout of airborne mobile-mapping systems

Apart from the image sensor(s), an airborne mobile-mapping system equipped for direct georeferencing involves one or several GPS receivers and antennas as well as an inertial measurement unit (IMU). In the most ideal case, all sensors are attached to a common rigid mounting structure, preventing variations in their relative positions and orientations. Further, the complete system requires synchronization to a common time scale, typically GPS time.

In practice, many airborne surveying companies use cameras with a retrofit IMU on a gyro-stabilized (gimbaled) platform. While this design does not affect the stability of the camera/IMU assembly, the GPS antenna is usually placed at other, remote, positions on the aircraft (Kremer 2006). In case the stabilization exerts rotations on the camera for guaranteeing an optimal image quality, the position offset (lever arm) of the GPS antenna from the IMU will change (even in the body frame of the IMU). Especially critical are designs with large along and/or lateral separations (referred to the aircraft frame); in contrast, vertical separations may be negligible due to the motion characteristics of aircraft. Such variations of the antenna offset will deteriorate the quality of the GPS/INS data, unless the gimbal angles of the camera are recorded and fed into the processing. Otherwise, the variable lever arm may be subject to poor observability in the GPS/INS integration, meaning that the estimation of the effects caused by the gimbal rotations will be critical in post-processing. Consequently, it could be difficult to correctly transfer the GPS/INS position to the image sensor.

#### 2.1.2 System calibration

Prior to the use of the system for mapping purposes, a calibration must be performed. This concerns both the calibration of individual sensors (e.g., an aerial camera or an IMU) and the system calibration due to the aircraft mount (Kremer 2006). Thereby, the differences in orientation between the IMU and the image sensors – known as boresight orientations – must be determined. The required approaches differ among passive and active sensors (see, e.g., Skaloud and Schaer 2003, Skaloud and Lichti 2006). Furthermore, the lever arms from the IMU towards the GPS antenna(s) and image sensor(s) must be derived. The latter task is usually fulfilled by classical geodetic surveying. As the position offsets are required in the body frame of the IMU (or in the camera frame), these measurements should be performed in conditions when the axis system of the IMU is well established and known (i.e., the systematic sensor errors of the IMU have been reliably estimated or can be considered as insignificant for the stated purpose).

#### 2.1.3 Nominal processing steps of the GPS/INS data

The processing of the GPS/INS data commences with the kinematic baseline determination between the mobile GPS equipment and one or several base stations located at precisely surveyed positions. Subsequently, the positions (and possibly also velocities) from GPS are integrated with the raw measurements of the IMU.

The difference in position and orientation between the IMU and the image sensor is either applied within the GPS/INS processing or in a subsequent step. Furthermore, the data need to be interpolated to the actual recording times of the image sensor. This yields the exterior orientation (EO) of the images in the earth-centered earth-fixed (ECEF) reference frame of GPS. However, as the final mapping products are usually demanded in some national coordinate frame, the EO data must be transformed accordingly (Legat 2006):

- With reference to the positions, this may require the transformation to a national geodetic datum, the application of some national map projection, and the consideration of the geoid heights. Moreover, an additional correction should be applied to minimize the distortions of the heights that arise from the curvature of the earth and the fact that an ellipsoid of revolution cannot be projected into the plane without length distortion.
- In case of the orientation angles, the transition to national coordinates may also require a datum-based transformation due to residual rotations of the national datum frame and the use of a locally best fitting ellipsoid of revolution. Further, the position-dependent convergence of meridians of the map projection must be accounted for.

Once these transformations have been applied, the EOs can be used for processing the image data. In many cases, however, an automated aero-triangulation (AAT) may be desired for controlling the quality of the direct-georeferencing results and/or improving the relative orientations of the images.

## 2.2 *Potential error sources*

Unfortunately, there are a number of potential error sources in direct georeferencing that may diminish or even ruin the quality of the EO data. Some of these error sources are (the order of items follows the sequence of the above descriptions):

- Lack of rigidity of the sensor assembly, including lever-arm variations caused by the platform stabilization.
- Synchronization errors or non-compensated sensor delays, e.g., time shifts between a camera trigger command and the actual shutter time of the camera.
- Calibration errors of sensor lever arms and boresight angles or failure to apply these parameters correctly.
- False settings or assumptions of the GPS/INS processing, e.g., concerning the modelling of systematic errors in the IMU.
- Use of wrong parameters of the national geodetic datum.
- Use of a wrong map projection, e.g., an approximate projection instead of some specific projection type that may not be supported by particular software packages.
- Failure to apply the geoid heights (if necessary) and/or the height correction required due to the length distortions arising from a map projection.

In addition to these rather technical items, another very important issue may cause severe difficulties: A lack of information exchange between different partners involved in a common mapping project

(especially with respect to metadata) and/or misunderstandings about the processing steps applied by the other partners.

We will encounter several of these errors in the case study described in Sect. 3.

### 3 Case study

To avoid offending any parties that participated in the project that serves as the basis of this case study, all references to these parties have been neutralized. Further, no details are given concerning the location of the project area.

#### 3.1 *Project characteristics*

The project was performed by two partners with several years of experience in their respective fields of work. The responsibility of Company A was to perform the image flight with a frame-based camera and transform the image EOs derived by GPS/INS to national coordinates. The task of Company B was to perform an AAT with the transformed EOs supplied by Company A and a number of ground control points (GCPs) provided by the client of the project.

Some other relevant project characteristics were as follows:

- The image data were recorded in two separate flight sections with scales 1:4000 (5 lines, 174 images with IDs 1 through 174) and 1:2500 (6 lines, 401 images with IDs 180 through 585). Considering the camera focal length of approximately 30 cm, the relative flight heights above the terrain were about 1200 m and 750 m, respectively. Separate AATs had to be done for each scale.
- The results of the photogrammetric processing were requested in national coordinates of the European country in question. The definition of the national geodetic datum is general which requires a 3D similarity transformation with respect to the ECEF frame and involves a locally best fitting ellipsoid of revolution. The map projection is a non-standard variant of the Transverse Mercator (TM). Furthermore, the client requested orthometric heights.

A two-dimensional plot of the image positions of both flight sections is shown in Figure 1. The data are given in national coordinates relative to a suitable position within the project area. The flight lines were almost parallel with alternate mean azimuths of  $-40^\circ$  (roughly north-west) and  $+140^\circ$  (roughly south-east), respectively.

#### *Encountered difficulties*

When Company B attempted to run the AATs, it turned out that the EO data provided by Company A were not consistent with the GCPs. While the image positions could be used – notably by allowing an individual drift correction per flight line – the discrepancies of the orientation angles were out of tolerance, rendering them completely unusable.

To cope with these problems, a number of additional GCPs were measured by the client and GPS-supported ATs (mainly based on the GCPs and tie points) were performed by Company B. The first author of this report was also invited to investigate the encountered difficulties.

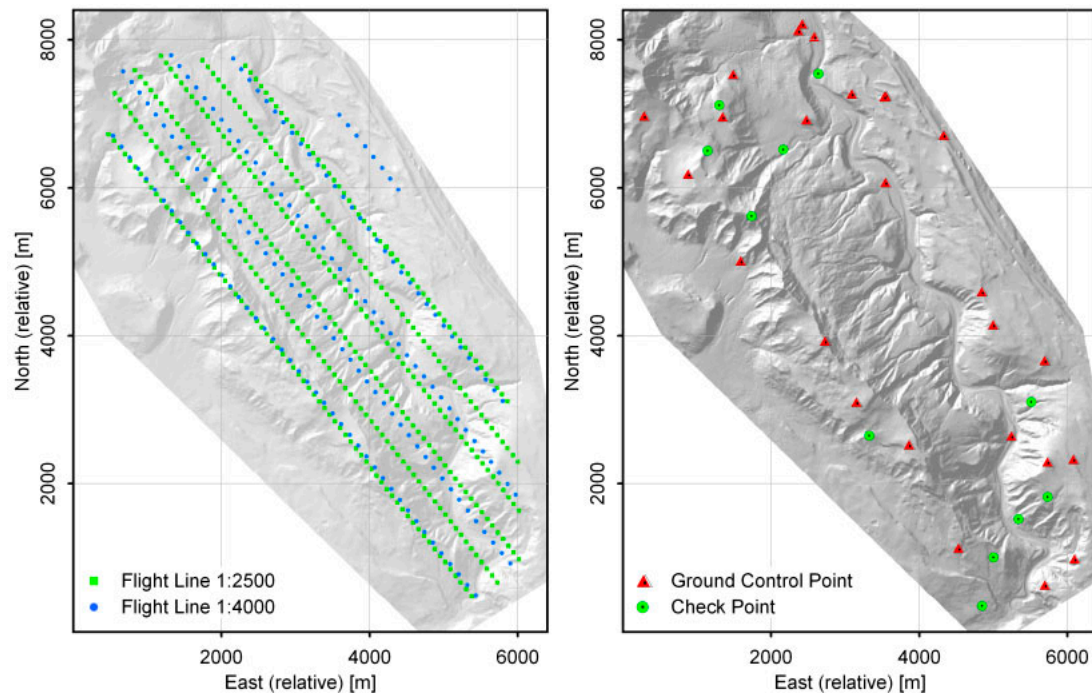


**Figure 1: Overview of the 1:4000 and 1:2500 flight lines and object point distribution**

### 3.2 *Provided data and information*

Our investigation was dictated by the provided data and information. Essentially, the following items were made available:

#### *GPS/INS processing files and transformed EOs*

Company A used GPS/INS hardware and software provided by Applanix (a high-quality POS/AV 510 system). The IMU of the navigation system (Litton LN-200) was retrofit to the airborne camera (Intergraph/Zeiss RMK TOP 30). The camera was placed in a stabilized mount that allows small relative rotations ( $\omega$ ,  $\phi$ ) with respect to the aircraft. The encoding angles of the camera gimbals were not recorded.

The GPS/INS data were processed using the software package POSpac 4.0 by Applanix. Among others, this package includes a GPS/INS integration module (POSProc) and an EO transformation tool (POSEO). Two types of result files from POSProc were used here, namely the final (i.e., smoothed) outcome of the GPS/INS processing and the corresponding file of standard deviations. In addition, Company A provided the POSEO result file that had been submitted to Company B for the AAT. Although desired, the EO data were not provided in national coordinates.

#### *AT processing protocols, project report, and further information*

Company B supplied protocols of the two GPS-supported ATs performed using the software package Match AT 4.0 by INPHO GmbH. In addition, the project report that had been delivered to the client was provided.

### 3.3 Identified problems and solutions

#### 3.3.1 Erroneous image positions – Horizontal effects

In the original setup, the GPS/INS data were transformed to national coordinates using POSEO. A comparison of these results with the image positions from the ATs revealed significant discrepancies. These are shown for the 1:2500 flight lines in Figure 2 (the variable background color of the figures always indicates the different flight lines). Despite the obvious offsets in each coordinate direction, the north and east coordinates include trends that depend on the flight lines.

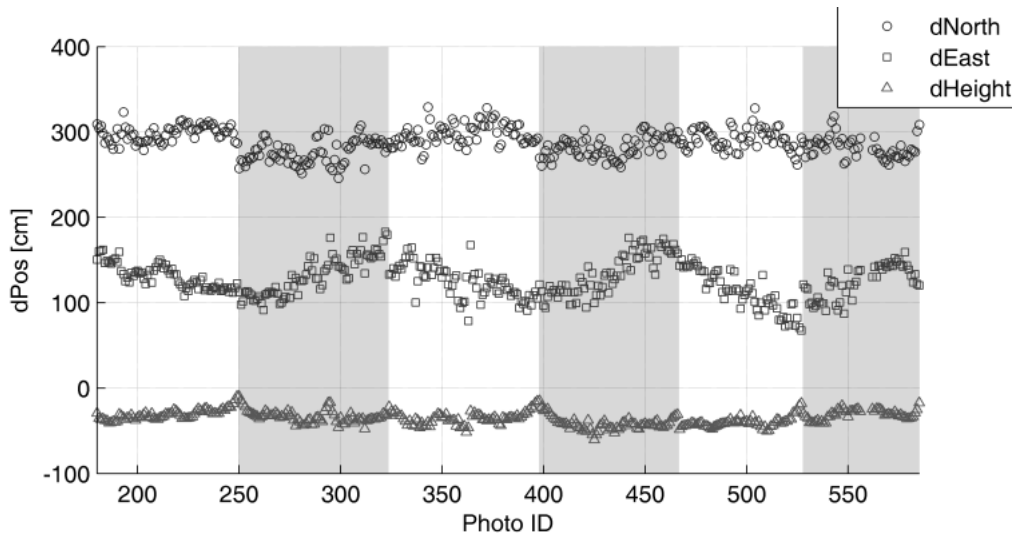


**Figure 2: Position differences POSEO minus AT, flight section 1:2500**

Considering these deviations, it is clear that the image positions from POSEO could only be used in the ATs by applying individual linear drift corrections for each flight line. As an example, the constant offsets of the 1:2500 flight lines computed by Match-AT are shown in Table 1. Clearly, the results in east and north are again correlated with the flight line. Furthermore, the values are unrealistically large: If the image positions had been transformed correctly, the constant shifts should be close to the magnitude of the GPS positioning errors (typically, some 10 cm in case of kinematic carrier-phase positioning). However, they are more than ten times greater, attesting errors in the processing.

Line	Direction	East offset [cm]	North offset [cm]	Height offset [cm]
1	NW	170.4	310.0	-124.0
2	SE	93.0	265.9	-126.8
3	NW	164.4	305.3	-128.9
4	SE	95.2	271.0	-135.3
5	NW	153.0	302.8	-133.6
6	SE	72.0	276.8	-126.4
	<b>Mean</b>	<b>124.7</b>	<b>288.6</b>	<b>-129.2</b>

**Table 1: GPS position bias per line as estimated by Match-AT for the 1:2500 flight**



Three reasons were identified that have contributed to the large position disparities in Figure 2:

1. In the AT, Company B introduced the eccentricity (lever arm) of the GPS antenna with respect to the camera as [18.6, 39.7, 128.3] cm (these values had been provided by Company A). However, as the results of the GPS/INS processing had already been referred to the centre of projection of the camera by Company A, the (re-) application of the eccentricity in the AT has, in fact, falsified the positions. While the vertical component corresponds to height offset of Table 1 (the camera was stabilized in the horizon), the horizontal deviations are only partly caused by this failure.

It is worth noting that it is probably the terminology of the user interface of Match AT that has added to this serious misunderstanding between Company A and B as it instructs the user to enter the “GPS antenna eccentricity”. This is correct when performing a GPS-supported AT; when using GPS/INS, however, it is usually not the eccentricity of the GPS antenna that is relevant for the AT but the lever arm of the IMU with respect to the camera. While the latter can also be accounted for at some other stage, the GPS-INS lever arm should be introduced for a correct GPS/INS integration.

2. The dominant part of the horizontal coordinate discrepancies is due to the non-standard character of the national map projection which is not supported by POSEO and was probably only “approximated” by selecting a projection of a similar type from the available choices.
3. The residual vertical disparities were partly caused by the failure of Company A to correct the national ellipsoidal heights derived from GPS/INS by the geoid heights. Additionally, the correction required for minimizing the distortion of the heights was ignored (this feature is not supported by POSEO).

Note that while problems 2 and 3 were caused by failures in the GPS/INS processing chain, problem 1 was induced in the AT. The effects of problem 1 on the results of the AT were regarded as negligible due to the GPS drift correction and the large number of GCPs (up to 40).

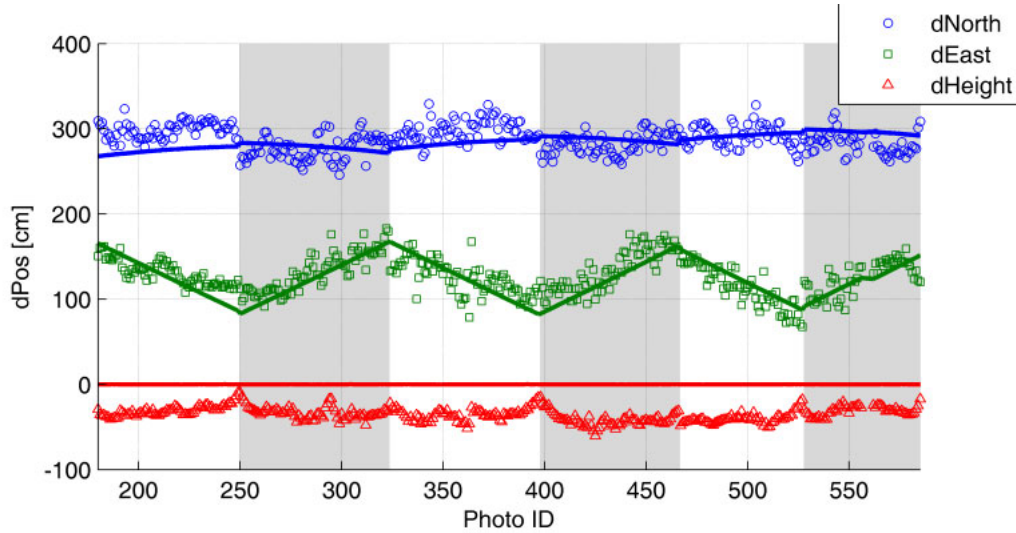
#### *Re-transformation of the GPS/INS to national coordinates*

The GPS/INS results from POSProc were transformed with the direct-georeferencing software utility CAMEO (Skaloud and Legat, 2006). This tool corrected the errors mentioned under items 2 and 3 above, as it supports both the national map projection required for the project and the necessary height corrections. Nevertheless, CAMEO was first configured to also calculate the height over the national ellipsoid while the height correction due to the projection was deactivated.

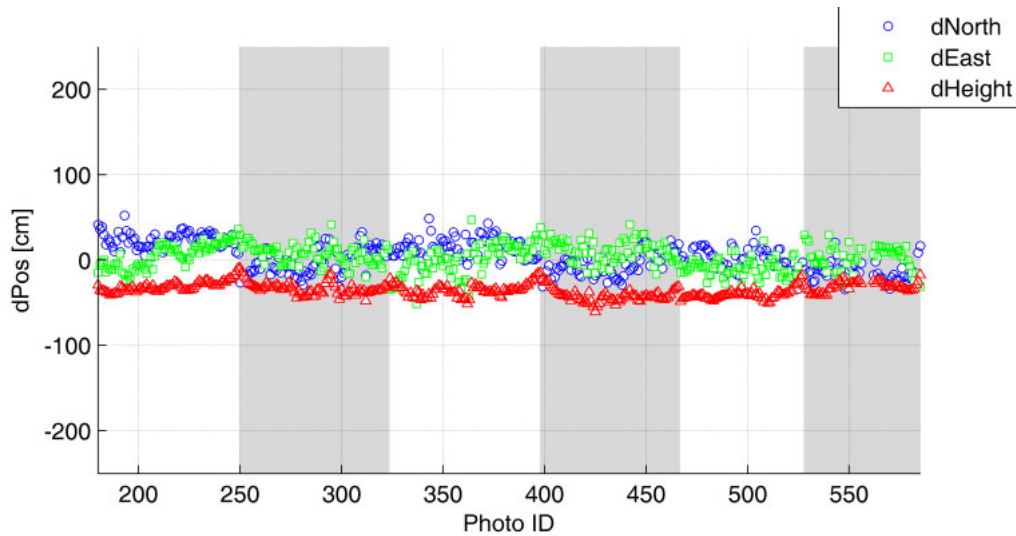
The POSEO-minus-AT discrepancies already depicted in Figure 2 are again plotted in Figure 3. The POSEO-minus-CAMEO differences are also shown. As documented by this figure, the latter correspond very well to the systematic “trends” appearing in the POSEO-minus-AT results in the horizontal coordinates, i.e., to the errors caused by the inadequate projection choice in POSEO. In contrast, the intermediate heights of CAMEO and those of POSEO are (practically) identical (max. deviations of  $\pm 0.1$  cm). This proves that both variants involved equivalent parameters for the national geodetic datum and that the output provided by POSEO included plain ellipsoidal heights. Hence, Company A ignored to account for the geoid undulations in the EO parameters while orthometric heights were used for the GCPs in the AT.

Figure 4 displays a direct position comparison between CAMEO and the AT (1:2500), also prior to the height corrections. Clearly, the remaining horizontal coordinate differences are mainly dominated by noise. The residuals are  $+3.1 \text{ cm} \pm 15.6 \text{ cm}$  (east) and  $+3.6 \text{ cm} \pm 18.0 \text{ cm}$  (north), respectively.

While the mean differences are now close to zero, their standard deviations still appear a bit elevated. This effect, however, is partly due to the noise of the AT results and partly due to the uncorrected variation of the GPS/IMU lever arm caused by the camera stabilization.



**Figure 3: Position differences POSEO minus CAMEO (smooth lines) and POSEO minus AT (noisy lines), flight section 1:2500**



**Figure 4: Position differences CAMEO minus AT, flight section 1:2500**

### 3.3.2 Erroneous image positions – Vertical effects

While the horizontal coordinates behave similarly in both flight sections, the residual height offsets with respect to the AT differ significantly among them. They amount to  $-35.4 \text{ cm} \pm 7.9 \text{ cm}$  (1:2500)

and  $-26.3 \text{ cm} \pm 12.4 \text{ cm}$  (1:4000), respectively. This apparent inconsistency is, in fact, a very important finding. There are two sources for this inconsistency:

1. The geoid height in the project area.
2. The vertical distortion of direct georeferencing due to the length distortion of the map projection.

#### *Application of geoid undulation*

The mean value of the geoid height is approximately  $-40 \text{ cm}$  and its variation across the project area may be ignored in this investigation. Since its effect is the same for the two flight sections, it does not explain the significant differences of their respective mean-height residuals. After application of the average geoid height the mean residual differences become  $+4.6 \text{ cm}$  (1:2500) and  $+13.7 \text{ cm}$  (1:4000), respectively.

#### *Correction of residual vertical distortions*

While the horizontal scale of the projection depends on position, the vertical scale is constant as it leaves the heights unchanged (in the numerical sense) but replaces the skew ellipsoidal normals by parallel lines. This effect may be corrected by a simple analytic function depending on the absolute flight height, the average terrain height, and the local scale factor of the map projection (Legat 2006). The dependence of this correction on the absolute flight height clarifies the diversity of the mean residual differences: Inserting the required values for each camera position, the final mean residuals between CAMEO and the AT become as low as  $+2.0 \text{ cm}$  (1:2500) and  $-2.7 \text{ cm}$  (1:4000), respectively. Finally, note that the virtue of this correction could be even further increased by replacing the assumed average terrain height by a better estimate (obtained, e.g., from an existing DTM) and by accounting for the variations of the geoid height across the project area.

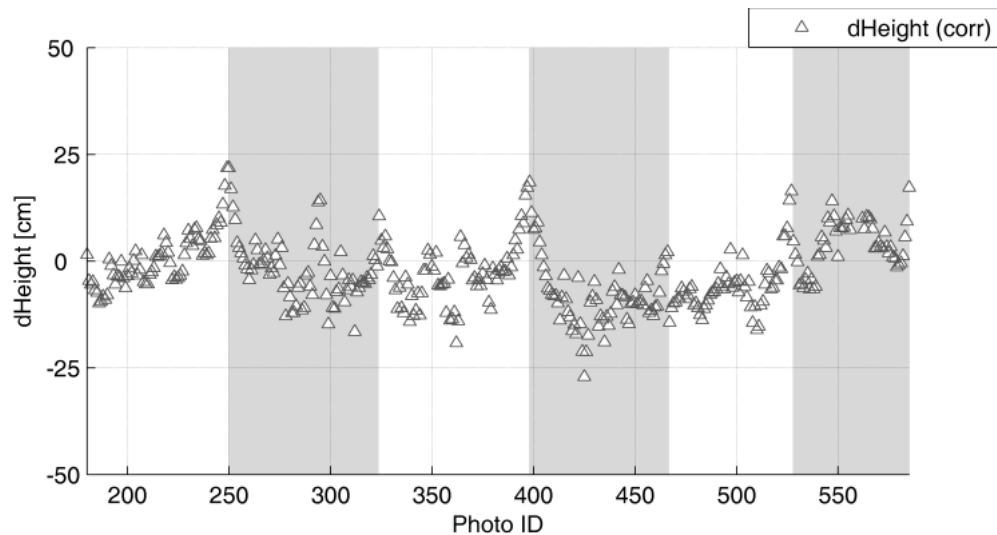


**Figure 5: Height differences CAMEO minus AT after consideration of the geoid heights and the analytic height correction, flight section 1:2500**

The final individual height residuals for the 1:2500 flight lines are shown in Figure 5 (note the change in scale of the ordinate axis). The remaining variations (with standard deviation of  $7.7 \text{ cm}$ ) are due to

residual errors in the GPS/INS and AT results. They are in accordance with the accuracy expectations (i.e., it appears that there are no additional undetected gross errors in either of the two data sources).

### 3.3.3 Erroneous image-orientation angles

In photogrammetry, the orientation of an image is conventionally described by three Euler-angles denoted as omega ( $\omega$ ), phi ( $\phi$ ), and kappa ( $\kappa$ ). Actually, the physical units of the angles and the order of individual rotations differ among commercial AT software packages. In particular, Match AT expects grads (gons) and adopts the definition omega-phi-kappa as the primary-secondary-tertiary rotations about axis 1, 2, and 3 of the terrain frame, respectively. This definition differs from that in POSProc.

Although the issues related to the definition of rotation-sequences were correctly tackled by Company A, significant discrepancies remained between the orientation angles of POSEO and Match-AT, especially for omega and phi (see Figure 6 for the results of the 1:2500 flight section). A comparison of these differences with the azimuth of the flight lines (alternating between  $-40^\circ$  and  $+140^\circ$ ) disclosed an obvious correlation of these quantities.

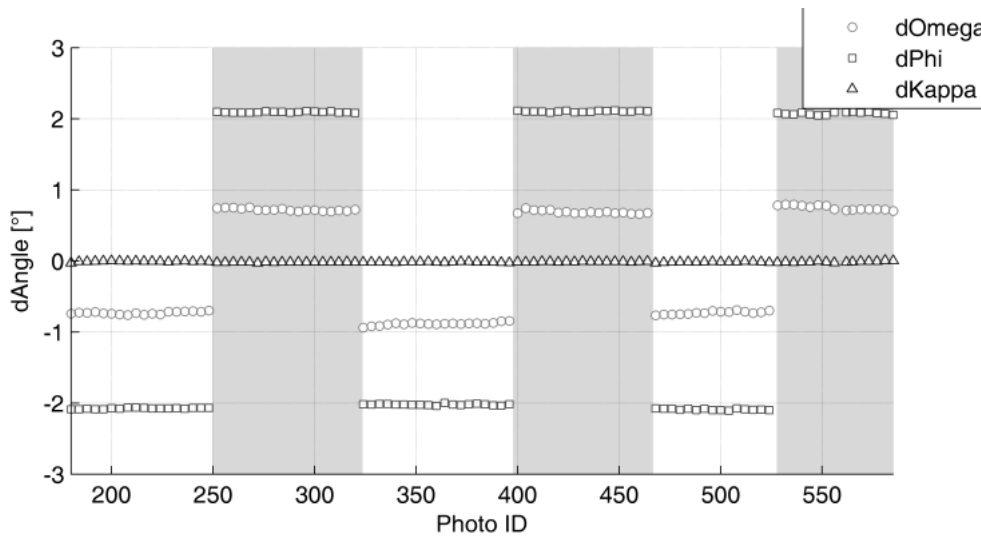


**Figure 6: Angle differences POSEO minus AT, flight section 1:2500**

#### *Re-processing of the orientation angles from GPS/INS*

The orientation angles obtained from CAMEO were (practically) identical to those of POSEO (max. differences of  $\pm 0.003^\circ$ ). Benefiting from the high correlation with the flight azimuth mentioned above, it was found that the discrepancies follow from an uncompensated mounting orientation difference (boresight) between the IMU and the camera. In other words, the orientation angles from POSEO were probably referred to the IMU instead of the camera as needed for the AT.

The boresight angles were estimated from the 1:4000 flight lines as angular differences between the (GPS-supported) AT and the results from GPS/INS. The statistical evaluation of this process is shown in Table 2. The given standard deviations are those of the angle sequences; the standard deviations of the mean angles are even lower by about one order of magnitude.

Boresight angle	Mean [°]	Rms [°]
About axis 1 (IMU)	1.191	0.0114
About axis 2 (IMU)	1.864	0.0085
About axis 3 (IMU)	0.002	0.0055

**Table 2: Mean boresight angles and standard deviations, flight section 1:4000**

As follows from the low standard deviations, these angles are well estimated. Once they are applied to the GPS/INS results in the 1:2500 profiles, the newly determined angles agree very well with those provided by the AT as demonstrated by Figure 7. Note the different scale of the ordinate axis compared to the previous figure. The RMS values for the angle differences amount to  $0.01^\circ$  for omega, phi and  $0.006^\circ$  for kappa, respectively. This magnitude of the residuals approximately corresponds to the expected angular accuracy of the IMU (LN-200) used by Company A. Similar level of agreement between GPS/INS-AT is reached in the experimental setup reported by Madani and Mostafa (2002). Also in this case, the reduced noise level of the kappa difference is probably due to its higher accuracy in the AT (about two times better than for omega and phi).

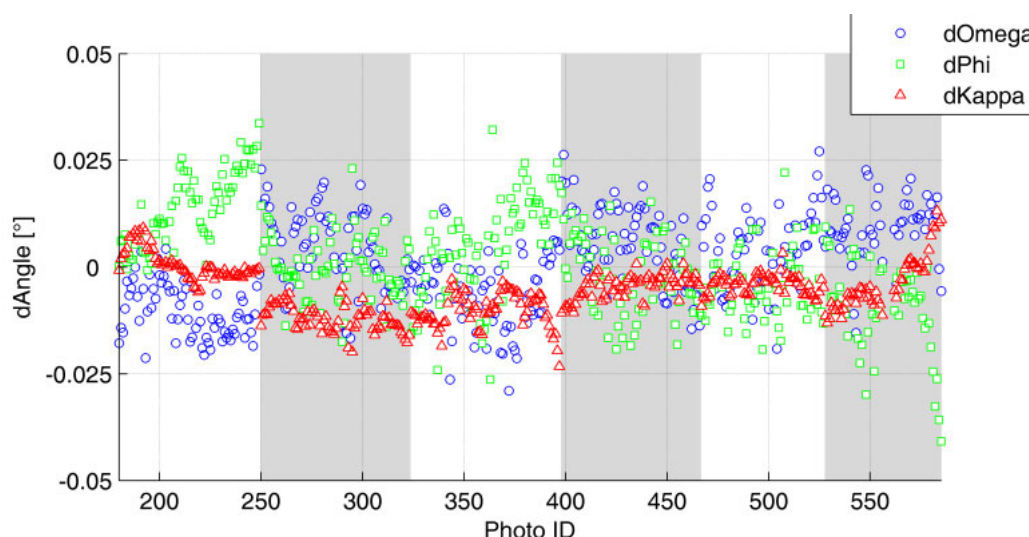


**Figure 7: Boresight-corrected angle differences CAMEO minus Match AT, flight section 1:2500**

### 3.4 Summary

As was shown in the previous sections, the direct- and indirect-georeferencing results of this project fit together very well once the processing is performed correctly. This confirms the expected benefits of the direct approach which provides a significant improvement of economy by reducing the number of GCPs to a minimum suitable for quality control and by speeding up the overall process when AT is necessary due to project requirements.

## 4 Conclusions and recommendations

The following recommendations represent a synthesis of the experiences gained through this project as well as many others within more than ten-year use of direct georeferencing. Nevertheless, these recommendations should not be used blindly and are not intended to replace but rather to complete the existing manuals and suggested measures recommended by the technology providers.

### *Boresight and lever-arm calibration*

The IMU/sensor orientation offset (boresight) must be carefully calibrated. In case of a frame-camera, the calibration requires specific flight patterns and block configuration. The support by GCPs is not required for this purpose. The position offsets between the IMU, the GPS antenna, and the camera should be determined by terrestrial geodetic measurements, ideally after a flight for tactical-grade IMUs. See Kresse et al. (2006) for details.

### *Gyro-stabilized mount*

The gyro stabilization of the camera (or other image sensor) should either be deactivated or the imposed gimbal angles should be recorded. Only in these two cases, the lever arm between the GPS antenna and the IMU can be correctly accounted for. Otherwise, it creates undesirable influences within GPS/INS integration and introduces positioning errors in the subsequent transfer of the results to the sensor EO.

### *EO transformation to national coordinates*

When transforming the EO data derived from GPS/INS to national coordinates, the correct datum definition and map projection are required. In this context, the situation of some countries is very specific as their non-standard map projections may not be supported by provided software packages. Such a situation requires the use of specific transformation tools like CAMEO or the extension of commercial software packages like POSEO. The same is true for the treatment of the systematic residual height errors of direct georeferencing (Legat 2006).

### *Aero triangulation*

When the GPS/INS processing is done carefully, the GPS drift correction within the AT software must be deactivated. The GPS/INS positions will fit to within some 10 cm if the lever arm was correctly treated, at least in the horizontal plane. As mentioned above, the vertical direction will require some additional corrections if the terrain is difficult and if the average terrain and flight heights are great. Lever arms and orientation differences among the sensors should be calibrated and applied prior to the AT.

As was shown in the previous section, the EO elements from direct georeferencing fit very well with those from indirect georeferencing. Thus, it is very beneficial to use the GPS/INS results not only as initial orientation estimates but also to broaden the applications field where the AT is completely dispensable and no GCPs are required. Nevertheless, one should always take counter-measures against possible systematic errors in the GPS/INS data that cannot be determined by filtering and smoothing due to the complementary error behavior of these navigation systems (Skaloud 2006).

## Acknowledgments

The data used in this study have been provided by the Sihlwald Data Center at the Department of Geography, University of Zurich ([www.sihlwald.unizh.ch](http://www.sihlwald.unizh.ch)). The authors are grateful to the Austrian Science Fund (FWF) for financing the research fellowship of Dr. Legat at the TOPO lab of the EPFL from June 2005 until September 2006 under contract number J2460-N10.

## References

- Kremer, J., 2006. System Calibration of Aerial Camera/GPS/IMU Systems – Procedures and Experiences. Proceedings of the International Calibration and Orientation Workshop EuroCOW, Castelldefels, Spain, 25-27 January: 6 pages (on CDROM).
- Kresse, W., Skaloud, J., Hinsken, L., 2006. Requirements for an orientation and calibration standard for digital aerial cameras and related sensors. “From Sensors to Imagery” – Symposium of ISPRS Commission 1, Paris, 3-6 July.  
[http://topo.epfl.ch/personnes/jsk/Papers/ISPRS06\\_Paris\\_KresseSkaloud.pdf](http://topo.epfl.ch/personnes/jsk/Papers/ISPRS06_Paris_KresseSkaloud.pdf)
- Legat, K., 2006. Approximate direct georeferencing in national coordinates. ISPRS Journal of Photogrammetry & Remote Sensing 60: 239-255.  
<http://topo.epfl.ch/documents/EuroSDR/legat05.pdf>
- Madani, M., Mostafa, M., 2002. ISAT Direct Exterior QA/QC Strategy Using POS Data. In: Heipke, C., Jacobsen, K., Wegmann, H. (Eds.): OEEPE Official Publication No 43: Integrated Sensor Orientation – Test Report and Workshop Proceedings, 281-297.  
<http://www.eurosdrr.net/publications/43.pdf>
- Madani, M., 2004. Photogrammetric applications, In: McGlone, J.C., Mikhail, E.M., Bethel, J., Mullen, R. (Eds.): Manual of Photogrammetry, 5th edition. American Society of Photogrammetry and Remote Sensing, Bethesda, MA: 1015-1026.
- Skaloud, J., Schaer, P., 2003. Towards a more rigorous boresight calibration. ISPRS International Workshop on Theory, Technology and Realities of Inertial/GPS/Sensor Orientation, Castelldefels, Spain.  
[http://topo.epfl.ch/personnes/jsk/Papers/ISPRS\\_Boresight.pdf](http://topo.epfl.ch/personnes/jsk/Papers/ISPRS_Boresight.pdf)
- Skaloud, J., 2006. Reliability of Direct Georeferencing Phase 1: An Overview of the Current Approaches and Possibilities. In: EuroSDR Official Publication No 51: Checking and Improving of Digital Terrain Models / Reliability of Direct Georeferencing.  
<http://www.eurosdrr.net/publications/51.pdf>
- Skaloud, J., Legat, K., 2006. CAMEO – Camera Exterior Orientation by Direct Georeferencing. Licensed software, Geodetic Engineering Laboratory (TOPO), Swiss Federal Institute of Technology Lausanne (EPFL), Switzerland.  
<http://topo.epfl.ch/research/techtransfer/>
- Skaloud, J., Lichti, D., 2006. Rigorous approach to boresight self-calibration in airborne laser scanning. ISPRS Journal of Photogrammetry & Remote Sensing 61 (2006) 47-59.  
<http://topo.epfl.ch/documents/EuroSDR/skaloud05.pdf>

## Index of Figures

Figure 1: Overview of the 1:4000 and 1:2500 flight lines and object point distribution .....	175
Figure 2: Position differences POSEO minus AT, flight section 1:2500 .....	176
Figure 3: Position differences POSEO minus CAMEO (smooth lines) and POSEO minus AT (noisy lines), flight section 1:2500 .....	178
Figure 4: Position differences CAMEO minus AT, flight section 1:2500 .....	178
Figure 5: Height differences CAMEO minus AT after consideration of the geoid heights and the analytic height correction, flight section 1:2500 .....	179
Figure 6: Angle differences POSEO minus AT, flight section 1:2500 .....	180
Figure 7: Boresight-corrected angle differences CAMEO minus Match AT, flight section 1:2500...	181

## Index of Tables

Table 1: GPS position bias per line as estimated by Match-AT for the 1:2500 flight .....	176
Table 2: Mean boresight angles and standard deviations, flight section 1:4000 .....	181



## LIST OF OEEPE/EuroSDR OFFICIAL PUBLICATIONS

State – November 2006

- 1 *Trombetti, C.*: „Activité de la Commission A de l'OEEPE de 1960 à 1964“ – *Cunietti, M.*: „Activité de la Commission B de l'OEEPE pendant la période septembre 1960 – janvier 1964“ – *Förstner, R.*: „Rapport sur les travaux et les résultats de la Commission C de l'OEEPE (1960–1964)“ – *Neumaier, K.*: „Rapport de la Commission E pour Lisbonne“ – *Weele, A. J. v. d.*: „Report of Commission F.“ – Frankfurt a. M. 1964, 50 pages with 7 tables and 9 annexes.
- 2 *Neumaier, K.*: „Essais d'interprétation de »Bedford« et de »Waterbury«. Rapport commun établi par les Centres de la Commission E de l'OEEPE ayant participé aux tests“ – „The Interpretation Tests of »Bedford« and »Waterbury«. Common Report Established by all Participating Centres of Commission E of OEEPE“ – „Essais de restitution »Bloc Suisse«. Rapport commun établi par les Centres de la Commission E de l'OEEPE ayant participé aux tests“ – „Test »Schweizer Block«. Joint Report of all Centres of Commission E of OEEPE.“ – Frankfurt a. M. 1966, 60 pages with 44 annexes.
- 3 *Cunietti, M.*: „Emploi des blocs de bandes pour la cartographie à grande échelle – Résultats des recherches expérimentales organisées par la Commission B de l'O.E.E.P.E. au cours de la période 1959–1966“ – „Use of Strips Connected to Blocks for Large Scale Mapping – Results of Experimental Research Organized by Commission B of the O.E.E.P.E. from 1959 through 1966.“ – Frankfurt a. M. 1968, 157 pages with 50 figures and 24 tables.
- 4 *Förstner, R.*: „Sur la précision de mesures photogrammétriques de coordonnées en terrain montagneux. Rapport sur les résultats de l'essai de Reichenbach de la Commission C de l'OEEPE“ – „The Accuracy of Photogrammetric Co-ordinate Measurements in Mountainous Terrain. Report on the Results of the Reichenbach Test Commission C of the OEEPE.“ – Frankfurt a. M. 1968, Part I: 145 pages with 9 figures; Part II: 23 pages with 65 tables.
- 5 *Trombetti, C.*: „Les recherches expérimentales exécutées sur de longues bandes par la Commission A de l'OEEPE.“ – Frankfurt a. M. 1972, 41 pages with 1 figure, 2 tables, 96 annexes and 19 plates.
- 6 *Neumaier, K.*: „Essai d'interprétation. Rapports des Centres de la Commission E de l'OEEPE.“ – Frankfurt a. M. 1972, 38 pages with 12 tables and 5 annexes.
- 7 *Wiser, P.*: „Etude expérimentale de l'aérotiangulation semi-analytique. Rapport sur l'essai »Gramastetten«.“ – Frankfurt a. M. 1972, 36 pages with 6 figures and 8 tables.
- 8 „Proceedings of the OEEPE Symposium on Experimental Research on Accuracy of Aerial Triangulation (Results of Oberschwaben Tests)“ *Ackermann, F.*: „On Statistical Investigation into the Accuracy of Aerial Triangulation. The Test Project Oberschwaben“ – „Recherches statistiques sur la précision de l'aérotiangulation. Le champ d'essai Oberschwaben“ – *Belzner, H.*: „The Planning. Establishing and Flying of the Test Field Oberschwaben“ – *Stark, E.*: „Testblock Oberschwaben, Programme I. Results of Strip Adjustments“ – *Ackermann, F.*: „Testblock Oberschwaben, Program I. Results of Block-Adjustment by Independent Models“ – *Ebner, H.*: „Comparison of Different Methods of Block Adjustment“ – *Wiser, P.*: „Propositions pour le traitement des erreurs non-accidentelles“ – *Camps, F.*: „Résultats obtenus dans le cadre du project Oberschwaben 2A“ – *Cunietti, M.*; *Vanossi, A.*: „Etude statistique expérimentale des erreurs d'enchaînement des photogrammes“ – *Kupfer, G.*: „Image Geometry as Obtained from Rheidt Test Area Photography“ – *Förstner, R.*: „The Signal-Field of Baustetten. A Short Report“ – *Visser, J.*; *Leberl, F.*; *Kure, J.*: „OEEPE Oberschwaben Réseau Investigations“ – *Bauer, H.*: „Compensation of Systematic Errors by Analytical Block Adjustment with Common Image Deformation Parameters.“ – Frankfurt a. M. 1973, 350 pages with 119 figures, 68 tables and 1 annex.
- 9 *Beck, W.*: „The Production of Topographic Maps at 1 : 10,000 by Photogrammetric Methods. – With statistical evaluations, reproductions, style sheet and sample fragments by

Landesvermessungsamt Baden-Württemberg Stuttgart.“ – Frankfurt a. M. 1976, 89 pages with 10 figures, 20 tables and 20 annexes.

- 10 „Résultats complémentaires de l’essai d’«Oberriet» of the Commission C de l’OEEPE – Further Results of the Photogrammetric Tests of «Oberriet» of the Commission C of the OEEPE“  
*Hárry, H.*: „Mesure de points de terrain non signalisés dans le champ d’essai d’«Oberriet» – Measurements of Non-Signalized Points in the Test Field «Oberriet» (Abstract)“ – *Stickler, A.*; *Waldhäusl, P.*: „Restitution graphique des points et des lignes non signalisés et leur comparaison avec des résultats de mesures sur le terrain dans le champ d’essai d’«Oberriet» – Graphical Plotting of Non-Signalized Points and Lines, and Comparison with Terrestrial Surveys in the Test Field «Oberriet»“ – *Förstner, R.*: „Résultats complémentaires des transformations de coordonnées de l’essai d’«Oberriet» de la Commission C de l’OEEPE – Further Results from Co-ordinate Transformations of the Test «Oberriet» of Commission C of the OEEPE“ – *Schürer, K.*: „Comparaison des distances d’«Oberriet» – Comparison of Distances of «Oberriet» (Abstract)“ – Frankfurt a. M. 1975, 158 pages with 22 figures and 26 tables.
- 11 „25 années de l’OEEPE“  
*Verlaine, R.*: „25 années d’activité de l’OEEPE“ – „25 Years of OEEPE (Summary)“ – *Baarda, W.*: „Mathematical Models.“ – Frankfurt a. M. 1979, 104 pages with 22 figures.
- 12 *Spiess, E.*: „Revision of 1 : 25,000 Topographic Maps by Photogrammetric Methods.“ – Frankfurt a. M. 1985, 228 pages with 102 figures and 30 tables.
- 13 *Timmerman, J.*; *Roos, P. A.*; *Schürer, K.*; *Förstner, R.*: On the Accuracy of Photogrammetric Measurements of Buildings – Report on the Results of the Test “Dordrecht”, Carried out by Commission C of the OEEPE. – Frankfurt a. M. 1982, 144 pages with 14 figures and 36 tables.
- 14 *Thompson C. N.*: Test of Digitising Methods. – Frankfurt a. M. 1984, 120 pages with 38 figures and 18 tables.
- 15 *Jaakkola, M.*; *Brindöpke, W.*; *Kölbl, O.*; *Noukka, P.*: Optimal Emulsions for Large-Scale Mapping – Test of “Steinwedel” – Commission C of the OEEPE 1981–84. – Frankfurt a. M. 1985, 102 pages with 53 figures.
- 16 *Waldhäusl, P.*: Results of the Vienna Test of OEEPE Commission C. – *Kölbl, O.*: Photogrammetric Versus Terrestrial Town Survey. – Frankfurt a. M. 1986, 57 pages with 16 figures, 10 tables and 7 annexes.
- 17 *Commission E of the OEEPE*: Influences of Reproduction Techniques on the Identification of Topographic Details on Orthophotomaps. – Frankfurt a. M. 1986, 138 pages with 51 figures, 25 tables and 6 appendices.
- 18 *Förstner, W.*: Final Report on the Joint Test on Gross Error Detection of OEEPE and ISP WG III/1. – Frankfurt a. M. 1986, 97 pages with 27 tables and 20 figures.
- 19 *Dowman, I. J.*; *Ducher, G.*: Spacelab Metric Camera Experiment – Test of Image Accuracy. – Frankfurt a. M. 1987, 112 pages with 13 figures, 25 tables and 7 appendices.
- 20 *Eichhorn, G.*: Summary of Replies to Questionnaire on Land Information Systems – Commission V – Land Information Systems. – Frankfurt a. M. 1988, 129 pages with 49 tables and 1 annex.
- 21 *Kölbl, O.*: Proceedings of the Workshop on Cadastral Renovation – Ecole polytechnique fédérale, Lausanne, 9–11 September, 1987. – Frankfurt a. M. 1988, 337 pages with figures, tables and appendices.
- 22 *Rollin, J.*; *Dowman, I. J.*: Map Compilation and Revision in Developing Areas – Test of Large Format Camera Imagery. – Frankfurt a. M. 1988, 35 pages with 3 figures, 9 tables and 3 appendices.
- 23 *Drummond, J.* (ed.): Automatic Digitizing – A Report Submitted by a Working Group of Commission D (Photogrammetry and Cartography). – Frankfurt a. M. 1990, 224 pages with 85 figures, 6 tables and 6 appendices.
- 24 *Ahokas, E.*; *Jaakkola, J.*; *Sotkas, P.*: Interpretability of SPOT data for General Mapping. – Frankfurt a. M. 1990, 120 pages with 11 figures, 7 tables and 10 appendices.

- 25 *Ducher, G.*: Test on Orthophoto and Stereo-Orthophoto Accuracy. – Frankfurt a. M. 1991, 227 pages with 16 figures and 44 tables.
- 26 *Dowman, I. J.* (ed.): Test of Triangulation of SPOT Data – Frankfurt a. M. 1991, 206 pages with 67 figures, 52 tables and 3 appendices.
- 27 *Newby, P. R. T.; Thompson, C. N.* (ed.): Proceedings of the ISPRS and OEEPE Joint Workshop on Updating Digital Data by Photogrammetric Methods. – Frankfurt a. M. 1992, 278 pages with 79 figures, 10 tables and 2 appendices.
- 28 *Koen, L. A.; Kölbl, O.* (ed.): Proceedings of the OEEPE-Workshop on Data Quality in Land Information Systems, Apeldoorn, Netherlands, 4–6 September 1991. – Frankfurt a. M. 1992, 243 pages with 62 figures, 14 tables and 2 appendices.
- 29 *Burman, H.; Torlegård, K.*: Empirical Results of GPS – Supported Block Triangulation. – Frankfurt a. M. 1994, 86 pages with 5 figures, 3 tables and 8 appendices.
- 30 *Gray, S.* (ed.): Updating of Complex Topographic Databases. – Frankfurt a. M. 1995, 133 pages with 2 figures and 12 appendices.
- 31 *Jaakkola, J.; Sarjakoski, T.*: Experimental Test on Digital Aerial Triangulation. – Frankfurt a. M. 1996, 155 pages with 24 figures, 7 tables and 2 appendices.
- 32 *Dowman, I. J.*: The OEEPE GEOSAR Test of Geocoding ERS-1 SAR Data. – Frankfurt a. M. 1996, 126 pages with 5 figures, 2 tables and 2 appendices.
- 33 *Kölbl, O.*: Proceedings of the OEEPE-Workshop on Application of Digital Photogrammetric Workstations. – Frankfurt a. M. 1996, 453 pages with numerous figures and tables.
- 34 *Blau, E.; Boochs, F.; Schulz, B.-S.*: Digital Landscape Model for Europe (DLME). – Frankfurt a. M. 1997, 72 pages with 21 figures, 9 tables, 4 diagrams and 15 appendices.
- 35 *Fuchs, C.; Gülch, E.; Förstner, W.*: OEEPE Survey on 3D-City Models.  
*Heipke, C.; Eder, K.*: Performance of Tie-Point Extraction in Automatic Aerial Triangulation. – Frankfurt a. M. 1998, 185 pages with 42 figures, 27 tables and 15 appendices.
- 36 *Kirby, R. P.*: Revision Measurement of Large Scale Topographic Data.  
*Höhle, J.*: Automatic Orientation of Aerial Images on Database Information.  
*Dequal, S.; Koen, L. A.; Rinaudo, F.*: Comparison of National Guidelines for Technical and Cadastral Mapping in Europe (“Ferrara Test”) – Frankfurt a. M. 1999, 273 pages with 26 figures, 42 tables, 7 special contributions and 9 appendices.
- 37 *Koelbl, O.* (ed.): Proceedings of the OEEPE – Workshop on Automation in Digital Photogrammetric Production. – Frankfurt a. M. 1999, 475 pages with numerous figures and tables.
- 38 *Gower, R.*: Workshop on National Mapping Agencies and the Internet. *Flotron, A.; Koelbl, O.*: Precision Terrain Model for Civil Engineering. – Frankfurt a. M. 2000, 140 pages with numerous figures, tables and a CD.
- 39 *Ruas, A.*: Automatic Generalisation Project: Learning Process from Interactive Generalisation. – Frankfurt a. M. 2001, 98 pages with 43 figures, 46 tables and 1 appendix.
- 40 *Torlegård, K.; Jonas, N.*: OEEPE workshop on Airborne Laserscanning and Interferometric SAR for Detailed Digital Elevation Models. – Frankfurt a. M. 2001, CD: 299 pages with 132 figures, 26 tables, 5 presentations and 2 videos.
- 41 *Radwan, M.; Onchaga, R.; Morales, J.*: A Structural Approach to the Management and Optimization of Geoinformation Processes. – Frankfurt a. M. 2001, 174 pages with 74 figures, 63 tables and 1 CD.
- 42 *Heipke, C.; Sester, M.; Willrich, F.* (eds.): Joint OEEPE/ISPRS Workshop – From 2D to 3D – Establishment and maintenance of national core geospatial databases. *Woodsford, P.* (ed.): OEEPE Commission 5 Workshop: Use of XML/GML. – Frankfurt a. M. 2002, CD.
- 43 *Heipke, C.; Jacobsen, K.; Wegmann, H.*: Integrated Sensor Orientation – Test Report and Workshop Proceedings. – Frankfurt a. M. 2002, 302 pages with 215 figures, 139 tables and 2 appendices.
- 44 *Holland, D.; Guilford, B.; Murray, K.*: Topographic Mapping from High Resolution Space Sensors. – Frankfurt a. M. 2002, 155 pages with numerous figures, tables and 7 appendices.

- 45 *Murray, K.* (ed.): OEEPE Workshop on Next Generation Spatial Database – 2005. *Altan, M. O.; Tastan, H.* (eds.): OEEPE/ISPRS Joint Workshop on Spatial Data Quality Management. 2003, CD.
- 46 *Heipke, C.; Kuittinen, R.; Nagel, G.* (eds.): From OEEPE to EuroSDR: 50 years of European Spatial Data Research and beyond – Seminar of Honour. 2003, 103 pages and CD.
- 47 *Woodsford, P.; Kraak, M.; Murray, K.; Chapman, D.* (eds.): Visualisation and Rendering – Proceedings EuroSDR Commission 5 Workshop. 2003, CD.
- 48 *Woodsford, P.* (ed.): Ontologies & Schema Translation – 2004. *Bray, C.* (ed.): Positional Accuracy Improvement – 2004. *Woodsford, P.* (ed.): E-delivery – 2005. Workshops. 2005, CD.
- 49 *Bray, C.; Rösndorf, C.* (eds.): Achieving Geometric Interoperability of Spatial Data, Workshop – 2005. *Kolbe, Th. H.; Gröger, G.* (eds.): International Workshop on Next Generation 3D City Models – 2005. *Woodsford, P.* (ed.): Workshop on Feature/Object Data Models. 2006, CD.
- 50 *Kaartinen, H.; Hyypä J.*: Evaluation of Building Extraction. *Steinmocher, K.; Kressler, F.*: Change Detection. *Bellmann, A.; Hellwich, O.*: Sensor and Data Fusion Contest: Information for Mapping from Airborne SAR and Optical Imagery (Phase I). *Mayer, H.; Baltsavias, E.; Bacher, U.*: Automated Extraction, Refinement, and Update of Road Databases from Imagery and Other Data. 2006, 280 pages.

The publications can be ordered using the electronic orderform of the EuroSDR website  
[www.eurosdrr.net](http://www.eurosdrr.net)